Raman spectroscopy based strategies for prevention and early detection of respiratory tract infections in susceptible individuals

FRIEDRICH-SCHILLER-
UNIVERSITÄT
JENA

Dissertation

(kumulativ)

zur Erlangung des akademishen Grades

doctor rerum naturalium (Dr. rer. nat.)

Vorgelegt dem Rat der Chemisch-Geowissenschaftlichen Fakultät der

Friedrich-Schiller-Universität Jena

von M. Sc. Olga Žukovskaja

geboren am 7. Oktober 1990 in Vilnius, Litauen

Gutachter

1. Prof. Dr. Jürgen Popp
   Friedrich-Schiller-Universität Jena
2. Prof. Dr. Ute Neugebauer
   Friedrich-Schiller-Universität Jena

Tag der Disputation: 07.08.2019

TABLE OF CONTENTS

INDEX OF ABBREVIATIONS

RTIs	Respiratory tract infections
WHO	World Health Organization
COPD	Obstructive pulmonary disease
CF	Cystic fibrosis
ABPA	Allergic bronchopulmonary aspergillosis
CXR	Chest radiography
CT	Computed tomography
BAL	Bronchoalveolar lavage fluid
PCR	Polymerase chain reaction
ELISA	Enzyme-linked immunosorbent assay
RS	Raman spectroscopy
RRS	Resonance Raman Spectroscopy
SERS	Surface-enhanced Raman Spectroscopy
RST	Raman spectroscopic techniques
UV	Ultraviolet
LSPRs	Local surface plasmon resonances
NPs	Nanoparticles
PLS-DA	Partial Least Squares-Discriminant Analysis
PCA	Principal Component Analysis
SVM	Supporting Vector Machine
LDA	Linear Discriminant Analysis
LBOCV	Leave-one-batch-out cross-validation
LMOCV	Leave-one-mouse-out cross-validation
PCs	Principal components
LOD	Limit of detection
SD	Standard deviation
RSD	Relative standard deviation
SiNWs	Si nanowires
MACE	Metal-assisted chemical etching
PSA	Prostate specific antigen
CRP	C-reactive protein
PCT	Procalcitonin

PYO	Pyocyanin
IL	Interleukin
DPA	Dipicolinic acid
HF	Hydrofluoric acid
NDI	Nephrogenic diabetes insipidus
dRTA	Distal renal tubular acidosis

TABLE OF FIGURES

1 MOTIVATION

"His lungs were so bad they couldn't supply the oxygen his body needed. A respiratory therapist told us his lungs were so hard and infected that it was like trying to pump air into a brick."

Scott Smith.

Our lungs are essential organs for life. We never fully appreciate this being healthy, but as soon as respiratory function is impaired, nothing else but our breathing really matters. Nowadays respiratory tract infections (RTIs) constitute a large and growing public health problem. They are one of the most common cases of primary care visits and account for major antibiotic prescriptions. [1-3] In 2016 RTIs killed approximately 3 million people worldwide, which makes them the leading infectious cause of death and the fourth-leading cause of death overall. [4]

Like other infectious diseases, the outcome of RTIs is a complex interplay between the ability of the pathogen to infect, colonize and damage tissues, and the capacity of the host to mount an effective immune response. The average human inhales approximately 23,000 breaths of air each day along with any contaminating bacteria, virus and fungal particles present in the environment. Fortunately, the respiratory tract has evolved to withstand this invasion of potential pathogens by building a variety of innate and acquired immune defenses. For example, mechanical barriers limit the upper respitatory tract's exposure to potential pathogens, while the mucociliary apparatus and cough reflexes work to expel any microorganisms that may bypass the initial defenses. If infectious agents manage to sneak into the lower respiratory tract, the alveolar macrophage and recruited phagocytes significantly decrease their chances of establishing infection. [5] However, if the defense mechanisms are not working properly, pathogens have a higher likelihood of occupying the organism. This is the case, for instance, for immunocompromised patients. Potent immunosuppressive therapies used for transplantations, the broad use of corticosteroids and immunosuppressant drugs for cancer, the lymphoproliferative and systemic diseases, tumour necrosis factor alpha inhibitors, monoclonal antibodies, and the pandemic of HIV/AIDS have created a favorable environment for the emergence of various infections. [6, 7] Pulmonary complications appear in 60 % of such patients and are associated with high mortality rates, especially in patients with mechanical ventilation. [8, 9]

Also susceptible are people suffering from chronic respiratory diseases such as asthma or obstructive pulmonary disease (COPD) as well as those who have genetic disorders affecting the lungs, like cystic fibrosis (CF). [10] In the case of chronic respiratory diseases, RTIs are the most common causal factors that disturb airway stability and lead to life-threating acute exacerbation of the main disease. [11, 12] CF is a disease characterized by the buildup of thick, sticky mucus,

which inhibit the clearance of microorganisms from the lungs. Thus, lower respiratory tract of CF patients is often colonized by pathogens. Ultimately, 80 to 95 % of patients with CF succumb to respiratory failure caused by chronic bacterial infection and concomitant airway inflammation. During infancy and early childhood, the main colonizing bacterium is the Gram-positive *Staphylococcus aureus*, which is later replaced by Gram-negative *Pseudomonas aeruginosa.* [13]

The last group of people at increased risk involves children, especially in low-income countries, and older adults. RTIs, predominantly pneumonia and bronchiolitis, are a major cause of death for children under 5 years of age. [14] Moreover, acute lower RTIs in childhood predispose individuals for chronic respiratory diseases later in life. [15] Considering older individuals (>65 years old) the morbidity rates of RTIs are similar as by younger people, but mortality rates are significantly higher. Reasons for this include: delayed diagnosis due to a frequent absence of typical signs and symptoms such as fever or leukocytosis; complications because of another chronic diseases, like diabetes; and often no response to the therapy. [16]

Taking into account the gradually ageing and constantly growing number of immunocompromised patients and individuals with chronic respiratory diseases, the growing mortality rates of RTIs are not surprising. Managing RTIs in susceptible patients is difficult: they often present atypically, progress rapidly and their identification and differentiation from noninfectious causes of fever and pulmonary infiltrates is far from simple. The development of prevention techniques as well as the improvement of diagnostic and treatment methods is essential to decreasing the fatal outcome of RTIs, especially in the susceptible groups mentioned above.

Strategies for preventing RTIs consider enhancing lung defenses and avoiding aspiration. Effective prevention against specific organisms can be provided by immunization. For example, influenza vaccination reduces the risk of medically attended influenza virus infection by approximately 50 %, though there is considerable heterogeneity by season, setting, and population subgroup. [17-19] Vaccination for preventing pneumococcal infection has also shown to be effective in healthy adults, but might not provide as much protection in individuals with chronic conditions. [20] Despite the moderate success, the biggest drawback of the immunization approach is the selective spectrum of protection and the time required for the development of the protective antibody. Avoiding the aspiration of pathogens is barely possible because no environment is totally sterile. However, by being aware of the exact composition of the microorganisms in the air, susceptible individuals could avoid being in the places with more dangerous pathogens. For instance, some susceptible individuals can have hypersensitivity to *Aspergillus* species, which can lead to allergic bronchopulmonary aspergillosis (ABPA) or other complications. [21] People with immunosuppression due to B-cell abnormalities are predisposed to infection with encapsulated bacteria such as *Streptococcus pneumoniae*. [22, 9] Individuals with CF should particularly avoid coloniza-

tion of *P. aeruginosa*. [23] Thus, the development of techniques for fast and automated identification of the microorganisms in the air could be beneficial for the prevention of RTIs.

The crucial requirement for decreasing mortality rates is an early and accurate diagnosis of the infections, which leads to appropriate treatment. Chest radiography (CXR) continues to be the preferred initial diagnostic imaging test for detecting suspected RTI. However, some researches have suggested that CXR may lack sensitivity for diagnosing, especially at early stages of infection [24, 25] and computed tomography (CT) may be diagnostically superior [26]. Regardless, both CXR and CT are associated with a dose of ionizing radiation, which limits frequency of imaging and thereby hinders the use of those techniques for tracking the disease's progres and treatment. Thus, it would be advantageous to develop other screening methods, which would enable easy, non-invasive and rapid detection of the infection at an early stage and would provide information about the severity of the disease.

Unfortunately, just the diagnosis of a RTI in the organism is not enough to establish correct treatment. Here, the detection of the exact infectious agent is highly important. [27] In current clinical practice, identification of the pathogens is based on cultures from sputum and bronchoalveolar lavage fluid (BAL). However, depending on the microorganism species culturing can take several days. Moreover, some species are not cultivable or contamination by organisms unrelated to the cause of infection may occur. As an alternative, nucleic acid-based and immunological techniques were developed. Nucleic acid-based detection methods usually rely on the amplification of DNA or RNA via polymerase chain reaction (PCR). They provide a high level sensitivity and specificity and are also very rapid. However, PCR methods require expensive reagents and the design of target-specific primers. Moreover, if the sample matrix contains substances inhibiting the PCR reaction, more or less complicated procedures will be necessary for the extraction of the target DNA. The method is also sensitive to contamination and experimental conditions. Immunological methods rely on antibodies' binding to specific antigens of target microorganisms. Commonly used techniques include enzyme-linked immunosorbent assay (ELISA) and serological assays. These methods improved the microbial diagnosis because of their high-throughput capacity and time- and cost-efficiency along with ease-of-use. However, for ELISA both specificity and sensitivity are reduced due to the difficulty in generating selective antibodies and the need for large amounts of antigens for quantification. Serological assays are usually limited due to their long time the antibodies need to be produced within the human body. [28, 29]

Given limitations of all introduced methods increase attention to the one more alternative approach, namely, the indirect identification of the infectious agent by detection of metabolites released to body-fluids either by pathogen or reflecting the host response.

To sum up, there are three strategies, which should be considered for reducing mortality from RTIs in susceptible individuals:

1) Prevention – fast and automatic monitoring of the composition of microorganisms in the air so that people could avoid being in places with potential pathogens.
2) Screening – periodic checking of susceptible individuals to diagnose the disease at an early stage.
3) Exact diagnosis of infectious agent directly from respiratory body-fluids.

The continuous effort should be devoted to developing new and improving already existing methods of addressing these clinical tasks. Moreover, apects such as rapidness, reliability, cost-effectiveness and simplicity should be considered. Simultaneously to fulfill all of these requirements is not easy, but one of the techniques which holds such promises is Raman spectroscopy (RS). RS is a vibrational spectroscopic method based on the inelastic scattering of light. This technique is able to non-invasively and rapidly provide the molecular information about the chemical composition of the sample, which could be used for certain medical needs. [30-33] Depending on the task, simple conventional RS can be used, or the techniques providing enhanced Raman signal, namely Resonance Raman Spectroscopy (RRS) and Surface-enhanced Raman Spectroscopy (SERS), can be applied.

The aim of this thesis is to assess the potential and limitations of these Raman spectroscopic techniques (RST) for the prevention, screening and diagnosis of RTIs. In the following section, the theoretical basics of three RST will be briefly introduced. Subsequently, keeping the three mentioned clinical tasks in focus, the current state of the application of RST in the medical field will be critically reviewed and summarized. In the last section of the thesis, the results published in four different manuscripts will be discussed, highlighting the potential and challenges of the applied methods. Here, firstly, the UV-RRS for the identification of fungal spores dangerous to susceptible individuals will be demonstrated. Next, utilizing mouse model of aspergillosis, conventional RS of urine will be introduced as an easy tool for screening the RTI and its diagnostic performance will be compared to that for other diseases. Lastly, the SERS detection of the metabolite of *P. aeruginosa* bacterium directly in complex matrixes of saliva and artificial sputum using easily prepared SERS substrates will be introduced and discussed.

2 THEORETICAL FUNDAMENTALS

2.1 Raman Spectroscopy

When light interacts with matter, most photons are elastically scattered. This effect is called Rayleigh scattering and means that the energy of the incident photon is equal to that of the scattered photon. However, one photon out of 10^7 is scattered inelastically, meaning that the energy between incoming and scattered photons differs. This effect was first experimentally observed by C.V. Raman in 1928 and was named in his honor. [34]

During the Raman effect, an initial photon with energy $\hbar\omega_0$ is annihilated and the molecule is excited from its initial vibrational energy state $|i\rangle$ to a virtual state $|m\rangle$ (this virtual state is neither a stationary state nor a solution of time-independent Schrödinger equation and it does not correspond to a well-defined value of energy). Next, the molecule relaxes to its final state $|f\rangle$ and a new photon with lower (Stokes Raman scattering) or higher (anti-Stokes Raman scattering) energy than the initial one is created. Stokes Raman scattering takes place when the scattering process starts from the vibrational ground state and ends up in a vibrational excited state via a transition into the virtual state. For the anti-Stokes Raman scattering the molecule is initially already in an excited vibrational state and by the scattering process is transferred into the vibrational ground state. [35, 36] As the majority of the molecules at room temperature are in the vibrational ground state, the Stokes Raman scattering is more dominant.

According to the classical description of light scattering, the intensity $\left(I_{i\to f}\right)$ of the Raman scattered light depends on the number of Raman active molecules (*N*), on the intensity of the incoming light $\left(I_0\right)$, the frequency of the incident laser radiation $\left(\omega_0\right)$ as well as the frequency for a Raman transition from state $|i\rangle$ to state $|f\rangle$ $\left(\omega_{fi}\right)$, and on a sum over the polarizability tensor components $\left(\alpha_{\rho\sigma}\right)$:

$$I_{i\to f} = const \cdot N \cdot I_0 \cdot (\omega_0 \pm \omega_{fi})^4 \cdot \sum_{\rho,\sigma} \left|\alpha_{\rho\sigma}\right|^2 . \tag{1}$$

In 1990, the first Raman spectroscopic investigations on biological cells were performed by Puppels *et al*. [37] Later on, the interest of applying RS in biomedicine related studies steadily increased. [38-41] The reason for this upswing in interest is the label-free, non-invasive and non-destructive nature of the technique together with the ability to instantly provide information about the molecular composition of the sample. Additionally, it requires simple to no sample preparation

and only a small sample amount. However, although RS is characterized by high molecular specificity, its scattering efficiency is rather poor, especially for the molecules with small Raman cross-sections. In addition to it, investigating biological samples using excitation wavelengths in the VIS or near infrared region, Raman scattering is very often interfered with the more intense fluorescence emission. To overcome these disadvantages of weak signal and overwhelming fluorescence background, special Raman signal-enhancing approaches, such as resonance Raman spectroscopy [42, 36] or surface enhanced Raman spectroscopy [43, 44] can be applied.

2.2 Resonance Raman spectroscopy

In resonance Raman spectroscopy, the dispersion relation of the polarizability α (i.e., its frequency dependence) is utilized to enhance the Raman scattering intensity. Using second-order perturbation theory Kramers, Heisenberg, and Dirac derived an expression for the transition polarizability tensor for a transition $i \to f$ [45]:

$$\left(\alpha_{\rho\sigma}\right)_{fi} = \sum_{\psi_r} \frac{\langle \psi_f | \mu_\rho | \psi_r \rangle \langle \psi_r | \mu_\sigma | \psi_i \rangle}{\hbar\omega_{ri} - \hbar\omega_o - i\Gamma_r} + \frac{\langle \psi_f | \mu_\sigma | \psi_r \rangle \langle \psi_r | \mu_\rho | \psi_i \rangle}{\hbar\omega_{rf} + \hbar\omega_o - i\Gamma_r} \tag{2}$$

with μ_ρ and μ_σ being the transition dipole moments, ω_o and ω_{ri} being the angular frequency of the incident and of the $i \to r$ radiation, respectively, and Γ_r is a damping factor which can be related to the life time of the excited vibronic state $|\psi_r\rangle$.

This equation describes Raman scattering as a two-photon process with a transition from the initial state with the vibronic wave function $|\psi_i\rangle$ to the entire manifold of eigenstates with the wave function $|\psi_r\rangle$ of the unperturbed molecule, followed by a transition to the final state with the wave

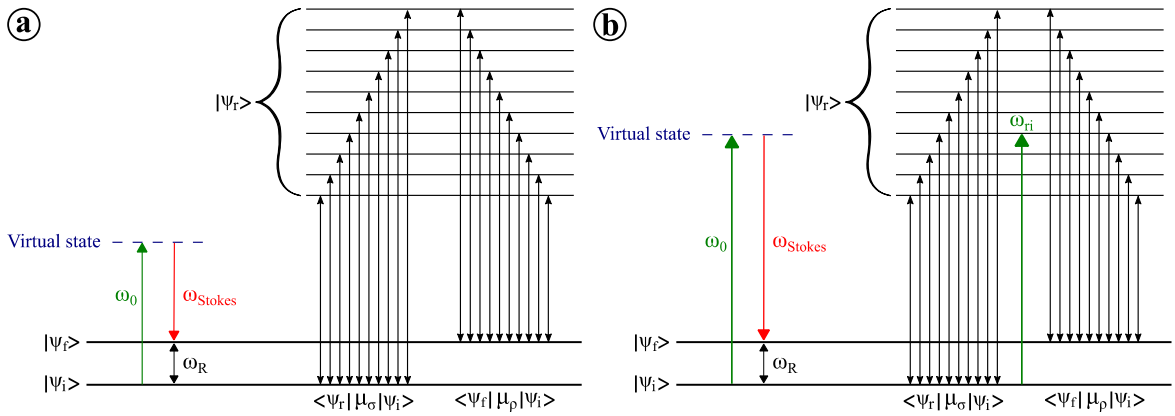

Figure 1. Energy level diagram illustrating the sum-over states description of the Raman transition polarizability tensor. **(a)** Nonresonant Raman scattering; **(b)** resonance Raman scattering, where the Raman excitation frequency matches the electronic transition of the molecule: $\omega_o \approx \omega_{ri}$.

function $|\psi_f\rangle$ as depicted in **Figure 1.**

For normal Raman scattering ($\omega_{ri} \gg \omega_o$, **Figure 1a**) the weighted summation over all possible states results in no information about the eigenstates $|\psi_r\rangle$. The initial $|\psi_i\rangle$ and final state $|\psi_f\rangle$ play the determining role. That changes, however, when the incident laser frequency ω_o matches the energy gap ω_{ri} to an electronically excited eigenstate $|\psi_r\rangle$ (**Figure 1b**). This electronic eigenstate will dominate the whole sum, because the denominator of the first term in the sum in Equation 2 becomes really small, causing the first term to become very large, while the second term becomes negligible. This explains the signal enhancement up to six to eight orders of magnitude that is observed in resonance Raman compared to normal Raman scattering.

As resonance Raman scattering occurs involving an excited electronic state, the technique can be used to gain information about the molecular structure and dynamic of the excited electronic state. However, in this work RRS is not used because of its high power for photochemical analysis, but rather because of its high sensitivity and selectivity. By choosing an appropriate wavelength, excitation of specific macromolecular biomarkers can be achieved, which allows for the detection of low concentrations in a complex biological environment. For instance, using excitation wavelength in the deep ultraviolet (UV) region, macromolecules such as proteins or DNA in the presence of other molecules, for instance, in whole cells, can be studied. [46] However, if the Stokes shift between the absorption and fluorescence of the molecule is not large enough, Raman bands can overlap with the fluorescence emission. The good way to avoid it is to use excitation wavelengths bellow 260 nm. Using such energy-rich UV-light, higher electronic excited states are incorporated. While Raman scattering occurs within the first few femtoseconds (10^{-15} s) directly from the high electronic state, fluorescence process occurs only on a time scale of nanoseconds (10^{-9} s) in most cases from the vibrational ground state of the first excited electronic state (Kasha's rule). Therefore, the Raman and fluorescence signals are well separated on the energy scale. [36] However, due to high power excitation light, photodegradation of the sample can occur, which is a primary drawback of this technique.

2.3 Surface enhanced Raman spectroscopy

The weak Raman signal can be greatly enhanced by the introduction of SERS. Historically, the SERS effect was first observed and reported by Martin Fleischmann and co-workers for pyridine adsorbed onto the surface of roughened silver electrodes. [47] After decades of debate, it is now generally agreed that there are two primary enhancement mechanisms: electromagnetic and chemical enhancement.

The electromagnetic (EM) enhancement results from the amplification of the light by the excitation of localized surface plasmon resonances (LSPRs). Surface plasmons are collective charge density fluctuations at metal/dielectric (or metal/vacuum) interface. If the metal surface is roughened, the plasmons are no longer confined and the electric field can radiate both in parallel and perpendicular directions to the surface. Because of its resonant character, the oscillation may result in a polarization and induction of a strong electromagnetic field on the metallic nanostructure. This light concentration occurs preferentially in the gaps, crevices, or sharp features of plasmonic materials, which are traditionally noble and coinage metals (e.g., silver, gold, and copper) with nanoscale features. As a result, the Raman modes of a molecule located in close vicinity to the nanostructure are enhanced because the Raman intensity is proportional to the squared incident electromagnetic field intensity (Equation 1). The EM enhancement mechanism was proved to account for signal enhancements of up to 10^{11}. [48-50] The particle size and shape were found to have a strong influence on the resonance frequency. It is also known that the electromagnetic field of the excited surface plasmons has evanescent character and quickly decreases with the distance *d* from the surface. By McCall derived dipolar plasmon approximation for silver spherical metal particle with radius *r* resulted in such dependency:

$$EM_{enhance} \propto \left(\frac{r}{r+d} \right)^{12}. \tag{3}$$

The other mechanism involved in signal enhancement is chemical enhancement, which combines three different processes: (1) chemical interaction of the nanoparticle and molecule in the electronic ground state; (2) resonant excitation of the charge-transfer process between the molecule and the nanoparticle; and (3) the resonance Raman enhancement appearing when the energy of the incident radiation matches the energy needed for an electronic dipole transition within the molecule. The magnitude of contribution from the chemical enhancement is highly variable with reported estimates ranging from 10^1 to as high as 10^6. [51-53]

Comparing the SERS spectra to the normal Raman spectra the shift in vibrational bands and changed intensity pattern might be observed. Shift in the bands could be explained by redistribution of electron density inside the molecule caused by analyte-metal interaction and resulting in the change in bond lengths and molecular polarizability. [43, 54] The change in intensity pattern of the SERS spectrum is associated with the orientation of the molecule to the metallic surface. According to the surface selection rules, only vibrational modes which have a nonvanishing component of the transition dipole moment normal to the metallic surface will be enhanced. [55] Moreover, due to evanescent nature of the EM field, modes being closer to the surface will exhibit greatly higher enhancement (Equation 3).

The application of SERS in the biomedical field requires SERS substrates to allow reproducible and quantitative SERS measurements, to be non-toxic for the biological system under investigation and to have a good lifetime. Aiming to fulfill these requirements, different designs and fabrication processes of the SERS-active substrates have been investigated. [56-58] The most common SERS substrates can be classified as colloidal nanoparticles (NPs) and planar nanostructures. However, to this point there is no 'best SERS substrate', as the performance of each substrate strongly depends on the desired application and analyte molecule. More specifically, on the Raman scattering cross-section of the molecule, its affinity towards metallic surface and the orientation on the surface.

3 STATE OF THE ART - MEDICAL APPLICATIONS OF RAMAN SPECTROSCOPIC TECHNIQUES

3.1 Identification of microorganisms

Rapid and reliable methods that enable the detection and identification of microorganisms are of great importance in medicine, food safety, and environmental or agricultural purposes. The early detection and subsequent elimination of highly pathogenic agents in the air or in food could prevent cases of a variety of diseases. For already established infections, the early identification of causative pathogens in the organism could significantly improve the outcome of the treatment and decrease overall health care costs. [59] Nowadays, the gold standard for the identification of microorganisms is cultivation followed by an investigation of the morphological and metabolic characteristics of grown cultures. Even though this technique is well established and reliable, it nonetheless entails two significant disadvantages. Firstly, depending on the bacterial species, culturing can take several days; moreover, some species are not cultivable or require a specific environment. Secondly, as the identification is based on careful observation and measurement of morphological characteristics of the organism, it requires highly trained and experienced personnel. Therefore, in recent decades many new methods have emerged for microorganism identification. [60-62] The most widespread ones are immunoassays and PCR. However, these methods also suffer from certain limitations such as an inability to detect organisms not represented in an immunoassay or PCR panel, or to discriminate between living and dead organisms in a sample. [63-65]

Among other alternatives, RS is a valuable and attractive tool in pathogen diagnostics because it provides information about the molecular structure and the chemical composition of the investigated samples. Different microbes vary, for example, in the composition of the proteome or the cell wall and accordingly exhibit a slightly different Raman spectrum. The first attempt to identify bacteria with RST was reported in 1987 by employing UV-RRS. [66] Relying on visual inspection of acquired spectra, authors confirmed spectroscopic differences between five different bacteria types and assigned them mostly to cellular RNA, DNA and the amino acids tyrosine and tryptophan. More recently, visual analysis of spectra has been replaced by more objective, powerful and automatic chemometric approaches, which capture even slight differences between the samples and use them for the subsequent identification. Such symbiosis of RS and chemometrics significantly raised the potential of different RST for the fast differentiation and identification of microbial species and even strains. [67-70]

Independent of the statistical algorithm used, all Raman-based pathogen classification methods require an extensive database of reference spectra of relevant microorganisms. With an established

database and well-trained statistical analysis algorithms [71], a broad range of pathogens could be identified with high accuracy. For instance, Hamasha *et al.* reported a differentiation of pathogenic and non-pathogenic *Escherichia coli* strains using conventional RS combined independently with principal component-discriminant function analysis or partial least squares-discriminant analysis (PLS-DA). For both multivariate chemometric techniques, the sensitivity and specificity exceeded 95 %. [72] Rebrošová *et al.* performed a RS study with 277 staphylococcal strains belonging to 16 species and, based on their Raman spectra, they were able to achieve the successful identification rate of more than 99 % for individual spectra on the species level. [73] This result is even more impressive knowing that bacterial colonies were investigated directly on solid medium after 24-hour culturing. A few more studies showed that the successful identification of bacteria can be still achieved if culturing time is decreased to 6 [74] or even 3 hours [75]. This indicates the potential of RS to exclude the human factor from the identification process and speed up the clinical routine of the pathogen identification. Some studies showed that the cultivation step can, in general, be excluded and single bacteria can be detected and identified with conventional RS directly from body-fluids. [76-78] However, in this case some bacteria isolation and enrichment strategies should be used. [79]

The main requirement for the RS-based identification of pathogens is providing for statistical analysis spectra with high signal to noise ratio. For some pigmented species of microorganisms, that could be a challenging task. For instance, Ghosal *et al.* performing a visible range RS study on several different microfungi spores relevant to indoor contamination pointed out that registration of a good spectrum was difficult due to combined fluorescence background and induced photodegradation. [80] Similar difficulties were reported by Verwer *et al.* when trying to discriminate *Aspergillus lentulus* from *Aspergillus fumigatus*. The good quality spectra and classification accuracy of 78 % were achieved only after whitening conidia. [81] One of the technical ways to minimize fluorescence background from pigmented species is to use UV-RRS with excitation wavelength lower than 260 nm, as, in this case, fluorescence and Raman signal are energetically separated. Moreover, with this technique the selective information about taxonomically important cellular components such as DNA/RNA bases and aromatic amino acids can be collected and utilized for the identification of microorganisms. Recently, UV-RRS was used to differentiate between 22 *Candida* strains of 12 clinically relevant species. Principal Component Analysis (PCA) combined with a Supporting Vector Machine (SVM) was used to build the model, which was evaluated with leave-one-batch-out cross-validation (LBOCV). Reliable identification results were observed with accuracies ranging from 93 %, all the way up to 100 %. [82] UV-RRS was also performed for discriminating between the common causal agents of urinary tract infection, namely *E. coli*, *Klebsiella* spp., *Enterococcus* spp. and *Proteus mirabilis*. Cluster analysis performed on the acquired data, correctly

grouped the spectra according to the genus. [83] Lopez-Diez and coauthors achieved successful discrimination on the species level between endospore-forming bacteria belonging to the genera *Bacillus* and *Brevibacillus*. [84] Despite the good performance, the UV-RRS has the disadvantage of inducing a 'burning effect' due to the high photon energy used for the Raman scattering excitation. To overcome this problem, microorganisms in the mentioned studies were analyzed on a rotating stage. However, this is suitable only for bulk samples requiring larger amount of biomass, thus the cultivation step cannot be omitted.

In recent years, the potential of SERS to speed up the pathogen identification was also widely explored. To this point, most SERS studies on microorganisms are based on two principal approaches: label-based and label-free. [85] In the case of label-based detection, plasmonic NPs are modified with specific target antibody or oligonucleotide and with Raman reporter molecule having large Raman cross-section. [86] Here, measurements provide spectral information on the Raman label, not on the bacterial cell itself, thus losing intrinsic SERS spectral information on the identity of the bacterial cell. Identification of the microorganism is based on the prior expectation of antibody or oligonucleotide specificity. [87, 88] Therefore, the label-based SERS can be used only when the target microorganism is known, which is very rarely the case in a clinical practice. Moreover, the complicated design of the SERS tags is time consuming and increases the analysis costs.

Label-free SERS tends to be a simpler alternative. Here, three strategies are possible. The predominant one is mixing of pre-prepared gold or silver nanoparticles of various shapes or aggregates with bacterial cell suspension. [89-92] Using such method, the limit of detection (LOD) of 10^3 CFU/mL was achieved [93] and identification of different bacteria (even in a mixture) was reported [94]. However, due to not uniform mixture of nanoparticles and bacterial cells, spectral reproducibility is often poor. To overcome this drawback, the synthesis of the nanoparticles directly on the bacterial wall was introduced. [95] This *in situ* strategy ensures homogenous contact of constituents of the bacterial cells to NPs and thus gives an intense spectrum with better reproducibility. [96-99] For instance, Dina *et al.* using *in situ* Ag NPs in less than 5 min successfully grouped Gram-negative and Gram-positive bacteria [100] and identified three fungal species [101]. The third strategy entails placing microorganisms on the top of different SERS-active planar substrates. [102, 103] For example, Henderson and coauthors introduced an Ag nanorrod array for the identification of *Mycoplasma pneumonia* from a panel of 12 other human commensal and pathogenic mycoplasma species with 100 % cross-validated statistical accuracy. [104]

Despite some reported success and actively ongoing research in this area, there is one major concern about using the SERS technique for the identification of microorganisms. While the Raman spectra include spectral information on the entire bacteria cell, the SERS spectra exhibit the

spectral information mostly just from the cell wall components, which are binding to the SERS-active surfaces, such as adenine or xanthine. [105] Thus, it is questionable whether this information is really enough willing to discriminate taxonomically similar species, not even talking about different strains. There is no binary answer to this question. For example, some studies showed that SERS spectrum of Mycobacteria is dominated by the mycolic acid, which is the characteristic component of the mycobacteria cell membrane. [106] As it is known that the mycolic acid structure slightly varies between species, the SERS spectra provide enough input for successful identification. Unfortunately, this is not the generally the case for all microorganisms. Muhamadali *et al.* compared conventional RS and SERS for the classification of a range of industrial, environmental or clinically relevant bacteria. Although SERS displayed unique clustering patterns which allowed for the perfect differentiation of Gram-positive and Gram-negative bacterial samples, the overall accuracy on species level using SERS spectral data was lower than when conventional RS was used (74.9 % *vs* 97.8 %). [107]

To sum up, numerous studies have shown the ability to use RST for the identification of microorganisms at different taxonomic levels. Indeed, careful thought is required prior to selection of one or more of these techniques, especially regarding sample type, format, preparation, and the biological questions being asked. Furthermore, some work should be performed on standardization of the sample preparation and measurement protocols, as well as on statistical evaluation processes, because a huge variety of applied methods makes the results comparability difficult and inhibits the transition to the clinics.

3.2 Body-fluids based screening of the diseases

The objective of medical screening is to detect disease in its early stages and thereby increase the chances for its successful treatment. Some criteria established by World Health Organization (WHO) underline that screening tests should be easy to perform and interpret, should be cost effective for the healthcare system and, of course, highly accurate. [108] Examples of current screening tests include the pap smear for cervical cancer, cholesterol level for heart disease and X-ray/CT for lung cancer. [109] The analysis of body-fluids is particularly attractive for screening purposes due to a minimal or non-invasive collection of samples and the possibility of performing multiple screening tests. Metabolomics studies already proved that in the presence of the different disease the biochemical profile of the body fluids changes. [110, 111] Thus, the development of an easy and cheap technique that is able to register those changes would be advantageous for clinical applications.

In this scope, RS holds significant diagnostic promises, because it provides a snapshot of the biomolecular composition of the sample and the variations therein. Moreover, it offers rapid and non-

destructive analysis with less sample quantity required and minimal or no sample preparation. Within the last years, a combination of conventional RS or SERS with advanced multivariate data analysis was actively explored for a wide range of diseases using different bio-fluids. [112, 113] The general workflow for such studies includes the acquisition of spectral data from samples obtained from control and atypical cohorts, preprocessing of spectra, building of a classification model and verification of the model on an independent data set or by using cross-validation methods. [114]

Currently, the majority of the biofluid-based RS research has focused on serum and plasma, since those samples are rich in proteins and contain verified or proposed markers for a variety of diseases. For instance, Gonzales-Solis *et al.* analyzed serum samples with conventional RS and, with the help of PCA combined with Linear Discriminant Analysis (LDA), could not only correctly distinguish between healthy volunteers and patients with leukemia, but also accurately classify three leukemia types. [115] Other serum-based Raman studies demonstrated higher than 90 % accuracies in differentiating normal subjects from patients with breast [116], ovarian [117] or nasopharyngeal [118] cancer. The applicability of the method was also explored for infectious diseases, such as Hepatitis B [119], Hepatitis C [120], or dengue infection [121].

In general, the good performance of RS for differentiation between healthy individuals and sick ones is not so surprising. The appearance of the disease activates the immune and metabolic systems, leading to some changes in the biochemical composition of blood and other bio-fluids, which can be reflected in 'biomolecular spectral fingerprint'. However, in clinical reality it is not enough to know that a person is sick, it is extremely important to identify the disease. Therefore, the question is: how different are the biomolecular changes for different diseases and is RS powerful enough to differentiate between them? In the case of sepsis and non-infectious systemic inflammatory response syndrome, Neugebauer *et al.* demonstrated that conventional RS has such potential. Measurements were performed on dry droplets of blood plasma and subsequent analysis of the spectral data with PCA-LDA algorithms resulted in sensitivity of 100 % and specificity of 82 %. [122] Much lower efficiency of the method (65 %) was reported for differentiation between individuals with head and neck cancer and patients with respiratory illnesses. [123] But here, when building the classification model authors utilized Raman spectra without background correction, which could explain comparably worse results.

Some studies demonstrated that conventional RS on blood serum extra to the diagnosis of the disease can provide information about its stage. [124, 125] For example, an assay carried out on serum samples from 44 asthma patients of different grades showed that changes in protein structure and an increase in DNA- and glycosaminoglycan-specific Raman bands were linked with an increase in asthma severity. [126]

SERS analysis of serum or plasma for disease diagnosis was also actively explored during the last decade, motivating it with the fact that it can enhance weak Raman signal and provide information about molecules, which were not visible on the Raman spectrum or were hindered by fluorescence. So far, aqueous Ag or Au colloids have proven to be the most efficient substrates for label-free analysis of bio-fluids, possibly because of the facile synthesis of colloidal NPs and the simplicity of adsorbing biomolecules on metal surface by mixing. [127, 128] For instance, Ag NPs were used to perform SERS investigation of the serum from 304 normal individuals, 333 patients with hepatopathy, and 99 patients with esophageal cancer. Using orthogonal PLS-DA a discrimination accuracy of 95 % was reached. [129] SERS applicability to detect other oncological diseases [130-132], chronic kidney disease [133], Hepatitis B virus infection [134] or diabetic complications [135] based on serum or plasma spectra was also reported.

Despite these positive results, there is still some concern about the SERS technique for screening purposes. Bonifacio *et al.* reported that proteins of serum or plasma can inhibit the aggregation of nanoparticles leading to very little or no surface enhancement. Therefore, it is beneficial to perform filtration of the sample prior to the analysis and get rid of the proteins. [136] However, this can lead to the loss of some potentially important diagnostic information. Moreover, authors showed that filtrated serum and plasma exhibit SERS spectrum strongly dominated by the bands from only two metabolites, namely uric acid and hypoxanthine. Thus, the choice of SERS for screening should be performed with extreme care, and should be foremost considered for diseases which may have a correlation with blood levels of these two metabolites. Another concern of using SERS relates to its strong dependency on the interaction between biomolecules and SERS active surfaces. This often influences the reproducibility of the spectra and brings extra variations, which could hinder the subtle spectral differences between the healthy and pathological samples. To check if SERS, in general, provides diagnostic benefits compared to conventional RS, Paraskevaidi *et al.* used both techniques to diagnose ovarian cancer based on blood plasma samples. Using the SVM algorithm, cancerous and healthy individuals were differentiated by RS with 94 % sensitivity and 96 % specificity and by SERS with 87 % sensitivity and 89 % specificity. [137] The outcome of the study leads to the conclusion that conventional RS may be advantageous for screening purposes using blood samples. Moreover, it is simpler than SERS and has lower costs.

Urine samples for the RST-based screening were investigated to a lesser extent, but there are still some studies that considered this excreted biofluid. Despite the fact that urine consists primarily of water, it possesses a huge amount of metabolic information for clinical usage. The pilot study of Bispo *et al.* showed that urine analysis with conventional RS leads to discrimination between normal subjects and diabetic/hypertensive patients with and without complications with overall 70 % accuracy. [138] The potential of the technique was also reported for the detection of oral can-

cer. [139] However, it is worth mentioning that reported Raman spectrum of urine is dominated by spectral signature of urea (peak at 1004 cm^{-1}), while other compounds have relatively low intensities and their many bands are convoluted.

In an attempt to receive some more information from other biomolecules found in urine, the SERS method was explored. Here, in contrast with serum and plasma (whose SERS spectra in literature have similar characteristics) urine spectra reported by different groups are more diverse. Some spectra are dominated by urea, other by creatinine or hypoxanthine. This can be explained by different experimental conditions or by high inter- and intra-individual variability of urine in terms of composition, concentration and pH, which is known to influence SERS signal. [140] Nevertheless, the application of SERS for urine screening resulted in accuracies between 80 and 95 % for prostate cancer [141], esophagus cancer [142], diabetes mellitus [143] and coronary heart disease [144].

Some research attention was also devoted for other bio-fluids, mostly evaluating their feasibility for the screening of the pathologies in a closer relation to the biofluid production. For instance, saliva samples were mostly considered for oral cavity and respiratory diseases. Gonchukov *et al.* performed RS of dry saliva for the early detection of periodontitis and showed that carotenoids contained in saliva correlate with the periodontitis level. [145] SERS was applied for the discrimination between saliva of healthy volunteers and patients with lung cancer [146, 147] or oral squamous cell carcinoma [148, 149]. However, for all studies, high spectral variability of saliva from sample to sample can be noticed and attributed to factors such as individuals' genetics, hydration frequency, smoking, etc.

Magee and coauthors analyzed induced sputum samples aiming to diagnose lung cancer cases and disease free patients with risk factor from healthy individuals. Conventional RS managed to identify people 'at risk' from healthy ones with a sensitivity of 90 % and specificity of 93 %. However, a lot of people 'at risk' were later misclassified as having cancer, resulting in 62 % specificity. [150] While, for screening test higher sensitivity is more desirable for not missing disease cases, low specificity rates are also a concern, because they lead to extra stress for individuals and higher costs. Spectral analysis of sputum samples combined with PCA appeared to be powerful for the distinguishing CF patients infected by *P. aeruginosa* and *S. aureus*. However, to achieve this result, authors had to perform a 30 min photobleaching of sputum samples to minimize huge fluorescence background hindering Raman signal. [151] The diagnostic use of SERS for sputum samples was not reported. This can be attributed to the highly viscous and inhomogeneous matrix of the sputum, which makes the use of SERS substrates challenging.

In conclusion, all of the mentioned studies confirm that the use of RST for disease screening is possible for a wide range of pathological conditions. However, most of them used relatively small

(less than 40) sample numbers. Therefore, additional research using much larger cohorts is certainly required for the transfer of the method to clinics. Moreover, studies including more groups of diseases are necessary in order to assess how specific a screening test can be. Finally, the practical benefits of using SERS for this clinical task are questionable, because it provides diagnostic value in the same range (or even lower) than conventional RS, but increases costs and analysis time, and brings some extra variations due to the interaction of biofluid components with metallic substrates.

3.3 Detection of biomarkers in body-fluids

The term biomarker could be generally described as "*a characteristic, that is objectively measured and evaluated as an indicator of normal biological processes, pathogenic processes, or pharmacologic responses to a therapeutic intervention*". [152] With the rise of genomics, metabolomics and other advances in molecular biology and biochemistry, biomarker studies have entered a whole new area and hold promise for early diagnosis and effective treatment of many diseases. Usually biomarkers are small molecules including metabolites, antigens, DNA, mRNA or enzymes, which are present at a low concentration in the complex mixture with different biomolecules. Thus, their detection and quantification, especially directly in body-fluids, is an analytical challenge. In the past few decades, significant progress has been made in this field and various promising detection methods have been developed, including ELISA, electrochemical immunoassay, fluorescence or surface plasmon resonance-based systems. [153-156] Although those and other methods are continuously improved, they still suffer from the lack of sensitivity and specificity required for clinical diagnostic applications. Thus, research for better alternatives is actively ongoing.

From the three RST discussed along this thesis, SERS, due to its ability to detect molecules of interest at trace levels, is the best candidate for this clinical task. The available literature provides a substantial number of examples confirming the potential of SERS for biomarker detection, especially in the field of cancer diagnostics. [157, 158, 128] However, in the frame of this thesis the focus is set to infectious diseases.

When it comes to infections, two diagnostic tasks are highly important: rapidly distinguishing between viral and non-viral infection cases and identification of the exact infectious agent. In the interplay between the host and the pathogen, a large number of molecules are released. From the initial interaction onwards, the majority of biomolecules available to measure are derived from the host, as pathogen numbers are very low. In a serious infection, when pathogens are able to overcome the early host response, their numbers increase at an exponential rate and the concentration of secreted biomolecules increases. However, the usefulness of many of them as biomarkers for diagnosis is predominantly in the validation process.

Some studies showed that increased levels of bacterial-induced host proteins like C-reactive protein (CRP) or procalcitonin (PCT) in the blood are a sign of bacterial infection. [159-161] For instance, CRP values in patients with an influenza-like illness varied between 12.97 and 32.41 mg/L for viral infections and exceeded 99.38 mg/L for bacterial infections, while in healthy individuals levels are considered to be less than 0.5 mg/L. [162] Diagnostically relevant levels of serum PCT begin from 0.1 ng/mL. [163]

SERS studies investigating the detection of those two proteins mainly utilized a label-based approach. For instance, Liu *et al.* proposed an ultrasensitive biosensor, in a sandwich immunoassay format, consisting of Au@Ag core−shell SERS nanotags as labels and photonic crystal beads as carriers. This biosensor was successfully used for CRP detection in real serum samples with achieved LOD of 70.2 pg/mL, which is many orders below the clinically relevant range. [164] As multiplex detection of few biomarkers can provide better diagnostic information, Nguyen *et al.* developed a mesoporous SERS substrate based on display of cysteine-rich peptide on M13 phages for the triplex detection of CRP, PCT and soluble triggering receptor expressed on myeloid cells-1 (sTREM-1). Substrates were functionalized with magnetic immune colloids gold-coated magnetic nanoparticles and specific antibodies to capture the biomarkers in the spiked serum samples. This method allowed detection till 27 pM (0.675 ng/mL), 103 pM (1.493 ng/mL), and 78 pM (2.34 ng/mL) for CRP, PCT and sTREM-1, respectively. [165]

The methods mentioned above have many advantages, such as ultralow LODs and versatility. However, their simplicity of use is limited by several drawbacks, including the necessity to synthesize two sets of nanoparticles with limited stability, usually complicated experimental design, high risk of nonspecific interactions between particles and non-targeted compounds attracted from a matrix, and an inability to monitor the direct bonding of target to a specific antibody. Therefore, the movement in the direction of label-free SERS approach should be considered. Kim *et al.* proposed performing label-free detection of CRP via monitoring of CRP-specific ligand-protein interactions using SERS chip with concentration-induced Ag nanoparticle aggregates. Here, the vibrational C-H stretching at 2930 cm^{-1} was an indicator of the interaction. More intense signal corresponded to higher concentration of CRP with minimum detection amount of 0.01 ng/mL in buffer and 0.1 ng/mL in 1 % serum. [166]

Van de Veeronk and colleagues, investigating serum samples from patients with Epstein-Bar virus, found that, for them, Interleukin (IL)-18 concentration was much higher than for healthy individuals (1018 pg/mL vs 200 pg/mL). Therefore, authors concluded that serum IL-18 may function as a marker of viral infection, similar to CRP and PCT for bacterial ones. [167] A few years later, Kaminska *et al.* demonstrated that a SERS-based immunoassay combined with a microfluidic device can simultaneously detect interleukins: IL-6, IL-8, IL-18 levels in blood plasma. For this, Au

NPs coated with different Raman reporter molecules and specific antibodies served as SERS tags, while Ag-Au bimetallic substrates functionalized with specific antigens performed the function of capturing substrates. Later, PCA was applied for segregation of the signal from three complexes and quantification of the interleukins in blood plasma. The reported method allowed for the achievement of LODs of 3.8 pg/mL, 7.5 pg/mL, and 5.2 pg/mL for IL-6, IL-8, and IL-18, respectively, which are lower than results using standard ELISA methods. [168]

Considering fungal infections, the sputum galactomannan is accepted as a biomarker for the invasive aspergillosis. [169] However, no SERS studies of this *Aspergillus* antigen could be found.

As mentioned before, the detection of biomarkers in the body-fluids can be helpful not only to determine the type of the infection in the organism but also to provide some information about the infectious agent. Therefore, extensive efforts of researchers are directed to identify biomarkers specific for certain pathogen. However, the number of SERS studies in this field is limited. One of a bit more with SERS investigated biomarkers is dipicolinic acid (DPA), which is attributed to the bacterial *Bacillus* spores. Yao *et al.* measured a different number of *B. subtilis* cells using 3D plasmonic trap array with the flower-like Ag microstructures and could see the Raman signature of secreted DPA, even when studying only one cell. [170] Another study reported the detection of DPA down to 5 ppb (29.9 nM) in aqueous solution using conventional Ag colloids. Moreover, applying multivariate data analysis allowed for the detection of DPA in complex extracts from viable spores. [171]

Another bacterial biomarker found in the literature is pyocyanin (PYO). PYO is a specific metabolite released by gram-negative bacteria *P. aeruginosa*, which is associated with persistent and chronic RTIs in patients with CF or weakend immune system. [172, 173] For CF patients, PYO concentration in the sputum samples varies between 7.7 µM and 76 µM. [174, 175] Although a few SERS studies on PYO are published, direct detection of PYO in sputum was still not reported. The study of Wu and collaborators considered clinical sputum samples, but direct detection was not possible due to high background signal from sputum matrix. Therefore, authors first extracted PYO by chloroform and then successfully measured it by employing silver nanorod arrays. [176] SERS detection of PYO was also performed in a medium from a bacterial culture, using surfaces with controlled nanometer gap spacing between plasmonic Au nanospheres. [177] For better quantification of PYO in this more complex matrix, machine-learning algorithms were applied and concentrations down to 1 ng/mL were detected. Moreover, it was concluded that SERS detection of PYO, besides potential diagnostic application, can also be used for the imaging of quorum sensing in *P. aeruginosa* biofilm communities. [178, 177]

To conclude, despite some progress in the field of infectious biomarkers, most of them are still not validated and only a limited number were successfully investigated with SERS. Label-based

SERS appeared to be a more explored and promising approach, as it allows overcoming problems connected with the complex composition of body-fluids. However, it has a complicated design with possible instability issues and risk of nonspecific interaction. Therefore, further improvements should be done in SERS-tags development. Moreover, studies often report very low LODs willing to demonstrate the power of their approach but forgetting to consider its clinically relevant range. Ultra-sensitivity is not always needed and simplicity of the test along with lower costs is more important. Thus, the applicability of label-free SERS in the biomarker detection should still be explored.

4 OWN RESEARCH RESULTS

As described in the previous section, RST have already been broadly investigated for various clinical applications. However, while a plethora of information can be found about application of RST for oncological diseases, infections (especially the ones of respiratoty tract) have thus far attracted significantly less attention. Moreover, often in the studies, in pursuit of high accuracies or low detection limits, some other important factors, such as simplicity or cost-effectiveness, were put aside. Therefore, in this thesis, the main focus was set for developing RST-based sensitive, reliable, but simultaneously simple and inexpensive solutions for better management of RTIs.

In the following section, the research results achieved within the framework of this thesis will be presented and discussed. A schematic overview of the included studies is presented in **Figure 2**. Firstly, UV-RRS technique will be suggested as a tool for improving prevention methods for RTIs by demonstrating the analysis and identification of fungal spores [OZ1]. Afterwards, urine-based screening of respiratory tract and other diseases using conventional RS will be presented [OZ2]. In the final part, indirect identification of the infectious agent by detecting bacterial metabolite in complex body fluids will be described [OZ3-OZ4].

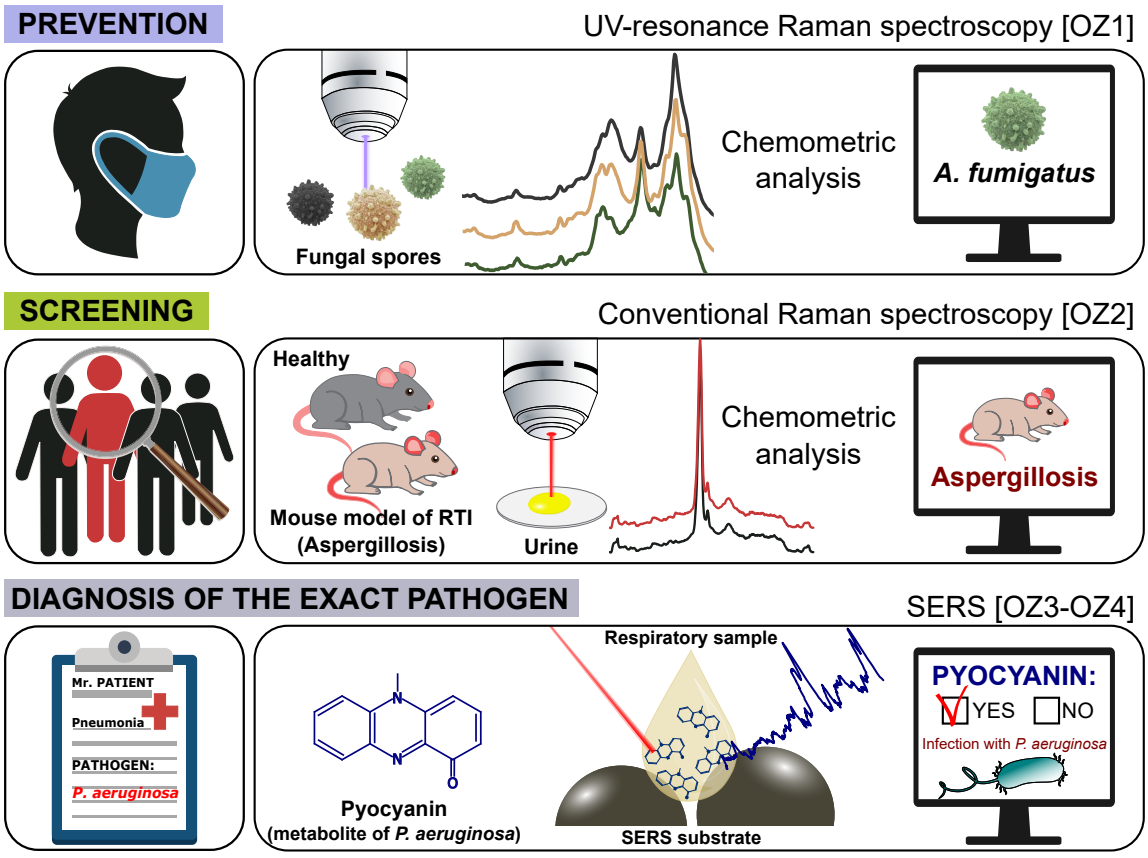

Figure 2. Schematic overview of the studies presented in the thesis.

4.1 UV Raman spectroscopy for identification of highly pigmented fungal spores in the air [OZ1]

Fungal spores were found to be one of the most common classes of airborne biological aerosols. [179, 180] Accordingly, humans inhale substantial numbers of fungal spores from outdoor and indoor air. Health risks of such fungal exposure strongly depend on the inhaled species, as different fungi produce different allergens and mycotoxins. [181, 182] Another important factor is sensitivity of the person. For instance, asthmatic individuals and people with CF are most commonly sensitive to *Aspergillus* species, which could lead to their symptoms worsening or developing of ABPA. [183, 184] Thus, avoidance of the aspiration of dangerous species is an important component of preventing infection. In order to do so, individuals need to be aware of the composition of fungal spores in the air. In the previous section mentioned limitations of currently used identification methods (culturing together with microscopical analysis, PCR, immunoassay) arise the need for the development of alternative techniques. The potential of RST for identification of microorganisms was already presented in the section 3.1 of this thesis and the need for careful choice of the technique was underlined.

Within the publication [OZ1] spores from eight different filamentous fungal species, implicated to a varied extent in respiratory diseases worldwide: *Aspergillus fumigatus*, *Aspergillus niger*, *Aspergillus nidulans*, *Aspergillus calidoustus*, *Cladosporium herbarum*, *Alternaria alternata*, *Penicillium rubens*, and *Lichtheimia corymbifera* were investigated. For this, fungi were grown for 7 days at room temperature; next, the spores were collected and inactivated with formaldehyde. Fungal spores of all the investigated species were highly pigmented, having dark brown, grey or green color, which makes achieving a high quality Raman spectra challenging. It has been previously reported that using visible excitation wavelengths for RS measurements of pigmented samples leads to high fluorescence background, which can partially or totally overwhelm the Raman signal. [185, 81] Therefore, for the spectroscopic examination the excitation wavelength in the UV region, namely 244 nm, was chosen, since at this wavelength fluorescence and Raman scattering are spectrally well separated. [186] Moreover, most taxonomic markers of microorganisms absorb in the UV region, leading to selective resonant enhancement of the Raman signals of taxonomically-important macromolecules (e.g. DNA/RNA bases and aromatic amino acids, which can be beneficial for the identification). [187-189] Unfortunately, these advantages of the UV-RRS come along with the risk of sample photodegradation due to the high photon energy of the UV radiation. To minimize the ‘burning effect’, samples were continuously rotated during the measurements with a speed 60 rotations/min and moved in the *x*, *y* direction after each rotation. This also allowed obtaining an average spectrum over a large amount of spores, which means that one spectrum already comprises metabolic and developmental diversity within the spore population.

To evaluate whether UV-RRS was a good method of choice for obtaining high quality spectra from deeply colored and highly absorbing samples, firstly, *A. fumigatus* spores were compared to non-pigmented spores of a same strain with a mutation in the *pksP* gene. [190] Mean Raman spectra of both samples is demonstrated in **Figure 3 (a)**. It can be seen that, despite the rotation of the samples, both experienced 'burning effect', which manifests itself by two broad carbon bands around 1360 and 1610 cm^{-1} [191]. However, spore-related spectral features, necessary for the spore identification process, are still clearly distinguishable for both samples. The primary bands observed in fingerprint region in the UV-RRS are typically associated with different nucleic acids and protein subunits. More specifically, the signal at 1648 cm^{-1} can be assigned to thymine, and the one at 1612 cm^{-1} to the aromatic amino acids tyrosine and tryptophan. Guanine and adenine exhibit peaks at 1574 and 1479 cm^{-1}, and together with tyrosine contribute to the signal at 1335 cm^{-1}. The Raman mode at 1526 cm^{-1} originates from cytosine. Thymine and adenine have a band at 1365 cm^{-1}. The peak at 1171 cm^{-1} can be assigned to tyrosine and the ones at 758 and 1008 cm^{-1} come from tryptophan. [187, 84, 192] Although the mentioned bands are more prominent for non-pigmented strain, it still can be concluded that UV-RRS can be used for investigating highly pigmented spores as well.

As a next step, Raman spectra from all fungal spores were obtained and their mean spectra are plotted in **Figure 3 (b)**. The differences between the spectra can be noticed by the naked eye. Additionally, to different carbonization background, relative intensity of the main bands varies among the fungal species. This provides insight into the different compositions of the DNA/RNA and protein subunits. During the study, three different batches of each strain were measured and the standard deviation (SD), illustrated as grey shade around each spectrum, displays the good reproducibility of the method. The higher deviation appeared for the *A. fumigatus* species but only because three different strains of it were included in this study. Moreover, for the growth of *A. fumigatus* and *P. rubens*, two different culturing media were used. Although, after collecting, fungal spores were washed several times, the influence of different growing conditions was observable when comparing spectra of the same species grown on different media (for the details see **Figure S-2 in Supporting Information (SI) for [OZ1]**). Despite this, it was decided to include all strains grown on different agars for building classification models in order to check if the differences from cultivation conditions are smaller than the differences due to species affiliation.

Keeping clinical needs in mind, three different models were established. As health hazards strongly vary between different genera, first of all, the statistical model was built to differentiate between species of *Penicilium*, *Cladosporium*, *Aspergillus*, *Alternaria* and *Lichtemnia.* To achieve this, firstly, PCA was performed to reduce the dimensionality of the Raman data and keep only the most significant information for classification. Generally, the choice of the number of principal components (PCs) is crucial, because, selecting too low risks missing some important information,

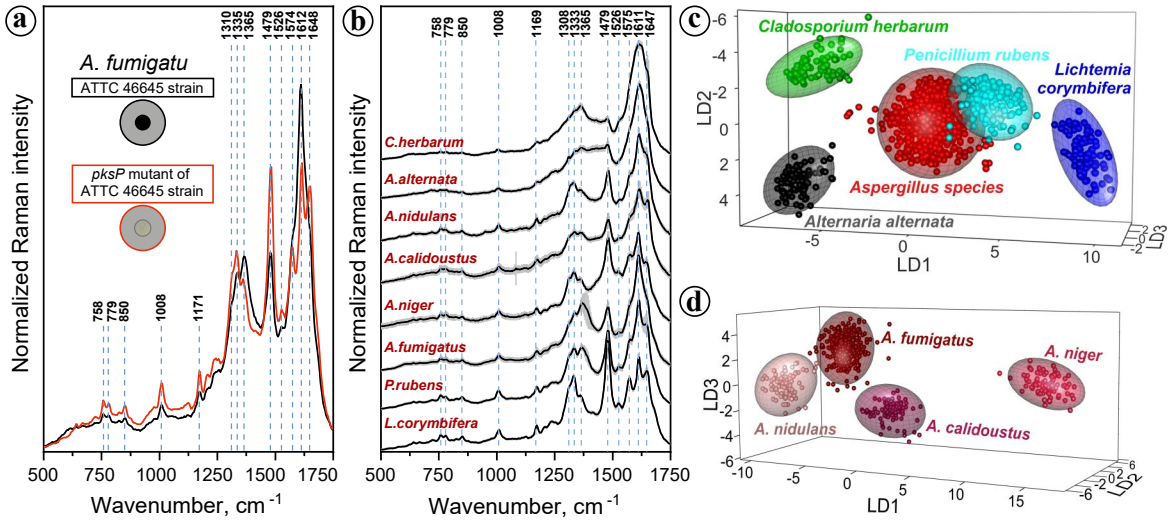

Figure 3. **(a)** Mean UV-Raman spectra of the pigmented *A. fumigatus* ATCC 46645 strain and the non-pigmented pksP mutant strain. **(b)** Mean UV-Raman spectra of the all batches from different fungal spores plotted together with their SD (grey area). For the *A. fumigatus* the mean spectrum represents all investigated strains. **(c)** LDA score plots for the classification model on the genus level. **(d)** LDA score plots for the classification model on the species level. Adapted from [OZ1].

while taking too high number can result in overfitting of the model. Unfortunately, there is no common algorithm to determine the optimal number of the PCs, and different approaches can be found in the literature. [193, 194] In the presented study, the optimal number of PCs was chosen by finding a saturation point of the accuracy as a function of the number of PCs (for the details see **Figures S-3, S-4, S-6 in SI for [OZ1]**). For the classification on a genus level, 6 PCs were selected as optimal input for the following LDA. The performance of the created LDA model was estimated with LBOCV. During this process, each batch was used once as the secondary dataset and predicted by the model built with the remaining two batches. Achieved results showed not only high accuracy of 97.50 % in classification, but also reflected the phylogenetic relationship between the different genera. From the LDA score plot of the classification model, which is depicted in **Figure 3 (c)**, it can be seen that *A. alternata* and *C. herbarium* belonging to the same class of Dothideomycetes were nicely separated from *Penicillium* and *Aspergillus* spores - affiliated to the class of Eurotiomycetes, and from *L. corymbifera* spores belonging to a lower group of fungi, the phylum Zygomycota. The most often misclassification occurred for the *Aspergillus* species. Here, 22 spectra out of 629 were assigned to *P. rubens*. The reason for it could be their taxonomic relation within the same class or the fact that spores grown on different media were included in both groups, which led to more variations. However, despite these mistakes the sensitivity for identifying of *Aspergillus* spores was still high (95.87 %). This is very promising, because *Aspergillus* fungi are often of special danger for immunocompromised patients and people with chronic respiratory diseases. [183, 184, 195, 196] But it should be noted that, out of hundreds of

Aspergillus species, only tens of them are known to cause infections. Therefore, to assess the health risks from fungal exposure, in addition to genus level, the identification on a species level should be performed.

In this study, four different *Aspergillus* species with different levels of danger were considered. Among them, *A. fumigatus* is the most common fungal pathogen, followed by *A. niger*. [197] *A. calidoustus* and *A. nidulans* are also classified as opportunistic pathogens, but cause infections relatively rarely. [198] To perform discrimination between these four species a LDA model with 7 PCs was created. Validation of this model with LBOCV resulted in the correct assignment of all spectra, which means 100 % accuracy. **Figure 3 (d)** demonstrates LDA score plot of the classification model. To the best of my knowledge, identification of fungal spores on a species level with RS was demonstrated before only once, where *Aspergillus lentulus* was differentiated from *A. fumigatus* with 78 % accuracy. [81] Our achieved accuracy is noticeably higher, suggesting that information provided by UV-RRS about DNA/RNA bases and aromatic amino acids may be beneficial for the classification of microorganisms.

To investigate the power of the technique more precisely, fungal spore identification at the strain level was also performed. For this purpose, three strains of *A. fumigatus* were considered. To know the exact strain of this fungus is useful, as the difference in virulence among strains was also reported. [199] The visual differentiation between the spectra from three strains was already not possible (see **Figure 5 [OZ1]**), due to their close phylogenetic relationship. For building the LDA model, the number of PCs was set to 10. The classification resulted in an overall accuracy of 89.42 % and 321 spectra out of 359 were assigned to correct strain. RS-based identification of the fungal spores at a strain level was not found in the literature before.

To conclude, in the focus of this study, it was shown that UV-RRS is a suitable method for the analysis of the highly pigmented fungal spores. Combining this technique with chemometrical methods, the highly accurate identification of the spores on genus (97.50 %), species (100 %) and strain levels (89.42 %) was achieved. Such results indicate undeniable potential of the UV-RRS for microorganism identification, however, it should be noted that the usage of the technique is limited to the biomass of the samples. At this point in time, measurements of few spores with the used Raman setup are challenging, because the device is not combined with microscope and finding the small spores on the slide would not be possible, nor would avoiding photodamage by the sample rotation. Therefore, currently, UV-RRS will not exclude the culturing step, but will provide an alternative for the conventional methods of fungal spore identification based on microscopic observation and morphological characterization of reference spores. Implementing UV-RRS in clinical routine would exclude human factor from the identification and make process more automated and objective.

4.2 Raman spectroscopy of urine for screening of respiratory tract diseases [OZ2]

The diagnosis of RTIs in patients with another underlying illness is challenging, as usual symptoms of RTIs, like fever or cough, can overlap with symptoms of the main disease or can be simply absent. Thus, the diagnosis of the infection often happens after it reaches a more acute stage. Such diagnostic delay complicates the treatment and causes higher mortality rates. Therefore, an effort should be devoted to the exploration of new screening technologies that can detect early signs of RTI, preferably in an easy and non-invasive manner. In this context, analysis of body fluids is particularly attractive because, along with a relatively easy collection procedure, they are rich in biochemical information of certain diagnostic value.

Among different body-fluids, the attention in the publication [OZ2] was directed towards urine samples due to the simple and completely non-invasive collection in people of all ages, possibility of multiple sampling, and low cells and protein content with a high number of metabolites [200]. Aiming to develop an easy and cheap screening test, urine analysis was performed with conventional RS. The main goal of the study was to evaluate whether RS of urine can provide enough information for the diagnosis of respiratory tract diseases and to compare its diagnostic ability with the one for kidney diseases. Respiratory tract diseases included aspergillosis infection and asthma. Asthma is a chronic inflammatory disorder, while aspergillosis is a fungal RTI associated with increased danger for immunocompromised patients and possible lethal outcomes, especially for late diagnosis cases [201, 202]. Although these diseases do not directly influence urine formation, some changes in the metabolic profile of urine are still expected as a response of the organism to the infection or external trigger. [203-205] On the other hand, to have more comprehensive study, diseases known to be in direct connection with urine generation were also included. This involved nephrogenic diabetes insipidus (NDI), characterized by inability to concentrate the urine and distal renal tubular acidosis (dRTA) which leads to more acidic urine. [206, 207]

To have more defined parameters and better comparison, it was decided to investigate mice models of all mentioned diseases before starting with a clinical study with the patients. After collection, urine samples were frozen and stored at -80 °C untill Raman measurements. To decrease the fluorescence contribution in the Raman spectrum, it was decided to use an excitation wavelength of 785 nm and to measure the samples as dried droplets. Schematic representation of the measurement workflow is depicted in **Figure 4 (a)**. Here, mapping of three different areas was performed, aiming to include the intrinsic heterogeneity of the sample and collect a big amount of data for each mouse. **Figure 4 (b)** demonstrates mean spectra for the different groups included in different disease models together with their SD (presented as a shaded area). It can be seen that, for all groups, Raman spectrum has the same shape with the most intensive peak at 1004 cm^{-1}. This band together with the smaller ones at 589, 1162, 1605 cm^{-1} can be assigned to urea, which is the most prominent component of the urine. The peaks at 839 and 1046 cm^{-1} are originating from cre-

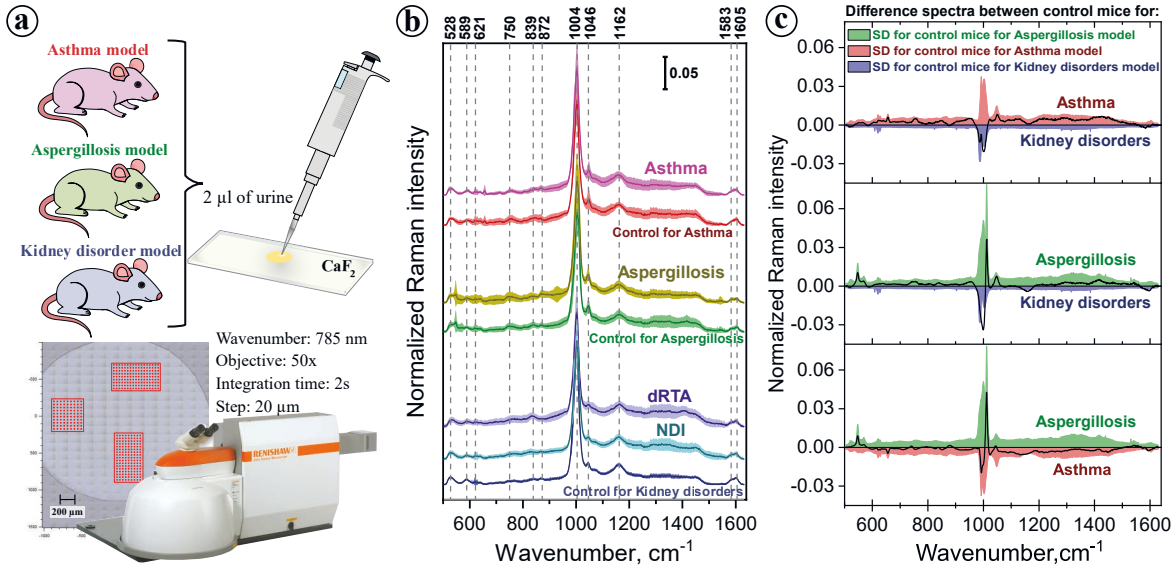

Figure 4. **(a)** Schematic illustration of the workflow of the Raman measurements. **(b)** Mean Raman spectra of the urine samples obtained from different groups in all included models, plotted together with the SD (shaded area); **(c)** Difference spectra between the mean urine spectra of control mice for different disease models with SD of the groups. Adapted from [OZ2].

atinine, while the Raman bands at 872 and 1076 cm^{-1} may be attributed to nitrogenous compounds. [208, 209] SDs for the mean spectra indicate that there is the intra- and inter-sample heterogeneity inside the groups. The lowest calculated SD was for the healthy mice, which were considered as a control for the kidney diseases. The control mice for asthma, to be a proper control, underwent a treatment with PBS, while control mice for the aspergillosis model were immunosuppressed with cortisone acetate. Moreover, in all models different type of mice were used. Therefore, the first step in the study [OZ2] was to clarify how different control mice of the included models are and whether all models can be analyzed together. For this, difference spectra between control groups were calculated and depicted in **Figure 4 (c)** together with SD for each group. Clear differences can be observed between all of the control mice, being higher than SDs of appropriate groups. This means that control mice are already so different that it is incorrect to combine all of the diseases in one model, as doing so can lead to the classification based not on the disease but on other factors. Thus, different disease models should be considered individually.

Firstly, the potential of urine-based RS was examined for kidney diseases. Since kidneys are the organs responsible for urine generation, it is expected that urine composition correlates with their health and RS has a high chance to monitor it. To prove this hypothesis, Raman spectra from urine samples from four mice with NDI, ten mice with dRTA and four healthy mice were obtained (**Figure 4 (b)**). To highlight the differences between these groups, the difference spectra were calculated and presented in **Figure 5 (a)**. One can see that urine from the mice with kidney diseases had lower intensities of the band around 1004 cm^{-1}, which can be correlated with the decreased

concentrations of urea. It is known that NDI is characterized by a genetic loss of urea transporters or inability of nephrons to respond to adequate concentrations of vasopressin, which reduces the interstitial concentration of urea and the concentrating ability of urine. [210] However, in the case of dRTA, decrease in the urea concentration is unclear. Comparing urine spectra from both diseases, NDI urine had higher intensities of peaks at 991 and 1013 cm^{-1}, which tentatively can be assigned to higher uric acid concentrations, while dRTA had more prominent Raman bands at 837 and 1407 cm^{-1}. The last peaks could originate from protein compounds, as it was also found that urine from dRTA mice contains more proteins, especially albumin. [211]

To support visual comparison, advanced multivariate data analysis was applied and discrimination between the diseases was performed. Like in the previous section, for this classification PCA-LDA was applied and the number of PCs was chosen by the same principal of finding the maximal accuracy as a function of the number of PCs (for the details see **Figures S1-S5 in SI for [OZ2]**). Evaluation of the model was performed with leave-mouse-out cross-validation (LMOCV). For this, spectral data of one mouse was removed from the data set and the LDA model was built with the remaining data. This procedure was repeated for all of the mice and provided a reliable, unbiased classification model. Using 6 PCs, 50387 spectra out of 52567 were assigned correctly and the overall accuracy of 95.85 % on spectral level was achieved. However, for the clinical needs, classification on a patient level is required. Therefore, the percentage of correctly identified spectra for every mouse should be calculated and compared with the set threshold. In the present study, a threshold of 50 % was applied, which means that a mouse was diagnosed as healthy or sick if more than half of her spectra were assigned to that group. In this manner obtained classification results on mouse level are presented in **Figure 5 (b)**. It can be seen that all of the mice were correctly classified. This not only confirms the starting hypothesis that urine-based RS is very informative for detecting disorder in kidney function but also shows that presented approach has a high potential for the identification of the exact disease.

After successful diagnosis of diseases directly influencing urine composition, respiratory tract diseases, which are not connected with urine production, were investigated. Here, the main goal was to evaluate the potential of Raman spectroscopic profiling of urine for the detection of respiratory tract infection, namely, aspergillosis. For this, 14 mice were immunosuppressed and 10 of them were exposed to *A. fumigatus* conidia, while four were kept as a control. Mean Raman spectra for both groups are presented in **Figure 4 (b)**, while difference spectrum between the groups is shown in **Figure 5 (c)**. Differences here are already not as obvious as for the kidney diseases. Moreover, spectral variability inside the groups is much higher than between them. Thus, there is an extreme need to apply chemometrics. To build the classification model, 11 PCs were used. Achieved results on mouse level are summarized in **Figure 5 (d)**. Two healthy mice were misclassified as sick and one sick mouse was assigned as healthy, that resulted in the model sensitivity of

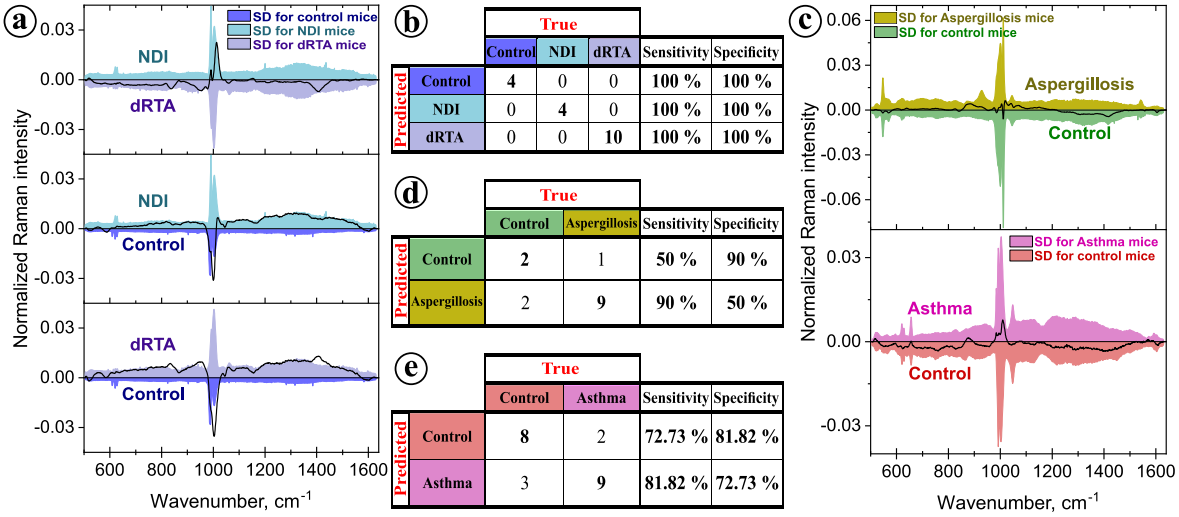

Figure 5. **(a)** Difference spectra between the mean urine spectra of mice with kidney disorders and control ones with SD of the groups. **(b)** Results of the mouse level classification model for kidney disorders evaluated with LMOCV. **(c)** Difference spectrum between the mean urine spectra of mice with aspergillosis and control ones, plotted together with SD of both groups. **(d)** Results of the mouse level classification model for aspergillosis infection evaluated with LMOCV. **(e)** Difference spectrum between the mean urine spectra of mice with asthma and control ones plotted together with SD of the both groups. **(f)** Results of the spectral level classification model for Aspergillosis infection evaluated with LMOCV. Adapted from [OZ2].

50 % and specificity of 90 %. In general, for the screening tests specificity is of higher priority, as false negative results can cost human life. Nevertheless, sensitivity should also be high to avoid expenses on further, in fact unnecessary, diagnostic tests and minimize stress for the individuals. To investigate appeared misclassification more precisely, the clinical data of the false negative mouse was checked in more details. It appeared that this mouse, together with one other, did not show any signs of the infection, which was proved by a pathological check of their lungs. However, the second mouse was still assigned to aspergillosis group. Furthermore, one extra mouse in the infected group developed only mild aspergillosis. All these facts may lead to the assumption that false positive results of the model appeared due to an incorrectly defined sick group. To check this, the aforementioned mice were excluded and the classification was repeated using the four control mice and seven mice with developed severe aspergillosis. To build the LDA model, 7 PCs were selected. Subsequent LMOCV resulted in 100 % accuracy on the mouse level. Such a result suggests that urine based RS holds the promise to be used as a diagnostic tool for the RTIs, however, train data set should be defined with special care.

Finally, the asthma model was considered. Here, asthma was chosen to check if urine reflects only the response of the organism to acute RTI or if inflammation of the airways also results in a change of metabolic and, consequently, in spectroscopic profile of urine. This model included 11 control and 11 mice with Ovalbumin-induced allergic asthma. For the second group, urine was collected 1, 5 and 9 days after exposure to the allergen. Mean spectra for the both groups can be

seen in **Figure 4 (b)** and the difference spectrum in **Figure 5 (e)**. Variations in the both groups were higher than the difference between them, thus, for the discrimination, the application of PCA-LDA model was required. As an input for LDA, 7 PCs were selected. The results of the classification on a mouse level are summarized in **Figure 5 (f)**. Misclassification occurred for three control and two asthmatic mice. This resulted in an overall accuracy of 77.27 %. The false negative results appeared for the urine samples collected on the fifth and ninth days after exposure to the Ovalbumin aerosol. Theoretically, it could be that the organism of these mice, after few first days, started to recover from the allergenic reaction. However, no clinical data was provided to check this hypothesis.

The present study reveals that RS generally has a great potential to monitor the changes appearing in urine due to pathological conditions. However, the performance of the method is diverse and depends significantly on the level of disease caused alterations in the urine samples. As kidney diseases directly influence the composition of the urine, the changes in urine are more obvious and RS, combined with PCA-LDA, can with 100 % accuracy discriminate not only between healthy and sick mice, but also between different kidney diseases. In the case of aspergillosis infection and asthma, the changes in urine reflect the overall organism response to the established infection or external trigger, thus variations are relatively small and their detection with RS becomes more challenging. Nevertheless, promising results for diagnosing these diseases were achieved. Asthmatic mice were discriminated from the control group with 77.27 % accuracy, while mice infected with *A. fumigatus* could be differentiated from the control ones with 78.57 % accuracy. Moreover, considering only mice with severe aspergillosis, accuracy is increasing untill 100 %. Such results show that urine based RS holds some promises for detection of the diseases not directly influencing urine composition and it could be useful for the screening of the RTIs. Ideally, spectroscopic analysis of urine could be performed periodically for susceptible individuals to monitor any deviations from 'normality'. However, to come to this point, firstly, more detailed clinical studies including much larger data sets should be performed. Moreover, to understand the molecular mechanism of altered spectral signature and to find the biochemical reasons, systemic studies combining RS with mass spectrometry or nuclear magnetic resonance spectrometry are required.

4.3 Fast and sensitive SERS detection of bacterial biomarker directly in complex matrices [OZ3-OZ4]

In the current clinical practice, treatment of the patients diagnosed with RTIs is initiated rather empirically without an accurate diagnosis of the infectious agent. This leads to the overuse of antibiotics, higher medical costs, prolonged hospital stays and increased mortality. The development of rapid, accurate and specific point-of care diagnostic tests able to screen for major pathogen groups, to enable identification of the causative organisms, and to define their antibiotic resistance profiles

would significantly improve the situation. [212] Within this scope, direct detection of the biomarkers, specific for the pathogen or reflecting the response of the host, may be a good approach. Thus, in the studies [OZ3] and [OZ4], the SERS detection of the bacterial biomarker pyocyanin directly in body-fluids was investigated.

PYO is a specific metabolite of *P. aeruginosa*, which is a Gram-negative, opportunistic pathogen causing acute and chronic infections, particularly in patients with CF or compromised host defense. [172, 173] The chemical structure of the PYO molecule is depicted in **Figure 6 (a)**. Previous studies reported that concentration of PYO in the sputum samples can vary between 7.7 µM and 76 µM for CF patients and can reach up to 130 µM for patients with bronchiectasis. [174, 175] There is no universal 'best' SERS platform, so the careful consideration of the analytical problem is required before choosing or designing a SERS sensor. [213]

One of the objectives of the thesis was to assess the capabilities and limitations of the SERS technique using conventional and easy-to-prepare SERS active surfaces. Therefore, in the study [OZ3], the preference was given to Ag colloids prepared by the easy and fast protocol of Leopold and Lendl. [214] Moreover, colloidal solution allows direct SERS analysis within the analyte natural solution medium. Before moving to the detection of PYO in complex matrices, the nature of the SERS spectrum of the molecule was investigated in 10 % ethanol solution due to its low solubility in purified water. All measurements were performed using 514 nm excitation wavelength, as it matches with the absorption region of Ag colloids (see **Figure S1 in SI for [OZ3]**). To achieve automated measurements and to obtain reproducible SERS spectra of different PYO concentrations, the droplet-based microfluidic setup presented in **Figure 6 (b)** was employed. A more detailed discussion about the combination of SERS with microfluidics and an overview of the recent developments and advancements in this field can be found in the review paper [OZ5-Review] prepared in the frame of this thesis. During the presented study, to create a segmented continuous flow, mineral oil was pumped to one of the inlets with a flow rate of 9 nl/s, while Ag colloids and analyte solution were pumped to other inlets with a flow rate of 7 nl/s. No aggregation agent was required, because PYO exhibit the ability to induce the aggregation by itself (see **Figure S3 in SI for [OZ3]**). In this manner, PYO concentrations between 0.5 µM and 85 µM were measured. The mean Raman spectra for every concentration, as well as for the blank water-ethanol solution are presented in **Figure 6 (c)**. It can be seen that the SERS spectra of PYO had a rich fingerprint in the 200-1800 cm^{-1} spectral range with the most prominent bands at 547, 676, 1353, 1564 and 1594 cm^{-1}. According to the literature, the peak at 547 cm^{-1} originates from ring-breathing and C-N torsion, the Raman mode at 676 cm^{-1} corresponds to the ring-deformation, the band at 1353 cm^{-1} is assigned to the combined C-C stretching, C-N stretching and C-H in-plane bending modes of the aromatic ring and, finally, the double peak at 1564 and 1594 cm^{-1} is ascribed to the ring deformation and the C-C stretch vibration. [178, 176]

Measuring PYO concentrations untill 10 µM ethanol Raman bands at 880, 1047 and 1087 cm^{-1} can be detected. With the further increase of PYO concentration, they became less prominent and more convoluted with PYO bands. Additionally, the Raman peaks at 221 and 240 cm^{-1} could be observed and assigned to the Ag-N and Ag-O stretching vibrations, respectively. [215] This confirms the hypothesis that interaction with the silver surface is achieved via the oxygen and nitrogen atoms of the PYO molecule. With the increase of PYO concentration, the Ag-O band becomes dominant, which suggests that, due to the steric hindering, PYO might adopt an upright orientation and interact with the metallic surface only via the O atom.

To assess the LOD and capability of SERS for quantitative analysis, the integrated peak area of the Raman bands at 240 and 667 cm^{-1} were plotted as a function of the in-droplet concentration (see **Figure 3 in [OZ3]**). The concentration curves for both peaks present an exponential increase until the concentration of 55 µM. However, the underlying mechanism is different. The Raman mode at 240 cm^{-1} is due to the PYO molecules in the first layer on the surface of the metallic nanoparticles, whereas the intensity of the 676 cm^{-1} band also increases due to the molecules present in the upper layers, but still located in the 'hot-spots'. As a result, the Raman band ascribed to the Ag-O vibration was implemented as internal standard and its use resulted in a linear response over the

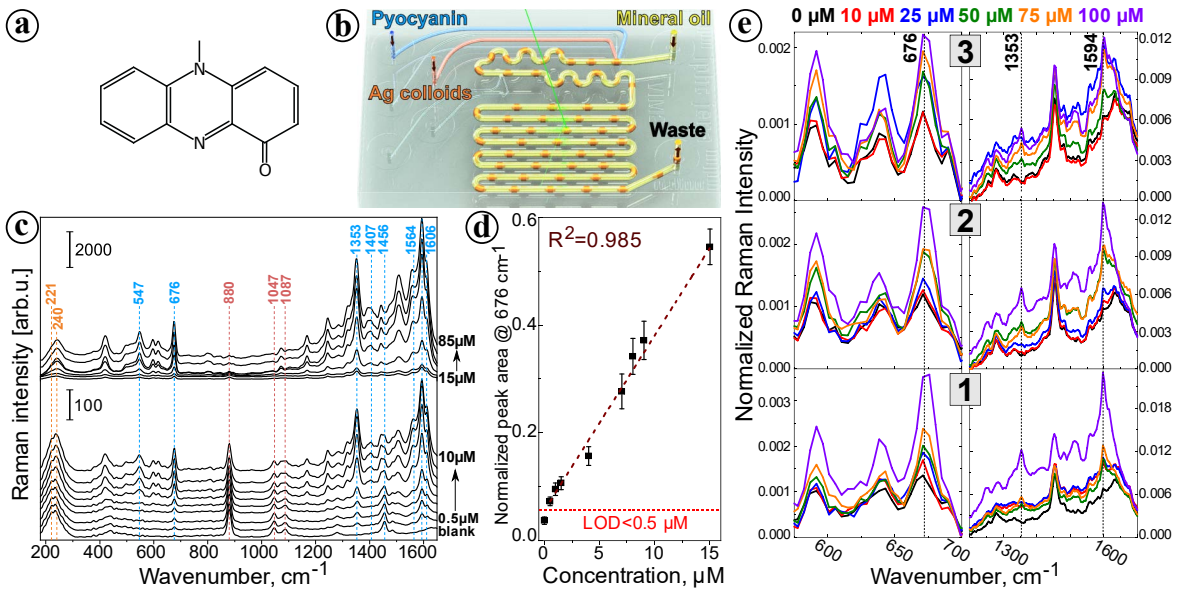

Figure 6. **(a)** Chemical structure of the PYO molecule ($C_{13}H_{10}N_2O$). **(b)** Scheme of the droplet based microfluidic chip used for LoC-SERS measurements. **(c)** Mean SERS spectra of PYO with concentrations between 0.5 and 85 µM in aqueous solution measured in the microfluidic platform. The mean spectrum of the blank (when only water-ethanol solution is pumped through at the first dosing unit) is also presented. **(d)** The peak area ratio of the 676 cm^{-1} and 240 cm^{-1} Raman modes as a function of PYO concentration in aqueous solution in the range between 0.5 and 15 µM with linear fitting. The red line indicates the calculated LOD. **(e)** Zoomed regions of mean SERS spectra of the different concentrations of PYO in the saliva samples from three volunteers. Adapted from [OZ3].

0.5-15 μM concentration range, which is demonstrated in **Figure 6 (d)**. The calculated LOD was below the lowest measured concentration of 0.5 μM, which is ~10 times lower than minimal concentration found in clinical sputum samples (7.7 μM). Measurements were repeated with another microfluidic chip and demonstrated a good reproducibility of the method (see **Figure S6-S7 in the SI for [OZ3]**).

However, the SERS detection in more complex matrixes is much more challenging due to the competition between matrix components and the target analyte for metallic sides of the SERS active surface. This is especially important if the SERS surfaces are not functionalized to capture one specific molecule, which was the case for the studies dicussed within this thesis. As a first step towards increasing the complexity of the matrix and switching to real world respiratory samples, saliva was chosen. Despite the fact that saliva is composed mainly of water, it contains a variety of electrolytes and enzymes, immunoglobulins and other antimicrobial factors, expectorated bronchial and nasal secretions, microorganisms and their products. [216] In the [OZ3] study, for the proof of concept, saliva from three healthy volunteers was spiked with the appropriate amount of PYO in ethanol solution to achieve the final concentrations of 10, 25, 50, 75 and 100 μM. As a negative control, saliva samples were spiked only with ethanol. Next, filtration was performed to remove the oral epithelial cells and food debris. SERS spectra were recorded in plastic cuvettes with the addition of silver colloids and KCl for the aggregation of nanoparticles. Here, the addition of the aggregation agent was beneficial, because saliva components reduced PYO ability to aggregate the Ag colloids.

SERS spectrum of pure saliva in the fingerprint area contained many small, convoluted peaks, which are difficult to interpret due to the unknown exact composition of the samples (see **Figure S8 in SI for [OZ3]**). By adding PYO to the matrix, new bands at 676, 1353 and 1594 cm^{-1} (which were previously assigned to PYO molecule) appeared. The zoomed spectral regions for every volunteer are shown in **Figure 6 (e)**. For the first and second volunteer, spectral changes were already seen at the lowest investigated PYO concentration of 10 μM, while for the third volunteer changes noticeable by eye appeared at a concentration of 25 μM. Compared to the aqueous solution, the sensitivity of the method decreased by two orders of magnitude. Despite the fact that it remained on the border of the clinically relevant range, it was clear that for a more complex and viscous matrix like sputum, the described method would not be sensitive enough and other strategies should be considered. Functionalization of Ag colloids with capture molecule specific for PYO might be a possible option. However, design of the capture scheme as well as modification of the nanoparticles surface is a complicated task and the focus of this thesis was set on researching a fast and easy detection scheme.

Therefore, in the [OZ4] study, development of the planar substrates for SERS detection of PYO in more complex respiratory samples was performed. The main advantage of the planar substrates

over colloidal NPs is that, beside the chemical affinity of the target molecule towards metallic surface, the simple static physical attachment also plays a role. During this study, as a complex matrix, artificial sputum was investigated, not only because it closely simulates clinical samples but also due to its known composition it also offers the possibility to study the interaction of the matrix components and target analyte with plasmonic nanostructures. Prepared artificial sputum included DNA, mucin, bovine serum albumin (BSA), egg yolk, NaCl, KCl, diethylenetriaminepentaactetic acid and tris(hydroxymethyl)aminomethane hydrochloride. [77] For the SERS investigations, 900 µL of artificial sputum were spiked with 100 µL of 1 mM PYO ethanol solution to achieve a concentration of 100 µM of PYO in the sputum. After this, serial dilutions were performed to get the final concentrations of 100, 75, 50, 25, 12.5 and 6.25 µM of the analyte in the sputum samples. As negative control sputum was spiked only with ethanol.

For the SERS measurements, silicon nanowires (SiNWs) based substrates were considered. The attention was drawn to SiNWs due to their low-cost and relatively easy fabrication. Moreover, they have a very high surface area, which allows packing of high number of the NPs, leading to higher enhancement factors. [217] In the context of the study, four different designs of the substrates, which are schematically represented in **Figure 7 (a)**, were fabricated. For this, SiNWs were prepared by metal-assisted chemical etching (MACE) in hydrofluoric acid (HF) solution using Ag NPs. [218] Next, for two substrates the Ag NPs on the bottom of the SiNWs were left and for two they were removed. This was followed by Ag NPs deposition on the top of the SiNWs for one of each substrate type. Finally, on all substrates the reduction of gold(III) chloride in 5 M hydrofluoric acid was performed [219], which resulted in the formation of Au NPs on the SiNWs or around the previously deposited Ag NPs on the top. In this way, at the end four SERS substrates were prepared: (1) Ag$_*$Au*SiNWs – SiNWs with native layer of Ag NPs at the bottom and deposited Au NPs on the top; (2) Ag$^*_*$Au*SiNWs – SiNWs with native Ag NPs at the bottom and bimetallic Ag/Au NPs on the top; (3) Ag*Au*SiNWs – SiNWs with bimetallic Ag/Au NPs on the top; (4) Au*SiNWs – SiNWs with Au NPs deposited on the top. Investigation of substrates' morphology with SEM showed that for all of the substrates SiNWs acquired a conical shape, which can be caused by simultaneous etching in HF during the deposition of Ag NPs and the gold reduction process (see **Figure 1 in [OZ4]**). Native Ag NPs on the bottom of the substrate were sized around 100 nm and the ones on the top around 50 nm. For all of the substrates, gold formed fine-grained structures consisting of NPs with sizes between 10-20 nm.

To compare the SERS ability between the different designs of the substrates, artificial sputum with PYO concentration of 50 µM was selected as a sample. All substrates were incubated for 30 min in PYO-artificial sputum solution, which was previously diluted 5 times with deionized water. Here, dilution was performed to reduce the matrix effects and optimize the SERS signal. [220, 221] As negative control, substrates were incubated in pure artificial sputum. After incubation substrates

were air-dried and subjected to Raman measurements performed with 785 nm excitation wavelength. Investigation of the substrates under the microscope revealed that during the drying process 'coffee-ring effect' appears and the sample is concentrated around the edge of the substrate. Thus, the scanning areas were selected closer to the edges of substrates. For every substrate ten areas with 100 point were measured. Obtained mean SERS spectra are depicted in **Figure 7 (b)**. First of all, it can be seen that the blank sputum by itself has intensive bands at 732, 960 and 1327 cm^{-1}. Based on the SERS measurements of all the sputum components and on the literature, these bands were assigned to the DNA base adenine. [222]

Despite this contribution of the matrix, the peaks of PYO at 597, 676, 1353, 1600 and 1615 cm^{-1} also can be observed for all the investigated substrates. For a better comparison, the ring deformation vibrational mode of PYO at 676 cm^{-1} was integrated and plotted in **Figure 7 (c)** together with the SD. More intensive signal was received from the substrates with the native Ag NPs on the bottom. This can be explained by the fact that some analyte molecules diffuse to the bottom of the substrate and their signal can be still enhanced by Ag NPs lying on the bottom. In the case of other two substrates with removed Ag NPs, Raman signal of those molecules is not enhanced, as they are too far away from the metal NPs on the top. The highest signal of PYO was achieved for the $Ag^{*}_{*}Au^{*}SiNWs$ substrate. Moreover, it also demonstrated the smallest relative standard deviation (RSD), which is highly important for the SERS studies. Therefore, only this substrate was considered for further investigation.

To estimate the detection sensitivity of the $Ag^{*}_{*}Au^{*}SiNWs$ substrate, the PYO concentrations of 100, 75, 50, 25, 12.5 and 6.25 µM in artificial sputum were measured and the resulting mean

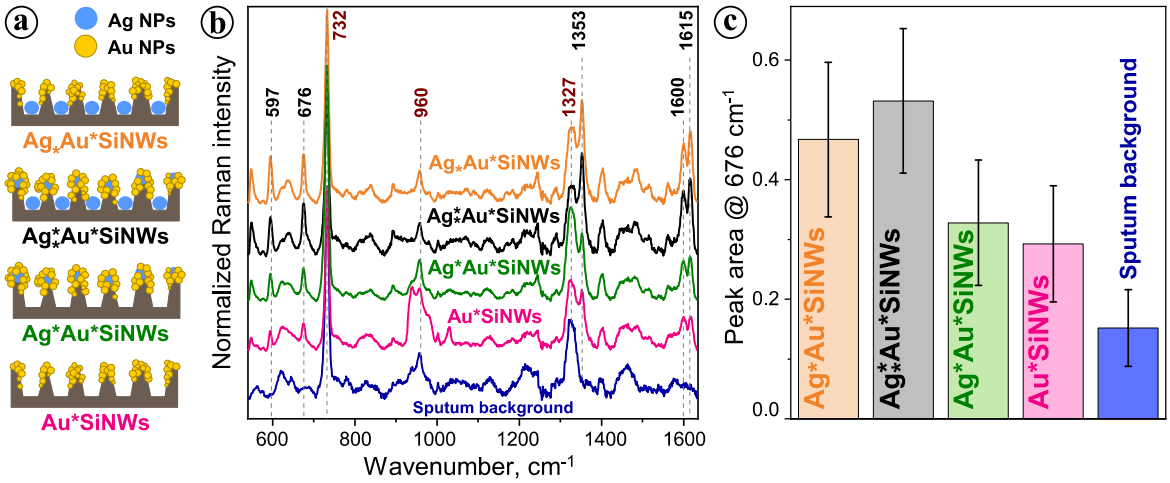

Figure 7. **(a)** Schematic representation of the fabricated SERS substrates. **(b)** Mean SERS spectra of 50 µM PYO in artificial sputum measured on four different types of SiNWs substrates and the mean SERS spectra of artificial sputum. **(c)** Normalized peak area for the peak at 676 cm^{-1} for four different types of SiNWs substrates. Adapted from [OZ4].

spectra are plotted in **Figure 8 (a).** Despite some background from the artificial sputum components, the characteristic peaks of PYO already appear for the 6.25 µM concentration. For a better visualization, the integrated peak area of the PYO band at 1353 cm^{-1} (zoomed region is depicted in **Figure 8 (b))** was calculated and plotted against the concentration of PYO. **Figure 8 (c)** shows the linear response in the concentration range from 6.25 µM to 100 µM.

Parallel to the detection in artificial sputum, PYO detection in aqueous solution was also performed aiming to evaluate the effects brought by complex matrix. Analyzing aqueous solutions PYO signal was clearly visible down to concentration of 1 nM (see **Figure S8 in SI for [OZ4]**). This proves that, in the case of artificial sputum, the competition for the free binding sites on the metallic surface occurs, and leads to decrease in SERS signal of PYO. Nevertheless, achieved detection of PYO in artificial sputum down to 6.25 µM perfectly fits the clinically relevant limit. This indicates the high potential of using the described substrates for the direct detection and quantification of PYO in artificial sputum, which, to the best of my knowledge, has not been reported before.

However, even though SERS offers a great potential for bioanalytical applications, often plasmonic substrates have been hindered by poor reproducibility. Therefore, the SERS signal reproducibility of the $Ag^{*}_{*}Au^{*}$SiNWs substrate was studied more precisely. For this, 50 µM concentration of PYO in artificial sputum was used and the signal variations from point-to-point were checked. Measuring 100 spectra with 5 µm step, SERS signal of PYO appeared to be quite stable demonstrating RSD around 11.6 %. Considering ten different areas within the substrate, deviation became higher and reached 22.7 % (see **Figure 3 [OZ4]**). This can be in the main explained by inhomogeneous drying of the sputum. Additionally to the point-to-point, SERS substrates should have very good batch-to-batch reproducibility, which ensures that all new substrates made with the same pro-

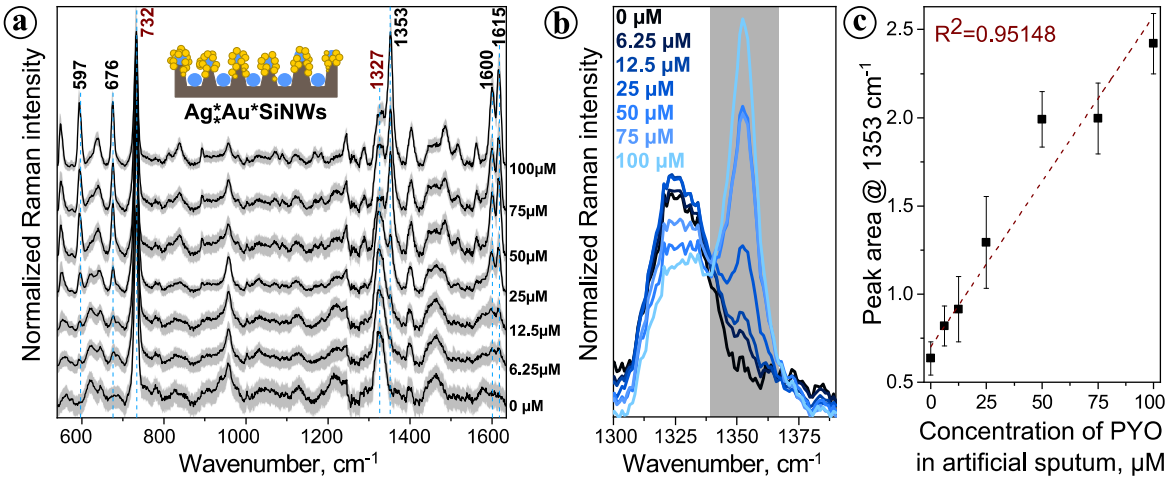

Figure 8. **(a)** Vector normalized mean SERS spectra of artificial sputum spiked with different PYO concentrations. **(b)** Zoomed mean spectra for different PYO concentrations. **(c)** The peak area of the band at 1353 cm^{-1} as a function of the PYO concentration in the range between 6.25 and 100 µM. Adapted from [OZ4].

cedure will provide the same results. During the study, four different batches of the $Ag^{*}_{*}Au^{*}$SiNWs substrates were prepared by two different researchers. All batches were similarly SERS active exhibiting RSD of the SERS signal around 12 %. Such variations suggest that there is still some room for the optimization of the substrates. MACE protocol used for production of SiNWs involves very short (15 s, 30 s) incubation steps in etching solutions and manual performing of them can lead to shorter or longer incubation, which result in small morphological variations between the substrates. Therefore, automation of the fabrication process would be beneficial.

To conclude, the presented studies show the high potential of the label-free SERS for the detection of the bacterial biomarker PYO directly in the body-fluids. Moreover, proposed SERS detection platforms with Ag colloids or SiNWs-based planar substrates are easy to prepare within a few minutes and require no special equipment. Although, in comparison to aqueous solution, the presence of interfering components of saliva or artificial sputum increased PYO detection limits, SERS signal of PYO in those complex fluids could still be clearly visible in the micromolar concentration range. This indicates that SERS, in prospect, can be implemented in real clinical setting because clinically relevant PYO concentrations in sputum lie between 7 and 130 μM. Furthermore, the achieved linear responses raise the question of a potential use of SERS not only for detection but also for quantification of this biomarker in body fluids. Clinical sputum samples should be considered in order to further explore the capabilities of this method.

5 SUMMARY AND OUTLOOK

The burden of respiratory tract infections (RTIs) is a substantial public health concern. High mortality rates worldwide highlight the extreme need for improving management of this type of infections. In particular, intense focus should be set on the individuals with higher susceptibility to RTIs, as they make up a significant part of the infection cases and are at higher risk of lethal outcome. To this group can be assigned people with any type of immunosuppression, individuals suffering from chronic respiratory tract diseases, persons with some genetic disorders affecting the respiratory organs, children till the age of five and elderly generation. To decrease the mortality of RTIs, especially among these people, improvement of prevention techniques as well as searching for faster and more accurate diagnostic methods leading to a more effective treatment, should be performed. The aim of this thesis was to investigate the potential and limitations of Raman spectroscopic techniques (RST) for these clinical tasks.

First of all, the role of RST for prevention purposes was demonstrated. Since currently available vaccinations for the prevention of infections provide selective spectrum of protection and have controversial effectiveness for susceptible individuals, some other actions should be considered. Taking into account that humans are constantly breathing and no environment is totally sterile, avoiding the aspiration of potential pathogens seems to be impossible. However, if they are aware of the exact composition of the microorganisms in the air, susceptible individuals could avoid being in the places with pathogens of high danger. To do so, a fast identification of the microorganisms found in the air should be performed. That is there RST enters the battlefield as an alternative to the time consuming and personnel-dependent culturing methods or to nucleic acid-based and immunological techniques requiring the complicated generation of selective antibody and large amount of antigens. RST were already broadly investigated for identification of microorganisms, however the application of it was mainly limited to not colored samples. In the frame of this thesis, it is demonstrated that highly pigmented and darkly colored fungal spores can also be identified based on their 'spectral fingerprint'. Fungal spores are often found in the air, and depending on the species, can cause the RTIs, especially in susceptible individuals, or trigger the exacerbation of an already developed respiratory disease. Raman measurements were carried out using UV-RRS, due to possibility of avoiding the fluorescence and obtaining the enhanced signal from taxonomically important biomolecules such as DNA/RNA. Subsequent spectral classification performed with PCA-LDA and evaluated with leave-batch-out cross-validation (LBOCV) demonstrated accuracies higher than 97 % not only in discrimination between spores of five different genera, but also for identification of four different *Aspergillus* species. This is highly relevant because out of hundreds

of *Aspergillus* species, only tens are known as opportunistic pathogens. The power of the technique was also assessed on the never before reported strain level and the accuracy of 89.42 % in differentiating between three strains of *A. fumigatus* was achieved. Since the usage of the Raman setup was limited to the biomass of the sample, the omission of the cultivation step was not possible at this point in time. However, combining of UV-RRS with chemometrical methods completely excludes the human factor from the identification process and makes it more automated. To make a full use of the potential of the technique, further studies should be directed towards technical improvements of the setup enabling measurements of spores directly from collection filters. This would allow for the susceptible individuals to perform online monitoring of the microorganisms' composition in the air and to take appropriate preventitive steps.

Another crucial point in managing RTIs is their rapid diagnosis, which allows earlier intervention and results in more effective treatment. However, for susceptible individuals it is often a challenging task, as usual symptoms of RTIs, like fever or cough, can overlap with symptoms of the main disease or can be simply absent. Therefore, a periodically performed easy and non-invasive screening test could be extremely beneficial. Nowadays there is no real screening program for the RTIs and detection of suspected infections is initially performed with chest radiography. However, frequent use of this imaging test is limited by the accompanied dose of ionizing radiation. In the scope of this thesis, conventional RS of urine was investigated as a possible screening technique for RTIs, which were represented by the mice model of aspergillosis infection. Here, urine attracted the interest due to simple and completely non-invasive collection in people of all ages, possibility of multiple sampling and possessing large amount of metabolites, which could reflect the developing infection. To assess more precisely the diagnostic value of urine and ability of RS to monitor changes in its composition, along with aspergillosis infection, the mice model of allergic asthma was included together with two kidney diseases known to have a direct influence on urine formation. Comparison of spectral data from control mice for all of the models revealed significant differences between them, which forced separated investigation of each model. Discrimination between sick and healthy mice was done using PCA-LDA and resultant model was evaluated with leave-mouse-out cross-validation (LMOCV). The classification accuracy of 100 % was achieved for the kidney disease model, which supported the starting hypothesis that urine is very informative for the diseases with direct connection to its formation and RS is able to read out this information. Considering respiratory tract diseases, which have no direct influence on urine composition, much smaller differences between control and sick mice were registered, but RS still showed promise for diagnosis. For detecting the allergic asthma, the accuracy of 77.27 % was achieved; however, it is worth noticing that occurred false negative results could have been caused by organism's capacity for self-regeneration, as the included urine samples were collected on different days after exposure

to allergens. Analyzing the aspergillosis model, firstly the sensitivity of 50 % and specificity of 90 % were achieved, but more detailed clinical data revealed that some of the infected mice did not develop the infection, which could lead to misclassifications. Rebuilding the model only with mice diagnosed with acute aspergillosis, the identification accuracy reached 100 %. This shows that urine-based RS holds some promises for the screening of RTIs but further clinical studies including significantly larger cohorts should be conducted for more precise validation of the method.

Finally, to increase the chances for the successful treatment of the RTIs, fast identification of the exact infectious agent is required. Within this scope, indirect detection of the pathogens by identifying the biomarkers released to body fluids by the microorganism or reflecting the host response may be a good alternative approach to the routine time consuming bacteriological culture. In the framework of the thesis, a highly sensitive SERS technique is suggested for this purpose by demonstrating, as an example, the detection of *P. aeruginosa* biomarker – pyocyanin (PYO) directly in respiratory body-fluids. With the focus on the clinical application, the main goal was to provide a cost-effective, sensitive, rapid and easy-to-use detection platform, which is able to detect clinically relevant PYO concentrations (7 – 130 µM in sputum samples). Initially, as SERS active agent easy-to-prepare Ag NPs were considered. To achieve more automated and reproducible measurements, SERS was combined with a microfluidic platform. To assess the suitability of the method, firstly, detection of PYO in aqueous solution was performed and the linear response of the SERS intensity in the concentration range of 0.5 – 15 µM was achieved with calculated limit of detection being lower than 0.5 µM. As a next step towards matrix complexity, spiked saliva samples from the volunteers were considered. Despite the more compounded solution, signatures of PYO were still visible for two volunteers down to 10 µM and for one down to 25 µM. Although these values are still in the clinically relevant range, such a drop of the detection sensitivity, compared to aqueous solution, provided insight that using the same strategy, PYO detection in a more complex biofluid such as sputum would be already challenging. Therefore, for the next measurements SERS performance of planar substrates was considered. Keeping in mind the requirement of simple and cost-effective detection platform, chemically within 20 min produced SiNWs variously decorated with Ag and/or Au NPs were introduced as SERS substrates. Investigating different designs was concluded that, for the SERS signal, it is beneficial to have the Ag NPs on the bottom of the NWs, because the Raman signal from the analyte molecules diffused to the bottom can be also enhanced. Moreover, placing on the top of SiNWs bimetallic Ag/Au NPs rather than only Au NPs improved the stability of the signal. Using such substrate the detection of PYO in artificial sputum, which mimics clinical samples, was performed. To decrease the influence of the matrix, dilution of the samples was suggested and PYO signal down to 6.25 µM concentration could be observed by the eye. Moreover, the linear response of SERS intensity in the concentration range of

6.25 - 100 μM was achieved. These results indicate that label-free SERS is suitable candidate for the PYO detection in respiratory bio-fluids and this technique holds significant promise for the quantitative analysis. Future studies should be focused on the optimization of the fabrication process of introduced SERS substrates and on the investigation of real sputum samples.

In conclusion, within the framework of this thesis, the potential role of RST for improving prevention and diagnostic strategies of RTIs in susceptible individuals was assessed, highlighting the need of careful choice of the technique according to the desired clinical task. To do so, UV-RRS spectroscopy was successfully applied for the identification of highly pigmented fungal spores samples, conventional RS of urine was investigated for the fast screening of the RTIs and SERS was used for the detection of a bacterial metabolite in complex matrixes for the rapid and more precise diagnosis. Along with the promising results, the challenging aspects such as (i) laser induced photodegradation and the need of spore' biomass for obtaining the good quality spectra for identification; (ii) decreased diagnostic value of urine for the diseases not directly connected with urine formation and (iii) interfering contribution of the complex matrix components to the SERS signal of target analyte, were discussed. Therefore, there remains a need for further investigations with clinical samples before RST can be accepted as an effective tool in clinical applications. However, the results achieved in the frame of this thesis represent a significant step forward toward this direction.

6 ZUSAMMENFASSUNG UND AUSBLICK

Infektionen der Atemwege (engl. *respiratory tract infection*, RTI) haben nicht nur einen sehr negativen Einfluss auf die Gesundheit der gesamten Weltbevölkerung, sondern auch erhebliche finanzielle und humanitäre Auswirkungen. Weltweit hohe Sterblichkeitsraten weisen auf die dringende Notwendigkeit eines verbesserten Managements bei dieser Art von Infektionen hin. Hierbei sollte der Fokus auf Personen mit einer erhöhten Anfälligkeit für RTI gelegt werden, da sie einen erheblichen Teil der Gesamtheit derartiger Infektionen ausmachen und ein besonders hohes Sterblichkeitsrisiko aufweisen. Zu dieser Gruppe zählen Personen mit jeder Art von Immunsuppression, wie auch Menschen, welche an chronischen Erkrankungen der Atemwege leiden oder die bestimmte genetische Störungen der Atmungsorgane aufweisen, aber auch Kinder bis zu einem Alter von fünf Jahren sowie alte Menschen. Um die Mortalität bei RTI, speziell bei diesen Personen, zu senken, sollten die Bemühungen zur Verbesserung der Präventionstechniken sowie die Erforschung von schnelleren und genaueren Diagnoseverfahren intensiviert werden, damit schließlich eine effektivere Behandlung erfolgen kann.

Ziel dieser Arbeit war es, das Potential und die Grenzen Raman-spektroskopischer Verfahren (RSV) für die Prävention und Diagnostik von RTI zu untersuchen.

Zunächst wurden die Möglichkeiten von RSV für Präventionszwecke erforscht. Da derzeit verfügbare Impfungen zur Verhinderung von Infektionen nur einen unvollständigen Schutz bieten und die Wirksamkeit bei anfälligen Personen umstrittenen ist, sollten auch andere Maßnahmen in Betracht gezogen werden. Weil der Mensch ständig atmen muss und praktisch keine Umgebung vollkommen steril ist, scheint es unmöglich, den Kontakt mit potentiellen Krankheitserregern gänzlich zu vermeiden. Wäre jedoch die genaue Zusammensetzung der Mikroorganismen in der Atemluft bekannt, könnten anfällige Personen sich gezielt von Orten mit hochgefährlichen Krankheitserregern fernhalten. Dazu ist eine schnelle Identifizierung der in der Luft vorkommenden Mikroorganismen erforderlich. Für diese Aufgabe sind RSV eine attraktive Alternative zu Kultivierungsmethoden, die sehr zeitaufwendig sind und deren Resultate von der durchführenden Person abhängig sind. Nukleinsäure-basierte und immunologische Techniken sind zwar ebenfalls schneller als kultivierungsbasierte Ansätze, erfordern aber eine komplizierte und kostspielige Erzeugung von selektiven Antikörpern und eine große Menge an Antigenen oder sehr teure Spezialreagenzien. Die Nutzung von RST zur Identifizierung von Mikroorganismen wurde bereits umfassend untersucht, jedoch war die Anwendung hauptsächlich auf Proben, welche keine Farbpigmente enthielten, beschränkt. Im Rahmen dieser Arbeit wird gezeigt, dass hochpigmentierte und dunkel gefärbte Pilzsporen auch anhand ihres „spektralen Fingerabdrucks“ identifiziert werden können. Pilzsporen sind häufig in der Luft zu finden und können, abhängig von ihrer Spezies, RTI insbesondere bei anfälligen Individuen verursachen oder bereits bestehende Atemwegserkrankungen verschlimmern. Um

diese zu charakterisieren wurde die Methode der Ultraviolett-Resonanz-Raman-Spektroskopie (UV-RRS) angewandt. Dabei wird das störende Fluoreszenzsignal der Probe vermieden, während die Raman-Banden von taxonomisch wichtigen Biomolekülen wie DNA / RNA verstärkt werden. Die nachfolgende spektrale Klassifizierung, die mit der Hauptkomponentenanalyse (engl. *Principal Component Analysis*, PCA) und der lineare Diskriminanzanalyse (engl. *Linear Discriminant Analysis*, LDA) durchgeführt und mit der „*Leave-One-Batch-Out*"-Kreuzvalidierung (engl. *leave-one-batch-out cross validation*, LBOCV) ausgewertet wurde, zeigte Genauigkeiten von mehr als 97 %. So wurde nicht nur die Unterscheidung von Sporen fünf verschiedener Gattungen, sondern auch die Identifizierung von vier verschiedenen Aspergillus-Arten ermöglicht. Dies ist äußerst relevant, da von Hunderten von *Aspergillus*-Arten nur zehn als opportunistische Erreger bekannt sind. Die Leistungsfähigkeit dieser Technik konnte ebenfalls anhand eines noch nie zuvor erreichten Spezifizierungslevels untermauert werden, wobei eine Genauigkeit von 89% bei der Differenzierung zwischen drei Stämmen von *A. fumigatus* erreicht wurde. Da der verwendete Raman-Messaufbau eine gewisse Menge an Biomasse der Probe erforderte, war der Verzicht auf einen Kultivierungsschritt zu diesem Zeitpunkt noch nicht möglich. Die Kombination von UV-RRS mit chemometrischen Methoden schließt jedoch den Faktor Mensch vollständig aus dem Identifizierungsprozess aus und macht ihn automatisierbar. Um das Potential dieses Ansatzes voll ausnutzen zu können, sollten weitere Anstrengungen im Hinblick auf die technische Verbesserung des Aufbaus ausgerichtet sein, sodass eine direkte Messung von Sporen aus Luftfiltern möglich ist. Dies würde es dem gefährdeten Personenkreis ermöglichen, eine Online-Überwachung der aktuell in der Luft vorhandenen Mikroorganismen durchzuführen und gegebenenfalls geeignete Präventionsmaßnahmen zu ergreifen.

Weitere entscheidende Punkte bei der Bekämpfung von RTI sind die schnelle Diagnose und die genaue Identifizierung der Erreger, wodurch ein früheres Eingreifen und eine wirksamere Behandlung möglich wird. Für die Patienten selbst sowie für die behandelnden Ärzte ist beides jedoch häufig schwer realisierbar, da die üblichen Symptome von RTI, wie Fieber oder Husten, von den Symptomen der Haupterkrankung überlagert werden können oder ganz fehlen. Ein regelmäßig durchgeführter einfacher und nichtinvasiver Screening-Test wäre hier von großem Nutzen. Bislang gibt es jedoch kein echtes Screening-Programm für die RTI. Die Erkennung von vermuteten Infektionen wird zunächst mit der Thorax-Radiographie durchgeführt. Die regelmäßige Verwendung dieses bildgebenden Tests ist aber durch die damit verbundene Dosis ionisierender Strahlung begrenzt. Im Rahmen dieser Arbeit wurde die konventionelle Raman-Spektroskopie (RS) von Urin als mögliches Screening-Verfahren für RTI, repräsentativ am Mausmodell der Aspergillose-Infektion, untersucht. Urin wurde deswegen als Probenmatrix gewählt, weil er einfach und nicht-invasiv bei Menschen jeden Alters entnommen werden kann, die Möglichkeit der Mehrfa-

chentnahme besteht und eine große Menge an Metaboliten aufweist, welche ihre Zusammensetzung ändern können, wenn sich eine Infektion entwickelt. Um den diagnostischen Wert des Urins und die Fähigkeit von RS zur Überwachung von Änderungen in seiner Zusammensetzung genauer zu erforschen, wurde neben einer Aspergillose-Infektion am Mausmodell auch allergisches Asthma zusammen mit zwei Nierenerkrankungen eingeschlossen, von denen bekannt ist, dass sie einen direkten Einfluss auf die Urinbildung haben. Ein Vergleich der Spektraldaten von Kontrollmäusen für alle Modelle ergab signifikante Unterschiede zwischen ihnen, was eine getrennte Untersuchung jedes Modells notwendig machte. Die Diskriminierung zwischen kranken und gesunden Mäusen wurde unter Verwendung von PCA-LDA durchgeführt und das resultierende Modell mit einer „*Leave-One-Mouse-Out*"-Kreuzvalidierung (engl. *leave-one-mouse-out cross validation*, LMOCV) bewertet. Eine Klassifizierungsgenauigkeit von 100 % wurde für das Nierenkrankheitsmodell erreicht, welche die Ausgangshypothese unterstützte, dass Urin bei Krankheiten, welche in direktem Zusammenhang mit seiner Produktion stehen, einen hohen Informationsgehalt besitzt, der mit RS ausgelesen werden kann. Im Hinblick auf Atemwegserkrankungen, die keinen direkten Einfluss auf die Zusammensetzung des Harns haben, wurden geringere Unterschiede zwischen Kontrollmäusen und erkrankten Mäusen festgestellt, jedoch zeigte die RS immer noch vielversprechende Ergebnisse in Bezug auf eine Diagnose. Beim Nachweis des allergischen Asthmas wurde eine Genauigkeit von 77 % erreicht. Zu berücksichtigen ist hierbei jedoch, dass aufgetretene falsch-negative Ergebnisse durch die Fähigkeit des Organismus zur Selbstregeneration verursacht werden könnten, da die verwendeten Urinproben an verschiedenen Tagen nach der Allergenexposition entnommen wurden. Bei der Analyse des Aspergillosemodells wurden zunächst eine Sensitivität von 50 % und eine Spezifität von 90 % erreicht. Eine detailliertere Analyse der klinischen Daten zeigte aber, dass bei einigen der infizierten Mäuse keine Symptome auftraten bzw. keine Infektion nachweisbar war, was vermutlich zu Fehlklassifizierungen führte. Bei der erneuten Generierung eines Modells nur mit den Mäusen, bei denen eine akute Aspergillose diagnostiziert wurde, erreichte die Erkennungsgenauigkeit 100 %. Dies zeigt, wie vielversprechend RS auf Urinbasis für das Screening von RTI ist. Für eine genauere Validierung der Methode sollten jedoch weitere klinische Studien mit deutlich größeren Kohorten durchgeführt werden.

Um die Chancen für eine erfolgreiche Behandlung der RTI zu erhöhen, ist eine schnelle Identifizierung des genauen Infektionserregers erforderlich. Dazu ist zum Beispiel ein indirekter Nachweis der Erreger durch charakteristische Biomarker, die durch den Mikroorganismus abgegeben werden, oder vom Wirt als Reaktion auf die Infektion gebildet werden, eine geeignete Alternative zu zeitraubenden Kultivierungsverfahren. Im Rahmen der Dissertation wurde für diesen Ansatz die hochsensitive oberflächenverstärkte Raman-Spektroskopie (engl. *Surface enhanced Raman spectroscopy*, SERS) gewählt und exemplarisch der Nachweis des von *P. aeruginosa* gebildeten

Biomarkers - Pyocyanin (PYO) direkt in der Atemwegsflüssigkeit realisiert. Mit dem Fokus auf die diagnostische Anwendung bestand das Hauptziel darin, eine kostengünstige, empfindliche, schnelle und benutzerfreundliche Erkennungsplattform bereitzustellen, mit der klinisch relevante PYO-Konzentrationen (7 – 130 µM in Sputumproben) nachgewiesen werden können. Als SERS-Substrat wurden zunächst einfach herzustellende Silber-Nanopartikel (Ag-NPs) verwendet. Um automatisierte und reproduzierbare Messungen durchführen zu können, wurde SERS mit einem Mikrofluidik-System kombiniert. Zur Beurteilung der generellen Eignung des Verfahrens, wurde zunächst der Nachweis von PYO in wässriger Lösung und die Korrelation der SERS-Intensität mit der Konzentration im Bereich von 0,5 – 15 µM untersucht. Dabei wurde eine Nachweisgrenze von weniger als 0,5 µM berechnet. Für den nächsten Schritt in Richtung einer erhöhten Matrixkomplexität wurden mit PYO-versetzte Speichelproben von freiwilligen Probanden analysiert. Trotz der komplexeren Zusammensetzung des Speichels waren die Signaturen von PYO bei zwei Probanden bis zu 10 µM und bei einem bis zu 25 µM messbar. Obwohl diese Werte noch im klinisch relevanten Bereich liegen, war die Nachweisempfindlichkeit im Vergleich zu wässriger Lösung deutlich verringert. Um den PYO-Nachweis in komplexeren Biofluiden wie Sputum mit dieser Methode dennoch durchführen zu können, wurden die nächsten Messungen mit einer planaren SERS-Substratvariante durchgeführt. Unter Berücksichtigung der Forderung nach einer einfachen und kostengünstigen Nachweisplattform wurden chemisch hergestellte Silizium-Nanodrähte (engl. *silicon nano wires*, SiNWs), die mit Ag- und / oder Au-NPs versehen waren, als SERS-Substrate eingeführt. Bei der Untersuchung verschiedener Designs wurde schließlich festgestellt, dass es für die SERS-Signalintensität vorteilhaft ist, die Ag-NPs an der Unterseite der NWs zu platzieren, da auf diese Weise das Raman-Signal von den nach unten diffundierten Analytmolekülen ebenfalls verstärkt werden kann. Darüber hinaus verbesserte das Aufbringen von Bimetall-Ag / Au-NPs anstelle von Au-NPs auf die Spitze der SiNWs die Stabilität des Signals. Mit einem solchen Substrat wurde der Nachweis von PYO in künstlichem Sputum, welches klinische Proben nachahmt, durchgeführt. Um den Einfluss der Matrix zu verringern, wurde eine Verdünnung der Proben vorgenommen. Das PYO-Signal konnte dabei bis zu einer Konzentration von 6,25 µM im Spektrum eindeutig mit bloßem Auge erkannt werden. Darüber hinaus wurde ein lineares Verhalten der SERS-Intensität im Konzentrationsbereich von 6,25 – 100 µM beobachtet. Diese Ergebnisse zeigen, dass markerfreies SERS für den PYO-Nachweis in Biofluiden der Atemwege gut geeignet und diese Technik zudem vielversprechend für die quantitative Analyse ist. Weiterführende Studien sollten sich somit auf die Optimierung des Herstellungsprozesses der eingeführten SERS-Substrate und auf die Untersuchung realer Sputumproben konzentrieren.

Im Rahmen dieser Arbeit wurde insgesamt das Potential von RSV zur Verbesserung der Präventions- und Diagnosestrategien von RTI bei anfälligen Personen untersucht, wobei besonders

Wert darauf gelegt wurde, die zum Einsatz kommende Technik sorgfältig auf die jeweiligen klinischen Anforderungen abzustimmen. So wurde die UV-RRS-Spektroskopie erfolgreich zur Identifizierung hochpigmentierter Pilzsporenproben eingesetzt und mittels konventioneller RS eine schnelle Screeningmethode für RTI an Urinproben realisiert. Darüber hinaus wurde demonstriert, dass SERS zum Nachweis eines bakteriellen Metaboliten in komplexen Proben geeignet ist und damit für eine schnelle und genauere Diagnose verwendet werden kann. Neben diesen vielversprechenden Ergebnissen wurden die herausfordernden Aspekte, wie (i) der laserinduzierte Photoabbau und der Bedarf an Sporenbiomasse, um Spektren mit guter Qualität für die Identifizierung zu erhalten; (ii) der verminderte diagnostische Wert des Urins für die Krankheiten, die nicht direkt mit der Urinbildung zusammenhängen, und (iii) der störende Beitrag der komplexen Matrixkomponenten zum SERS-Signal des Zielanalyten kritisch diskutiert. Demnach gibt es aktuell immer noch Bedarf an weiteren Untersuchungen und Studien mit klinischen Proben, bevor RSV als wirksames Instrument in der klinischen Anwendung akzeptiert werden kann. Die in dieser Arbeit erzielten Ergebnisse sind jedoch ein großer Schritt in diese Richtung.

7 PUBLICATIONS

In the present section the reprints of the publications included in the frame of the thesis are shown.

[OZ1] UV-Raman spectroscopic identification of fungal spores important for respiratory diseases

Olga Žukovskaja, Sandra Kloß, Matthew G. Blango, Oleg Ryabchykov, Olaf Kniemeyer, Axel A. Brakhage, Thomas W. Bocklitz, Dana Cialla-May, Karina Weber, Jürgen Popp

Analytical Chemistry, 2018, **90** (15), 8912–8918

DOI: 10.1021/acs.analchem.8b01038

[OZ2] Towards Raman spectroscopy of urine as a screening tool

Olga Žukovskaja, Oleg Ryabchykov, Maria Straßburger, Thorsten Heinekamp, Axel A. Brakhage, Christopher Hennings, Christian Hübner, Michael Wegmann, Dana Cialla-May, Thomas Bocklitz, Karina Weber, Jürgen Popp

Submitted to *Journal of Biophotonics*

[OZ3] Detection of *Pseudomonas aeruginosa* metabolite pyocyanin in water and saliva by employing the SERS technique

Olga Žukovskaja, Izabella Jolan Jahn, Karina Weber, Dana Cialla-May, Jürgen Popp

Sensors 2017, **17**(8), 1704

DOI: 10.3390/s17081704

[OZ4] Rapid detection of the bacterial biomarker Pyocyanin in artificial sputum using a SERS-active silicon nanowire matrix covered by bimetallic noble metal nanoparticles

Olga Žukovskaja*, Svetlana Agafilushkina*, Vladimir Sivakov, Karina Weber, Dana Cialla-May, Liubov Osminkina, Jürgen Popp

Talanta. 2019, **202**,171-177

DOI: 10.1016/j.talanta.2019.04.047

[OZ5-Review]

Surface-enhanced Raman spectroscopy and microfluidic platforms: challenges, solutions and potential applications

Izabella Jolan Jahn, Olga Žukovskaja, Xiao-Shan Zheng, Karina Weber, Thomas. W. Bocklitz, Dana Cialla-May, Jürgen Popp

Analyst, 2017, **142**(7), 1022-1047

DOI: 10.1039/c7an00118e

* Equally contributed authors

7.1 UV-Raman spectroscopic identification of fungal spores important for respiratory diseases [OZ1]

Olga Žukovskaja, Sandra Kloß, Matthew G. Blango, Oleg Ryabchykov, Olaf Kniemeyer, Axel A. Brakhage, Thomas W. Bocklitz, Dana Cialla-May, Karina Weber, Jürgen Popp

Analytical Chemistry, 2018, 90 (15), pp 8912–8918

https://pubs.acs.org/doi/10.1021/acs.analchem.8b01038

Declaration on authorship and copyright in a cumulative doctoral thesis

[1]**Žukovskaja, O.**, [2]Kloss, S., [3]Blango, M. G., [4]Ryabchykov, O., [5]Kniemeyer, O., [6]Brakhage, A. A., [7]Bocklitz, T. W., [8]Cialla-May, D., [9]Weber, K., [10]Popp, J., 2018. UV-Raman Spectroscopic Identification of Fungal Spores Important for Respiratory Diseases. *Analytical chemistry*, *90*(15), pp.8912-8918										
Involved in										
	1	2	3	4	5	6	7	8	9	10
Conceptual research design	X	X	X		X	X	X	X	X	X
Planning of research activities	X	X	X				X	X	X	X
Data collection	X	X								
Data analyses and interpretation	X			X			X			
Manuscript writing	X			X			X	X	X	X
Suggested publication equivalence value	**1.0**			0.5						

Author Contribution

Olga Žukovskaja	concept development UV-RRS measurements data analysis and interpretation writing of manuscript
Sandra Kloß	concept development first test measurements UV-RRS measurements discussion of results proofreading of manuscript
Matthew G. Blango	concept development culturing of fungal spores discussion of results proofreading of manuscript
Oleg Ryabchykov	data analysis and interpretation discussion of data analysis concepts and results
Olaf Kniemeyer	discussion of experimental concept and results proofreading of manuscript
Axel A. Brakhage	discussion of results proofreading of manuscript
Thomas W. Bocklitz	discussion of data analysis concepts and results proofreading of manuscript
Dana Cialla-May	discussion of experimental concept and results proofreading of manuscript
Karina Weber	discussion of experimental concept and results proofreading of manuscript
Jürgen Popp	project management discussion of concepts and results discussion and proofreading of manuscript

analytical chemistry

Article

Cite This: *Anal. Chem.* 2018, 90, 8912−8918

pubs.acs.org/ac

UV-Raman Spectroscopic Identification of Fungal Spores Important for Respiratory Diseases

Olga Žukovskaja,[†,‡,§] Sandra Kloß,[†] Matthew G. Blango,[∥] Oleg Ryabchykov,[†,§] Olaf Kniemeyer,[∥] Axel A. Brakhage,[∥,⊥] Thomas W. Bocklitz,[†,§] Dana Cialla-May,[†,‡,§] Karina Weber,[*,†,‡,§] and Jürgen Popp[†,‡,§]

[†]Institute of Physical Chemistry and Abbe Center of Photonics, Friedrich Schiller University Jena, Helmholtzweg 4, 07745 Jena, Germany

[‡]Research Campus Infectognostic, Philosophenweg 7, 07743 Jena, Germany

[§]Leibniz Institute of Photonic Technology Jena—Member of the Research Alliance "Leibniz Health Technologies", Albert-Einstein-Straße 9, 07745 Jena, Germany

[∥]Department of Molecular and Applied Microbiology, Leibniz Institute for Natural Product Research and Infection Biology (HKI), Adolf-Reichwein-Straße 23, 07745 Jena, Germany

[⊥]Department of Microbiology and Molecular Biology, Institute for Microbiology, Friedrich Schiller University Jena, Neugasse 25, 07743 Jena, Germany

Supporting Information

ABSTRACT: Fungal spores are one of several environmental factors responsible for causing respiratory diseases like asthma, chronic obstructive pulmonary disease (COPD), and aspergillosis. These spores also are able to trigger exacerbations during chronic forms of disease. Different fungal spores may contain different allergens and mycotoxins, therefore the health hazards are varying between the species. Thus, it is highly important quickly to identify the composition of fungal spores in the air. In this study, UV-Raman spectroscopy with an excitation wavelength of 244 nm was applied to investigate eight different fungal species implicated in respiratory diseases worldwide. Here, we demonstrate that darkly colored spores can be directly examined, and UV-Raman spectroscopy provides the information sufficient for classifying fungal spores. Classification models on the genus, species, and strain levels were built using a combination of principal component analysis and linear discriminant analysis followed by evaluation with leave-one-batch-out-cross-validation. At the genus level an accuracy of 97.5% was achieved, whereas on the species level four different *Aspergillus* species were classified with 100% accuracy. Finally, classifying three strains of *Aspergillus fumigatus* an accuracy of 89.4% was reached. These results demonstrate that UV-Raman spectroscopy in combination with innovative chemometrics allows for fast identification of fungal spores and can be a potential alternative to currently used time-consuming cultivation.

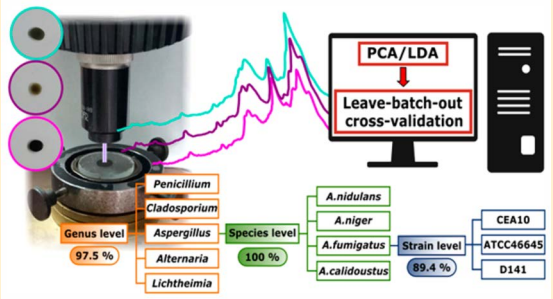

Hundreds of millions of people of all ages suffer every day from chronic respiratory diseases. According to the latest WHO estimates (2004), which are considered conservative, >300 million people are afflicted with asthma, 210 million people suffer from chronic obstructive pulmonary disease (COPD), while >400 million suffer from some other form of respiratory disease.[1] These diseases all have a negative impact on the quality of life of those affected and in many instances can be life threatening, especially in cases of acute exacerbation. Exacerbations of allergic respiratory disease occur frequently in COPD and asthma patients, likely triggered by exposure to environmental stimuli. Although debated, these exacerbations are generally characterized by increased airway inflammation, mucus production, and impaired lung function.

Outdoor fungal spores are one of several environmental factors responsible not only for causing respiratory diseases in humans,[2−4] but also for triggering exacerbations during chronic forms of lung diseases such as asthma and COPD. For example, it was reported that asthma hospitalization cases increase during thunderstorms due to the increased aerosolization of fungal spores.[5] Since different fungi may produce different allergens and mycotoxins, the severity of asthma exacerbation may vary between spores of different fungal taxa,[6] e.g., some patients have hypersensitivity only to *Aspergillus spec.*, which can lead to allergic bronchopulmonary aspergillosis

Received: March 7, 2018
Accepted: June 29, 2018
Published: June 29, 2018

DOI: 10.1021/acs.analchem.8b01038
Anal. Chem. 2018, 90, 8912−8918

(ABPA) or other complications in patients suffering from asthma, cystic fibrosis, or COPD.[7] Therefore, it would be beneficial to identify and eliminate fungal spores before they trigger respiratory disease or exacerbations in patients with chronic respiratory diseases.

Currently the "gold standard" for fungal identification is the cultivation of sampled organisms coupled with careful observation and measurement of macroscopic and microscopic morphological characteristics of the organism of interest, including reproductive structures like spores. However, this method is laborious and requires highly trained and experienced personnel. Additional difficulties in fungal identification include the presence of a wide range of nonculturable organisms and/or contamination of fungal cultures with fast-growing bacteria, as these factors make the analysis of morphological information complicated.[8] A fast, highly automated method, which can identify fungal spores via pattern recognition, would exclude the human factor from the identification process and would improve turn-around times for spore identification. As an alternative approach to the more classic culture methods, polymerase chain reaction (PCR)-based detection methods for fungal spore identification have been reported.[8−11] PCR methods require expensive reagents and design of target-specific primers and tend to produce false-positive results. Another possibility is offered by vibrational spectroscopy, a technique which utilizes molecular vibrations to provide information about the molecular composition, structure and behavior within a sample.

Among the vibrational spectroscopic methods, Raman spectroscopy is a very promising tool for the characterization of microorganisms.[12,13] This method offers specific molecular information about the chemical species in the samples in a noninvasive and label-free manner. The abilities of Raman spectroscopy for investigation and characterization of airborne allergens, such as individual pollen grains, has been demonstrated by various groups.[14−16] The characterization of fungal spores using Raman spectroscopy with visible excitation wavelengths has been previously also reported. However, in these studies, the excitation wavelengths utilized could only be applied to white or light-colored spores.[17,18] Several different microfungi spores relevant to indoor contamination were successfully characterized and identified with Raman spectroscopy, describing the biochemical composition of a single spore.[19] A study of C. Wang et al. reported measurements of Raman spectra in 1600−3400 cm^{-1} spectral range from individual pollen particles and Bermuda grass smut spores held in a photophoretic trap. Due to the small size of spores the spectrum had high background and only three Raman bands were visible.[20] Raman spectroscopy with visible excitation wavelengths was also used to discriminate *Aspergillus lentulus* from *Aspergillus fumigatus* with an accuracy of only 78%.[17] K. De Gussem et al. combined Raman spectroscopy with linear discriminant analysis (LDA) and reached around 90% accuracy in assigning the spectra of spores to the correct genus,[18] while identification on the species level was not possible. Instead of applying visible Raman excitation wavelengths various studies on mammalian cells,[21,22] bacteria,[23−25] and pollen[26] showed that utilizing electronically resonant excitation wavelengths in the UV region can be beneficial for the identification of microorganisms due to a selective resonant enhancement of the Raman signals of taxonomically important macromolecules, e.g., DNA/RNA bases and aromatic amino acids. Furthermore, the fluorescence background in UV resonance Raman spectra is negligible for excitation wavelengths below 260 nm, which lead to Raman spectra with high signal-to-noise ratio.[27−31]

In the present study, for the first time the UV-Raman spectroscopic identification of fungal spores is demonstrated. Eight different filamentous fungal species, implicated to a varied extent in respiratory diseases worldwide, were examined: *Aspergillus fumigatus*, *Aspergillus niger*, *Aspergillus nidulans*, *Aspergillus calidoustus*, *Cladosporium herbarum*, *Alternaria alternata*, *Penicillium rubens*, and *Lichtheimia corymbifera*. Except for the mucoralean fungus *Lichtheimia corymbifera*, a basal fungal lineage, all other species belong to the division Ascomycota. In contrast to previous studies,[17,18] highly pigmented spores were successfully investigated. The identification of spores was based on a combination of principal component analysis (PCA) and LDA of the UV resonance Raman spectral data and was applied at a genus, species, and strain level. The performance of the models was evaluated with leave-one batch-out cross-validation. The presented results highlight the possibility of UV-Raman spectroscopy as a promising method for the automated identification of fungal spores.

MATERIALS AND METHODS

Fungal Spores. For this study 11 fungal strains from 8 different species were utilized, namely *A. fumigatus*, *P. rubens*, *A. niger*, *C. herbarum*, *A. alternata*, *A. nidulans*, *A. calidoustus*, and *L. corymbifera* (Table S-1 of the Supporting Information, SI). The *A. fumigatus pksP* mutant has been described previously.[32,33] The fungi were grown for 7 days, in the dark, on 10 cm agar plates at room temperature (~22 °C). Growth was conducted on *Aspergillus* minimal media (AMM; 6.0 g/L $NaNO_3$, 0.52 g/L KCl, 1.52 g/L KH_2PO_4, 0.52 g/L $MgSO_4 \cdot 7H_2O$, 1% (wt/vol) glucose, and 1 mL of trace element solution [1 g/L $FeSO_4 \cdot 7H_2O$, 8.8 g/L $ZnSO_4 \cdot 7H_2O$, 0.4 g/L $CuSO_4 \cdot 5H_2O$, 0.15 g/L $MnSO_4 \cdot 4H_2O$, 0.1 g/L $Na_2B_4O_7 \cdot 10H_2O$, 0.05 g/L $(NH_4)_6Mo_7O_{24} \cdot 4H_2O$] per liter),[34] malt agar (MA) (Sigma-Aldrich), or modified SUP agar plates (4.1 g/L KH_2PO_4, 1.1 g/L NH_4Cl, 0.9 g/L K_2HPO_4, 0.1 g/L $MgSO_4$, 1% (wt/vol) glucose, and 0.5% (wt/vol) yeast extract).[35] AMM was supplemented with 0.06 mg/L biotin and 5 mM arginine for growth of *A. nidulans* A89. Conidia (asexually produced spores) from each strain were collected in 10 mL of water and separated from hyphae through a 40 μm pore filter. After centrifugation for 10 min at 1800 × *g*, conidia were resuspended in 3% (v/v) formaldehyde and incubated for 1 h for inactivation. Following formaldehyde-inactivation, each conidial-mixture was washed with water to remove any contaminating formaldehyde. The inactivation of the spores was confirmed by the lack of growth on appropriate media. Each growth condition was tested in triplicate, on three separate days. For the UV-Raman measurements 10 μL of spore suspensions was spread on a fused-silica surface and allowed to dry at room temperature.

Spectroscopic Instrumentation. Raman measurements were performed using a LabRam HR 800 spectrometer from Horiba Jobin-Yvon (Bensheim, Germany) with a 2400 lines/mm grating. As excitation wavelength, a frequency doubled argon-ion laser (Coherent Innova 300, MotoFReD, Coherent, Dieburg, Germany) operating at 244 nm was applied. The samples were illuminated via a microscope (Olympus BX 41) equipped with a 20× magnification antireflection coated UV objective (LMU UVB) with a numerical aperture of 0.4. The laser power at the laser head was ca. 10.5 mW and on the

DOI: 10.1021/acs.analchem.8b01038
Anal. Chem. 2018, 90, 8912−8918

sample ca. 0.8 mW at a spot diameter of ~1 μm, corresponding to ~10^5 W/cm^2 irradiance. The entrance slit was set to 300 μm. The Raman scattered light was detected by a nitrogen-cooled CCD camera with an integration time of 20 s with 2 accumulations. The samples were rotated with a speed 60 rotations/min and moved in the *x*,*y* direction after each rotation to obtain an average spectrum over a large sample area to minimize possible photodegradation by UV radiation. Ten spectra were collected per sample. Measurements were performed by two independent operators.

Data Analysis. Data processing was performed using an in-house developed script in the programming language R.[36] First, the spectra were wavenumber calibrated by using the Teflon Raman spectrum measured prior to each sample measurement as reference. Next, the Raman spectra were background corrected using the sensitive nonlinear iterative peak (SNIP) clipping algorithm[37] with a second-order clipping filter. Finally, all spectra were vector normalized and used as input for PCA, which was performed to reduce the dimensionality of the data while retaining the most significant information for classification. PCA was followed by LDA. The performance of the created LDA model for classification of fungal spores was estimated using the leave-one batch-out-cross-validation (LBOCV) approach.[38] In this method, one batch was held out from the data set, and the LDA model was redeveloped using the remaining spectra. The resultant model was then used to classify the removed batch. This process was repeated with every batch until all spectra were classified. In this manner LBOCV of the PCA-LDA model was utilized for all number of principle components (PCs). Then, an optimal number of PCs was chosen by finding a saturation point of the accuracy as a function of the number of PCs. For spectral comparison across the groups, mean Raman spectra for each fungal species were calculated using preprocessed, vector-normalized spectra of all batches.

RESULTS AND DISCUSSION

The primary goal of this study was to determine the feasibility of UV-Raman spectroscopy for the identification of melanised fungal spores. The selected fungal spores were all highly pigmented: black for *A. alternata* and *A. niger*, dark green for *A. fumigatus* strains and *P. rubens*, brown for *A. calidoustus* and *C. herbarum* and light gray for *L. corymbifera* and *A. nidulans* (Figure S-1). The difficulties of recording Raman spectra using visible excitation wavelengths from such dark conidia were previously reported; the dark pigments result in a strong interfering fluorescent signal, which masks the original spectrum.[17] Therefore, initially, the possibility of obtaining good quality spectra with UV-Raman from deeply colored, highly absorbing samples was investigated. For this purpose, wild-type *A. fumigatus* conidia were compared to non-pigmented conidia of a strain with a mutation in the *pksP* gene, essential for the formation of the gray-green spores containing dihydroxynaphthalene (DHN)-melanin.[32] The UV-Raman spectra of these samples are depicted in Figure 1.

During the measurements, the samples were continuously rotated; however, this rotation was insufficient to completely eliminate the laser-induced degradation of spore proteins into polymeric hydrogenated amorphous carbon. Thus, a carbon background manifesting itself by the two broad bands at approximately 1360 and 1610 cm^{-1} is observed.[39−41] For the nonpigmented *pksP* mutant strain, the graphitization level was lower, and therefore the bands originating from the spores in

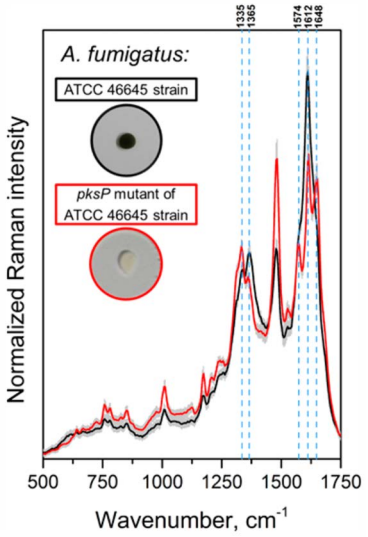

Figure 1. Mean UV-Raman spectra and their double standard deviation of the pigmented *A. fumigatus* ATCC 46645 strain and the nonpigmented *pksP* mutant strain.

the region of 1500−1700 cm^{-1} are more prominent. However, the general shape of the spectra and the peak positions are the same for both samples. In the pigmented wild-type spores of *A. fumigatus*, the unique spore-related spectral features necessary for the spore identification process are still easily visible. Hence, it can be concluded that UV-Raman can be used for the measurement of highly pigmented spores.

To compare a diverse range of allergenic fungi, we had to cultivate these organisms on several different media to promote sporulation due to different nutrient requirements. To test the variability induced by different culture media, we cultivated *P. rubens* strain ATCC 28089 and *A. fumigatus* strain ATCC 46645 on both MA and AMM medium for direct comparison. The mean UV-Raman spectra of the collected spores are presented in Figure S-2. The influence of the culture medium on the spectra was visible and can be best seen in the 1250−1700 cm^{-1} wavenumber region. In the case of *A. fumigatus* grown on MA medium, the signal at 1365 cm^{-1} is more intense, whereas for *P. rubens* the peak at 1648 cm^{-1} is more prominent. Despite this observation, all strains grown on different agars were included into the classification model, proving that the differences from cultivation conditions are smaller than the differences due to species affiliation.

The representative preprocessed mean Raman spectra of the studied fungal spores are depicted in Figure 2.

For all species, primary bands were observed in the wavenumber region between 750 and 1700 cm^{-1}, which is typically associated with various nucleic acids and protein subunits in UV-Raman spectroscopy. The band positions are in good agreement with previously published UV-Raman spectroscopic studies of microorganisms.[24,23,42] The signal at 1648 cm^{-1} can be assigned to thymine and the one at 1612 cm^{-1} to the aromatic amino acids tyrosine and tryptophan. Guanine and adenine exhibit peaks at 1574 and 1479 cm^{-1}; they also contribute to the signal at 1335 cm^{-1}. The latter band (at 1333 cm^{-1}) also contains information from tyrosine. The signal at 1526 cm^{-1} can be assigned to cytosine. Thymine and

DOI: 10.1021/acs.analchem.8b01038
Anal. Chem. 2018, 90, 8912−8918

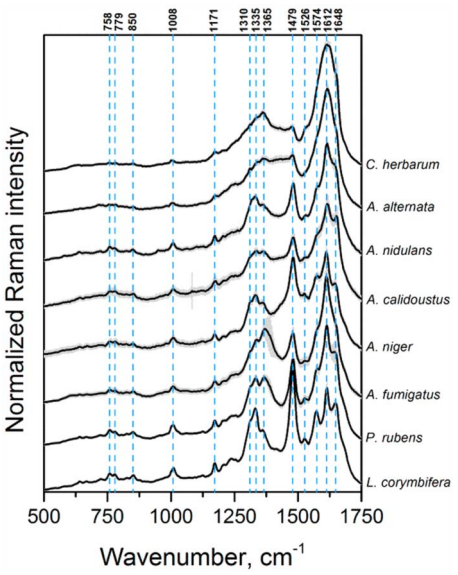

Figure 2. Mean UV-Raman spectra of the all batches from different fungal spores plotted together with double standard deviation (gray area). For the *A. fumigatus* the mean spectrum represents all investigated strains.

adenine exhibit a band at 1365 cm^{-1}. The peak at 1171 cm^{-1} can be assigned to tyrosine. Tryptophan exhibits characteristic bands at 758 and 1008 cm^{-1}. In this study, measurements were performed on the bulk sample under continuous rotation; so several spores contribute to one spectrum. Therefore, one spectrum already comprises metabolic and developmental diversity within the spore population. The reproducibility of these spectra was tested by measuring the Raman spectra from three independent batches.

It is evident from Figure 2 that the fungal spores belonging to different genera display distinct Raman spectral signatures and are easily distinguishable based on their spectra. The peak positions for all analyzed spores are the same, however the relative intensities for the bands in the region of 1250 and 1750 cm^{-1} differ. For the *C. herbarum* and *A. alternata* measurements, three Raman modes at 1574, 1612, and 1648 cm^{-1} are strongly convoluted due to a higher carbonization background. In addition to a visual comparison, a PCA/LDA model was applied and verified using the leave-one batch-out-cross-validation. Three different models on genus, species, and strain level were established (see Figure 3). Health hazards related to fungal spores may differ across genera and species due to the difference between allergenicity and types of mycotoxins produced. It is known for example that the severity of asthma exacerbation may vary between spores of different taxa.[6] To prevent exacerbations, it is important to define the composition of spores in the air on the genus level. Thus, the classification model was first trained to distinguish spores on the genus level. Prior to LDA, the data size was reduced by PCA. The optimal number of PCs was chosen by finding a saturation point of the accuracy as a function of the number of PCs; in this case, 6 PCs were selected (Figure S-3). The LDA model was trained with 2 batches of spores and then tested with one independent batch of the same strain. This allowed for three different batch permutations for validation and gave a reliable unbiased classification model. The sensitivity, specificity, and accuracy of the LDA model in each run were calculated and averaged. Table 1 shows the number of spectra that were classified correctly for each species of the fungi and also summarizes sensitivity and specificity.

Out of 1079 spectra, 27 were misclassified; this resulted in 97.5% accuracy. In Figure 4, the LDA score plot of the classification model is depicted, whereby each dot represents one spectrum and the ellipsoids correspond to confidence regions for the scores on a level of 95% of the spectral data for each class. The biggest amount of errors appeared to be due to the misclassification of *Aspergillus* species to the closely related genus *Penicillium*. The LDA score plot also nicely reflects the phylogenetic relationship between the different genera: *A. alternata* and *C. herbarium* belong to the same class of Dothideomycetes, while the closely related genera *Penicillium* and *Aspergillus* are grouped into the class Eurotiomycetes. The species *L. corymbifera* belongs to a lower group of fungi, the phylum Zygomycota that diverged early in the evolution of true fungi.[43]

In the second step, the model distinguishes between four different *Aspergillus* species. Several *Aspergillus* species are able to cause infections like invasive pulmonary aspergillosis or allergic reactions like ABPA, while others are nearly non-pathogenic.[44] In addition, antifungal drug susceptibility is wide-ranging among even quite similar organisms.[45] Thus, the

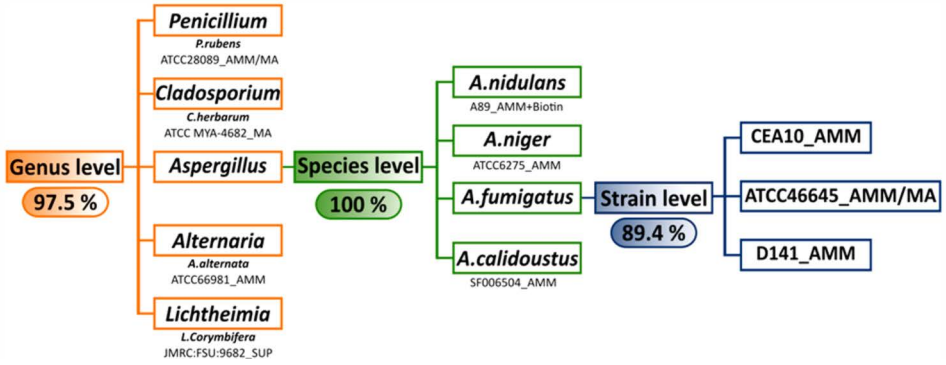

Figure 3. 3-Level PCA/LDA classification model of fungal spores cultured in three independent batches (the percentage represents the accuracies of the model achieved by LBOCV).

DOI: 10.1021/acs.analchem.8b01038
Anal. Chem. 2018, 90, 8912−8918

Table 1. Identification Results for Different Fungal Spores on the Genus Level

True / Predicted	*Altenaria alternata*	*Aspergillus* species	*Cladosporium herbarum*	*Lichtheimia corymbifera*	*Penicillium rubens*	Sensitivity, %	Specificity, %
Altenaria alternata	90	0	0	0	0	**100**	**100**
***Aspergillus* species**	0	603	0	0	1	**95.87**	**99.78**
Cladosporium herbarum	0	4	90	0	0	**100**	**99.6**
Lichtheimia corymbifera	0	0	0	90	0	**100**	**100**
Penicillium rubens	0	22	0	0	179	**99.44**	**97.55**

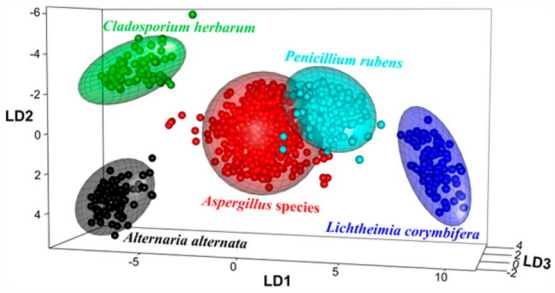

Figure 4. LDA score plots for the classification model on the genus level.

knowledge of the species identity may influence the choice of appropriate antifungal therapy. The visual differentiation of the spectra from *A. fumigatus*, *A. nidulans*, *A. calidoustus*, and *A. niger* is already not as obvious as it was for different genera (Figure 2). For building the identification model on the species level, the number of PCs was set to 7 (Figure S-4). All 629 spectra were assigned correctly resulting in 100% accuracy. The differentiation was based mostly on the different amount of DNA in the spores, mainly resulting in the intensity differences for the peaks at 1365, 1479, and 1648 cm^{-1} (Figure S-5). The achieved accuracy was higher than the one reported by P.E.B. Verwer et al., where the discrimination of *Aspergillus lentulus* from *Aspergillus fumigatus* with VIS-Raman spectroscopy was correct for 78% of spectra.[17]

Finally, the model was trained to classify three different strains of *A. fumigatus*, since diversity in virulence among different *A. fumigatus* strains is also well-documented.[46] The UV-Raman spectra of the three investigated *A. fumigatus* strains are presented in Figure 5. By comparing the spectra, it is clear that the main spectral characteristics of the investigated strains were the same, as a consequence of their close phylogenetic relationship. The LDA model was built with 10 PCs (Figure S-6), and the classification was correct for 89.4% of spectra. The results of this classification model are summarized in Table 2. The misclassification occurred mostly between the ATCC 46445 and D141 strains. The identification of fungal spores on the strain level using Raman spectroscopy was not previously reported.

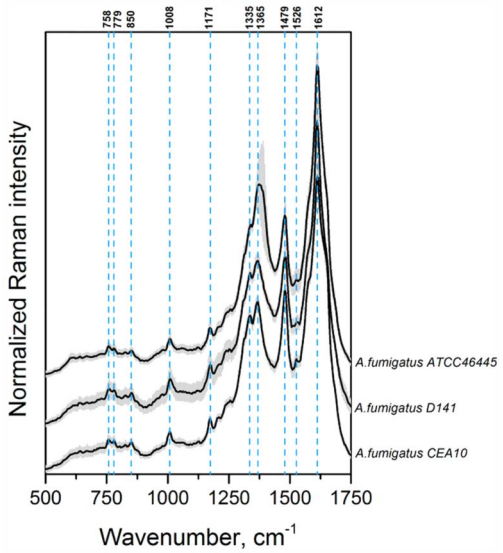

Figure 5. Mean UV-Raman spectra of three *A. fumigatus* strains.

Table 2. Results of the Identification of *A. fumigatus* Strains

True / Predicted	ATCC 46645	CA10	D141	Sensitivity, %	Specificity, %
ATCC 46645	151	1	8	**83.89**	**94.97**
CEA10	6	89	0	**98.89**	**97.77**
D141	23	0	81	**91.01**	**91.48**

CONCLUSIONS

In the case of respiratory fungal infections, identification of the fungal agent is often incredibly challenging due to a diverse array of potential organisms and relatively poor diagnostic possibilities. Thus, the development of sensitive and automated methods for the identification of fungal spores is of particular medical interest. In this study, a combination of UV resonance

DOI: 10.1021/acs.analchem.8b01038
Anal. Chem. 2018, 90, 8912−8918

Raman spectroscopy and chemometrical methods allowed for a highly accurate identification of fungal spores on a genus, species, and even strain level. In all analyzed classification models, strains grown on different agars were included. The promising results presented here indicate that the differentiation of spectra is not determined by the cultivation conditions, but instead based on the differences in the amounts of DNA, RNA, and protein aromatic amino acid units in spores of each species. Moreover, it has been demonstrated that darkly colored spores can be directly examined with UV-Raman spectroscopy, and the contribution of amorphous carbon in the spectra does not inhibit the correct identification of the spores. The obtained classification ratios in the range between 89% and 100% demonstrate that UV resonance Raman spectroscopy represents a powerful tool for fungal spore identification and should be considered for further investigations.

■ ASSOCIATED CONTENT

Supporting Information

The Supporting Information is available free of charge on the ACS Publications website at DOI: 10.1021/acs.analchem.8b01038.

Table S-1: Strains used in the study; Figure S-1: Images of dried spore biomass from the studied fungal species on the fused silica substrate; Figure S-2: Mean UV-Raman spectra and their double standard deviation of the *A. fumigatus* (A) and *P. rubens* (B) strains cultured on different media; Figure S-3: Accuracy as a function of the number of PCs for the genus level; Figure S-4: Accuracy as a function of the number of PCs for the species level; Figure S-5: Loading vectors for the species level model; and Figure S-6: Accuracy as a function of the number of PCs for the strain level (PDF)

■ AUTHOR INFORMATION

Corresponding Author

*Phone: +49 (0)3641-206309. Fax: +49 (0)3641-206399. E-mail: karina.weber@leibniz-ipht.de (K.W.).

ORCID

Olaf Kniemeyer: 0000-0002-9493-6402
Axel A. Brakhage: 0000-0002-8814-4193
Thomas W. Bocklitz: 0000-0003-2778-6624
Karina Weber: 0000-0003-4907-8645
Jürgen Popp: 0000-0003-4257-593X

Author Contributions

The manuscript was written through contributions of all authors. All authors have given approval to the final version of the manuscript.

Notes

The authors declare no competing financial interest.

■ ACKNOWLEDGMENTS

We gratefully acknowledge the Federal Ministry of Education and Research, Germany (BMBF) for the continued support for the InfectoGnostics (13GW0096F) and EXASENS (13N13856 and 13N13861) grants.

■ REFERENCES

(1) WHO. *Global Surveillance, Prevention and Control of Chronic Respiratory Diseases. A Comprehensive Approach*; WHO: Switzerland, 2007.
(2) Kohler, J. R., Casadevall, A., Perfect, J. *Cold Spring Harbor Perspect. Med.* **2015**, *5*, a019273
(3) Sorenson, W. G. *Environ. Health Perspect* **1999**, *107*, 469−472.
(4) Wilson, L. S.; Reyes, C. M.; Stolpman, M.; Speckman, J.; Allen, K.; Beney, J. *Value Health* **2002**, *5*, 26−34.
(5) Dales, R. E.; Cakmak, S.; Judek, S.; Dann, T.; Coates, F.; Brook, J. R.; Burnett, R. T. *Chest* **2003**, *123*, 745−750.
(6) Atkinson, R. W.; Strachan, D. P.; Anderson, H. R.; Hajat, S.; Emberlin, J. *Occup. Environ. Med.* **2006**, *63*, 580−590.
(7) Agarwal, R.; Hazarika, B.; Gupta, D.; Aggarwal, A. N.; Chakrabarti, A.; Jindal, S. K. *Med. Mycol.* **2010**, *48*, 988−994.
(8) Dean, T. R.; Betancourt, D.; Menetrez, M. Y. *J. Microbiol. Methods* **2004**, *56*, 431−434.
(9) Hernandez, A.; Martinez, J. L.; Mellado, R. P. *World J. Microbiol. Biotechnol.* **1999**, *15*, 33−36.
(10) Ward, E. *Methods Mol. Biol.* **2009**, *508*, 147−159.
(11) Williams, R. H.; Ward, E.; McCartney, H. A. *Appl. Environ. Microbiol.* **2001**, *67*, 2453−2459.
(12) Stockel, S.; Kirchhoff, J.; Neugebauer, U.; Rosch, P.; Popp, J. *J. Raman Spectrosc.* **2016**, *47*, 89−109.
(13) Muhamadali, H.; Subaihi, A.; Mohammadtaheri, M.; Xu, Y.; Ellis, D. I.; Ramanathan, R.; Bansal, V.; Goodacre, R. *Analyst* **2016**, *141*, 5127−5136.
(14) Guedes, A.; Ribeiro, H.; Fernandez-Gonzalez, M.; Aira, M. J.; Abreu, I. *Talanta* **2014**, *119*, 473−478.
(15) Ivleva, N. P.; Niessner, R.; Panne, U. *Anal. Bioanal. Chem.* **2005**, *381*, 261−267.
(16) Schulte, F.; Lingott, J.; Panne, U.; Kneipp, J. *Anal. Chem.* **2008**, *80*, 9551−9556.
(17) Verwer, P. E. B.; Leeuwen, W. B.; Girard, V.; Monnin, V.; Belkum, A.; Staab, J. F.; Verbrugh, H. A.; Bakker-Woudenberg, I.; Sande, W. W. J. *Eur. J. Clin. Microbiol. Infect. Dis.* **2014**, *33*, 245−251.
(18) De Gussem, K.; Vandenabeele, P.; Verbeken, A.; Moens, L. *Anal. Bioanal. Chem.* **2007**, *387*, 2823−2832.
(19) Ghosal, S.; Macher, J. M.; Ahmed, K. *Environ. Sci. Technol.* **2012**, *46*, 6088−6095.
(20) Wang, C. J.; Pan, Y. L.; Hill, S. C.; Redding, B. *J. Quant. Spectrosc. Radiat. Transfer* **2015**, *153*, 4−12.
(21) Ashton, L.; Hogwood, C. E. M.; Tait, A. S.; Kuligowski, J.; Smales, C. M.; Bracewell, D. G.; Dickson, A. J.; Goodacre, R. *J. Chem. Technol. Biotechnol.* **2015**, *90*, 237−243.
(22) Yazdi, Y.; Ramanujam, N.; Lotan, R.; Mitchell, M. F.; Hittelman, W.; Richards-Kortum, R. *Appl. Spectrosc.* **1999**, *53*, 82−85.
(23) Gaus, K.; Rosch, P.; Petry, R.; Peschke, K. D.; Ronneberger, O.; Burkhardt, H.; Baumann, K.; Popp, J. *Biopolymers* **2006**, *82*, 286−290.
(24) Lopez-Diez, E. C.; Goodacre, R. *Anal. Chem.* **2004**, *76*, 585−591.
(25) Walter, A.; Schumacher, W.; Bocklitz, T.; Reinicke, M.; Rosch, P.; Kothe, E.; Popp, J. *Appl. Spectrosc.* **2011**, *65*, 1116−1125.
(26) Manoharan, R.; Ghiamati, E.; Britton, K. A.; Nelson, W. H.; Sperry, J. F. *Appl. Spectrosc.* **1991**, *45*, 307−311.
(27) Domes, C.; Domes, R.; Popp, J.; Pletz, M. W.; Frosch, T. *Anal. Chem.* **2017**, *89*, 9997−10003.
(28) Frosch, T.; Schmitt, M.; Noll, T.; Bringmann, G.; Schenzel, K.; Popp, J. *Anal. Chem.* **2007**, *79*, 986−993.
(29) Harz, M.; Krause, M.; Bartels, T.; Cramer, K.; Rosch, P.; Popp, J. *Anal. Chem.* **2008**, *80*, 1080−1086.
(30) Neugebauer, U.; Schmid, U.; Baumann, K.; Holzgrabe, U.; Ziebuhr, W.; Kozitskaya, S.; Kiefer, W.; Schmitt, M.; Popp, J. *Biopolymers* **2006**, *82*, 306−311.
(31) Petry, R.; Mastalerz, R.; Zahn, S.; Mayerhofer, T. G.; Volksch, G.; Viereck-Gotte, L.; Kreher-Hartmann, B.; Holz, L.; Lankers, M.; Popp, J. *ChemPhysChem* **2006**, *7*, 414−420.
(32) Jahn, B.; Koch, A.; Schmidt, A.; Wanner, G.; Gehringer, H.; Bhakdi, S.; Brakhage, A. A. *Infect. Immun.* **1997**, *65*, 5110−5117.

DOI: 10.1021/acs.analchem.8b01038
Anal. Chem. 2018, 90, 8912−8918

(33) Langfelder, K.; Jahn, B.; Gehringer, H.; Schmidt, A.; Wanner, G.; Brakhage, A. A. *Med. Microbiol. Immunol.* **1998**, *187*, 79−89.
(34) Brakhage, A. A.; Vandenbrulle, J. *J. Bacteriol.* **1995**, *177*, 2781−2788.
(35) Schwartze, V. U.; Hoffmann, K.; Nyilasi, I.; Papp, T.; Vagvolgyi, C.; de Hoog, S.; Voigt, K.; Jacobsen, I. D. *PLoS One* **2012**, *7*, 11.
(36) R. D. C Team. *R*; R Foundation for Statistical Computing: Vienna, Austria, 2011.
(37) Ryan, C. G.; Clayton, E.; Griffin, W. L.; Sie, S. H.; Cousens, D. R. *Nucl. Instrum. Methods Phys. Res., Sect. B* **1988**, *34*, 396−402.
(38) Guo, S. X.; Bocklitz, T.; Neugebauer, U.; Popp, J. *Anal. Methods* **2017**, *9*, 4410−4417.
(39) Ferrari, A. C.; Robertson, J. *Phys. Rev. B: Condens. Matter Mater. Phys.* **2001**, *64*, 13.
(40) Harz, M.; Claus, R. A.; Bockmeyer, C. L.; Baum, M.; Rosch, P.; Kentouche, K.; Deigner, H. P.; Popp, J. *Biopolymers* **2006**, *82*, 317−324.
(41) Kumamoto, Y.; Taguchi, A.; Smith, N. I.; Kawata, S. *Biomed. Opt. Express* **2011**, *2*, 927−936.
(42) Wu, Q.; Hamilton, T.; Nelson, W. H.; Elliott, S.; Sperry, J. F.; Wu, M. *Anal. Chem.* **2001**, *73*, 3432−3440.
(43) Blackwell, M.; Vilgalys, R.; James, T. Y.; Taylor, J. W. Fungi. Eumycota: mushrooms, sac fungi, yeast, molds, rusts, smuts, etc., 2012. http://tolweb.org/.
(44) Brakhage, A. A. *Curr. Drug Targets* **2005**, *6*, 875−886.
(45) Van Der Linden, J. W. M.; Warris, A.; Verweij, P. E. *Med. Mycol.* **2011**, *49*, S82−S89.
(46) Mondon, P.; De Champs, C.; Donadille, A.; Ambroise-Thomas, P.; Grillot, R. *J. Med. Microbiol.* **1996**, *45*, 186−191.

DOI: 10.1021/acs.analchem.8b01038
Anal. Chem. 2018, 90, 8912−8918

Supporting Information

UV-Raman Spectroscopic Identification of Fungal Spores Important for Respiratory Diseases

Olga Žukovskaja, [†,‡,§] Sandra Kloß,[†] Matthew G. Blango, [‖] Oleg Ryabchykov, [†,§] Olaf Kniemeyer, [‖] Axel A. Brakhage, [‖,⊥] Thomas W. Bocklitz,[†,§] Dana Cialla-May,[†,‡,§] Karina Weber,[*,†,‡,§] and Jürgen Popp[†,‡,§]

[†] Institute of Physical Chemistry and Abbe Center of Photonics, Friedrich Schiller University Jena, Helmholtzweg 4, 07745 Jena, Germany;

[‡] Research Campus Infectognostic, Philosophenweg 7, 07743 Jena, Germany;

[§] Leibniz Institute of Photonic Technology Jena, Albert-Einstein-Str. 9, 07745 Jena, Germany;

[‖] Department of Molecular and Applied Microbiology, Leibniz Institute for Natural Product Research and Infection Biology (HKI), Adolf-Reichwein-Straße 23, 07745 Jena, Germany;

[⊥] Department of Microbiology and Molecular Biology, Institute for Microbiology, Friedrich Schiller University Jena, Neugasse 25, 07743 Jena, Germany;

*Corresponding Author: Phone: +49 (0)3641-206309, Fax: +49 (0)3641-206399, Email: karina.weber@uni-jena.de;

Table of Content:

Table S-1. Strains used in the study

Organism	Strain	Growth Media
Aspergillus fumigatus	CEA10	AMM
Aspergillus fumigatus	ATCC 46645	MA / AMM
Aspergillus fumigatus	ATCC 46645 with *pksP* mutation	AMM
Aspergillus fumigatus	D141	AMM
Aspergillus calidoustus	SF006504	AMM
Aspergillus niger	ATCC 6275	AMM
Aspergillus nidulans	A89	AMM[1]
Cladosporium herbarum	ATCC MYA-4682	MA / AMM
Alternaria alternata	ATCC 66981	AMM
Penicillium rubens	ATCC 28089	MA / AMM
Lichtheimia corymbifera	JMRC:FSU:9682	SUP
*AMM = *Aspergillus* minimal media; AMM[1]= AMM +Biotin +Arginine; MA = Malt Agar; SUP = SUP-modified Media		

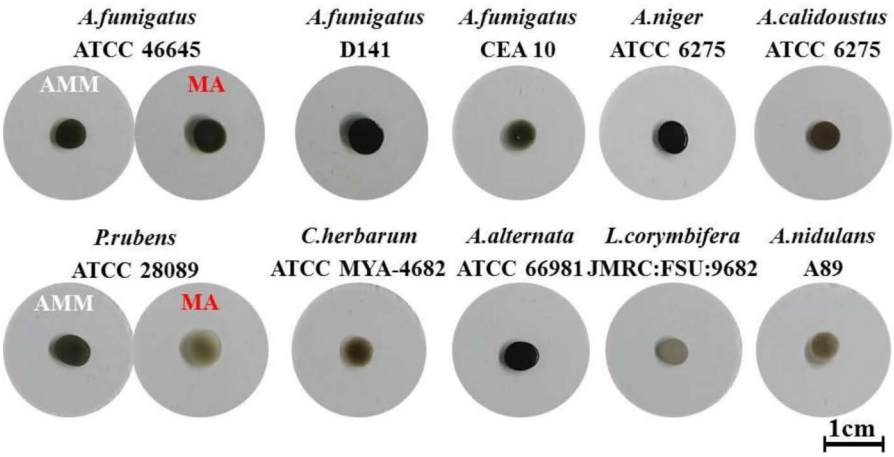

Figure S-1. Images of dried spore biomass from the studied fungal species on the fused silica substrate.

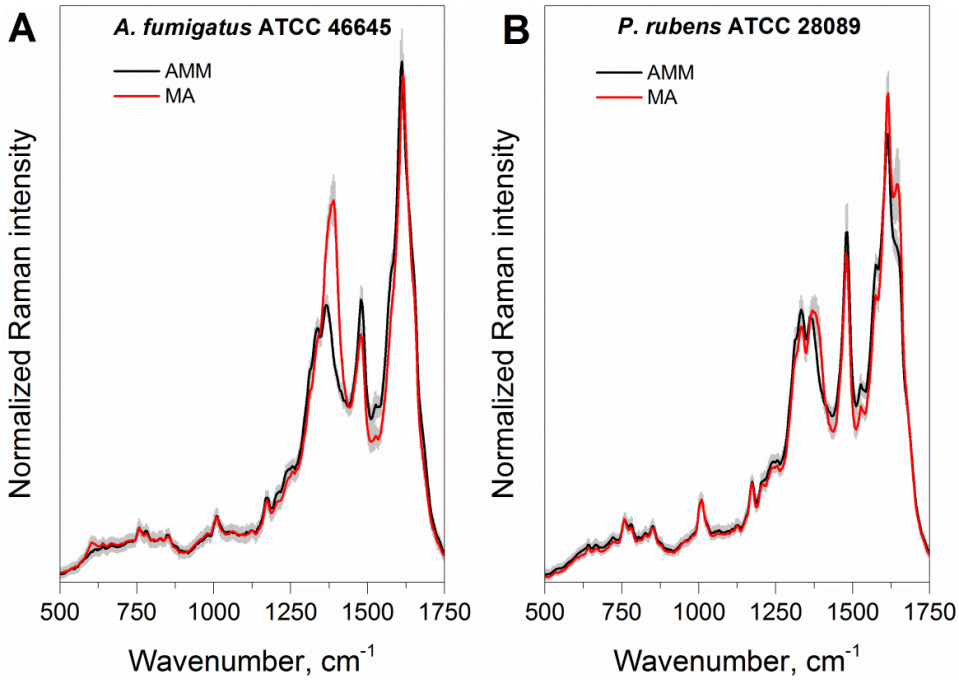

Figure S-2. Mean UV-Raman spectra and their double standard deviation of the *A. fumigatus* (A) and *P. rubens* (B) strains cultured on different media.

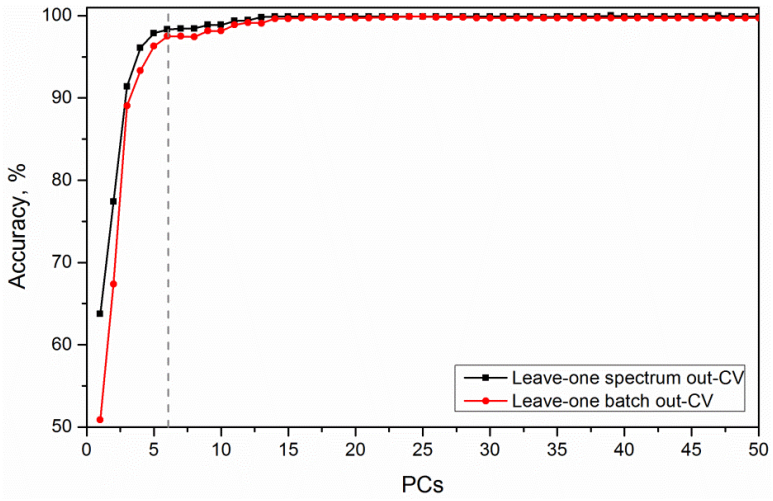

Figure S-3. Accuracy as a function of the number of PCs for the genus level.

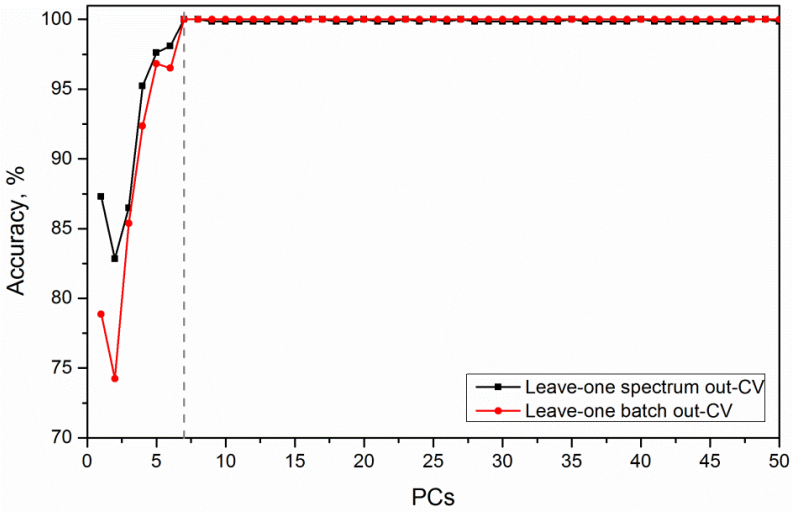

Figure S-4. Accuracy as a function of the number of PCs for the species level.

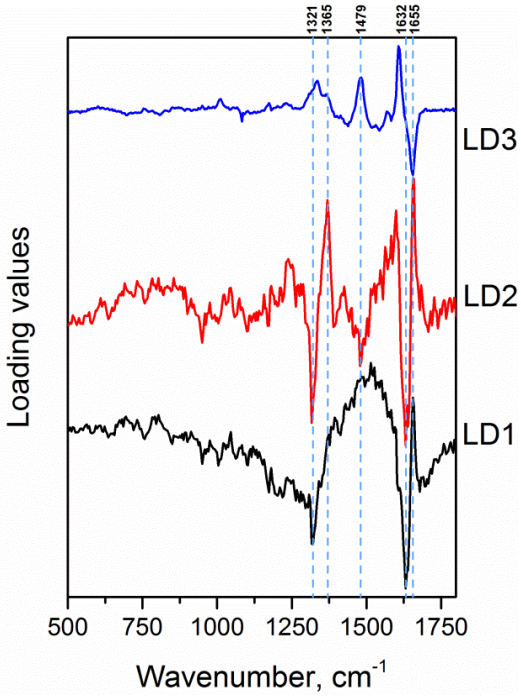

Figure S-5. Loading vectors for the species level model.

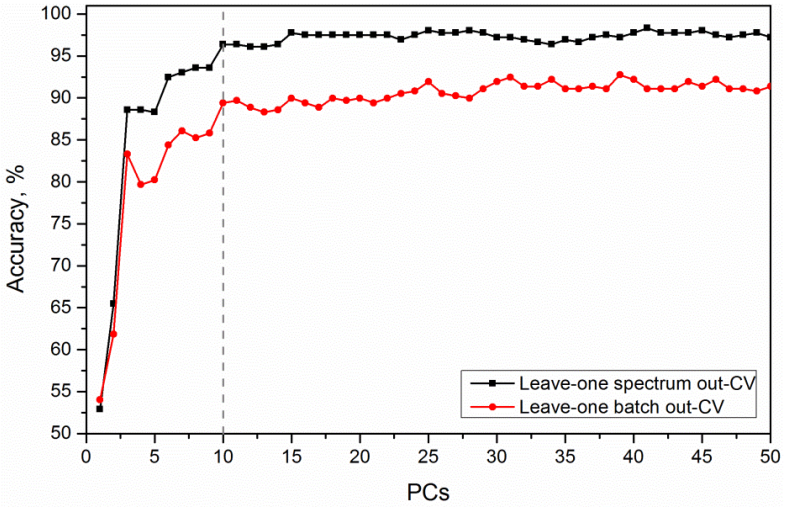

Figure S-6. Accuracy as a function of the number of PCs for the strain level.

7.2 Towards Raman spectroscopy of urine as a screening tool [OZ2]

Olga Žukovskaja, Oleg Ryabchykov, Maria Straßburger, Thorsten Heinekamp, Axel A. Brakhage, Christopher Hennings, Christian Hübner, Michael Wegmann, Dana Cialla-May, Thomas W. Bocklitz, Karina Weber, Jürgen Popp

Submitted to *Journal of Biophotonics* (16.04.2019).

Declaration on authorship and copyright in a cumulative doctoral thesis

[1]**Olga Žukovskaja**, [2]Oleg Ryabchykov, [3]Maria Straßburger, [4]Thorsten Heinekamp, [5]Axel A. Brakhage, [6]Christopher Hennings, [7]Christian Hübner, [8]Michael Wegmann, [9]Dana Cialla-May, [10]Thomas Bocklitz, [11]Karina Weber, [12]Jürgen Popp											
Involved in												
	1	2	3	4	5	6	7	8	9	10	11	12
Conceptual research design	X	X							X	X	X	X
Planning of research activities	X		X	X	X	X	X	X	X	X	X	X
Data collection	X											
Data analyses and interpretation	X	X								X		
Manuscript writing	X	X							X	X	X	X
Suggested publication equivalence value	**1.0**	0.5										

Author Contribution

Olga Žukovskaja	concept development Raman spectroscopic measurements data analysis and interpretation writing of manuscript
Oleg Ryabchykov	data analysis and interpretation proofreading of manuscript
Maria Straßburger	establishing of aspergillosis mouse model proofreading of manuscript
Thorsten Heinekamp	establishing of aspergillosis mouse model proofreading of manuscript
Axel A. Brakhage	establishing of aspergillosis mouse model proofreading of manuscript
Christopher Hennings	establishing of kidney disorders mouse model proofreading of manuscript
Christian Hübner	establishing of kidney disorders mouse model proofreading of manuscript
Michael Wegmann	establishing of asthma mouse model proofreading of manuscript
Dana Cialla-May	discussion of experimental concept and results proofreading of manuscript
Thomas W. Bocklitz	discussion of data analysis concepts and results proofreading of manuscript
Karina Weber	discussion of experimental concept and results proofreading of manuscript
Jürgen Popp	project management discussion of concepts and results discussion and proofreading of manuscript

Towards Raman spectroscopy of urine as screening tool

Olga Žukovskaja,[a,b,c] Oleg Ryabchykov,[a,c] Maria Straßburger,[d] Thorsten Heinekamp,[d] Axel A. Brakhage,[d,e] J. Christopher Hennings,[f] Christian A. Hübner,[f] Michael Wegmann,[g,h] Dana Cialla-May, [a,b,c] Thomas W. Bocklitz,[a,c] Karina Weber *[a,b,c] and Jürgen Popp [a,b,c]

[a] Institute of Physical Chemistry and Abbe Center of Photonics, Friedrich Schiller University Jena, Helmholtzweg 4, 07745 Jena, Germany;
[b] Research Campus Infectognostic, Philosophenweg 7, 07743 Jena, Germany;
[c] Leibniz Institute of Photonic Technology Jena - Member of the research alliance “Leibniz Health Technologies”, Albert-Einstein-Str. 9, 07745 Jena, Germany;
[d] Leibniz Institute for Natural Product Research and Infection Biology, Hans-Knöll-Institute, Beutenbergstr. 11a, 07745 Jena, Germany;
[e] Institute of Microbiology, Friedrich Schiller University Jena, D-07743 Jena, Germany
[f] Institut für Humangenetik, Universitätsklinikum Jena, Am Klinikum 1, 07747 Jena, Germany;
[g] Division of Asthma Exacerbation & Regulation, Program Area Asthma & Allergy, Leibniz-Center for Medicine and Biosciences, - Member of the research alliance “Leibniz Health Technologies”, Parkallee 1-40, 23845 Borstel, Germany;
[h] Airway Research Center North (ARCN), Member of the German Center for Lung Research, Borstel, Germany
* Corresponding author: karina.weber@leibniz-ipht.de

Abstract

For the screening purposes urine is an especially attractive biofluid, since it offers easy and non-invasive sample collection and provides a snapshot of the whole metabolic status of the organism, which may change under different pathological conditions. Raman spectroscopy (RS) has the potential to monitor these changes and utilize them for disease diagnostics. The current study utilizes mouse models aiming to compare the feasibility of the urine based RS combined with chemometrics for diagnosing kidney diseases directly influencing urine composition and respiratory tract diseases having no direct connection to urine formation. The diagnostic models for included diseases were built using principal component analysis with linear discriminant analysis and validated with a leave-one-mouse-out cross-validation approach. Considering kidney disorders, the accuracy of 100 % was obtained in discrimination between sick and healthy mice, as well as between two different kidney diseases. For asthma and invasive pulmonary aspergillosis achieved accuracies were noticeably lower, being, respectively, 77.27 % and 78.57 %. In conclusion, our results suggest that RS of urine samples not only provides a solution for a rapid, sensitive and non-invasive diagnosis of kidney disorders, but also holds some promises for the screening of non-urinary tract diseases.

Keywords: Raman spectroscopy, screening, urine, principal component analysis, linear discriminant analysis.

Introduction

Screening is the process by which unrecognized diseases or defects are identified, using tests, which can be applied rapidly for large numbers of people. In this context, the analysis of biofluids is particularly attractive, because they are rich in biochemical and biological information, offer minimal or non-invasive collection of samples and give a possibility to perform multiple screening tests. The rise in metabolomics demonstrated that metabolic profile of biofluids changes due to different pathological conditions and those changes can be utilized for diagnostic purposes.[1-3] Thus, there is a continuing effort devoted to the exploration of new technologies that can rapidly detect those changes.

In this field, Raman spectroscopy (RS) is a promising technique, since it provides a spectral "fingerprint" of the sample under investigation, which represents a snapshot of the biomolecular composition of the sample. Combining RS with multivariate statistical analysis, even minimal spectral changes from the 'normality' can be detected and correlated with the certain disease.[4-6] Moreover, it offers rapid and non-destructive analysis with minimal or no sample preparation, which is highly beneficial for the screening test. The literature provides numbers of examples of the successful application of biofluid based RS for screening of various cancer types, some infections and neurological diseases.[7-11] Blood serum and plasma samples are the most often used ones, because they provide an overview of the whole organism health status. However, some researchers assure that other biofluids, like urine, saliva or sputum, also should not be neglected. Among them urine is of high interest, because it allows a complete non-invasive sample collection procedure with no discomfort for the patient and it contains many metabolites, which physicochemical properties may vary due to some diseases.[12, 13]

RS of urine in terms of disease screening was rather slightly investigated and only few reports are available. Few studies performed RS analysis of urine aiming to assess the developing of kidney disease in patients with diabetes and hypertension. For this, quantitative information regarding important urine biomarkers (urea, creatinine, and

glucose) was obtained from Raman spectra and with a help of statistical models correlated with the renal impairment and other complications.[14-16] Except of this, RS based 'metabolic fingerprinting' of urine was used only for the screening of oral and breast cancer.[17, 18] Therefore, to assess the potential of urine based RS as a screening technique more precisely, a broader range of diseases should be investigated.

In this study, urine samples were considered for the RS based diagnosis from two groups of pathological states established in animal models. The first group included diseases in direct connection to the urine formation, namely, distal renal tubular acidosis (dRTA) and reversible nephrogenic diabetes insipidus (NDI) elicited by pharmacological intervention with excessive Lithium intake. Both disease states relate directly to the urine composition. NDI is characterized by the inability to concentrate the urine efficiently, leading to polyuria (excessive urine production) and polydipsia (excessive thirst),[19] while dRTA is characterized by defective renal acid-base regulation and as a result less acidic urine.[20] The second group considered diseases which possess no direct connection to the urine formation, namely, asthma and infection with *Aspergillus fumigatus* causing invasive pulmonary aspergillosis. Asthma is a chronic inflammatory disorder, which affects 339 million people in all regions of the world[21] and aspergillosis is a life-threatening fungal infection predominantly affecting immunocompromised patients.[22, 23] For both diseases, the access to easy screening test could lead to early intervention and better disease management.

The aim of this study is to investigate and compare the potential of urine based RS for the diagnosis of the mentioned diseases. Here, animal models were utilized, since they allow controlling the experiment parameters employing a defined model, before starting with a clinical study. Classification models were built using principal component analysis (PCA) followed by linear discriminant analysis (LDA) and evaluated with a leave-one mouse-out cross-validation (LOMOCV). The presented results identify that, although urine based RS are more suitable to diagnose diseases having direct and specific correlation with urine composition, spectroscopic screening of other diseases holds some potential as well.

Materials and methods

Animals. The urine samples of mice used within this study were provided from three different laboratories. All animals were cared for in accordance with the European animal welfare regulation and all experiments were approved by the responsible local authorities of Thuringia or Schleswig-Holstein States of Germany. All mice, except of the ones with DRTA disease, were supplied by Charles River, Germany. A brief description about the animals and treatment protocols is provided in **Table 1**.

Table 1 Description of the included mice models.

Model	Groups	Treatment	Mice type	Age	Number of mice
Kidney disorders	Control	no	C57BL/6J	3 months	4
	Nephrogenic diabetes insipidus (NDI)	1 week with 40 mM LiCl- and 3 weeks with 60 mM LiCl-supplemented diet	C57BL/6J	3 months	4
	Distal renal tubular acidosis (dRTA)	0.14 M Sodium bicarbonate during the first 2 months of age	Atp6v0a4-deficient	2.5 months	10
Aspergillosis	Control	Immunosuppression with cortisone acetate	CD-1 mice	6-8 weeks	4
	Aspergillosis	Immunosuppression with cortisone acetate + exposure to *A. fumigatus* conidia	CD-1 mice	6-8 weeks	10
Asthma	Control	Injection of PBS	BALB/c	6-8 weeks	11
	Asthma	Injection of OVA Exposure to 1% OVA aerosol	BALB/c	6-8 weeks	11

Kidney disorder models (NDI and dRTA). NDI in mice was induced according to Trepiccione *et al.[24]* Briefly, mice were fed a diet containing 40 mM/kg LiCl for one week and then 60 mM/kg LiCl for three weeks. Control mice received a LiCl-free mouse chow with otherwise identical ingredients. Water was provided *ad libitum*. As model of dRTA Atp6v0a4-deficient mice were used. Generation of those mice is described in Hennings *et al.*[25] For all mice urine was collected during 24 h using metabolic cages, frozen immediately after collection and stored at -80°C.

Invasive Pulmonary Aspergillosis model. Mice were immunosuppressed with two single doses of 1 g/kg body weight cortisone acetate (Sigma-Aldrich Chemie GmbH, Taufkirchen, Germany), which were injected intraperitoneally (i.p.) three days before and immediately prior to infection with *A. fumigatus*. Afterwards the mice were anesthetized intraperitoneally by an anesthetic combination of midazolam, fentanyl, and medetomidine. 2 x 10^5 conidia in 20 µl PBS were applied to the nares of the mice. Anesthesia was terminated by subcutaneous injection of flumazenil, naloxon and atipamezol. The infected animals were monitored at least twice a day

and humanely sacrificed if moribund (defined by severe lethargy, severe dyspnea, or hypothermia). A group of PBS infected mice served as control. Pathological changes in the lungs were recorded during postmortem analysis. The spontaneous urine was collected in sterile Petri dishes during the handling or invasively after sacrification. The urine samples were frozen immediately after collection and stored at -80°C.

Asthma mouse model. Mice were sensitized by i.p. injection of Ovalbumin (OVA) (Grade VI; Sigma-Aldrich Chemie GmbH, Munich, Germany) adsorbed to aluminium hydroxide (Imject Alum Adjuvant, Thermo Scientific Inc., Pierce Biotechnology, Rockford, IL, USA) in 200 µL sterile Dulbecco's phosphate-buffered saline (PBS) on days 1, 14, and 21 as described previoulsy.[26] The control group received sterile PBS via i.p. injection at the indicated time points. In order to induce allergic airway inflammation and formation of experimental allergic asthma, sensitized mice were subsequently exposed to a 1% OVA-aerosol (1% w/v in PBS) on days 26 to 28. The spontaneous urine was collected in sterile Petri dishes after one, five and nine days after exposure to 1% OVA-aerosol, frozen and stored at -80°C.

Spectral acquisition. After passive thawing, raw urine samples were subjected to Raman spectroscopy by analyzing two separated droplets of 2 µl of the sample deposited on a calcium fluoride slide and letting them dry at room temperature. Raman spectra were recorded using a Renishaw inVia Raman system equipped with 785 nm excitation laser and using a 1200 lines/mm grating. The samples were illuminated via a microscope equipped with a 50× magnification objective (Leica) with a numerical aperture of 0.75. The laser power at the laser head was ca. 300 mW. For every sample 3 scans of different areas of the dried droplets were performed with a step size of 20 µm, resulting in ca. 1200 spectra per sample. The integration time for every spectrum was 2 s.

Data Analysis. Prior to the statistical analysis, the spectra were preprocessed in order to improve the robustness and stability of the results.[27] The data processing was performed using an in-house developed script in the programming language R.[28] First, we removed the most corrupted spectra which contained signal intensities larger than upper limit of the detector range. These removed spectra featured either extremely large fluorescence background or highly intense cosmic ray spikes. After removing the most corrupted spectra, the wavenumber axis was calibrated using the Raman spectrum of the standard 4-acetamidophenol, which were collected on each day of measurement.[29] The calibrated Raman spectra were background corrected using the sensitive nonlinear iterative peak (SNIP) clipping algorithm with a second-order clipping

filter.[30] Next, all spectra were vector normalized and used as input for a PCA, which was performed to reduce the dimensionality of the data while retaining the most significant information for classification. The PCA was followed by a LDA.[31] The performance of the created LDA model for the classification of healthy and disease samples was estimated using a leave-mouse-out-cross-validation (LMOCV) approach.[32] In this method, the spectra of a mouse were held out from the data set, and the LDA model was redeveloped using the remaining spectra. The resultant model was then used to predict the spectra of the removed mouse. This process was repeated with every mouse until all spectra were classified. A LMOCV of a PCA-LDA model was performed for number of principle components (PCs) from 1 to 50. Then, an optimal number of PCs was chosen by finding a saturation point of the accuracy as a function of the PC number (see **Figures S1, S2, S3, S4** in the supplementary material). For spectral comparison across the groups, mean Raman spectra for each group were calculated using preprocessed, normalized spectra of all samples.

Results and discussion

The urine of healthy individuals consists primarily of water (approximately 96 %) with high concentrations of urea (from amino acid metabolism), inorganic salts (chloride, sodium, and potassium), creatinine, ammonia, organic acids, various water-soluble toxins and pigmented products of hemoglobin breakdown, including urobilin, which gives urine its characteristic color.[33] Since some variations in the urine composition can be brought by diet and hydration level of the individual, for this proof of concept study we utilized an animal model, which allows having more defined and controllable experimental parameters. The disease models presented here were established in different laboratories using different types of mice. Moreover, for asthma and aspergillosis models even not sick mice were somehow treated to be a proper control. Therefore, to evaluate if it is possible to analyze all models together, firstly, the urine samples from the control groups of the mice were compared. To collect a large amount of spectra from each sample, thereby characterizing their intrinsic heterogeneity, Raman spectral mapping was performed. **Figure 1 (a)** shows the mean Raman spectra obtained for each control group. For all mice the most prominent component in the urine Raman spectra is urea, which exhibits an intensive band around 1003 cm^{-1} and bands at 589, 1162, 1605 cm^{-1}. The peaks at 839 and 1046 cm^{-1} can be assigned to creatinine, while the Raman peaks at 872 and 1076 cm^{-1} may

be attributed to nitrogenous compounds.[34, 35] Comparing mean Raman spectra among the mice groups, one can notice that spectral variations for the control mice for kidney disorder model were much lower. For this, two reasons can be pointed out: firstly, those mice were healthy and had no treatment and, secondly, their urine was collected in metabolic cages during 24 h. Thus, variations in urine composition are balanced over the day. Control mice for asthma and aspergillosis models were somehow treated and mice included in those groups could react different to the treatment, which could affect the urine composition and subsequent spectral deviations.

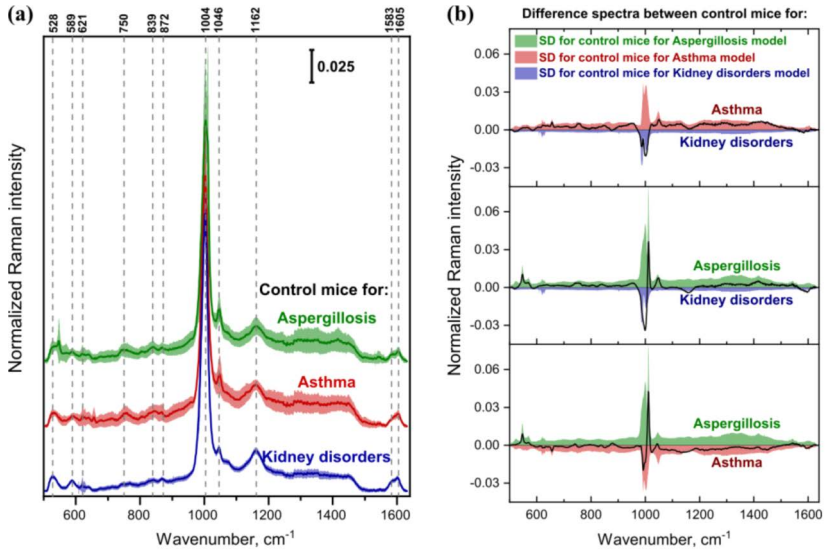

Figure 1 (a) Mean Raman spectra of the urine samples obtained from control mice for different disease models together with the standard deviation (SD) (shaded area); **(b)** Difference spectra between the mean urine spectra of control mice for different disease models with SD of the groups.

To better highlight differences between control mice of different models, difference spectra have been generated and are shown in **Figure 1 (b)**. One can observe that there are clear differences between different models, particularly when it comes to peak intensities. To support visual comparison, advanced multivariate data analysis was applied. Here, firstly, the data was reduced by a PCA using 11 PCs (**Figure S1**) and, next, LDA was performed. In order to evaluate the PCA-LDA model a leave-mouse-out-cross-validation (LMOCV) was applied. Thereby, the data from one mouse was removed from the data set and the LDA model was trained with the remaining data. The spectral data of the taken out mouse was subsequently predicted. This allowed for different mouse permutations for validation and gave a reliable unbiased classification model. **Table S1** shows that perfect

classification accuracy for mice from different models was achieved. This leads to the conclusion that the control mice of the included models are very different and it is not correct to evaluate different disease models together, since the potential discrimination might be caused not by differences in diseases but by other factors. Therefore, three disease models were considered separately.

The kidney disorder cohort included healthy mice and mice with two different kidney disease states. Four mice, due to nutrition with LiCl-supplemented diet, developed NDI and 10 other mice were Atp6v0a4 deficient, resulting in dRTA. **Figure 2 (a)** demonstrates the mean urine spectra for healthy mice and the ones having one of two kidney disease states, while in the **Figure 2 (b)** difference spectra among those groups are depicted. From the difference spectra it is obvious that urine from mice with induced kidney problem or dRTA have a lower urea concentration but higher concentration of other components. Urine from mice with Atp6v0a4 deficient mice was less acidic and contained more proteins, especially albumin.[25] Therefore, peaks around 835 and 1404 cm^{-1}, which are clearly more intensive for the dRTA mice, can be tentatively assigned to protein compounds.

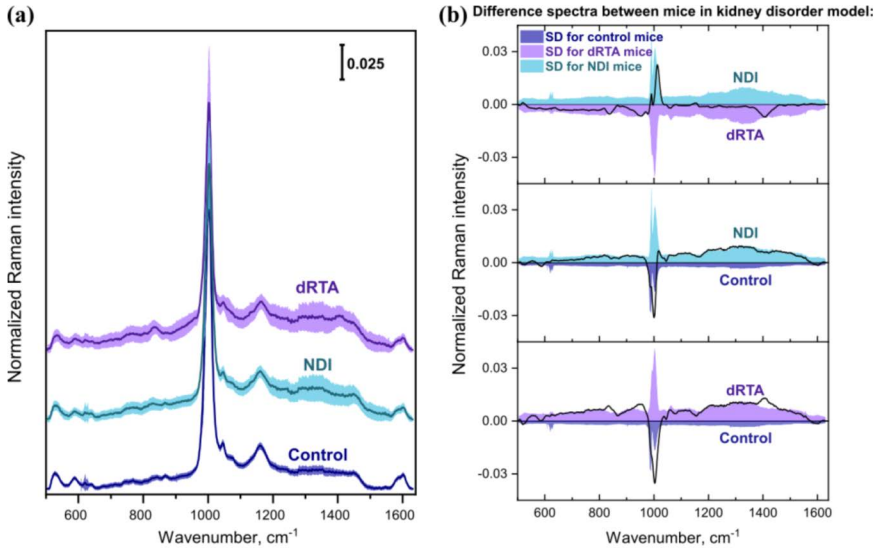

Figure 2 (a) Mean Raman spectra of the urine samples obtained from control mice and the ones having NDI or dRTA, plotted together with the standard deviation (SD) (shaded area); **(b)** Difference spectra between the mean urine spectra of mice with kidney disorders and control ones with SD of the groups.

To get more objective and automatic differentiation of the discussed kidney disorders, the already introduced PCA-LDA model was used. Here, the number of PCs was set to 6

(**Figure S2**). Because the PCA/LDA model assigns the spectra individually, firstly, the classification on spectral level was performed and after evaluation of the model with LMOCV resulted in overall accuracy of 95.85 % (**Table S2**). However, ultimately, the goal of the study is to determine an individual health status of a mouse. Therefore, the initial results must be aggregated in order to predict the disease at the mouse level. Here, a procedure must be applied to combine the predictions on the spectra level to a mouse level prediction. Within this study a voting scheme was utilized, which uses a threshold on the relative frequency of predictions. We used 50 % as threshold; thus, a single mouse is classified as healthy or sick if at least 50 % of its spectra are assigned to that group. The results of such classification on mouse level are shown in **Table 2**. Although the cohort size is limited, the classification accuracy is 100 % for differentiating between healthy and sick mice, as well as between NDI and dRTA mice. This indicates that urine based RS can not only successfully diagnose kidney disease states but also provide more exact diagnosis within the wide spectrum of them.

Table 2 Results of the mouse level classification model for kidney disorders evaluated with LMOCV.

		True				
		Control	**NDI**	**dRTA**	**Sensitivity**	**Specificity**
Predicted	**Control**	**4**	0	0	**100 %**	**100 %**
	NDI	0	**4**	0	**100 %**	**100 %**
	dRTA	0	0	**10**	**100 %**	**100 %**

Such good results for the kidney disorder model were rather expectable, since it is known that those diseases directly influence the composition of urine and changes therein can be depicted with RS. More intriguing is the question whether RS of urine can provide enough information for the diagnosis of diseases with no direct connection to kidney function. To answer that question two mouse models of respiratory tract disorders were used. Firstly, aspergillosis infection was considered. Similar as before, the analysis started from having a look on the mean urine spectra from control and with *A. fumigatus* infected mice, which are depicted in **Figure 3 (a)**, as well as on their difference spectrum shown in **Figure 3 (b)**. The mean spectra for those two groups are very similar in general spectral shape and peak positions. From **Figure 3 (b)** one can easily notice that the difference spectrum is less intense comparing with the ones for the kidney disorder model. Moreover, it is few times lower than spectral variations within the group, which are

demonstrated by the standard deviations (SD) and originate from the intra- and inter-sample heterogeneity. Therefore, here more than ever, the application of multivariate statistical analysis for the classification is required.

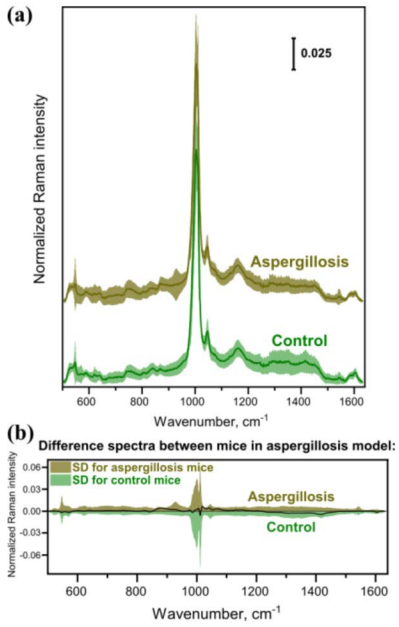

Figure 3 (a) Mean Raman spectra of the urine samples obtained from control and aspergillosis mice, plotted together with the standard deviation (SD) (shaded area); **(b)** Difference spectrum between the mean urine spectra of mice with aspergillosis and control ones (black solid line), plotted together with SD of both groups (shaded areas).

To build a classification model 11 PCs were selected (**Figure S3**) and the final results on spectral level are shown in **Table S3** and on mouse level in **Table 3**. It can be seen that for two mice false positive diagnosis took place, meanwhile one sick mouse was misclassified as healthy, which led to 50 % sensitivity and 90 % specificity of the model. Thought for the screening techniques higher specificity is in favour, since it guarantees that no disease cases will be missed, a sensitivity of 50 % is critical, because it leads to unnecessary stress for individuals and increased costs for subsequent more precise diagnostic tests.

Table 3 Results of the mouse level classification model for aspergillosis infection evaluated with LMOCV.

		True			
		Control	**Aspergillosis**	**Sensitivity**	**Specificity**
Predicted	**Control**	**2**	1	**50.00 %**	**90.00 %**
	Aspergillosis	2	**9**	**90.00 %**	**50.00 %**

Trying to find the reason for the false negative result for one mouse the medical information for the infected mice were rechecked and it appeared that this mouse, although it was infected with *A. fumigatus* conidia, did not show any signs of the infection, which was proved by pathological check of the lungs. The same happened with one more mouse but it still was classified correctly. Additionally one mouse developed only light infection. Knowing those facts could be presumed that built classification model got confused due to presence of not sick or lightly sick mice in the aspergillosis group. To check this hypothesis these three mice were excluded from the data set and the model was rebuilt for the remaining really sick mice. For building the LDA model 7 PCs were used (**Figure S4**) and after the evaluation with LMOCV the accuracy of 100 % on mouse level was reached (**Table S4**).

Finally, the RS was utilized for the asthma model. The potential of RS to diagnose asthma was demonstrated for blood serum samples with achieved 80.6 % accuracy discriminating between healthy people and patients with mild asthma.[36] However, the use of urine would be even more beneficial, especially for children, due to easy collection and possibility for multiple testing. For this study mouse urine samples were collected 1, 5 or 9 days after allergen exposure. The mean Raman spectra of control mice and the ones with induced asthma are demonstrated in **Figure 4 (a)**, followed by the difference spectrum between the groups shown in **Figure 4 (b)**. Similarly as for the aspergillosis model, the difference spectrum is lower than the SD of the both groups and visual comparison of the spectra is not suitable for the discrimination of asthmatic mice.

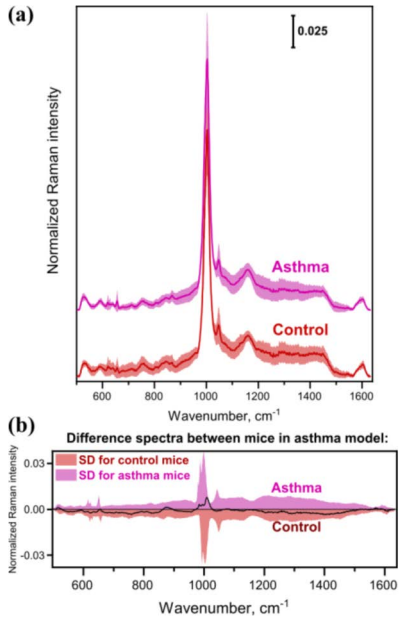

Figure 4 (a) Mean Raman spectra of the urine samples obtained from control mice and mice with asthma, plotted together with the standard deviation (SD) (shaded area); **(b)** Difference spectrum between the mean urine spectra of mice with asthma and control ones (black solid line) plotted together with SD of the both groups (shaded areas).

A LDA classification model was created with 7 PCs (**Figure S5**) and the results achieved after evaluation with LMOCV are summarized in **Table S5** on spectral level and in **Table 4** for each mouse. It can be seen that three control mice were classified as sick and two sick mice were assigned to the healthy ones. This resulted in sensitivity of 72.73 %, specificity of 81.82 % and final model accuracy of 77.27 %.

Table 4 Results of the spectral level classification model for aspergillosis infection evaluated with LMOCV.

		True			
		Control	**Asthma**	**Sensitivity**	**Specificity**
Predicted	**Control**	**8**	2	**72.73 %**	**81.82 %**
	Asthma	3	**9**	**81.82 %**	**72.73 %**

To check, which exactly mice were misclassified, the percentage of correctly classified spectra per mouse was calculated and presented in the **Table S6**. It can be seen that urine collected after the first day after exposure to the allergen, provided correct diagnosis for all mice, while one false negative classification appeared using urine of the fifth day and the second mistake using urine of the ninth day. This somehow correlates with medical

prognosis of asthma, which states that severe allergic reaction is most possible during first days after the contact with allergens and with the time organism starts to recover. However, to evaluate such correlation, a more detailed study is required involving much larger cohorts of subjects.

Conclusions

Within this study the applicability of urine based RS for diagnosis of kidney and respiratory tract diseases was investigated utilizing mouse models. Raman spectra were acquired from unprocessed dried urine samples and a PCA-LDA model was built. To ensure the reliability of the results the model was validated using a LMOCV approach. Considering kidney disorders perfect classification was achieved not only for distinguishing between healthy and sick mice but also for identifying the exact kidney disease from two included in the model. Such good results can be explained by the direct connection of kidney function to urine composition. For respiratory tract diseases, which included aspergillosis and asthma, already worse results were achieved reaching 78.57 % and 77.27 % accuracies, respectively. However, for both models occurred false negative results could be up to some level explained from medical data of mice, such as not developing of the infection in mice infected with *A. fumigatus* or possible recovery from the allergic asthma with time. Overall promising results were obtained, and more detailed clinical studies in this direction should be considered to develop urine based RS as a screening tool and path the way for further Raman based disease diagnostics.

Conflicts of interest

There are no conflicts to declare.

Acknowledgements

The funding of the grants InfectoGnostics (13GW0096F), InfectControl 2020 (03ZZ0803A) and EXASENS (13N13856) by the Federal Ministry of Education and Research, Germany (BMBF) supporting this study is gratefully acknowledged.

References

[1] S. Medina, R. Dominguez-Perles, J. I. Gil, F. Ferreres, A. Gil-Izquierdo *Curr Med Chem*. **2014**, *21*, 823-848.

[2] A. Zhang, H. Sun, P. Wang, Y. Han, X. Wang *J Proteomics*. **2012**, *75*, 1079-1088.

[3] A. H. Zhang, H. Sun, X. J. Wang *Anal. Bioanal. Chem.* **2012**, *404*, 1239-1245.

[4] M. J. Baker, S. R. Hussain, L. Lovergne, V. Untereiner, C. Hughes, R. A. Lukaszewski, G. Thiéfin, G. D. Sockalingum *Chem. Soc. Rev.* **2016**, *45*, 1803-1818.

[5] K. Kong, C. Kendall, N. Stone, I. Notingher *Adv. Drug Deliv. Rev.* **2015**, *89*, 121-134.

[6] L. B. Leal, M. S. Nogueira, R. A. Canevari, L. F. C. S. Carvalho *Photodiagnosis Photodyn Ther*. **2018**, *24*, 237-244.

[7] J. L. Gonzalez-Solis, J. C. Martinez-Espinosa, J. M. Salgado-Roman, P. Palomares-Anda *Lasers Med. Sci.* **2014**, *29*, 1241-1249.

[8] S. Khan, R. Ullah, A. Khan, R. Ashraf, H. Ali, M. Bilal, M. Saleem *Photodiagnosis Photodyn Ther*. **2018**, *23*, 89-93.

[9] K. Naseer, A. Amin, M. Saleem, J. Qazi *Spectrochimica acta. Part A, Molecular and biomolecular spectroscopy*. **2019**, *206*, 197-201.

[10] E. Ryzhikova, O. Kazakov, L. Halamkova, D. Celmins, P. Malone, E. Molho, E. A. Zimmerman, I. K. Lednev *J. Biophotonics*. **2015**, *8*, 584-596.

[11] H. Wang, S. Zhang, L. Wan, H. Sun, J. Tan, Q. Su *Spectrochimica acta. Part A, Molecular and biomolecular spectroscopy*. **2018**, *201*, 34-38.

[12] S. Bouatra, F. Aziat, R. Mandal, A. C. Guo, M. R. Wilson, C. Knox, T. C. Bjorndahl, R. Krishnamurthy, F. Saleem, P. Liu, Z. T. Dame, J. Poelzer, J. Huynh, F. S. Yallou, N. Psychogios, E. Dong, R. Bogumil, C. Roehring, D. S. Wishart *PLoS ONE*. **2013**, *8*, e73076.

[13] A. Zhang, H. Sun, X. Wu, X. Wang *Clin. Chim. Acta*. **2012**, *414*, 65-69.

[14] J. A. M. Bispo, E. E. D. Vieira, L. Silveira, A. B. Fernandes *J. Biomed. Opt.* **2013**, *18*.

[15] C. J. Saatkamp, M. L. d. Almeida, J. A. M. Bispo, A. L. B. Pinheiro, A. B. Fernandes, L. Silveira, Quantifying creatinine and urea in human urine through Raman spectroscopy aiming at diagnosis of kidney disease, SPIE, **2016**.

[16] E. E. D. Vieira, J. A. M. Bispo, L. Silveira, A. B. Fernandes *Lasers Med. Sci.* **2017**, *32*, 1605-1613.

[17] T. Bhattacharjee, A. Khan, G. Maru, A. Ingle, C. M. Krishna *Analyst*. **2015**, *140*, 456-466.

[18] B. Elumalai, A. Prakasarao, B. Ganesan, K. Dornadula, S. Ganesan *J. Raman Spectrosc.* **2015**, *46*, 84-93.

[19] C. Kavanagh, N. S. Uy *Pediatr. Clin. North Am.* **2019**, *66*, 227-234.

[20] J. Yaxley, C. Pirrone *Ochsner J.* **2016**, *16*, 525-530.

[21] G. A. Network in The Global Asthma Report 2018, Vol. (Ed.^Eds.: Editor), City, **2018**.

[22] R. AllergyAli, F. Ozkalemkas, T. Ozcelik, V. Ozkocaman, A. Ozkan, S. Bayram, B. Ener, A. Ursavas, G. Ozal, A. Tunali *Ann. Clin. Microbiol. Antimicrob.* **2006**, *5*, 17-17.

[23] G. A. Kliasova, N. A. Petrova, G. M. Galstian, L. N. Gotman, E. S. Vishnevskaia, E. P. Sysoeva, N. D. Khoroshko, E. A. Mikhailova, E. N. Parovichnikova, V. G. Isaev *Ter Arkh*. **2003**, *75*, 63-68.

[24] F. Trepiccione, G. Capasso, S. Nielsen, B. M. Christensen *Am. J. Physiol. Renal Physiol.* **2013**, *305*, F919-F929.

[25] J. C. Hennings, N. Picard, A. K. Huebner, T. Stauber, H. Maier, D. Brown, T. J. Jentsch, R. Vargas-Poussou, D. Eladari, C. A. Hübner *EMBO Mol. Med.* **2012**, *4*, 1057-1071.

[26] L. Lunding, S. Webering, C. Vock, A. Schroder, D. Raedler, B. Schaub, H. Fehrenbach, M. Wegmann *Allergy*. **2015**, *70*, 366-373.

[27] T. Bocklitz, A. Walter, K. Hartmann, P. Rösch, J. Popp *Anal. Chim. Acta*. **2011**, *704*, 47-56.

[28] R. D. C. Team. **2011**.

[29] T. W. Bocklitz, T. Dörfer, R. Heinke, M. Schmitt, J. Popp *Spectrochim. Acta A*. **2015**, *149*, 544-549.

[30] C. G. Ryan, E. Clayton, W. L. Griffin, S. H. Sie, D. R. Cousens *Nucl Instrum Methods Phys Res B*. **1988**, *34*, 396-402.

[31] T. W. Bocklitz, S. Guo, O. Ryabchykov, N. Vogler, J. Popp *Anal. Chem.* **2016**, *88*, 133-151.

[32] S. Guo, T. Bocklitz, U. Neugebauer, J. Popp *Anal. Methods*. **2017**, *9*, 4410-4417.

[33] D. F. Putnam *NASA Contractor Report No. NASA CR-1802*. **1971**.

[34] L. P. Moreira, L. Silveira, Jr., A. G. da Silva, A. B. Fernandes, M. T. T. Pacheco, D. Rocco *J Photochem Photobiol B*. **2017**, *176*, 92-99.

[35] W. R. Premasiri, R. H. Clarke, M. E. Womble *Lasers Surg Med.* **2001**, *28*, 330-334.

[36] A. Sahu, K. Dalal, S. Naglot, P. Aggarwal, C. Murali Krishna *PLoS ONE*. **2013**, *8*, e78921-e78921.

Supporting Information

Towards Raman spectroscopy of urine as screening tool

Olga Žukovskaja,[a,b,c] Oleg Ryabchykov,[a,c] Maria Straßburger,[d] Thorsten Heinekamp,[d] Axel A. Brakhage,[d,e] J. Christopher Hennings,[f] Christian A. Hübner,[f] Michael Wegmann,[g,h] Dana Cialla-May,[a,b,c] Thomas W. Bocklitz,[a,c] Karina Weber*[a,b,c] and Jürgen Popp[a,b,c]

a. Institute of Physical Chemistry and Abbe Center of Photonics, Friedrich Schiller University Jena, Helmholtzweg 4, 07745 Jena, Germany;
b. Research Campus Infectognostic, Philosophenweg 7, 07743 Jena, Germany;
c. Leibniz Institute of Photonic Technology Jena - Member of the research alliance "Leibniz Health Technologies", Albert-Einstein-Str. 9, 07745 Jena, Germany;
d. Leibniz Institute for Natural Product Research and Infection Biology, Hans-Knöll-Institute, Beutenbergstr. 11a, 07745 Jena, Germany;
e. Institute of Microbiology, Friedrich Schiller University Jena, D-07743 Jena, Germany
f. Institut für Humangenetik, Universitätsklinikum Jena, Am Klinikum 1, 07747 Jena, Germany;
g. Division of Asthma Exacerbation & Regulation, Program Area Asthma & Allergy, Leibniz-Center for Medicine and Biosciences, - Member of the research alliance "Leibniz Health Technologies", Parkallee 1-40, 23845 Borstel, Germany;
h. Airway Research Center North (ARCN), Member of the German Center for Lung Research, Borstel, Germany

*Corresponding author: karina.weber@leibniz-ipht.de

Table of Content:

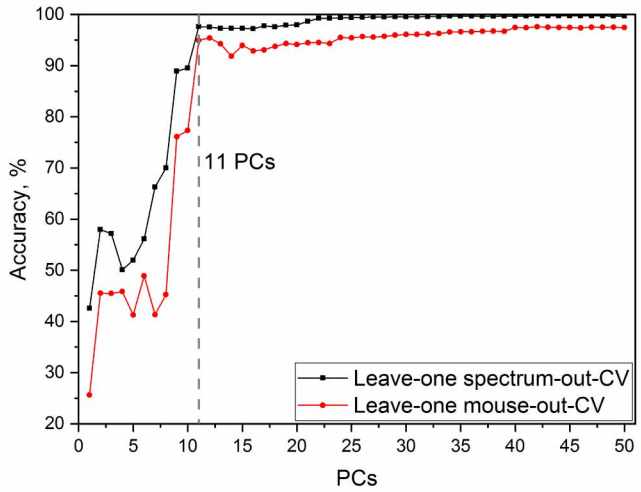

Figure S1. PCA/LDA model accuracy as the function of PCs for control mice from different disease models.

Table S1. Results of the mouse (spectral) level classification model for control mice for different diseases evaluated with leave-one mouse-out-CV.

Predicted \ True	Aspergillosis control	Asthma control	Kidney disorder control	Sensitivity, %	Specificity, %
Aspergillosis control	**4 (20572)**	0 (148)	0 (0)	**100 (89.76)**	**100 (99.58)**
Asthma control	0 (573)	**11 (24082)**	0 (5)	**100 (97.67)**	**100 (98.26)**
Kidney disorder control	0 (1774)	0 (426)	**4 (10362)**	**100 (99.95)**	**100 (95.38)**

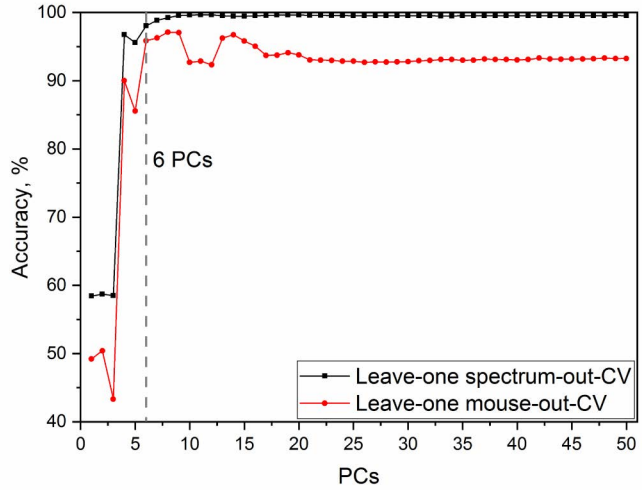

Figure S2. PCA/LDA model accuracy as the function of PCs for kidney disorder model.

Table S2. Results of the spectral level classification model for kidney disorders evaluated with LMOCV.

		True				
		Control	**NDI**	**DRTA**	**Sensitivity, %**	**Specificity, %**
Predicted	**Control**	**9931**	652	1023	**95.79**	**96.03**
	NDI	380	**10816**	42	**94.09**	**98.97**
	DRTA	56	27	**29640**	**96.53**	**99.62**

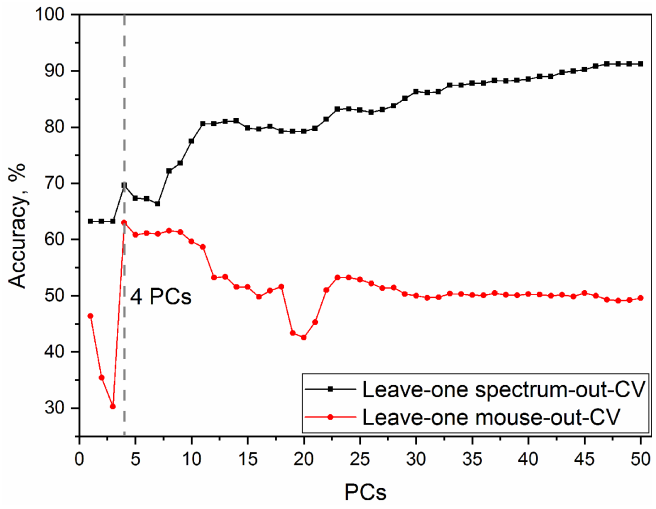

Figure S3. PCA/LDA model accuracy as the function of PCs for aspergillosis model.

Table S3. Results of the spectral level classification model for aspergillosis evaluated with LMOCV.

		True			
		Control	**Aspergillosis**	**Sensitivity, %**	**Specificity, %**
Predicted	**Control**	**10989**	11119	**47.95**	**71.76**
	Aspergillosis	11930	**28253**	**71.76**	**47.95**

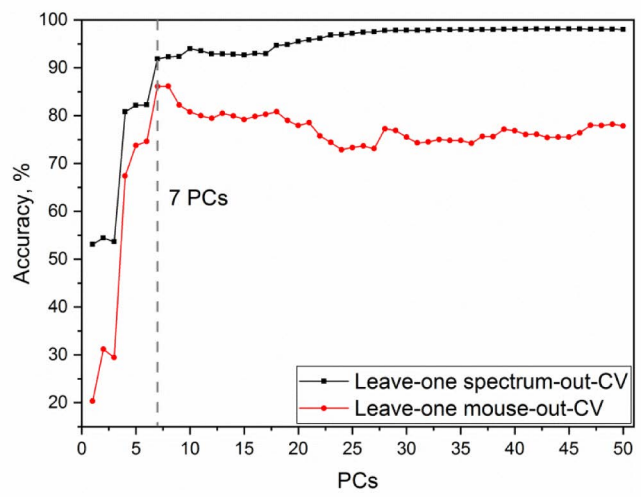

Figure S4. PCA/LDA model accuracy as the function of PCs for aspergillosis model including only very sick mice.

Table S4. Results of the mouse (spectral) level classification model for aspergillosis including only very sick mice evaluated with LMOCV.

		True			
		Control	**Aspergillosis**	**Sensitivity, %**	**Specificity, %**
Predicted	**Control**	**4 (21017)**	0 (4878)	**100 (91.70)**	**100 (81.2)**
	Aspergillosis	0 (1902)	**7 (21073)**	**100 (81.2)**	**100 (91.70)**

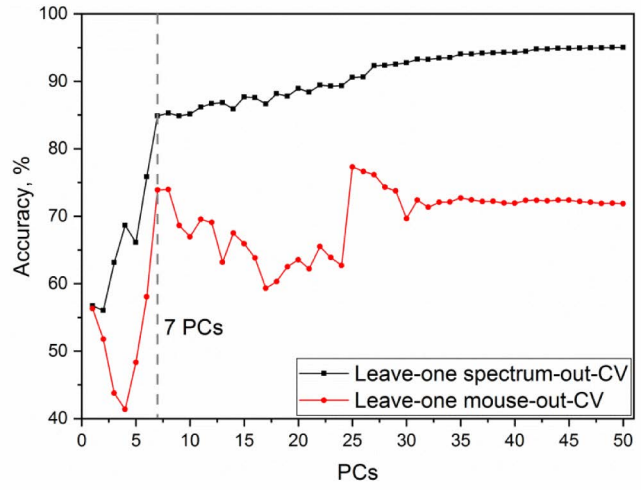

Figure S5. PCA/LDA model accuracy as the function of PCs for asthma model.

Table S5. Results of the spectral level classification model for aspergillosis evaluated with LMOCV.

		True			
		Control	**Asthma**	**Sensitivity, %**	**Specificity, %**
Predicted	**Control**	**18094**	6228	**73.39**	**74.42**
	Asthma	6562	**18118**	**74.42**	**73.39**

Table S6. Results of the classification for every mouse for the asthma model using leave-one mouse-out-CV.

Mouse			**Percentage of correctly classified spectra per mouse, %**	**Mouse diagnosis according to the RS**
Control	Day 1	5077	95.76	Healthy
	Day 1	5078	**42.04**	**Sick**
	Day 1	5079	100	Healthy
	Day 1	5080	99.95	Healthy
	Day 5	5141	99.40	Healthy
	Day 5	5143	74.37	Healthy
	Day 5	5144	66.6	Healthy
	Day 9	5117	**49.52**	**Sick**
	Day 9	5118	**30.73**	**Sick**
	Day 9	5119	94.49	Healthy
	Day 9	5120	67.89	Healthy
Asthma	Day 1	5081	77.78	Sick
	Day 1	5082	100	Sick
	Day 1	5083	100	Sick
	Day 1	5084	98.05	Sick
	Day 5	5146	89.6	Sick
	Day 5	5147	**0.47**	**Healthy**
	Day 5	5148	69.49	Sick
	Day 9	5121	99.44	Sick
	Day 9	5122	71.24	Sick
	Day 9	5123	**8.74**	**Healthy**
	Day 9	5124	65.23	Sick

7.3 Detection of Pseudomonas aeruginosa metabolite pyocyanin in water and saliva by employing the SERS technique [OZ3]

Olga Žukovskaja, Izabella Jolan Jahn, Karina Weber, Dana Cialla-May, Jürgen Popp

Sensors 2017, 17(8), 1704

https://doi.org/10.3390/s17081704

Declaration on authorship and copyright in a cumulative doctoral thesis

[1]**Olga Žukovskaja**, [2]Izabella Jolan Jahn, [3]Karina Weber, [4]Dana Cialla-May, [5]Jürgen Popp 2017, Detection of Pseudomonas aeruginosa metabolite pyocyanin in water and saliva by employing the SERS technique. *Sensors*, 17(8), 1704					
Involved in					
	1	2	3	4	5
Conceptual research design	X	X	X	X	X
Planning of research activities	X	X	X	X	X
Data collection	X				
Data analyses and interpretation	X	X			
Manuscript writing	X	X	X	X	X
Suggested publication equivalence value	**1.0**				

Author Contribution

Olga Žukovskaja	concept development SERS measurements data analysis and interpretation writing of manuscript
Izabella Jolan Jahn	concept development data analysis and interpretation discussion of experimental concept and results proofreading of manuscript
Dana Cialla-May	discussion of experimental concept and results proofreading of manuscript
Karina Weber	discussion of experimental concept and results proofreading of manuscript
Jürgen Popp	project management discussion of concepts and results discussion and proofreading of manuscript

sensors

MDPI

Article

Detection of *Pseudomonas aeruginosa* Metabolite Pyocyanin in Water and Saliva by Employing the SERS Technique

Olga Žukovskaja [1,2], Izabella Jolan Jahn [3], Karina Weber [1,2,3], Dana Cialla-May [1,2,3,*] and Jürgen Popp [1,2,3,*]

1 Institute of Physical Chemistry and Abbe Center of Photonics, Friedrich Schiller University Jena, Helmholtzweg 4, 07743 Jena, Germany; olga.zukovskaja@leibniz-ipht.de (O.Ž.); karina.weber@leibniz-ipht.de (K.W.)
2 Research Campus InfectoGnostics, Philosophenweg 7, 07743 Jena, Germany
3 Leibniz Institute of Photonic Technology Jena, Albert-Einstein-Str. 9, 07745 Jena, Germany; izabella.jahn@leibniz-ipht.de
* Correspondence: dana.cialla-may@leibniz-ipht.de (D.C.-M.); juergen.popp@leibniz-ipht.de (J.P.); Tel.: +49-(0)-3641-206-309 (D.C.-M.); +49-(0)-3641-206-300 (J.P.)

Received: 13 June 2017; Accepted: 20 July 2017; Published: 25 July 2017

Abstract: Pyocyanin (PYO) is a metabolite specific for *Pseudomonas aeruginosa*. In the case of immunocompromised patients, it is currently considered a biomarker for life-threating *Pseudomonas* infections. In the frame of this study it is shown, that PYO can be detected in aqueous solution by employing surface-enhanced Raman spectroscopy (SERS) combined with a microfluidic platform. The achieved limit of detection is 0.5 μM. This is ~2 orders of magnitude below the concentration of PYO found in clinical samples. Furthermore, as proof of principle, the SERS detection of PYO in the saliva of three volunteers was also investigated. This body fluid can be collected in a non-invasive manner and is highly chemically complex, making the detection of the target molecule challenging. Nevertheless, PYO was successfully detected in two saliva samples down to 10 μM and in one sample at a concentration of 25 μM. This indicates that the molecules present in saliva do not inhibit the efficient adsorption of PYO on the surface of the employed SERS active substrates.

Keywords: SERS; pyocyanin; microfluidics; diagnosis; artificial sputum

1. Introduction

Increasing antibiotic resistance impedes the successful treatment of infections, such as pneumonia or tuberculosis. This leads to longer hospital stays, higher medical costs and increased mortality [1]. Therefore, it is essential to identify the exact pathogen prior to the antibiotic treatment.

Pseudomonas aeruginosa is an important gram-negative bacterium and is the leading cause of respiratory tract infections in the case of patients with compromised host defense mechanisms. Therefore, this pathogen is responsible for the highest rates of acquired infections in intensive-care units [2]. Because of its intrinsic ability to develop antibiotic resistance, to form impenetrable biofilms and to release a large arsenal of virulence factors [3], *P. aeruginosa* is one of the greatest therapeutic challenges, and rapid detection, as well as the selection of the appropriate antibiotic to initiate the therapy, is critical to optimize the clinical outcome.

Currently, the routine detection and identification of *P. aeruginosa* in respiratory samples is performed by bacteriological culture. The time to achieve reliable results is at least 24 h. An alternative approach is the indirect detection of the bacteria by identifying the biomarkers released by the organism. *P. aeruginosa* produces several toxic metabolites, the most predominant of them being the

redox-active phenazine compound pyocyanin (PYO). PYO is capable of destroying host cells by altering critical cellular processes, generating reactive oxygen species and inducing neutrophil apoptosis [4]. *P. aeruginosa* is the only microorganism known to produce PYO, and for this reason PYO can be used as a potential biomarker. It was found that in clinical sputum samples PYO can reach concentrations up to 16.5 µg/mL (~76 µM) for cystic fibrosis patients and up to 27.3 µg/mL (~130 µM) for patients with bronchiectasis [5]. Moreover, Hunter et al. concluded that levels of PYO and its biosynthetic precursor, phenazine-1-carboxylic acid, varying between 7.7 µM and 46.8 µM in expectorated cystic fibrosis sputum samples are negatively correlated with lung function [6]. The presence and the concentration of PYO in clinical samples is traditionally determined through extraction of the pigment with chloroform and by subsequently performing high performance liquid chromatography (HPLC). However, HPLC is available only in academic and clinical centers and it is time consuming, costly and laborious.

Surface-enhanced Raman spectroscopy (SERS) was proven to be a molecular specific and highly sensitive analytical technique suitable for biological applications [7–10]. SERS allows the sensitive identification of the molecular fingerprint of the analyte brought in the proximity of plasmonic nanostructures by enhancing its Raman signal by several orders of magnitude. For example, Polisetti et al. demonstrated that SERS can be used for investigating PYO produced by laboratory and cystic fibrosis lung isolate strains of *P. aeruginosa* for different growing conditions [11]. Additionally, Bodelon et al. developed different Au nanorod structures and performed SERS measurements for studying the intercellular communication of growing *P. aeruginosa* biofilms on the basis of secreted PYO [12]. Further on, the detection of PYO in clinical sputum samples was also successfully performed using silver nanorod array substrates [13]. However, due to the complex sputum matrix, PYO was outcompeted for available adsorption sites on the metallic surface by other species and its SERS detection became possible only after extracting it from sputum samples by the traditional chloroform procedure. Additionally, even though SERS is a highly specific and sensitive detection method, traditional SERS measurements still suffer from low reproducibility. This hinders a quantitative analysis. Combining SERS with microfluidics overcomes this limitation and enables the handling of small sample volumes [14–16].

Within this study, SERS was first combined with a droplet-based microfluidic platform to obtain reproducible and automated measurement conditions for the detection of PYO in aqueous environment. This is essential because, as the majority of the already published SERS studies have demonstrated, for each targeted analyte, a smart experimental design is needed to obtain SERS spectra with an optimized signal-to-noise ratio [17–19]. By taking into account the ability of the biomarker to induce the aggregation of the employed silver nanoparticles and by carefully choosing the measurement design, PYO levels down to concentrations of 0.5 µM were detected with the lab-on-a-chip SERS (LoC-SERS) platform. In the second part of the study, saliva was considered to be a clinically relevant sample matrix. This body fluid can be collected in a simple, non-invasive manner and offers high chemical complexity. Additionally, when collecting sputum, the clinical samples also contain saliva. This makes saliva an important and easy-to-access sample. Consequently, the interferences brought by this matrix in the SERS spectra have to be assessed. The results demonstrate that despite the high complexity of the matrix, PYO spiked in saliva collected from healthy volunteers can be successfully detected in the micromolar range.

2. Materials and Methods

2.1. Chemicals and Reagents

Pyocyanin from *P. aeruginosa*, ≥98% (HPLC) in powder form, silver nitrate (ACS reagent, 99%), hydroxylamine hydrochloride (ReagentPlus, 99%) and mineral oil were purchased from Sigma Aldrich (St. Louis, MO, USA), whereas potassium chloride (KCl) (≥99.5% p.a. ACS, ISO) was acquired from Carl Roth (Karlsruhe, Germany).

2.2. Silver Nanoparticles (Ag NPs) Synthesis

The silver colloidal solution was prepared through the chemical reduction of silver nitrate by hydroxylamine in the presence of sodium hydroxide at room temperature, as established in the standard Leopold and Lendl protocol [20]. The synthesized nanoparticles were characterized by UV-Vis spectroscopy (Figure S1) and transmission electron microscopy (TEM) (Figure S2).

2.3. Pyocyanin Solution

Since PYO is sparingly soluble in water, first a stock solution of PYO at 1 mM concentration was prepared in ethanol by adding the appropriate amount of powder. Working solutions were obtained by diluting the stock solution with high-purity water, keeping a concentration of 10% of ethanol in the final solutions.

2.4. Saliva Sample Preparation

Saliva collected from the control group of the IDES (Innovative Diagnostik für Infectionserregern bei Pneumonien, InfectoGnostics research campus (13GW0096F)) study (ethical approval 4672-01/16) were used. The samples were obtained from two female and one male volunteer at least 1 h after a meal. The samples were stored at 4 °C until analysis. None of the individuals had undergone medical treatment at the time of sample collection and they were also not in medical evidence for chronic diseases. Prior to the measurements, PYO solutions in ethanol with different concentrations were added to the saliva samples in a ratio of 1 to 9. The as obtained samples had the following biomarker concentration: 10, 25, 50, 75 and 100 µM. As negative control, a sample containing only ethanol and saliva was considered. To remove oral epithelial cells and food debris, the samples were filtrated using a cellulose acelate membrane with a pore size of 0.2 µm (VWR International, Radnor, PA, USA).

2.5. Instrumentation

Raman and SERS spectra were acquired with a commercially available WITec Raman microscope (WITec GmbH, Ulm, Germany) equipped with a diode laser (Fandango, Cobolt) that emits at 514 nm. During the measurements, a 600 lines per mm grating was used with a spectral resolution of ~5 cm^{-1} and the same objective (Nikon 20 × 0.4 N.A., Tokyo, Japan) was employed for focusing the laser beam on the sample and for collecting the Raman backscattered light. For all measurements, a laser power of 38 mW and an integration time of 1 s were used. The reference Raman and SERS spectra of the water-ethanol, as well as of the PYO solution were measured in plastic cuvettes and each spectrum is the result of 50 accumulations.

In order to determine the limit of detection of PYO in aqueous solution, a droplet-based glass microfluidic chip was employed (Scheme 1).

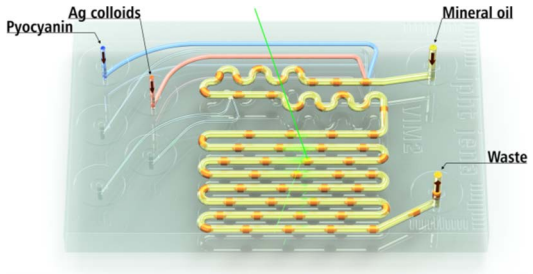

Scheme 1. Schematic representation of the droplet based microfluidic chip used for LoC-SERS measurements.

A detailed description of the chip has been published elsewhere [21]. The glass syringes (ILS Germany GmbH, Stützerbach, Germany) were filled with different solutions and connected with the chip via Teflon capillaries, having an inner diameter of 0.5 mm (WICOM GmbH, Heppenheim, Germany). The solutions were pumped into the chip via a computer controlled pump system (neMESYS Cetoni GmbH, Korbußen, Germany). To create a segmented continuous flow, mineral oil was pumped with a flow rate of 9 nL/s, while the analyte and the Ag NPs were both injected with 7 nL/s. All other ports were blocked. The SERS spectra were measured continuously with an integration time of 1 s.

To assess the interferences brought by the molecules present in the saliva, the control samples and the ones spiked with PYO were mixed with the silver colloidal solution in a 1 to 1 ratio, followed by the addition of 1 M KCl (final mixing ratio 1:1:0.2). Here, KCl was added to induce the aggregation process. Three independent measurements were recorded for each sample with 1 s integration time and 20 accumulations.

2.6. Data Processing

The data processing was performed using an algorithm developed in-house in the programming language R [22]. In the case of the LoC-SERS measurements, Raman/SERS spectra were measured continuously during the flow. Accordingly, alternating SERS spectra of the analyte containing droplets, Raman spectra of the oil phase and mixed spectra of both phases were recorded. Therefore, during the data processing, the oil and mixed spectra were removed first. Afterwards, spectra were background corrected using the Statistics-sensitive Non-linear Iterative Peak-clipping (SNIP) algorithm with 80 iterations and cut to the region of interest [23]. Univariate statistical analysis was performed by calculating the peak area of the band around 676 cm^{-1}. This Raman mode corresponds to the ring breathing mode of PYO. For peak integration, the Simpson's rule [24] was applied. The integrated peak area was plotted as function of the concentration. SERS spectra measured in plastic cuvettes were vector-normalized. The same background correction algorithm was also applied to the spectra recorded in cuvettes.

3. Results and Discussion

3.1. SERS Detection of Pyocyanin in Aqueous Solution

PYO is a redox-active phenazine and its chemical structure is depicted in Scheme 2. It is a heterocyclic nitrogen containing compound, which exist as a zwitterion at the pH value of blood (7.35–7.45). PYO can accept a single electron, yielding a relatively stable anion radical, and readily undergoes a redox cycle [25].

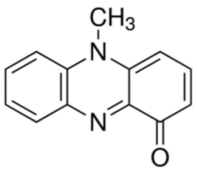

Scheme 2. Chemical structure of the PYO molecule ($C_{13}H_{10}N_2O$).

In Figure 1, the normalized Raman spectrum of PYO in a water-ethanol solution at a concentration of 0.5 mM and the normalized SERS spectrum of PYO at a concentration of 10 µM are plotted together with the Raman and the SERS spectra of the solvent without the analyte. Based on this, the normal Raman spectrum of the PYO solution is dominated by the Raman modes assigned to the molecular vibrations of ethanol at 880, 1047, 1087 and 1456 cm^{-1} (see Figure 1a). Nevertheless, at 676, 1353 and 1606 cm^{-1} clearly distinguishable Raman bands ascribed to the presence of the PYO molecule can be

Sensors **2017**, *17*, 1704

also noticed. A comprehensive band assignment of the Raman modes of the metabolite can be found in the literature [12,13]. Briefly, the band around 676 and 1606 cm^{-1} was assigned to the ring deformations, while the signal at 1354 cm^{-1} corresponds to the combined C-C stretching, C-N stretching and C-H in-plane bending modes of the aromatic ring. In the presence of the Ag nanoparticles, the already mentioned Raman marker bands are strongly enhanced and new ones appear. More exactly, the double band at 1564 cm^{-1} and 1594 cm^{-1}, ascribed to the ring deformation and the C-C stretch vibration, the two bands at 423 and 547 cm^{-1}, corresponding to the ring torsion and the ring breathing with C-N torsion, become prominent, whereas the Raman band at 1606 cm^{-1} is convoluted with the rest of the signal.

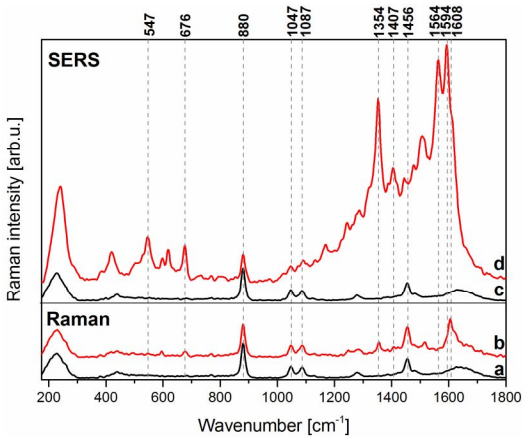

Figure 1. Normalized Raman spectra of 10% ethanol solution (a) and PYO 500 μM solution (b), as well as normalized SERS spectra of the same ethanol solution (c) and PYO 10 μM solution (d).

3.2. LoC-SERS Measurement of PYO in Aqueous Solution

In order to achieve automated measurements and to obtain reproducible SERS spectra of PYO in aqueous solution at different concentrations, the microfluidic setup depicted in Scheme 1 was employed. Generally, to get strong Raman signal enhancements, the aggregation of spherical nanoparticles is required [26]. Usually the creation of "hot-spots" is achieved by the addition of an active (e.g., KCl) or a passive (e.g., KNO_3) electrolyte to the colloid-analyte mixture. However, based on our performed experiments, PYO induces by itself the aggregation of the colloids and the addition of aggregation agents is not needed. This is demonstrated by recording the SERS spectra in the absence of salts as well as in the presence of KCl at different concentrations (Figure S3). For clarity, the integrated peak area of the Raman band located at ~676 cm^{-1} is represented in the inset of Figure S3 for different measurement conditions. This band was chosen because its intensity is not influenced by surrounding bands. According to the results, the most intensive and stable signal is achieved when no salts are present. The decrease of the signal with KCl addition can be explained by the fact that the presence of KCl causes over-aggregation and creates large clusters, which cannot support high electromagnetic enhancements at the used excitation wavelength. Therefore, all following measurements were carried out in the absence of any additional aggregation agent.

Another important factor for SERS measurements is the time elapsed between the induction of the aggregation and the measurements. Performing measurements in the microfluidic chip offers time-control by choosing the measurement position. For this purpose, during SERS measurements, the excitation laser was focused in the middle of each microfluidic channel. The results showed that the intensity of the signal was the same for different positions, but the lowest relative standard deviation

of the signal was achieved for the measurement done in the 3rd channel (Figure S4). Therefore, all subsequent measurements were performed with the laser beam fixed in the middle of the 3rd channel.

By taking the clinically relevant range into account (7–130 μM) [5,6], PYO solutions with concentrations between 0.5 μM and 85 μM were measured employing our proposed LoC-SERS-based detection scheme. In Figure 2, the mean SERS spectra for all concentration steps are plotted together with the blank spectrum. It can be observed that for concentrations higher than 20 μM, the most prominent ethanol band at 880 cm^{-1} becomes convoluted with the intense PYO spectra. The spectral signature of PYO at 676 cm^{-1} and 1353 cm^{-1} is still present at a concentration of 0.5 μM. For better visualization, the integrated peak area of the ring deformation vibration band at 676 cm^{-1} was plotted against the concentration of PYO (Figure 3). The concentration curve has a sigmoidal form, reaching a plateau for concentrations higher than 55 μM. This is explained by a full occupation of the Ag nanoparticle's surface with PYO molecules. Thus, by further increasing the concentration of the PYO molecules, no significant increase of the band intensity was observed due to an increased distance of the analyte molecule toward the metallic surface.

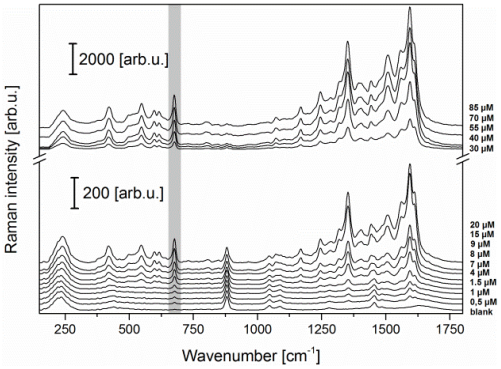

Figure 2. Mean SERS spectra of PYO with concentrations between 0.5 and 85 μM in aqueous solution measured in the microfluidic platform. The mean spectrum of the blank (when only water–ethanol solution is pumped through at the first dosing unit) is also presented.

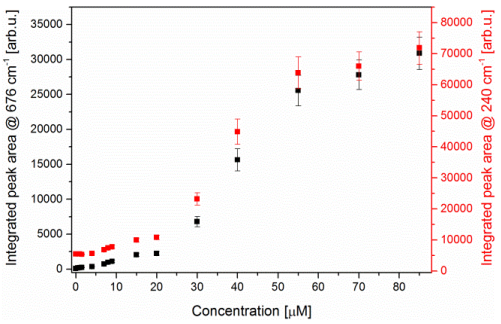

Figure 3. Integrated peak area of the PYO Raman mode at 676 cm^{-1} (black) and of the mode at 240 cm^{-1} which corresponds to the Ag-(adsorbed atom) (red).

It is known that usually the bonding of molecules to the silver surface takes place either through the lone pair electrons of the nitrogen or oxygen atoms or through the π electron system of the aromatic ring [27,28]. In the first two cases, Raman bands assigned to the vibrational modes of the Ag-adsorbed molecule (i.e., Ag-N, Ag-O) can appear in the low wavenumber region (200–260 cm^{-1}) because of the molecule adsorption. Furthermore, when electrolytes containing Cl^{-} are used for inducing the

Sensors **2017**, *17*, 1704

aggregation of the nanoparticles, a low wavenumber Raman band also appears due to the Ag-Cl vibration. Since PYO is causing the aggregation of the nanoparticles, no additional salts were added to the colloid-analyte mixture. Thus, the bands in the low wavenumber range in the recorded spectra cannot be assigned to this vibration.

Based on the molecular structure of PYO (see Scheme 2), it is expected that oxygen and nitrogen atoms carry partial negative charges, thus, most probably an interaction with the silver surface is achieved via these heteroatoms. As a result of the interaction of PYO with Ag nanoparticles, Raman bands in the low wavenumber region, at 221 and 239 cm^{-1}, can be observed and assigned to the Ag-N and Ag-O stretching vibrations [29]. The increase of their intensity (see Figure S5) can be attributed to the increment of the number of adsorbed PYO molecules on the Ag surface. The change of the ratio of these two bands with increasing PYO concentration might be caused by a change in the orientation of the target molecule on the surface of Ag nanoparticles. Namely, at low concentrations, the molecule might interact with the metallic surface via the free electron pairs of both N and O, while at high concentrations, due to the steric hindering, PYO might adopt an upright orientation and interact with the metallic surface only via the O atom.

The integrated peak area of the two convoluted bands in the low wavenumber range is presented by red scatter plot in Figure 3. Comparing it with the integrated peak area of the 676 cm^{-1} band, a similar sigmoidal behavior with saturation after 55 µM was observed. However, the underlying mechanism behind the increment of the signal is different for the two Raman bands. The Raman mode at 240 cm^{-1} band is due to the PYO molecules in the first layer on the surface of the silver nanoparticles. Meanwhile, the intensity of the 676 cm^{-1} is increasing also because of the molecules present in the upper layers but still found in the 'hot-spot' between the nanoparticles.

In the following, the Raman band centered at 240 cm^{-1} was used as an internal standard [30]. The normalized integrated peak area of the Raman marker band of the metabolite is plotted in Figure 4. After normalization, a linear response over the 0.5–15 µM concentration range is achieved. According to the IUPAC definition, the limit of detection is equal with the signal of the blank plus three times its standard deviation. The calculated limit of detection (LOD) is below the lowest measured concentration (0.5 µM) (the threshold is illustrated in Figure 4). Moreover, the normalization of the signal significantly improved the "chip-to-chip" reproducibility. As illustrated in the supporting information, the integrated peak area of the Raman mode at 676 cm^{-1} for two different microfluidic chips is difficult to compare (Figure S6); however, after normalization, the concentration curves gain the same profile (Figure S7). Therefore, the Ag-adsorbed atom mode can be considered to be an internal standard and it increases the comparability of different data sets.

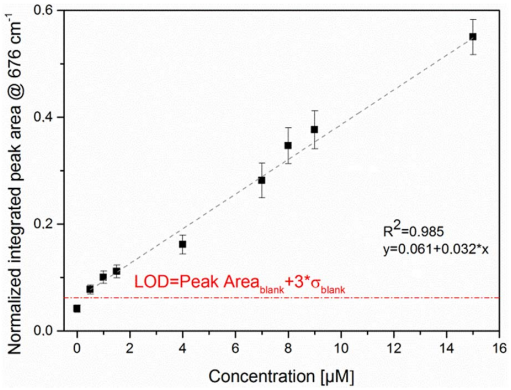

Figure 4. The peak area ratio of the 676 cm^{-1} and 240 cm^{-1} Raman modes as a function of PYO concentration in aqueous solution in the range between 0.5 and 15 µM with linear fitting. The red line indicates the calculated LOD.

Sensors **2017**, *17*, 1704

3.3. SERS Detection of PYO in Saliva

In order to move toward clinical applications, the feasibility of SERS for PYO detection in saliva was investigated. The spectroscopic analysis of clinical samples is often challenging due to the complex and heterogeneous nature of biological fluids. In the case of SERS, different components can interact with the metallic structures and the detection of the Raman modes of the molecules of interest present in low concentrations can be inhibited. In the current study, saliva was chosen as the test sample matrix. This biological fluid will be present in the respiratory tract samples. Despite the fact that saliva is composed mainly of water, it has a multitude of dissolved components, for example minerals, electrolytes, hormones, mucins and enzymes. It also contains expectorated bronchial and nasal secretions, serum and blood derivatives from oral wounds, bacteria and bacterial products, viruses, fungi, desquamated epithelial cells and food debris [31]. Since the composition of saliva varies among individuals, for the proof of concept, saliva samples from three healthy volunteers were used for this study. Six different solutions with different PYO salivary concentrations (0 M, 10 µM, 25 µM, 50 µM, 75 µM, 100 µM) were prepared for each sample by mixing 9 parts of human saliva with 1 part of ethanol solution containing the target molecule. To remove oral epithelial cells and food debris, the samples were filtrated prior to the measurement. The recorded mean SERS spectra of the samples originating from the three volunteers at different PYO concentrations are presented in Figure 5. Since the ethanol concentration in all samples was kept constant, for a better comparison, all spectra were normalized to the ethanol Raman mode at 880 cm^{-1}.

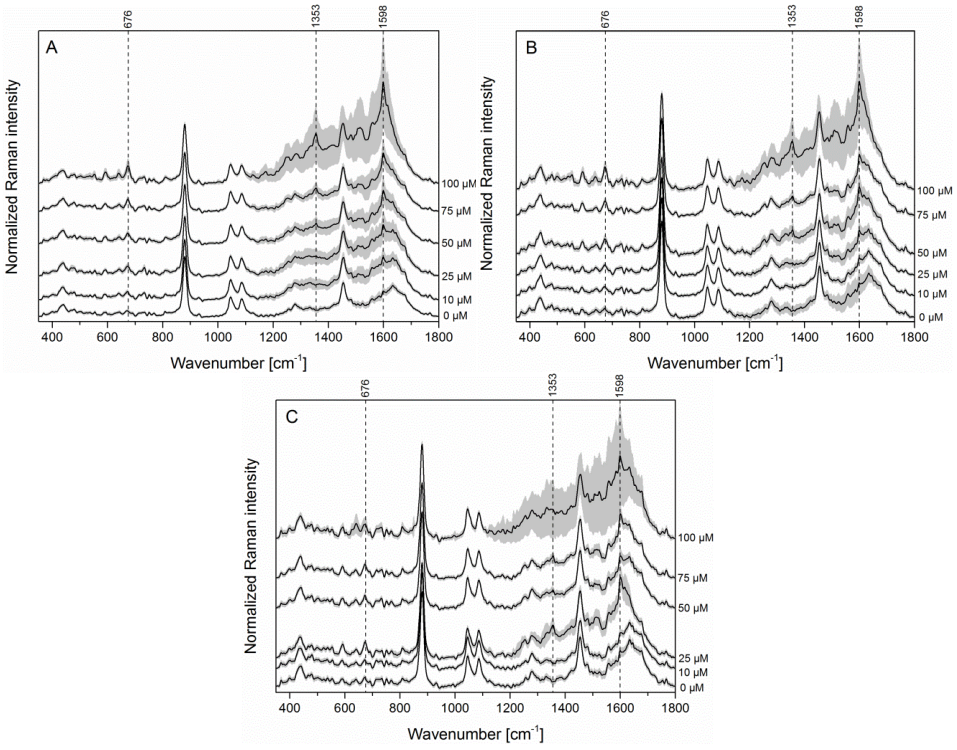

Figure 5. Mean SERS spectra and their double standard deviation of the different concentrations of PYO in the saliva sample from volunteer number one (**A**), two (**B**) and three (**C**).

The SERS signal of the pure saliva (Figure S8) is challenging to interpret because of the convolution of the Raman bands in the fingerprint region. However, the Raman modes around 1240, 1472, 1610

and 1653 cm^{-1} can be distinguished and tentatively assigned to proteins, amino acids, lipids and DNA and/or RNA bases [32,33]. Because PYO stock solutions were prepared in ethanol, as negative control for the current study a mixture of saliva with ethanol was considered. The latter molecule gives rise to the intensive Raman bands at 880, 1047, 1087 and 1456 cm^{-1} observed in Figure 5 for the 0 μM samples. By spiking PYO to the complex matrix, a new band appears at 1353 cm^{-1}, while the bands at 676 cm^{-1} and 1598 cm^{-1} gradually increase in intensity with the increment of PYO concentration. These three Raman modes are characteristic for the targeted molecule. In the case of the first and second volunteer, spectral changes can be seen already at the lowest investigated PYO concentration (10 μM) (Figure 5A,B and Figure S9), while for the third volunteer changes can be noticed by eye at a concentration of 25 μM (Figure 5C and Figure S9). In the case of the highest concentration, 100 μM, the increased standard deviation of the recorded spectra can be explained by the poisoning of the metallic surface by the high number of molecules present in the matrix. In comparison with the LOD previously obtained for PYO in water (below 0.5 μM), the complexity of the matrix affects the sensitivity of the method and the metabolite could be detected down to a 10 μM concentration. For these samples, the LOD was not calculated based on the IUPAC definition, but instead the lowest concentration causing observable changes in the SERS spectrum of the sample was considered. Nevertheless, by using easy to prepare silver nanoparticles, we showed that the detection of PYO in the clinical range can be achieved and the saliva collected from the three volunteers does not significantly affect the detection of the target molecule.

4. Conclusions

P. aeruginosa is an opportunistic human pathogen responsible for acute and chronic infections, particularly in individuals with compromised immune systems and host defenses. PYO is a virulence factor uniquely produced by this pathogen. Thus, its fast and selective detection can reveal the presence of *P. aeruginosa* in the organism, which can help with fast and successful antibiotic treatment.

In this study, the detection of pyocyanin (PYO) was performed through surface-enhanced Raman spectroscopy (SERS) combined with a microfluidic platform. It was shown that the aggregation of the silver nanoparticles is induced by the presence of the analyte and no additional salts are necessary to achieve enhancement. PYO was successfully detected in aqueous solution in the clinically relevant range (7–130 μM) with the linearity in the 0.5 μM–15 μM region and a limit of detection <0.5 μM. This demonstrated that the described LoC-SERS approach is versatile and allows the detection of bacteria metabolites. In the second part of the paper, as proof of concept, saliva collected from three volunteers was considered as a matrix. As none of the individuals were under treatment for pneumonia, PYO was artificially added to the saliva and it was successfully detected in this chemical environment down to the 10 μM concentration for two of the investigated samples, while in the case of the third sample spectral changes were observed at 25 μM. The results establish the potential for the detection of PYO directly from complex matrixes. For further studies, other respiratory specimens will be also considered. Additionally, the measurement principle used can be significantly improved by replacing the bench-top Raman setup with a miniaturized or even portable system, by integrating the sample clean-up step in the platform and by opting for a pressure driven pumping system.

Supplementary Materials: The following are available online at http://www.mdpi.com/1424-8220/17/8/1704/s1.

Acknowledgments: The funding of the grants InfectoGnostics (13GW0096F) and EXASENS (13N13856) by the Federal Ministry of Education and Research, Germany (BMBF) supporting this study is gratefully acknowledged.

Author Contributions: O.Ž. designed, performed and analyzed all the experimental work in the reported study. I.J.J. contributed with scientific discussion of the content and reviewing the manuscript. D.C.-M., K.W. and J.P. contributed by supervising and reviewing the paper.

Conflicts of Interest: The authors declare no conflict of interest.

References

1. World Health Organization. Antibiotic Resistance. Available online: http://www.who.int/mediacentre/factsheets/antibiotic-resistance/en/ (accessed on 27 February 2017).
2. Lambert, M.L.; Suetens, C.; Savey, A.; Palomar, M.; Hiesmayr, M.; Morales, I.; Agodi, A.; Frank, U.; Mertens, K.; Schumacher, M.; et al. Clinical outcomes of health-care-associated infections and antimicrobial resistance in patients admitted to European intensive-care units: A cohort study. *Lancet Infect. Dis.* **2011**, *11*, 30–38. [CrossRef]
3. Lau, G.W.; Hassett, D.J.; Ran, H.M.; Kong, F.S. The role of pyocyanin in Pseudomonas aeruginosa infection. *Trends Mol. Med.* **2004**, *10*, 599–606. [CrossRef] [PubMed]
4. Palmer, G.C.; Whiteley, M. Metabolism and Pathogenicity of Pseudomonas aeruginosa Infections in the Lungs of Individuals with Cystic Fibrosis. *Microbiol. Spectr.* **2015**, *3*, 185–213. [CrossRef]
5. Wilson, R.; Sykes, D.A.; Watson, D.; Rutman, A.; Taylor, G.W.; Cole, P.J. Measurement of Pseudomonas-aeruginosa phenazine pigments in sputum and assessment of their contribution to sputum sol toxicity for respiratory epithelium. *Infect. Immun.* **1988**, *56*, 2515–2517. [PubMed]
6. Hunter, R.C.; Klepac-Ceraj, V.; Lorenzi, M.M.; Grotzinger, H.; Martin, T.R.; Newman, D.K. Phenazine Content in the Cystic Fibrosis Respiratory Tract Negatively Correlates with Lung Function and Microbial Complexity. *Am. J. Respir. Cell Mol. Biol.* **2012**, *47*, 738–745. [CrossRef] [PubMed]
7. Cheng, H.W.; Luo, J.; Zhong, C.J. SERS nanoprobes for bio-application. *Front. Chem. Sci. Eng.* **2015**, *9*, 428–441. [CrossRef]
8. Cialla, D.; Pollok, S.; Steinbrucker, C.; Weber, K.; Popp, J. SERS-based detection of biomolecules. *Nanophotonics* **2014**, *3*, 383–411. [CrossRef]
9. Pahlow, S.; Marz, A.; Seise, B.; Hartmann, K.; Freitag, I.; Kammer, E.; Bohme, R.; Deckert, V.; Weber, K.; Cialla, D.; et al. Bioanalytical application of surface- and tip-enhanced Raman spectroscopy. *Eng. Life Sci.* **2012**, *12*, 131–143. [CrossRef]
10. Sharma, B.; Frontiera, R.R.; Henry, A.I.; Ringe, E.; Van Duyne, R.P. SERS: Materials, applications, and the future. *Mater. Today* **2012**, *15*, 16–25. [CrossRef]
11. Polisetti, S.; Baig, N.F.; Morales-Soto, N.; Shrout, J.D.; Bohn, P.W. Spatial Mapping of Pyocyanin in Pseudomonas Aeruginosa Bacterial Communities Using Surface Enhanced Raman Scattering. *Appl. Spectrosc.* **2017**, *71*, 215–223. [CrossRef] [PubMed]
12. Bodelon, G.; Montes-Garcia, V.; Lopez-Puente, V.; Hill, E.H.; Hamon, C.; Sanz-Ortiz, M.N.; Rodal-Cedeira, S.; Costas, C.; Celiksoy, S.; Perez-Juste, I.; et al. Detection and imaging of quorum sensing in Pseudomonas aeruginosa biofilm communities by surface-enhanced resonance Raman scattering. *Nat. Mater.* **2016**, *15*, 1203–1211. [CrossRef] [PubMed]
13. Wu, X.M.; Chen, J.; Li, X.B.; Zhao, Y.P.; Zughaier, S.M. Culture-free diagnostics of Pseudomonas aeruginosa infection by silver nanorod array based SERS from clinical sputum samples. *Nanomed. Nanotechnol. Biol. Med.* **2014**, *10*, 1863–1870. [CrossRef] [PubMed]
14. Huang, J.A.; Zhang, Y.L.; Ding, H.; Sun, H.B. SERS-Enabled Lab-on-a-Chip Systems. *Adv. Opt. Mater.* **2015**, *3*, 618–633. [CrossRef]
15. Jahn, I.J.; Zukovskaja, O.; Zheng, X.S.; Weber, K.; Bocklitz, T.W.; Cialla-May, D.; Popp, J. Surface-enhanced Raman spectroscopy and microfluidic platforms: Challenges, solutions and potential applications. *Analyst* **2017**, *142*, 1022–1047. [CrossRef] [PubMed]
16. Wang, C.; Yu, C.X. Analytical characterization using surface-enhanced Raman scattering (SERS) and microfluidic sampling. *Nanotechnology* **2015**, *26*, 092001. [CrossRef] [PubMed]
17. Andreou, C.; Hoonejani, M.R.; Barmi, M.R.; Moskovits, M.; Meinhart, C.D. Rapid Detection of Drugs of Abuse in Saliva Using Surface Enhanced Raman Spectroscopy and Microfluidics. *ACS Nano* **2013**, *7*, 7157–7164. [CrossRef] [PubMed]
18. Israelsen, N.D.; Hanson, C. Nanoparticle properties and synthesis effects on surface-enhanced Raman scattering enhancement factor: An introduction. *Sci. World J.* **2015**, *2015*, 124582. [CrossRef] [PubMed]
19. Tong, L.M.; Righini, M.; Gonzalez, M.U.; Quidant, R.; Kall, M. Optical aggregation of metal nanoparticles in a microfluidic channel for surface-enhanced Raman scattering analysis. *Lab Chip* **2009**, *9*, 193–195. [CrossRef] [PubMed]

20. Leopold, N.; Lendl, B. A new method for fast preparation of highly surface-enhanced Raman scattering (SERS) active silver colloids at room temperature by reduction of silver nitrate with hydroxylamine hydrochloride. *J. Phys. Chem. B* **2003**, *107*, 5723–5727. [CrossRef]
21. Marz, A.; Ackermann, K.R.; Malsch, D.; Bocklitz, T.; Henkel, T.; Popp, J. Towards a quantitative SERS approach—Online monitoring of analytes in a microfluidic system with isotope-edited internal standards. *J. Biophotonics* **2009**, *2*, 232–242. [CrossRef] [PubMed]
22. R Development Core Team. *Development Core R: A Language and Environment for Statistical Computing*; The R Foundation for Statistical Computing: Vienna, Austria, 2011.
23. Ryan, C.G.; Clayton, E.; Griffin, W.L.; Sie, S.H.; Cousens, D.R. SNIP, a statistics-sensitive background treatment for the quantitative-analysis of pixe spectra in geoscience applications. *Nucl. Instrum. Methods Phys. Res. B* **1988**, *34*, 396–402. [CrossRef]
24. Atkinson, K. *An Introduction to Numerical Analysis*, 2nd ed.; Wiley: Hoboken, NJ, USA, 1989; pp. 251–263. ISBN 978-0-471-62489-9.
25. Hassan, H.M.; Fridovich, I. Mechanism of the antibiotic action of pyocyanine. *J. Bacteriol.* **1980**, *141*, 156–163. [PubMed]
26. Zhang, Y.Y.; Walkenfort, B.; Yoon, J.H.; Schlucker, S.; Xie, W. Gold and silver nanoparticle monomers are non-SERS-active: A negative experimental study with silica-encapsulated Raman-reporter-coated metal colloids. *Phys. Chem. Chem. Phys.* **2015**, *17*, 21120–21126. [CrossRef] [PubMed]
27. Baia, M.; Baia, L.; Kiefer, W.; Popp, J. Surface-enhanced Raman scattering and density functional theoretical study of anthranil adsorbed on colloidal silver particles. *J. Phys. Chem. B* **2004**, *108*, 17491–17496. [CrossRef]
28. Castro, J.L.; Lopez-Ramirez, M.R.; Arenas, J.F.; Soto, J.; Otero, J.C. Evidence of Deprotonation of Aromatic Acids and Amides Adsorbed on Silver Colloids by Surface-Enhanced Raman Scattering. *Langmuir* **2012**, *28*, 8926–8932. [CrossRef] [PubMed]
29. Chowdhury, J.; Mukherjee, K.M.; Misra, T.N. A pH dependent surface-enhanced Raman scattering study of hypoxanthine. *J. Raman Spectrosc.* **2000**, *31*, 427–431. [CrossRef]
30. Hidi, I.J.; Jahn, M.; Weber, K.; Cialla-May, D.; Popp, J. Droplet based microfluidics: Spectroscopic characterization of levofloxacin and its SERS detection. *Phys. Chem. Chem. Phys.* **2015**, *17*, 21236–21242. [CrossRef] [PubMed]
31. Greabu, M.; Battino, M.; Mohora, M.; Totan, A.; Didilescu, A.; Spinu, T.; Totan, C.; Miricescu, D.; Radulescu, R. Saliva—A diagnostic window to the body, both in health and in disease. *J. Med. Life* **2009**, *2*, 124–132. [PubMed]
32. Li, X.Z.; Yang, T.Y.; Lin, J.X. Spectral analysis of human saliva for detection of lung cancer using surface-enhanced Raman spectroscopy. *J. Biomed. Opt.* **2012**, *17*, 0370031–0370035. [CrossRef] [PubMed]
33. Yuen, C.; Zheng, W.; Huang, Z.W. Optimization of extinction efficiency of gold-coated polystyrene bead substrates improves surface-enhanced Raman scattering effects by post-growth microwave heating treatment. *J. Raman Spectrosc.* **2010**, *41*, 374–380. [CrossRef]

Supplementary material

Detection of *Pseudomonas aeruginosa* metabolite pyocyanin in water and saliva by employing the SERS technique

Olga Žukovskaja [1,2], Izabella Jolan Jahn [3], Karina Weber [1,2,3], Dana Cialla-May [1,2,3,] and Jürgen Popp [1,2,3]*

[1] Friedrich Schiller University Jena, Institute of Physical Chemistry and Abbe Center of Photonics, Helmholtzweg 4, 07745 Jena, Germany;
[2] Research Campus Infectognostic, Philosophenweg 7, 07743 Jena, Germany;
[3] Leibniz Institute of Photonic Technology Jena, Albert-Einstein-Str. 9, 07745 Jena, Germany;
* Correspondence: dana.cialla-may@leibniz-ipht.de; Tel.: +49-3641-206-309

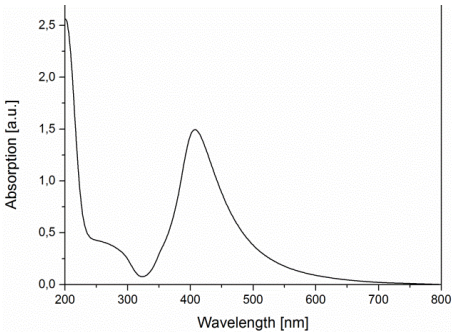

Figure S1. UV-Vis absorption spectra of the Ag nanoparticles.

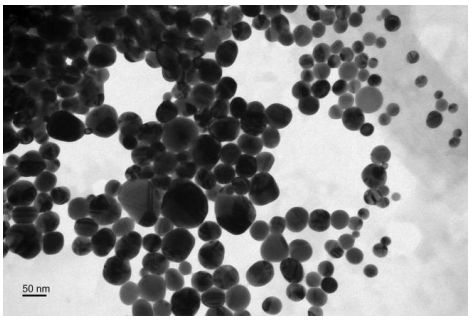

Figure S2. TEM image of Ag nanoparticles.

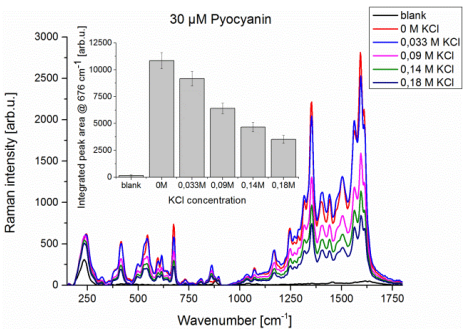

Figure S3. Mean SERS spectra of 30 µM PYO with different concentrations of KCl measured in the microfluidic platform. In the inset the integrated peak area of the PYO Raman mode at 676 cm^{-1} and

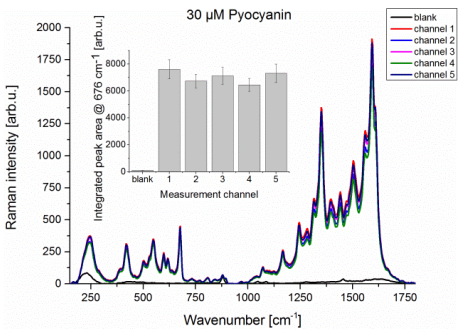

Figure S4. Mean SERS spectra of 30 µM PYO measured in different channels of the microfluidic chip. In the inset the integrated peak area of the PYO Raman mode at 676 cm^{-1} and its double standard deviation is illustrated.

its double standard deviation for different KCl concentrations is illustrated.

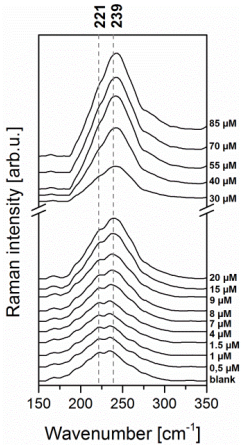

Figure S5. Mean SERS spectra of PYO with different concentrations in the region of Ag-O and Ag-N complexes vibrations.

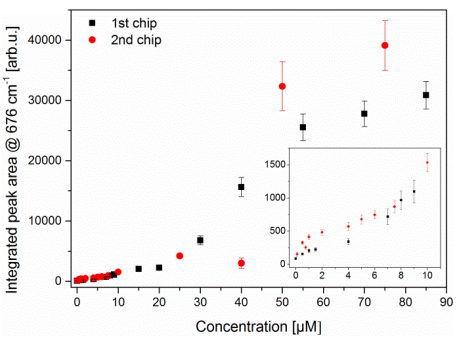

Figure S6. The peak area of the 676 cm^{-1} Raman mode as a function of PYO concentration for 2 different chips. In the inset zoomed area for concentrations till 10 μM.

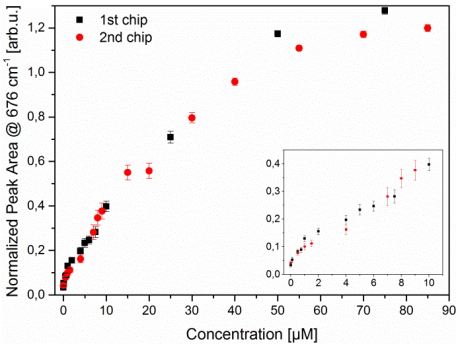

Figure S7. The peak area ratio of the 676 cm^{-1} and 240 cm^{-1} Raman modes as a function of PYO concentration. In the inset zoomed area for concentrations till 10 μM.

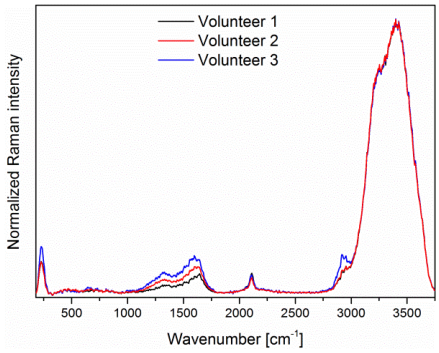

Figure S8. Mean SERS spectra of pure saliva of different volunteers

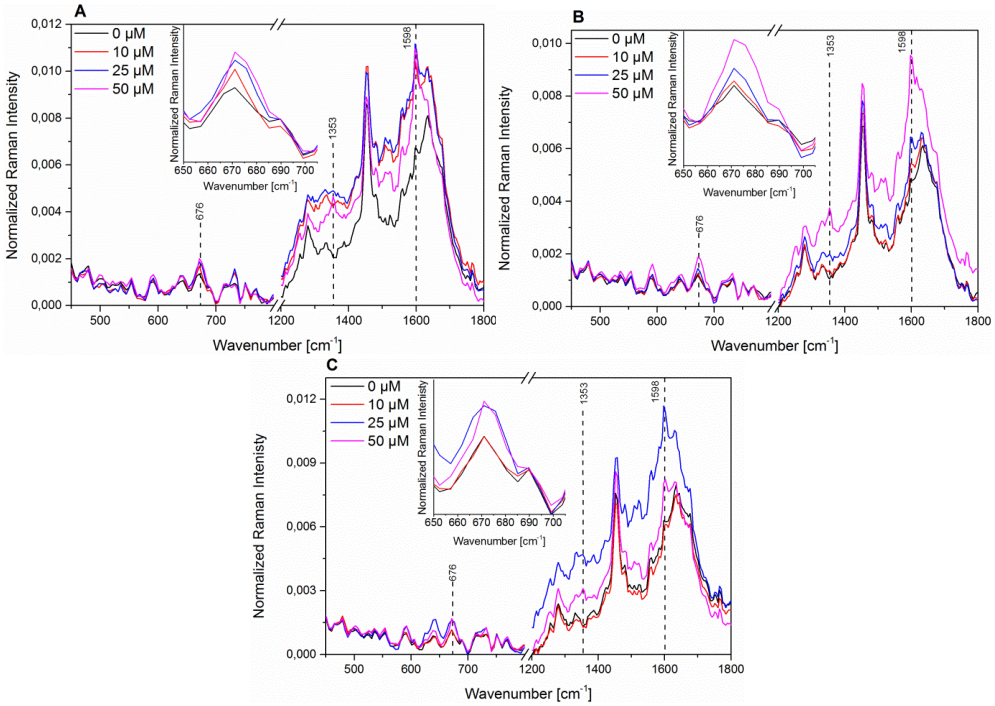

Figure S9. Mean SERS spectra in the fingerprint region of the three lowest concentrations of PYO in the saliva sample from volunteer number one (A), two (B) and three (C). In the inset the Raman band at 676 cm^{-1} is plotted.

7.4 Rapid detection of the bacterial biomarker Pyocyanin in artificial sputum using a SERS-active silicon nanowire matrix covered by bimetallic noble metal nanoparticles [OZ4]

Olga Žukovskaja*, Svetlana Agafilushkina*, Vladimir Sivakov, Karina Weber, Dana Cialla-May, Liubov Osminkina, Jürgen Popp

Talanta, 2019, 202, pp 171–177

https://doi.org/10.1016/j.talanta.2019.04.047

Declaration on authorship and copyright in a cumulative doctoral thesis

[1]**Olga Žukovskaja**, [2]Svetlana Agafilushkina, [3]Vladimir Sivakov, [4]Karina Weber, [5]Dana Cialla-May, [6]Liubov Osminkina, [7]Jürgen Popp. *Talanta*, 2019, 202, pp 171–177.							
Involved in							
	1	2	3	4	5	6	7
Conceptual research design	X	X	X	X	X	X	X
Planning of research activities	X	X	X	X	X	X	X
Data collection	X	X					
Data analyses and interpretation	X						
Manuscript writing	X	X	X	X	X	X	X
Suggested publication equivalence value	**1.0**	1.0					

Author Contribution

Olga Žukovskaja	concept development SERS measurements data analysis and interpretation writing of manuscript
Svetlana Agafilushkina	concept development fabrication of SERS substrates writing of manuscript
Vladimir Sivakov	back scattered electrons measurements discussion of experimental concept and results project management proofreading of manuscript
Karina Weber	discussion of experimental concept and results proofreading of manuscript
Dana Cialla-May	discussion of experimental concept and results proofreading of manuscript
Liubov Osminkina	discussion of experimental concept and results proofreading of manuscript
Jürgen Popp	project management discussion of concepts and results discussion and proofreading of manuscript

Talanta 202 (2019) 171–177

Contents lists available at ScienceDirect

Talanta

journal homepage: www.elsevier.com/locate/talanta

Rapid detection of the bacterial biomarker pyocyanin in artificial sputum using a SERS-active silicon nanowire matrix covered by bimetallic noble metal nanoparticles

Olga Žukovskaja[a,b,c,1], Svetlana Agafilushkina[d,1], Vladimir Sivakov[c], Karina Weber[a,b,c], Dana Cialla-May[a,b,c,*], Liubov Osminkina[d,e,**], Jürgen Popp[a,b,c]

[a] Friedrich Schiller University Jena, Institute of Physical Chemistry and Abbe Center of Photonics, Helmholtzweg 4, 07745, Jena, Germany
[b] Research Campus InfectoGnostics, Philosophenweg 7, 07743, Jena, Germany
[c] Leibniz Institute of Photonic Technology Jena - Member of the Research Alliance "Leibniz Health Technologies", Albert-Einstein-Str. 9, 07745, Jena, Germany
[d] Lomonosov Moscow State University, Physics Department, 119991, Moscow, Russia
[e] Institute for Biological Instrumentation of Russian Academy of Sciences, 142290, Pushchino, Moscow Region, Russia

ARTICLE INFO

Keywords:
Surface enhanced Raman spectroscopy (SERS)
Silicon nanowires (SiNWs)
Pyocyanin
Pseudomonas aeruginosa
Metabolite
Sputum

ABSTRACT

Early stage detection of *Pseudomonas* infections is life-saving, especially in the case of patients with cystic fibrosis. Pyocyanin (PYO) is a specific metabolite of the *Pseudomonas aeruginosa* bacteria, and detection of it directly in the sputum can significantly reduce the diagnosis time of the infection. In the present study, aiming to achieve this goal, a simple and cost-effective surface-enhanced Raman spectroscopy (SERS) detection platform was proposed. For this, a silicon nanowire (SiNW) matrix, produced by metal-assisted chemical etching of silicon substrates was variously modified by noble metal (silver and gold) nanoparticles (NPs) and tested for the detection of the metabolite PYO in the complex matrix of artificial sputum. We found the SERS substrate with Ag NPs on the bottom of SiNWs and deposited bimetallic Ag/Au NPs on the top of them the best suited for the sensitive detection of PYO. The investigated plasmonic substrate showed good point-to-point and batch-to-batch signal reproducibility and allowed for the detection of PYO in artificial sputum down to 6.25 μM, which is the required sensitivity for clinical applications.

1. Introduction

Pseudomonas aeruginosa is a common opportunistic pathogen of nosocomial infection in patients with impaired immunity connected with the management of malignancy, organ transplantation, autoimmune and inflammatory conditions, as well as being the major pathogen associated with respiratory tract infections in patients with cystic fibrosis (CF) [1–4]. Early identification of *P. aeruginosa* in CF patients provides the opportunity for early aggressive antibiotic treatment, as early isolates are generally nonmucoid, antibiotic-susceptible and present at low density [5–8]. Mucoid *Pseudomonas* is very challenging to treat and eradicate because of its ability to form impenetrable biofilms and rapidly develop resistance to antibiotics [9]. *P. aeruginosa* airway infection in CF patients is generally diagnosed by a culture of respiratory tract samples, such as spontaneously expectorated or induced sputum, oropharyngeal swabs or bronchoalveolar lavage (BAL) [7]. It usually takes more than 3 days to obtain accurate results. Moreover, there is a risk of inconsistent results due to sample contamination, and *P. aeruginosa* biofilms formed in CF lungs has decreased cultivability under standard conditions. Thus, in recent years, some attention has been given to alternative methods of diagnosis, such as serology or molecular techniques like polymerase chain reaction (PCR) [10–12]. Both methods exhibit high potential for the detection of *P. aeruginosa*; however, PCR methods require expensive reagents and the design of target-specific primers, while serological tests often fail to detect early colonization in young patients [13,14]. An alternative approach is the indirect detection of the *P. aeruginosa* by identifying the virulence factors secreted by the bacteria. One of these virulence factors is pyocyanin (PYO), which alters critical cellular processes, thereby generating reactive oxygen species and inducing neutrophil apoptosis

* Corresponding author. Friedrich Schiller University Jena, Institute of Physical Chemistry and Abbe Center of Photonics, Helmholtzweg 4, 07745, Jena, Germany.
** Corresponding author. Lomonosov Moscow State University, Physics Department, 119991, Moscow, Russia.
E-mail addresses: dana.cialla-may@leibniz-ipht.de (D. Cialla-May), osminkina@physics.msu.ru (L. Osminkina).
[1] Equally contributed authors.

https://doi.org/10.1016/j.talanta.2019.04.047
Received 14 December 2018; Received in revised form 12 April 2019; Accepted 18 April 2019
Available online 25 April 2019
0039-9140/

[15]. PYO is exclusively secreted by *P. aeruginosa*, giving this molecule high potential to be used as a diagnostic biomarker. In clinical sputum samples, PYO can reach concentrations up to 16.5 μg/ml (~76 μM) for cystic fibrosis patients and up to 27.3 μg/ml (~130 μM) for patients with bronchiectasis [16]. Hunter et al. observed a certain correlation between the concentration levels of PYO and its biosynthetic precursor, phenazine-1-carboxylic acid, in expectorated cystic fibrosis sputum samples and the severity of the disease. Patients with severe lung obstruction showed a significant progressive increase in PYO concentrations (46.8 μM) relative to those with normal lung function (7.7 μM) [17]. The development of a fully enclosed automatic technique for direct PYO detection in respiratory samples will shorten diagnostic turnaround time and reduce the risk of contamination.

Surface enhanced Raman spectroscopy (SERS) already has been proven to be a molecular-specific and highly sensitive analytical technique suitable for biological applications [18–20]. SERS allows for the sensitive identification of the molecular fingerprint of the analyte brought in the proximity of plasmonic nanostructures, which enhance the Raman signal by several orders of magnitude. Different SERS approaches have been described for studying *P. aeruginosa* biofilm formation and intercellular communication on the basis of the PYO signal [21,22]. In our previous study, we demonstrated direct detection of PYO spiked in the saliva of three volunteers using silver colloids as the SERS agent. PYO was successfully detected down to the 10 μM concentration in two saliva samples and down to 25 μM in the third one [23]. Moving to more complex biological environments, such as sputum or BAL, still represents a significant challenge, since the intrinsic complexity of the matrix may prevent the interaction of the target analyte with the metallic surface. In turn, this would hinder analysis by SERS, as other molecular species, e.g., proteins or DNA bases interacting with metal would increase the background signal. For instance, Wu et al., using an Ag nanorod arrays as the SERS substrate due to the dense matrix and volume dilution of processed sputum, could not detect PYO directly in clinical sputum samples from CF patients; prior to the measurements, PYO had to be extracted from sputum by chloroform [24]. That outcome makes the development of SERS substrates, which could overcome the limitations brought by complex matrix, of high importance.

Vertically aligned silicon nanowires (SiNWs) are imperative for the fabrication of such SERS substrates, because they have very high surface area and surface tailorability. Thus, a high number of metallic nanoparticles (NPs) could be packed on them, which would yield a high enhancement factor. SiNWs decorated with silver or gold were successfully used for ultrasensitive SERS detection of the standard analyte Rhodamine 6G [25,26], pesticides such as carbaryl [27], DNA [28] or avidin molecules [29].

In the current study, we present four different types of SiNWs substrates covered with the gold and/or silver for the direct, label-free SERS detection of PYO spiked in artificial sputum. Here, artificial sputum was selected since it simulates clinical samples and because its exactly known composition offers the possibility to study interaction of the matrix components and target analyte with plasmonic nanostructures. To the best of our knowledge, this is the first report proving the high potential of SERS for the direct determination of PYO in such a complex matrix as sputum.

2. Materials and methods

Chemicals and Reagents. Silver nitrate ($AgNO_3$), 48% Hydrofluoric acid (HF), Pyocyanin from *P. aeruginosa*, ≥98% (HPLC) in powder form, DNA from fish sperm and mucin from porcine stomach (type II) were purchased from Sigma Aldrich. Bovine serum albumin (BSA) and egg yolk emulsions from VWR Prolabo, potassium chloride (KCl) (≥99.5% p.a. ACS, ISO) and sodium chloride (NaCl) from Carl Roth, diethylenetriaminepentaacetic acid (DTPA) with tris(hydroxymethyl)aminomethane hydrochloride (TRIS × HCl pH 8) from Merck, nitric acid (HNO_3), 65% from Chimmed and gold(III) chloride ($AuCl_3$) from ABCR were also used.

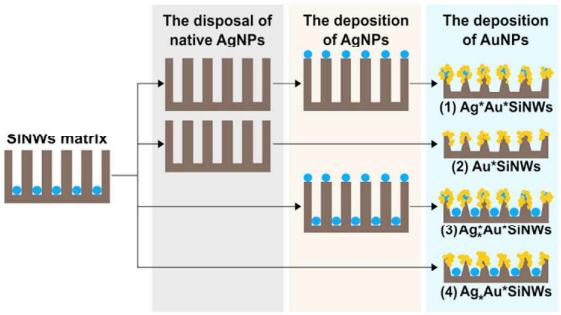

Scheme 1. Schematic representation of the formation of SiNWs based substrates covered with noble metal nanoparticles. (no color print).

Fabrication of the SERS substrates. Four SERS substrates based on SiNWs matrix were produced, as shown in Scheme 1: (1) Ag^*Au^*SiNWs, for which bimetallic Ag/Au NPs were deposited on the top of SiNWs matrix; (2) Au^*SiNWs, for which only Au NPs were deposited on the top of SiNWs matrix; (3) $Ag^*_*Au^*$SiNWs, where Ag NPs covered the bottom and bimetallic Ag/Au NPs were deposited on the top of SiNWs matrix; (4) Ag_*Au^*SiNWs, with Ag NPs at the bottom and Au NPs on the top of SiNWs matrix.

The SiNW matrix was prepared by metal-assisted chemical etching (MACE) of boron-doped 1–5 Ωcm (100) single crystalline silicon (Si) wafers using a similar procedure as published in our previous work [30]. Prior the MACE procedure, the Si surfaces were rinsed in acetone and isopropanol for 2 min to remove organic and inorganic residues, and then rinsed in 5% HF aqueous solution for 1 min to remove the native oxide. In the first step of MACE, Ag NPs were deposited on the surfaces by immersing them in aqueous solution of 0.02 M $AgNO_3$ and 5 M HF at a volume ratio of 1:1 for 15 s. In the second step, the Si surfaces covered with Ag NPs were immersed in the second etching solution containing 5 M HF and 30% H_2O_2 at a volume ratio of 10:1 in a Teflon vessel for 30 s. The etching step was performed at room temperature. After the MACE procedure, the typical SiNWs matrix of vertically aligned nanowire array with native Ag NPs at the bottom was observed, as shown in Fig. S1. If it was necessary, native Ag NPs were removed by immersing the samples in concentrated (65%) nitric acid (HNO_3) for 15 min. Finally, the samples were rinsed several times in deionized water and dried at room temperature.

For the formation of Ag, Au, or bimetallic Ag/Au NPs in SiNWs matrix, the matrix was immersed in 0.02 M $AgNO_3$ or in 0.01 M $AuCl_3$ and 5 M HF at a volume ratio of 1:1 for 10–30 s, similar to galvanic displacement and autometallography [31]. As a result, on the top of the nanowires appeared silver or gold NPS recovered from silver nitrate or from gold(III) chloride, respectively. In the case of bimetallic Ag/Au NPs, the silver was recovered first, and then the procedure was repeated for the gold.

SEM analysis. The morphology and composition of the SiNW matrix covered by noble metal (gold and silver) particles was studied by scanning electron microscopy (SEM) using a Carl Zeiss ULTRA 55, FE-SEM microscope. To carry out the SEM analysis, the samples were rinsed several times in deionized water and dried at room temperature. The surface morphology was investigated by detecting secondary electrons. The surface composition was studied by detecting back scattered electrons (BSEs).

Pyocyanin Solution. Since PYO is slightly soluble in water, a stock solution of 1 mM PYO was prepared in ethanol by adding the appropriate amount of powder. Next, serial dilutions were performed to prepare 1000, 500, 100, 50, 10, 5, 1, 0.5 nM PYO. Concentration of ethanol was kept 10% in all solutions.

Artificial sputum. The artificial sputum was prepared according to the protocol used by Kloß et al. [31] Briefly, 400 mg of DNA from fish sperm and 3 g of mucin from porcine stomach (type II) were each suspended in 25 mL of deionized water and solubilized in a rotation mixer (12–15 rpm) over the night at 4 °C 1 g of BSA was solubilized in 10 mL of deionized water. 500 mg of NaCl, 225 mg of KCl, and 0.6 mg of DTPA were dissolved in 10 mL of deionized water each. All solutions were mixed, and 5 mL of egg yolk emulsion was added. The pH was adjusted to 7.0 with 1 M TRIS × HCl at pH 8, and, finally, the solution was filled up to 100 mL with deionized water and vortexed. The artificial sputum was stored at −20 °C. Before measurements, the sputum was thawed at room temperature and vortexed. 900 µL of artificial sputum were spiked with 100 µL of 1 mM PYO solution in ethanol to achieve 100 µM PYO in the sputum. For reference, the artificial sputum was spiked just with ethanol. Next, serial dilutions of artificial sputum with 100 µM PYO were performed to prepare the final concentrations of 100, 75, 50, 25, 12.5 and 6.25 µM of the analyte in the sputum samples, keeping the same sputum amount. For the SERS measurements, the resulting solutions were diluted 5 times with deionized water.

SERS measurements. The SERS measurements were performed using a commercially available Renishaw inVia Qontor setup equipped with a 785 nm laser. During the measurements, a 1200 lines per mm grating was used with a spectral resolution of ~0.84 cm^{-1}, the same objective (Leica 50× 0.75 N A.) was employed for focusing the laser beam on the sample and for collecting the backscattered light. The laser power was set to 3 mW on the laser head. For the SERS measurements, the substrates were incubated for 30 min in the as-prepared solutions of the sputum and then air dried. For the artificial sputum samples, due to the surface tension and the evaporation of the sample liquid, the 'coffee-ring effect' occurred and the target sample was concentrated around the edge of the substrate [32]. Therefore, the scanning areas were chosen around the edges for artificial sputum solutions (Fig. S2). When incubating substrates in aqueous PYO solution, the 'coffee-ring effect' was not detected; thus, for the aqueous PYO solutions, scan areas were selected randomly within the whole substrate area. For every sample, 10 50 × 50 µm areas were scanned using a 5 µm step. This resulted in 100 spectra per scan and 1000 spectra per sample. An integration time of 1 s was used.

Data Processing. Data processing was performed using an in-house developed algorithm in the programming language R [33]. During data processing, the spectra were background corrected using the Statistics-sensitive Nonlinear Iterative Peak-clipping (SNIP) algorithm [34]. To estimate the peak area, the Simpson rule was applied.

3. Results and discussion

Characterization of the SiNWs decorated with metallic NPs. Fig. 1 shows top view and cross-sectional images of the SiNW matrix variously modified by noble metal (gold and silver) NPs. During the sample preparation process, the nanowires acquire a conical shape. This is due to the formation of an oxide SiO_2 layer on the surface of the nanowires in the process of the reduction of Au NPs from gold chloride and its simultaneous etching in hydrofluoric acid. The top view and cross-sectional images of SiNWs matrix covered by gold on the top, Au*SiNWs, are presented in Fig. 1 (a, b). It is clear that gold forms the branched structures consisting of NPs with sizes between 10 and 20 nm on top of the nanowires. The presence of Au nanostructures on top of SiNW matrix is also confirmed by BSE analysis, as shown in Fig. S3. Fig. 1 (c, d) shows SEM images of the SiNW matrix with native silver at the bottom and deposited gold on top of the nanowires (Ag◦Au*SiNWs). Based on SEM, as well as on the BSE images shown in Fig. S4, it can be argued that the native Ag NPs that remain after the SiNWs production process are approximately 100 nm. The fine-grained gold nanostructures, similar to the structures observed in Fig. 1 (b), are localized on the top of SiNWs, as shown in Fig. 1 (d). Fig. 1 (e, f) represents the top view and cross-sectional SEM images of SiNWs with bimetallic Ag/Au NPs on top (Ag*Au*SiNWs). The Ag NPs, formed during the reduction of silver nitrate, are approximately 50 nm and localized on the top of the SiNWs, as shown in Fig. S5. From the SEM and BSE images shown in Fig. 1 (e, f) and Fig. S6, it is clear that these Ag NPs are homogeneously coated with a fine-grained structure of 10–20 nm Au NPs. SEM images of the SiNW matrix with a native layer of Ag NPs at the bottom and bimetallic Ag/Au NPs on the top ($Ag^*_◦Au^*$SiNWs) are shown in Fig. 1 (g, h), and the corresponding BSE images are shown in Fig. S7. The morphology of Ag NPs at the bottom and bimetallic Ag/Au NPs on top of the SiNWs was similar to the previous cases.

SERS characterization of SiNWs matrices covered by metal NPs. To move toward clinical application, the feasibility of using the investigated substrates for SERS detection of PYO in artificial sputum was explored. Due to the inherent limitations of SERS, direct detection of target analytes in complex biological environments still represents a significant challenge, mainly because of the competition between matrix components and the target analyte for binding sites on the SERS-active metallic surface. To find which type of the investigated substrates is the most suitable, two substrates of each type were incubated in artificial sputum with 50 µM PYO and 1000 spectra per substrate were measured. This resulted in the dataset of 2000 spectra for every substrate type.

Here, it is worth to notice that prior to the substrate incubation the spiked sputum sample was diluted. The dilution step was introduced in order to reduce the matrix effects [35,36] and to optimize the incubation process, since an increased viscosity of artificial sputum leads to a non-homogeneous distribution of the sample on the substrate and the formation of a thicker layer of the sample, which results in a lower SERS signal. To select the optimal dilution ratio, different dilutions were prepared. The achieved SERS spectra are depicted in Fig. S8. It can be seen that with an increasing amount of water, all Raman peaks becomes more prominent, even if the concentration of all components is decreased. The highest SERS signal of the target molecule PYO was achieved for the dilution ratio of 1:4, which was implemented for all measurements. In parallel, as a negative control, substrates were incubated in sputum without the analyte. Subsequent Raman spectroscopy measurements revealed that artificial sputum by itself has intense Raman modes at 732, 960 and 1327 cm^{-1} (Fig. 2 (a)), which, based on previous studies, can be mainly assigned to adenine, which is the one of four nucleobases in the nucleic acid of DNA [37]. However, despite some background information from the matrix, the Raman modes characteristic of PYO at 597, 676, 1353, 1600 and 1615 cm^{-1} are clearly visible for the all investigated SERS templates. The molecular structure of PYO is presented in the inset of Fig. 2 (a). The Raman band at 597 cm^{-1} is related to C–C, C–N and C–H out-of-plane bending vibrations, the one at 676 cm^{-1} is assigned to the ring deformation, and the peak at 1353 cm^{-1} corresponds to the combined C–C stretching, C–N stretching and C–H in-plane bending. Finally, the double band at 1600 cm^{-1} and 1615 cm^{-1} is ascribed to the ring deformation, C–C stretching vibration and C–H in-plane bending.

More detailed assignment of the all Raman modes of PYO can be found in the literature [24]. To analyze which SERS substrate allows the highest SERS performance, the ring deformation vibrational mode at 676 cm^{-1} was integrated from the vector normalized spectra and plotted for each type of SiNW matrix (Fig. 2 (b)). The relative standard deviations (RSDs) for Ag*Au*SiNWs, $Ag^*_◦Au^*$SiNWs, Ag*Au*SiNWs and Au*SiNWs were 27.7, 22.7, 32.0 and 32.2%, respectively. It is clear that the most intense and stable SERS signal was obtained using $Ag^*_◦Au^*$SiNWs. The Ag◦Au*SiNWs substrate had a very similar SERS performance, while Ag*Au*SiNWs and Au*SiNWs substrates had already significantly lower SERS intensity and higher RSD. Thus, it can be concluded that keeping the native layer of Ag NPs at the bottom of the substrate is improving the SERS signal. Most probably in this case, molecules of PYO, which reached the bottom of the substrate, can also be enhanced and contribute to the SERS signal. From Fig. 2 (b) it can also be observed that creating on the top of SiNWs bimetallic Ag/Au

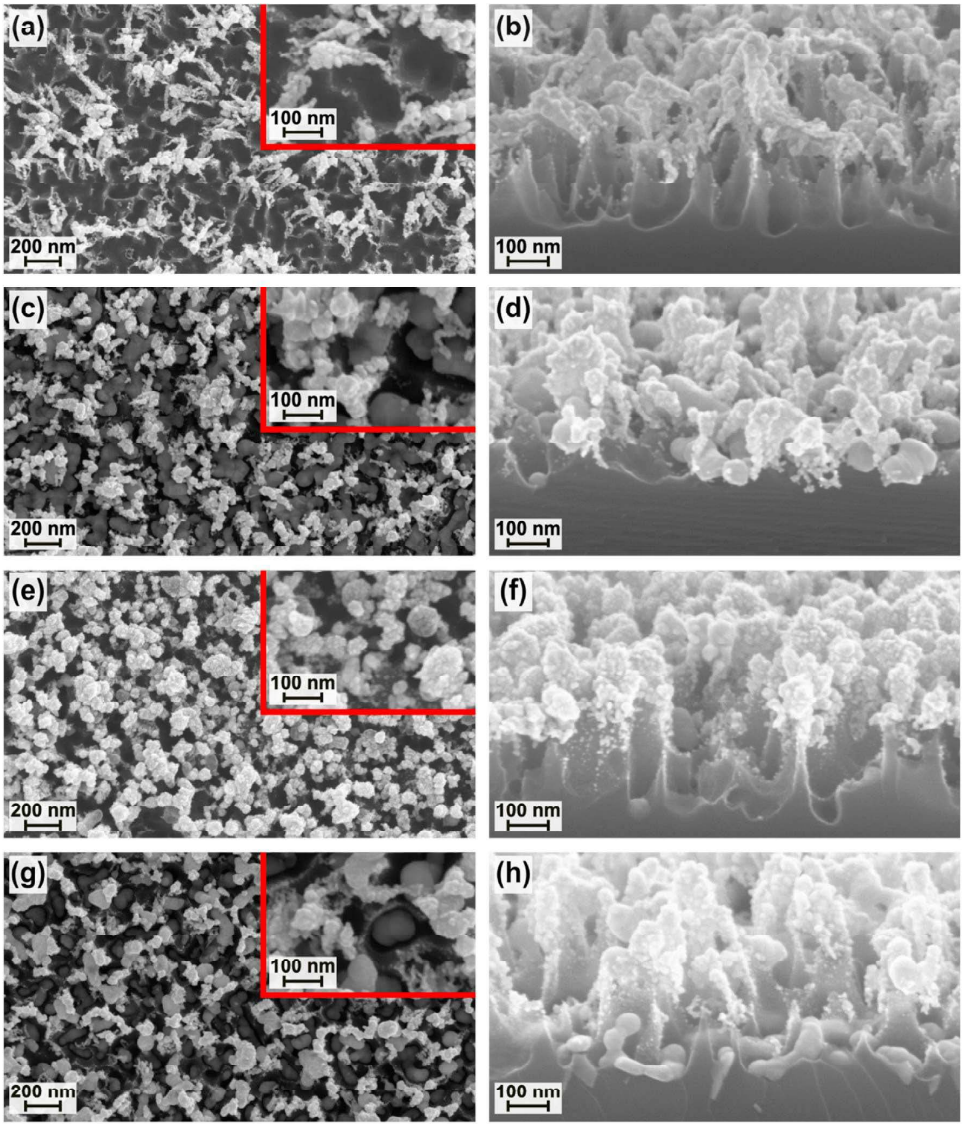

Fig. 1. SEM images of the SiNW matrix, differently modified by noble metal nanoparticles. Top view (a) and cross-sectional view (b) of Au*SiNWs; top view (c) and cross-sectional view (d) of Ag*Au*SiNWs; top view (e) and cross-sectional view (f) Ag*Au*SiNWs; top view (g) and cross-section view (h) of $Ag^{*}_{*}Au^{*}$SiNWs. (no color print). (For interpretation of the references to color in this figure legend, the reader is referred to the Web version of this article.)

NPs gives no significant signal improvement in comparison with just deposited Au NPs. However, it improves the RSD.

Based on those findings, for the further investigations, only $Ag^{*}_{*}Au^{*}$SiNWs substrates were utilized. This included the determination of the point-to-point and batch-to-batch SERS reproducibility of the nanostructures, performed by utilizing the same 50 μM PYO in artificial sputum.

The SEM analysis of the $Ag^{*}_{*}Au^{*}$SiNWs illustrates the morphological homogeneity across a large segment of the substrate (see Fig. 1). However, slight variations of the nanoparticles size, aggregation state and their distribution are still present. To investigate how it influences the SERS signal uniformity, SERS spectra were collected from 10 different randomly chosen 50 × 50 μm areas with a 5 μm step. Fig. 3 (a) presents the point-to-point SERS reproducibility of the measurements within one map. The characteristic Raman mode of PYO at 676 cm^{-1} was investigated for 100 individual spectra and plotted as a function of the spectrum number. The relative standard deviation (RSD) of the SERS intensity was approximately 11.6%, which is shown as the light red area. This demonstrates that the investigated chemically produced SERS substrate is capable of generating SERS signals with good reproducibility.

Fig. 3 (b) depicts the signal variation for different scans within the substrate. Each box represents 100 spectra measured within one scan. Here already higher deviations can be observed. This possibly can be caused by differences in the focus depth changing the measurement position as well by inhomogeneous drying of the sputum. The

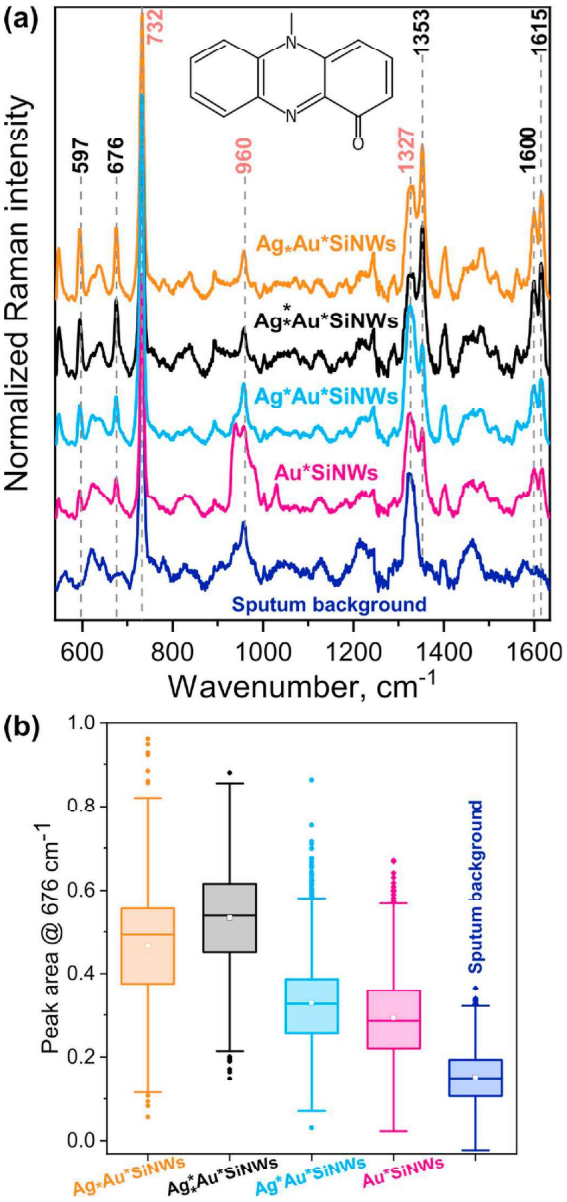

Fig. 2. (a) Mean SERS spectra of 50 µM PYO in artificial sputum measured on four different types of SiNWs substrates (2000 spectra per type of SERS substrate) and the mean SERS spectra of artificial sputum. Inset presents the molecular structure of Pyocyanin. **(b)** Normalized peak area for the peak at 676 cm^{-1} for four different types of SiNW substrates. (no color print). (For interpretation of the references to color in this figure legend, the reader is referred to the Web version of this article.)

illustrated variations still demonstrate that scanning some areas within a substrate is a reliable method for getting an overview of substrate SERS activity.

Additionally, four batches of substrates were prepared to investigate the batch-to batch SERS reproducibility. Here, two substrates from each batch were investigated by measuring 1000 spectra per substrate using 50 µM concentration of PYO. Similarly, as for previous analysis, the

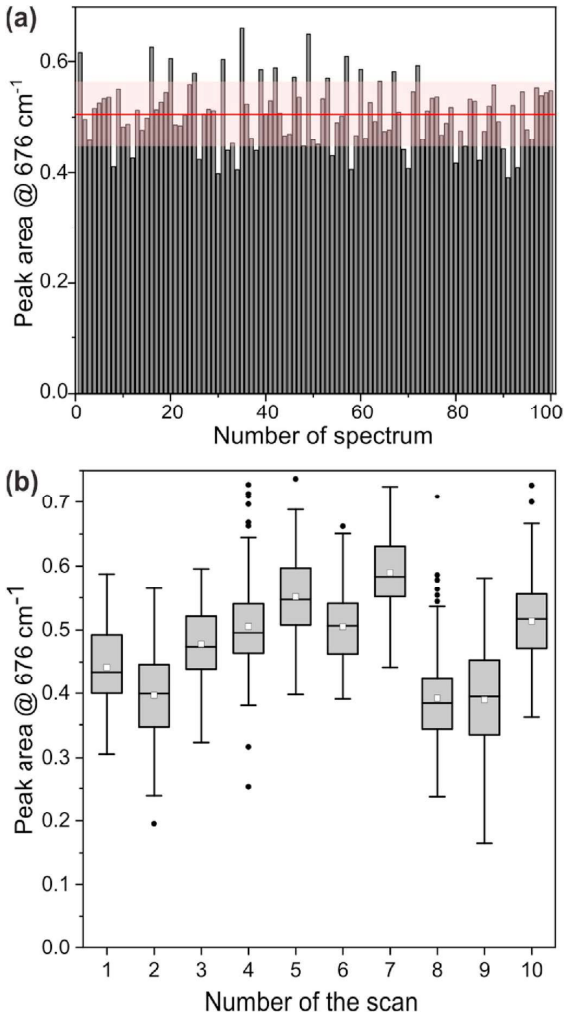

Fig. 3. (a) Point-to-point SERS reproducibility of 50 µM of PYO in artificial sputum obtained from 50 × 50 µm area with a 5 µm step. The red line shows the average intensity, and the light red area represents the standard deviation of the obtained spectra. (b) The scan-to-scan SERS reproducibility of 10 different scans consisting of 100 spectra. (no color print). (For interpretation of the references to color in this figure legend, the reader is referred to the Web version of this article.)

peak area for the ring breathing mode at 676 cm^{-1} was calculated and plotted for individual batches of substrates (Fig. 4). These investigations reveal that all batches of $Ag^{*}_{*}Au^{*}$SiNWs are SERS active and have similar performance with RSD for the mean for all batches being around 12%. This indicates the good reliability of the method.

Finally, the sensitivity of the substrates for the detection of PYO in artificial sputum was investigated. Prior to the measurements, different clinically relevant concentrations of PYO were spiked into the matrix. Fig. 5 (a) represents the mean spectra for the investigated concentrations, as well as the SERS spectrum from the sputum without the analyte. Despite some background from the matrix, already for 6.25 µM PYO, the peaks at 593, 676, 1353, 1600 and 1615 cm^{-1} appear, which are the signature of PYO. With the increase of the concentration, the peaks become even more prominent. For better visualization in Fig. 5 (b), the integrated peak area of the C—N stretching and C—H in-plane

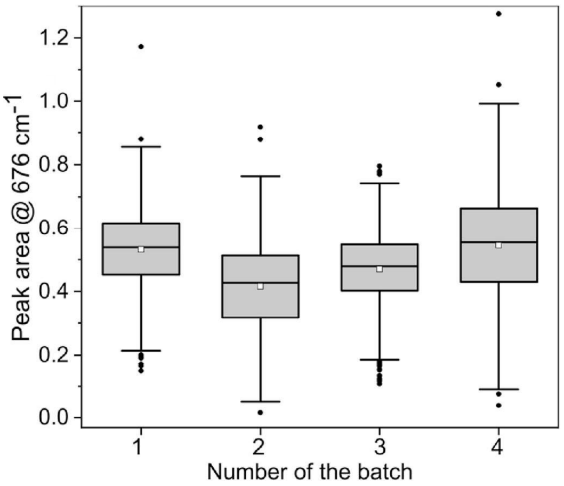

Fig. 4. Batch-to-batch reproducibility obtained by measuring two substrates from each batch (2000 spectra per batch) using a 50 µM concentration of PYO in artificial sputum. (no color print).

bending vibrations at 1353 cm^{-1} was plotted against the concentrations of PYO.

From Fig. 5 (b), it is obvious that the PYO band at 1353 cm^{-1} can be detected at 6.25 µM, which is the lowest expected concentration of the clinically relevant range for patients with cystic fibrosis. It can be concluded that the designed substrates are sensitive platforms for the SERS detection of biomolecules in complex matrices. In parallel to the visual assessment, the calculation of the limit of detection (LOD) was performed. Using the definition that the LOD is equal to the blank intensity plus three-times SD (3σ confidence level) divided by the slope of the calibration line [38] a LOD of 15 µM was achieved. Although in the literature lower LODs for SERS based PYO detection can be found (see Table S1), this is the first study reporting direct detection in such complex matrix as artificial sputum without complex sample preparation steps.

To investigate the influence of the complex matrix on the SERS performance, different concentrations of PYO in aqueous solution were investigated. Fig. S9 shows the PYO signal for different concentrations as well as the background signal of the substrate. The characteristic bands of PYO can be reliably detected down to 1 nM without any significant background contribution from the substrate. Thus, the competition for free binding sites on the metallic surface between the PYO and other components of artificial sputum results in a decrease of SERS signal by three orders of magnitude. Despite this, the proposed substrates have significant ability to directly detect clinically relevant concentrations in artificial sputum. This finding is highly important for solving the diagnostic issues of *P. aeruginosa* infections.

4. Conclusions

PYO is a virulence factor uniquely produced by *P. aeruginosa*. Thus, the fast and selective detection of this factor can reveal the presence of *P. aeruginosa* in an organism. The direct detection of PYO in sputum will reduce diagnosis time and lead to successful antibiotic treatment. SERS is a powerful technique for the identification and potential quantification of target analytes. However, its real application is challenging due to the multiple interferences from the complex matrix. Thus, suitable SERS substrates for such purposes should be designed. In this study, the fabrication process of a SiNW matrix differently modified with Ag and Au NPs was demonstrated. The process combines SiNW synthesis by the metal-assisted chemical etching with or without native Ag NPs and subsequent Ag and Au NPs chemical deposition. This fabrication method has short processing time, is cost-effective and provides structural variability with high potential for SERS applications. The

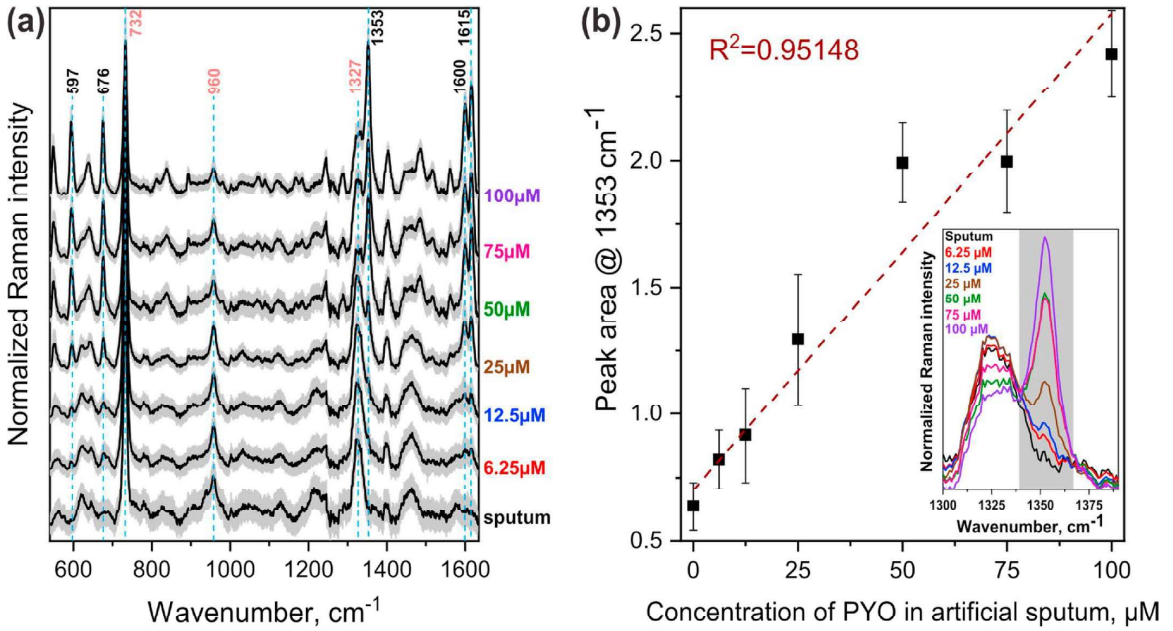

Fig. 5. (a) Vector normalized mean SERS spectra of artificial sputum spiked with different PYO concentrations. (b) The peak area of the band at 1353 cm^{-1} (in inset) as a function of the PYO concentration in the range between 6.25 and 100 µM. (no color print). (For interpretation of the references to color in this figure legend, the reader is referred to the Web version of this article.)

investigation of different substrates for PYO detection in artificial sputum revealed that keeping native Ag NPs on the bottom of the SiNWs is beneficial for the SERS performance. Furthermore, the deposition of Ag first, followed by that of Au, to achieve bimetallic Ag/Au NPs on top of the SiNWs, gives a more stable signal. Based on those findings, the $Ag^{*}_{s}Au^{*}$SiNWs substrate was selected for studying the sensitivity in detection of PYO in artificial sputum. Point-to-point and batch-to-batch investigations showed good stability of the signal, and PYO could be successfully detected in artificial sputum down to 6.25 μM, which is the lower extreme of the clinically relevant range.

Notes

The authors declare no competing financial interests.

Acknowledgment

The authors thank Ivan Bozhev for recording SEM images. We gratefully acknowledge the Federal Ministry of Education and Research, Germany (BMBF) for the continued support for the InfectoGnostics (13GW0096F) and EXASENS (13N13856) grants, and the financial support from the Russian Science Foundation (RSF) (grant No. 17-12-01386), additionally with the Foundation for the Advancement of Theoretical Physics and Mathematics "BASIS".

Appendix A. Supplementary data

Supplementary data to this article can be found online at https://doi.org/10.1016/j.talanta.2019.04.047.

References

[1] A.W. Artenstein, A.S. Cross, Serious infections caused by Pseudomonas aeruginosa, J. Intensive Care Med. 9 (1) (1994) 34–51.
[2] G.P. Bodey, R. Bolivar, V. Fainstein, L. Jadeja, Infections caused by Pseudomonas aeruginosa, Rev. Infect. Dis. 5 (2) (1983) 279–313.
[3] L.V.R.F. da Silva, F.d.A. Ferreira, F.J.C. Reis, M.C.A. de Britto, C.E. Levy, O. Clark, J.D. Ribeiro, Pseudomonas aeruginosa infection in patients with cystic fibrosis: scientific evidence regarding clinical impact, diagnosis, and treatment, J. Bras. Pneumol. 39 (4) (2013) 495–512.
[4] J.C. Davies, Pseudomonas aeruginosa in cystic fibrosis: pathogenesis and persistence, Paediatr. Respir. Rev. 3 (2) (2002) 128–134.
[5] G. Doring, S.P. Conway, H.G. Heijerman, M.E. Hodson, N. Hoiby, A. Smyth, D.J. Touw, Antibiotic therapy against Pseudomonas aeruginosa in cystic fibrosis: a European consensus, Eur. Respir. J. 16 (4) (2000) 749.
[6] F. Ratjen, G. Döring, W.H. Nikolaizik, Effect of inhaled tobramycin on early Pseudomonas aeruginosa colonisation in patients with cystic fibrosis, Lancet 358 (9286) (2001) 983–984.
[7] T.D. Starner, P.B. McCray Jr., Pathogenesis of early lung disease in cystic fibrosis: a window of opportunity to eradicate bacteria, Ann. Intern. Med. 143 (11) (2005) 816–822.
[8] N.H. Valerius, C. Koch, N. Hoiby, Prevention of chronic Pseudomonas aeruginosa colonisation in cystic fibrosis by early treatment, Lancet 338 (8769) (1991) 725–726.
[9] P.D. Lister, D.J. Wolter, N.D. Hanson, Antibacterial-resistant Pseudomonas aeruginosa: clinical impact and complex regulation of chromosomally encoded resistance mechanisms, Clin. Microbiol. Rev. 22 (4) (2009) 582–610.
[10] P. Deschaght, S. Van daele, F. De Baets, M. Vaneechoutte, PCR and the detection of Pseudomonas aeruginosa in respiratory samples of CF patients. A literature review, J. Cyst. Fibros. 10 (5) (2011) 293–297.
[11] R.M. Mauch, C.E. Levy, Serum antibodies to Pseudomonas aeruginosa in cystic fibrosis as a diagnostic tool: a systematic review, J. Cyst. Fibros. 13 (5) (2014) 499–507.
[12] Y. Tang, Z. Ali, J. Zou, G. Jin, J. Zhu, J. Yang, J. Dai, Detection methods for Pseudomonas aeruginosa: history and future perspective, RSC Adv. 7 (82) (2017) 51789–51800.
[13] T.A. Douglas, S. Brennan, L. Berry, K. Winfield, C.E. Wainwright, K. Grimwood, S.M. Stick, P.D. Sly, Value of serology in predicting *Pseudomonas aeruginosa* infection in young children with cystic fibrosis, Thorax 65 (11) (2010) 985.
[14] G.A. Tramper-Stranders, C.K. van der Ent, M.G. Slieker, S.W.J. Terheggen-Lagro, F.T. van Berkhout, J.L.L. Kimpen, T.F.W. Wolfs, Diagnostic value of serological tests against Pseudomonas aeruginosa in a large cystic fibrosis population, Thorax 61 (8) (2006) 689–693.
[15] S. Hall, C. McDermott, S. Anoopkumar-Dukie, A.J. McFarland, A. Forbes, A.V. Perkins, A.K. Davey, R. Chess-Williams, M.J. Kiefel, D. Arora, G.D. Grant, Cellular effects of pyocyanin, a secreted virulence factor of Pseudomonas aeruginosa, Toxins 8 (8) (2016) 236.
[16] R. Wilson, D.A. Sykes, D. Watson, A. Rutman, G.W. Taylor, P.J. Cole, Measurement of Pseudomonas aeruginosa phenazine pigments in sputum and assessment of their contribution to sputum sol toxicity for respiratory epithelium, Infect. Immun. 56 (9) (1988) 2515–2517.
[17] R.C. Hunter, V. Klepac-Ceraj, M.M. Lorenzi, H. Grotzinger, T.R. Martin, D.K. Newman, Phenazine content in the cystic fibrosis respiratory tract negatively correlates with lung function and microbial complexity, Am. J. Respir. Cell Mol. Biol. 47 (6) (2012) 738–745.
[18] H.-W. Cheng, J. Luo, C.-J. Zhong, SERS nanoprobes for bio-application, Front. Chem. Sci. Eng. 9 (4) (2015) 428–441.
[19] M.D. Porter, R.J. Lipert, L.M. Siperko, G. Wang, R. Narayanan, SERS as a bioassay platform: fundamentals, design, and applications, Chem. Soc. Rev. 37 (5) (2008) 1001–1011.
[20] X.S. Zheng, I.J. Jahn, K. Weber, D. Cialla-May, J. Popp, Label-free SERS in biological and biomedical applications: recent progress, current challenges and opportunities, Spectrochim. Acta A Mol. Biomol. Spectrosc. 197 (2018) 56–77.
[21] G. Bodelon, V. Montes-Garcia, V. Lopez-Puente, E.H. Hill, C. Hamon, M.N. Sanz-Ortiz, S. Rodal-Cedeira, C. Costas, S. Celiksoy, I. Perez-Juste, L. Scarabelli, A. La Porta, J. Perez-Juste, I. Pastoriza-Santos, L.M. Liz-Marzan, Detection and imaging of quorum sensing in Pseudomonas aeruginosa biofilm communities by surface-enhanced resonance Raman scattering, Nat. Mater. 15 (11) (2016) 1203–1211.
[22] C.Q. Nguyen, W.J. Thrift, A. Bhattacharjee, S. Ranjbar, T. Gallagher, M. Darvishzadeh-Varcheie, R.N. Sanderson, F. Capolino, K. Whiteson, P. Baldi, A.I. Hochbaum, R. Ragan, Longitudinal monitoring of Biofilm Formation via robust surface enhanced Raman scattering quantification of Pseudomonas aeruginosa-produced metabolites, ACS Appl. Mater. Interfaces 10 (15) (2018) 12364–12373.
[23] O. Zukovskaja, I.J. Jahn, K. Weber, D. Cialla-May, J. Popp, Detection of Pseudomonas aeruginosa metabolite pyocyanin in water and saliva by employing the SERS technique, Sensors (Basel) 17 (8) (2017).
[24] X. Wu, J. Chen, X. Li, Y. Zhao, S.M. Zughaier, Culture-free diagnostics of Pseudomonas aeruginosa infection by silver nanorod array based SERS from clinical sputum samples, Nanomed. Nanotechnol. Biol. Med. 10 (8) (2014) 1863–1870.
[25] C.-Y. Chen, L.-J. Hsu, P.-H. Hsiao, C.-T.R. Yu, SERS detection and antibacterial activity from uniform incorporation of Ag nanoparticles with aligned Si nanowires, Appl. Surf. Sci. 355 (2015) 197–202.
[26] M.F. Peng, H.Y. Xu, M.W. Shao, Ultrasensitive surface-enhanced Raman scattering based gold deposited silicon nanowires, Appl. Phys. Lett. 104 (19) (2014).
[27] X.T. Wang, W.S. Shi, G.W. She, L.X. Mu, S.T. Lee, High-performance surface-enhanced Raman scattering sensors based on Ag nanoparticles-coated Si nanowire arrays for quantitative detection of pesticides, Appl. Phys. Lett. 96 (5) (2010).
[28] Y. He, S. Su, T.T. Xu, Y.L. Zhong, J.A. Zapien, J. Li, C.H. Fan, S.T. Lee, Silicon nanowires-based highly-efficient SERS-active platform for ultrasensitive DNA detection, Nano Today 6 (2) (2011) 122–130.
[29] A. Convertino, V. Mussi, L. Maiolo, Disordered array of Au covered Silicon nanowires for SERS biosensing combined with electrochemical detection, Sci. Rep. 6 (2016).
[30] E. Tolstik, L.A. Osminkina, C. Matthäus, M. Burkhardt, K.E. Tsurikov, U.A. Natashina, V.Y. Timoshenko, R. Heintzmann, J. Popp, V. Sivakov, Studies of silicon nanoparticles uptake and biodegradation in cancer cells by Raman spectroscopy, Nanomedicine 12 (7) (2016) 1931–1940.
[31] S. Kloss, B. Lorenz, S. Dees, I. Labugger, P. Rosch, J. Popp, Destruction-free procedure for the isolation of bacteria from sputum samples for Raman spectroscopic analysis, Anal. Bioanal. Chem. 407 (27) (2015) 8333–8341.
[32] R.D. Deegan, O. Bakajin, T.F. Dupont, G. Huber, S.R. Nagel, T.A. Witten, Capillary flow as the cause of ring stains from dried liquid drops, Nature 389 (1997) 827.
[33] R.D.C. Team, R.:A. Language, And Environment for Statistical Computing, (2011).
[34] C.G. Ryan, E. Clayton, W.L. Griffin, S.H. Sie, D.R. Cousens, SNIP, a statistics-sensitive background treatment for the quantitative-analysis of pixe spectra in geoscience applications, Nucl. Instrum. Methods Phys. Res. B 34 (3) (1988) 396–402.
[35] I.J. Hidi, M. Jahn, M.W. Pletz, K. Weber, D. Cialla-May, J. Popp, Toward levofloxacin monitoring in human urine samples by employing the LoC-SERS technique, J. Phys. Chem. C 120 (37) (2016) 20613–20623.
[36] V. Peksa, M. Jahn, L. Štolcová, V. Schulz, J. Proška, M. Procházka, K. Weber, D. Cialla-May, J. Popp, Quantitative SERS analysis of azorubine (E 122) in sweet drinks, Anal. Chem. 87 (5) (2015) 2840–2844.
[37] F. Madzharova, Z. Heiner, M. Gühlke, J. Kneipp, Surface-enhanced hyper-Raman spectra of adenine, guanine, cytosine, thymine, and uracil, J. Phys. Chem. C 120 (28) (2016) 15415–15423.
[38] A. Shrivastava, V. Gupta, Methods for the determination of limit of detection and limit of quantitation of the analytical methods, Chronicles Young Sci. 2 (1) (2011) 21–25.

Supporting Information

Rapid detection of the bacterial biomarker Pyocyanin in artificial sputum using SERS active SiNWs matrix covered by bimetallic noble metal nanoparticles

Olga Žukovskaja[a,b,c,#], Svetlana Agafilushkina[d,#], Vladimir Sivakov[c], Karina Weber[a,b,c], Dana Cialla-May [a,b,c,*], Liubov Osminkina[d,e,*], and Jürgen Popp[a,b,c]

[a] Friedrich Schiller University Jena, Institute of Physical Chemistry and Abbe Center of Photonics, Helmholtzweg 4, 07745 Jena, Germany;

[b] Research Campus InfectoGnostics, Philosophenweg 7, 07743 Jena, Germany;

[c] Leibniz Institute of Photonic Technology Jena - Member of the research alliance "Leibniz Health Technologies", Albert-Einstein-Str. 9, 07745 Jena, Germany;

[d] Lomonosov Moscow State University, Physics Department, 119991 Moscow, Russia

[e] Institute for Biological Instrumentation of Russian Academy of Sciences, 142290 Pushchino, Moscow Region, Russia

*Corresponding authors e-mail address: dana.cialla-may@leibniz-ipht.de and osminkina@physics.msu.ru

# Equally contributed authors.

Table of Content:

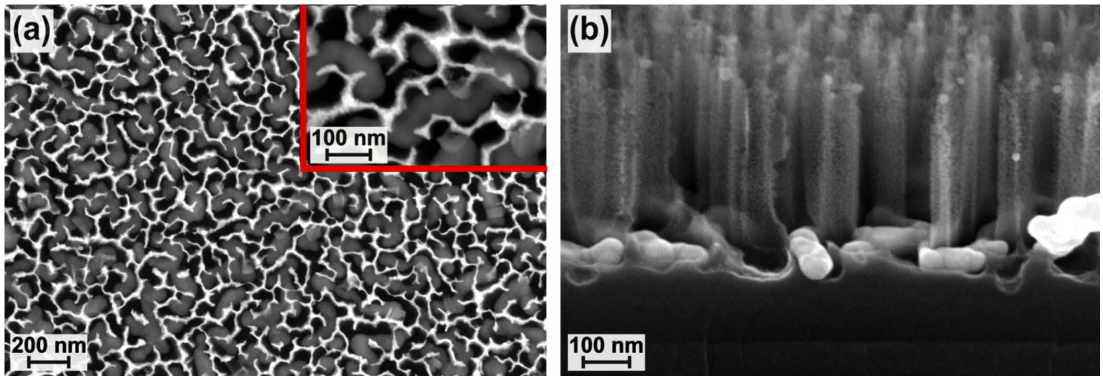

Figure S1. SEM images of SiNWs matrix with native silver nanopartcles. (a) top view and (b) cross-section view.

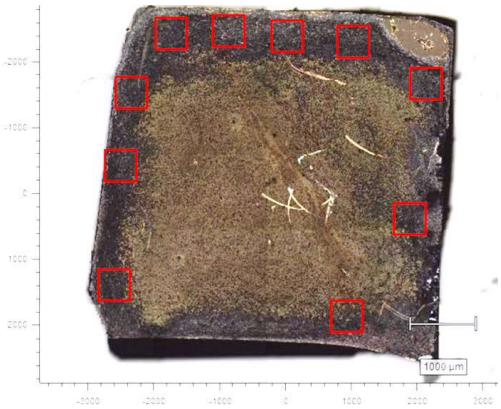

Figure S2. Microscopic image of the substrate incubated in artificial sputum with during drying formed 'coffee-ring' effect. Red squares indicate measurement areas.

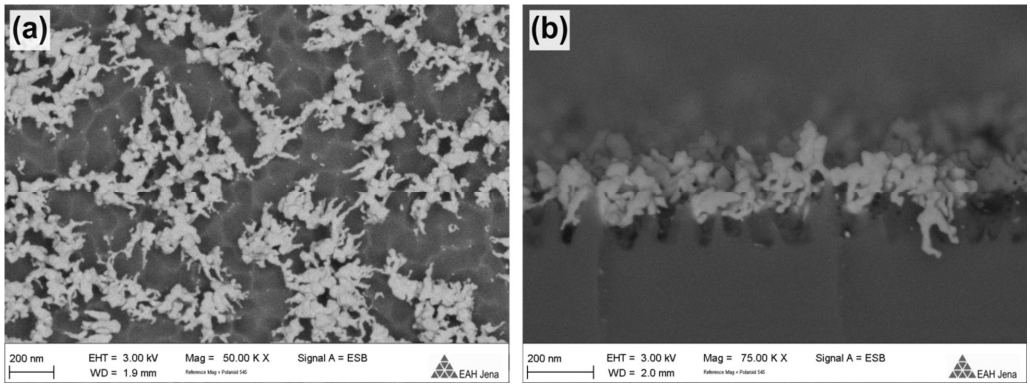

Figure S3. SEM images of Au*SiNWs: (a) top view; (b) cross-sectional view in BSE modus.

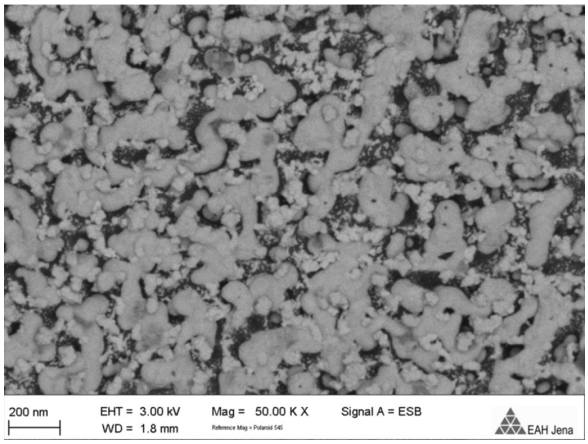

Figure S4. Top view SEM image of Ag*Au*SiNWs in BSE modus.

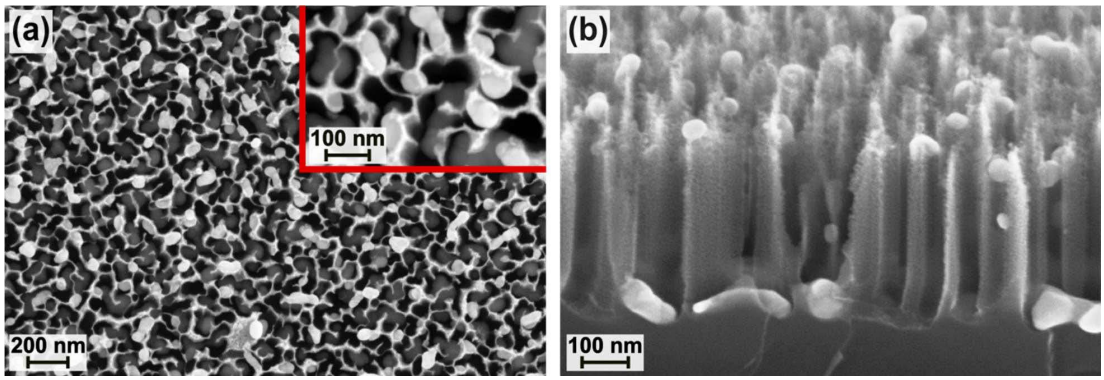

Figure S5. SEM images of SiNWs with native silver nanopartcles at the bottom and silver nanoparticles on the top (Ag*Ag*SiNWs): (a) top view and (b) cross-sectional view.

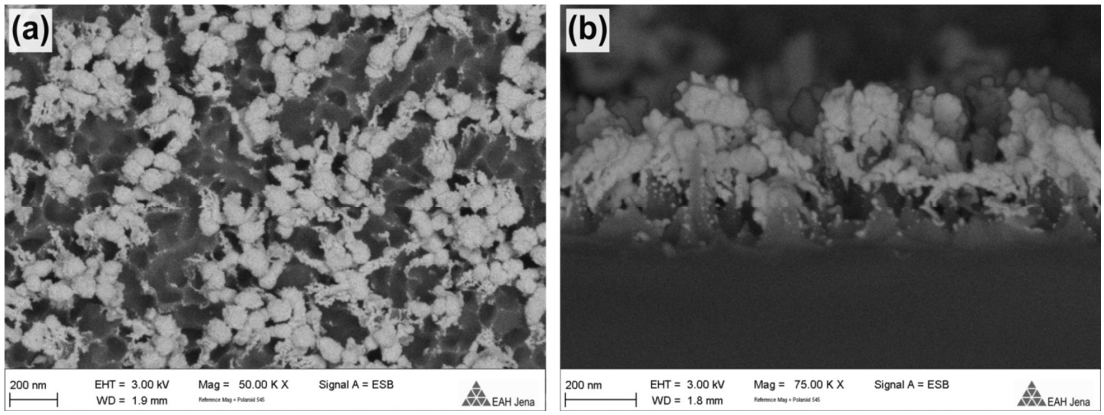

Figure S6. SEM images of Ag*Au*SiNWs: (a) top view; (b) top view in BSE modus.

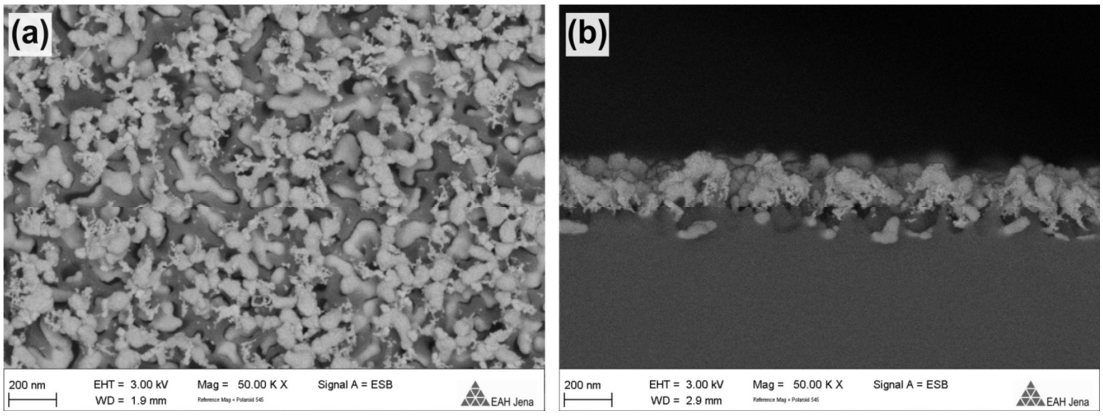

Figure S7. SEM images of $Ag^{*}_{e}Au^{*}SiNWs$ in BSE modus: (a) top view; (b) cross-sectional view.

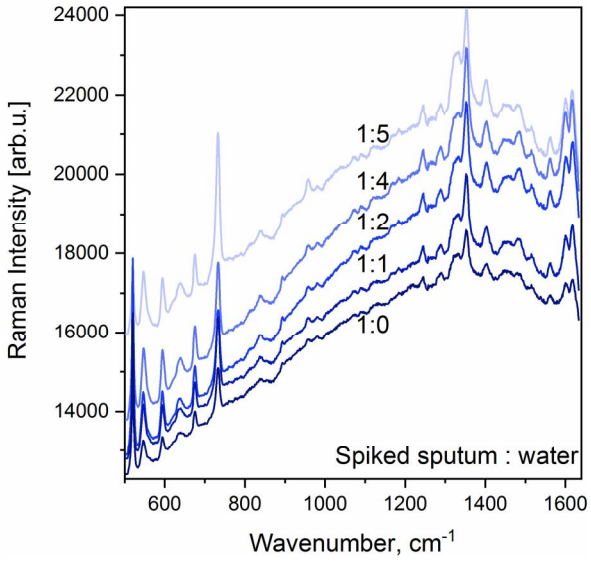

Figure S8. Mean raw SERS spectra of artificial sputum spiked with PYO and diluted with different amount of water.

Table S1. An overview of the reported SERS studies on PYO detection.

Substrate	Matrix	Lowest detected concentration	Linear range (μM)	Reference
Ag colloids	Water	0.5 μM	0.5 - 15	[23]
	Spiked saliva	10 μM	-	
Ag nanorrod array substrates	Water	23.8 nM	0.0238 – 47.6	[24]
	Spiked culture media	23.8 nM	0.0238 – 47.6	
	Spiked clinical sputum samples (PYO extraction by chloroform)	47.6 nM	0.0476 – 4.76	
Macroporous poly-N-isopropylacrylamide (pNIPAM) hydrogels loaded with Au nanorods (Au@pNIPAM)	Aqueous samples obtained from chloroform extracted *P. aeruginosa* culture supernatants	10^{-10} M	0.01 – 0.1	[21]
Mesostructured Au@TiO_2 substrates bearing a mesoporous TiO_2 thin film over a submonolayer of Au nanospheres;		10^{-9} M	0.01 – 0.1	
Mesoporous silica-coated micropatterned supercrystal arrays of Au nanorods (Au@SiO2)		10^{-14} M	0.001 – 0.1	
Au nanoparticle assemblies with controlled nanogap	Water	0.476 nM	0.00476 – 47.6	[22]
	LB media	4.76 nM	0.00476 – 476	

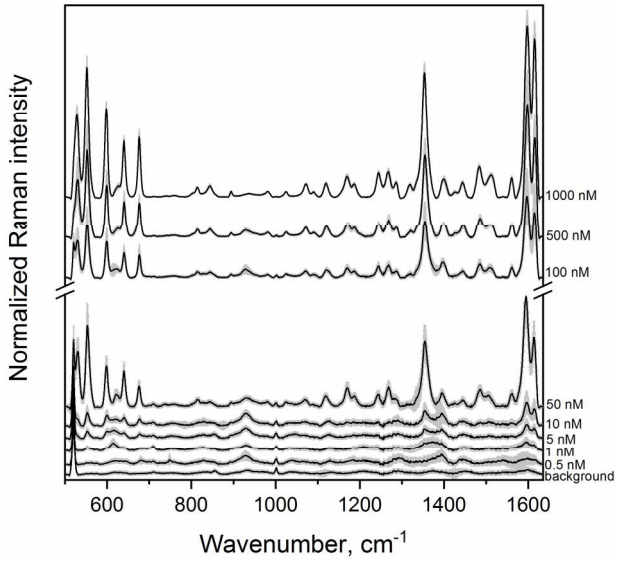

Figure S9. Mean SERS spectra of PYO with concentrations between 10^{-5} and 10^{-10} M in aqueous solution measured on the $Ag_*^*Au^*$SiNWs substrates. The mean spectrum of the blank (when substrate was incubated only in water-ethanol solution) is also presented.

7.5 Surface-enhanced Raman spectroscopy and microfluidic platforms: challenges, solutions and potential applications [OZ5-Review]

Izabella Jolan Jahn, Olga Žukovskaja, Xiao-Shan Zheng, Karina Weber, Thomas. W. Bocklitz, Dana Cialla-May, Jürgen Popp

Analyst, 2017,142, 1022-1047

Declaration on authorship and copyright in a cumulative doctoral thesis

[1]Izabella Jolan Jahn, **[2]Olga Žukovskaja**, [3]Xiao-Shan Zheng, [4]Karina Weber, [5]Thomas. W. Bocklitz, [6]Dana Cialla-May, [7]Jürgen Popp; *Analyst*, 2017,142, 1022-1047					
Involved in					
	1	**2**	3	4	5
Conceptual research design					
Planning of research activities					
Data collection					
Data analyses and interpretation					
Manuscript writing	X	X	X	X	X
Suggested publication equivalence value		**0.3**			

Author Contribution

Izabella Jolan Jahn	writing the introduction, theoretical basis and microfluidic parts
Olga Žukovskaja	writing application part
Xiao-Shan Zheng	writing application part
Karina Weber	concept development proofreading of manuscript
Thomas. W. Bocklitz	writing chemometric methods part
Dana Cialla-May	concept development proofreading of manuscript
Jürgen Popp	concept development proofreading of manuscript

Analyst

CRITICAL REVIEW

View Article Online
View Journal | View Issue

Cite this: *Analyst*, 2017, **142**, 1022

Surface-enhanced Raman spectroscopy and microfluidic platforms: challenges, solutions and potential applications

I. J. Jahn,[a,b] O. Žukovskaja,[a] X.-S. Zheng,[b] K. Weber,[a,b,c] T. W. Bocklitz,[a,b] D. Cialla-May[a,b] and J. Popp*[a,b,c]

The exhaustive body of literature published in the last four years on the development and application of systems based on surface-enhanced Raman spectroscopy (SERS) combined with microfluidic devices demonstrates that this research field is a current hot topic. This synergy, also referred to as lab-on-a-chip SERS (LoC-SERS) or nano/micro-optofluidics SERS, has opened the door for new opportunities where both techniques can profit. On the one hand, SERS measurements are considerably improved because the processes previously performed on a large scale in the laboratory and prone to human error can now be carried out in nanoliter volumes in an automatic and reproducible manner; on the other hand, microfluidic platforms need detection methods able to sense in small volumes and therefore, SERS is ideal for this task. The present review not only aims to provide the reader an overview of the recent developments and advancements in this field, but it also addresses the key aspects of fundamental SERS theory that influence the interpretation of SERS spectra, as well as the challenges brought about by the experimental conditions and chemometric data analysis.

Received 20th January 2017,
Accepted 23rd February 2017

DOI: 10.1039/c7an00118e

rsc.li/analyst

Introduction

There is a need for (bio)analytical methods in the field of life sciences to help improve the quality of life and to answer fundamental research questions about biological processes, and consequently, new platforms are continually sought and being developed. Among these methods, techniques based on chromatographic separation are the most widely used. They are

[a]*Friedrich Schiller University Jena, Institute of Physical Chemistry and Abbe Center of Photonics, Helmholtzweg 4, 07745 Jena, Germany. E-mail: juergen.popp@uni-jena.de*
[b]*Leibniz Institute of Photonic Technology Jena, Albert-Einstein-Str. 9, 07745 Jena, Germany*
[c]*Research Campus Infectognostic, Philosophenweg 7, 07743 Jena, Germany*

I. J. Jahn

Izabella Jahn studied physics at the Babes-Bolyai University in Cluj-Napoca, Romania. In 2012, she joined the group of Prof. Popp and received her PhD in 2016. During her work, she focused on assessing the potential and limitations of lab-on-a-chip SERS to determine and quantify antibiotics in human urine samples with the aim of therapeutic drug monitoring. Currently, she is a PostDoc at the Leibniz Institute of Photonic Technology, Jena, Germany, where her research interest is in point-of-care approaches for medical diagnosis.

O. Žukovskaja

Olga Žukovskaja received her bachelor degree in Physics in 2012 and two years later her Master's degree in Medical Physics from Vilnius University in Lithuania. As a PhD student, she joined the group of Prof. J. Popp in 2015. Her research focuses on the application of Raman spectroscopy and SERS for the identification of pathogens and their metabolites in biofluids with the use of microfluidic platforms.

applied in the clinical diagnosis of disease and disorders,[1–4] biopharmaceutical data screening,[5–7] water and environmental applications,[8–10] food,[11–15] pharmaceutics,[16–19] and forensic testing.[20–23] Although chromatography-based platforms are considered to be the reference analytical methods, they require a large initial capital investment and, later, high service costs. There is also a lack of standardization; therefore, results from different laboratories are not comparable.[24] Furthermore, they are sophisticated methods requiring qualified staff and are not suitable for on-site detection. Optical detection platforms, on the contrary, have been extensively miniaturized[25–30] in the last years and their potential for a multitude of applications has been demonstrated.[31–37]

Vibrational spectroscopies, infrared (IR) and Raman spectroscopy, are, in particular, well known for giving molecular specific information by taking advantage of the vibrational modes of molecules. Water, one of the main constituents of biological and environmental samples, has high absorption in the IR range, whereas its scattering cross-section is very low. Thus, for the analysis of aqueous samples, Raman spectroscopy is preferred instead of IR absorption spectroscopy. The Raman effect is based on the inelastic scattering of photons. Thus, it is a very weak process and consequently the detection of analyte molecules present at very low concentration is limited. One of the approaches to enhance the inherently weak Raman signal is to bring the target molecules into the proximity of metallic nanostructures. Thus, surface-enhanced Raman spectroscopy (SERS) combines the molecular specific information with the signal-enhancing power of plasmonic structures. The SERS effect was first observed in 1974 by Fleischmann while he was recording the Raman spectrum of pyridine adsorbed on a roughened silver electrode.[38] Forty years later, 15% of the overall Raman publications are still related to this topic. Over the years, SERS has advanced from being a technique mainly used to characterize molecule–metal interactions[39–41] and to detect dye molecules in pure water[42–44] to being applied in the quantification of biomolecules in clinical and environmental samples as well as to the detection of biomarkers of various diseases.[45–53] Nevertheless, compared with the reference analytical methods, SERS is considered to still be in its childhood when it comes to the available commercial platforms.

The main challenge to obtain reliable SERS measurements is represented by the quality of the plasmonic substrates. For analytical applications, the preparation of these structures has to be straightforward, reproducible, and cost effective, while at the same time the provided signal enhancement has to be homogenous. Silver and gold are the most commonly used metals for fabricating SERS-active substrates. They can be synthesized in numerous ways, such as bottom-up methods for obtaining metal colloids or core–shell nanoparticles, self-organization or template-assisted methods, and top-down processes.[54–57] From the measurement principle point of view, two strategies are commonly employed when recoding SERS spectra. In the first case, metallic colloidal solutions are mixed with the target analytes and with a so-called activation or aggregation agent and the measurements are performed in a cuvette. In the second case, analyte-containing solutions are drop-casted or incubated on the surface of solid (1D, 2D, or 3D) substrates and then the mapping measurements are carried out.

Both measurement approaches have their particular disadvantages. It was proven by Schlücker *et al.*[58] and is illustrated herein in Fig. 1, that single spherical metallic nanoparticles offer a signal enhancement of at most two orders of magnitude and that the aggregation of the nanoparticles is required for an optimal SERS signal. The creation of hot-spots can be achieved *via* the addition of an active (*i.e.*, KCl) or a passive

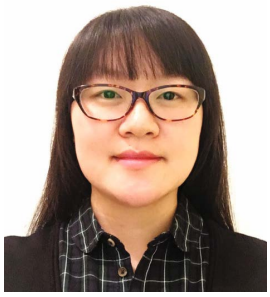

X.-S. Zheng

Xiao-Shan Zheng received her PhD at Xiamen University in 2015 under the supervision of Prof. Bin Ren on SERS-based live-cell study. She is now a PostDoc fellow in the Department of Spectroscopy and Imaging at the Leibniz Institute of Photonic Technology (Jena, Germany). Her current interests are focused on SERS-based multiplex detection and biosensing.

K. Weber

Karina Weber, during her PhD time, studied chemical and process engineering and defended her thesis in 2006 at the Technical University in Clausthal-Zellerfeld, Germany. In 2007, she joined the group of Prof. Jürgen Popp as a PostDoc and since 2011, she has been responsible for the Jenaer Biochip Initiative group at the Leibniz Institute of Photonic Technology Jena Germany. Her research is focused on the development and optimization of novel chip-based detection technologies for the multiplex analysis of biomolecules and low molecular weight substances. In particular, her research is focused on the implementation of a point-of-care technology that enables application outside of specialized laboratories.

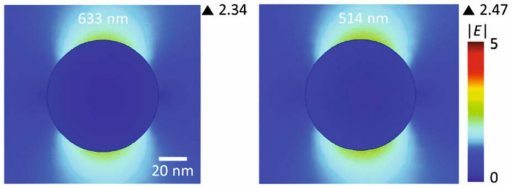

Fig. 1 Finite element method simulation of the incident electric field amplitude $|E|$ distribution on a 80 nm Ag sphere upon 633 (left) and 514 (right) nm excitation showing a maximum field enhancement of 2.34 and 2.47, respectively. This corresponds to a SERS enhancement factor of ~30 (in the $|E|^4$ approximation) (Zhang *et al.*[58] published by the PCCP Owner Societies).

(*i.e.*, KNO_3) electrolyte, by the presence of the analyte itself, or by the addition of polymers or long chain ions.[59] The aggregated metallic nanoparticles yield great signal enhancements, but the SERS spectrum of the molecule to be detected becomes dependent on the time elapsed between the induction of the aggregation and the measurement.[60,61] Furthermore, the order of addition and the mixing ratio of the nanoparticles, the analyte solution, and the aggregation agent have a crucial influence on the SERS signal.[62] In the second case, when solid substrates are employed for signal enhancement, the drop-casting procedure creates a heterogeneous layer of analyte molecules on the surface due to the coffee-ring effect, yielding SERS signals with low reproducibility. Furthermore, when the substrates are incubated into the sample, the incubation time will strongly influence the final SERS results.

Limitations brought about by the hard-to-control colloid aggregation and the need to ensure heterogeneous analyte layers on solid substrates can be overcome by injecting or integrating the SERS-active substrate in a microfluidic platform. The combination of SERS with microfluidics, also referred to as lab-on-a-chip SERS (LoC-SERS) or nano/micro-optofluidic SERS, opened new opportunities for system miniaturization and integration,[51,63–71] bringing the advantages of both techniques. On the one hand, SERS measurements are considerably improved because processes previously done on a large scale in the laboratory and that were prone to human error can now be carried out in nanoliter volumes in an automatic and reproducible manner. On the other hand, microfluidic platforms need detection methods able to sense in small volumes and therefore, SERS is ideal for this task.

The reported LoC-SERS platforms can be sorted into two distinct categories: flow through or continuous flow platforms[72–114] and segmented or droplet-based platforms.[60,115–126] The main body of literature is focused on the first type of microfluidic systems. Here, colloidal nanoparticles prepared *via* the chemical reduction of salts can be injected at the same, or at an additional inlet as the sample,[72–81] while stationary substrates prepared *via i.e.* top-down processes can be integrated in the channel system,[84–103] or the synthesis can be carried out *in situ*.[104–114] Compared with conventional SERS measurements on open platforms, liquid evaporation is avoided and the deposition of molecules along the perimeter of the liquid droplet due to the capillary flow at a pinned contact line is overcome. Furthermore, the diffusion of the analyte toward the substrate can be improved *via* electrokinetic concentration,[86] magnetic trapping,[80] hydrodynamic focusing,[87] or dielectrophoresis.[102] However, regardless of the chosen way to apply the SERS-active substrate, the sample permanently wets the channel walls of the microfluidic platform. This will lead, in

T. W. Bocklitz

Thomas Bocklitz received his diploma in Physics in 2007 in Jena, Germany, and then in 2011, he was awarded a PhD degree in Physical Chemistry/Chemometrics under the supervision of Prof. Popp. Afterwards, he started as a postdoctoral associate in the same group. In 2013, he started to establish a junior research group "Statistical Modelling and Image Analysis". In 2016, this group joined the Leibniz Institute of Photonic Technology Jena and finished his habilitation on "Extraction of biomedical information from photonic data". His work was honored with the Bruce-Kowalski-award in chemometrics and an invitation to be part of the "Prominent young spectroscopists special issue" in Vibrational Spectroscopy. Since 2016, he has been a member of the "Michael Stifel Center Jena for Data-Driven and Simulation Science".

D. Cialla-May

Dana Cialla-May studied chemistry and received her PhD in Chemistry from the Friedrich-Schiller University Jena, Germany. During her PhD thesis in the group of Prof. Popp, her research focused on the characterization and application of plasmonic structures for surface and tip-enhanced Raman spectroscopy. Since 2011, she has worked, together with Dr Karina Weber, as the head of the research group Jena Biochip Initiative at the Leibniz Institute of Photonic Technology (IPHT), Jena, Germany. Her main research focuses on surface-enhanced spectroscopic techniques, e.g., *the generation of powerful SERS substrates and their application in life science and environmental analysis.*

View Article Online
Analyst Critical Review

most cases, to the so-called memory effect, where the molecules of the sample get enriched over time on the surface of the channels. This will result, for example, in an overestimation of the detection limits, especially when stationary substrates are used for signal enhancement. Consequently, Meier *et al.*[127] reported an approach to regenerate on-chip SERS substrates by applying a high electrical potential (100 V) leading to analyte desorption. However, one has to make sure that the nanostructure of the SERS-active substrates is not affected during this process.

The segmented flow, and especially droplet-based LoC-SERS platforms,[115–122,124–126,128] completely inhibit the cross-contamination by assuring that no or very low cross-talk exists between the liquid compartments. This is achieved by dispensing the sample and colloidal nanoparticles into individual droplets surrounded by an immiscible liquid phase. The droplets can be trapped, sorted, mixed, or split, based on the specific experimental requirements.[65,129] Commonly, the employed nanoparticles are previously synthesized and then injected into the chip, although *in situ* nanoparticle synthesis has also been reported.[125,126] This offers a great advantage because the challenges represented by the batch-to-batch reproducibility and colloidal solution aging effect can be avoided. Furthermore, each droplet can be considered as a micro-cuvette or a micro-reactor. The colloids are mixed with the analyte in a reproducible way and, by mounting the chip on the microscope stage and fixing the focus point, the aggregation time can be easily controlled. Nevertheless, these platforms are limited to the detection of analyte molecules with good water solubility, as most often the segmented flow is achieved by forming aqueous droplets in the continuous flow of oil.

Although the feasibility of most of the reported LoC-SERS platforms has been tested only with analyte molecules with a high scattering cross-section, such as rhodamine 6G, the ultimate goal should be their application in life sciences or other fields. Considerable efforts have been undertaken in the last years in pathogen identification,[80,92,116,130] the quantitative measurement of low weight molecular species,[79,88,103,110,131] and in the biomarker detection of various diseases.[77,122,132,133] As most of these applications are based on databases, calibration data, or are multi-parameter problems, chemometric approaches have to be applied for correct and complete result interpretation. This is also necessary because the amount of recorded data is extensive and their analysis cannot be carried out manually with conventional software.

In the last two years, two reviews, one by Zhou and Kim[71] and a second one by Huang *et al.*[70] have been published regarding microfluidic approaches combined with SERS as a detection method. These reviews provide an excellent overview of the fabrication methods of the nanostructures integrated in such platforms and address the influence of certain morphologies on the function of the device. The authors approach the topic from the perspective of technology and address the questions: what can be achieved? what can be fabricated? However, in practice, for the final aim of commercializing LoC-SERS platforms, one needs to be directed toward overcoming the challenges associated with specific applications and solutions. Therefore, in the present review, besides offering an overview of the recently published studies on microfluidic platform development, SERS-active substrate fabrication, and the application of LoC-SERS systems, aspects of fundamental SERS theory influencing the interpretation of SERS spectra, challenges brought by experimental conditions and chemometric data analysis will also be addressed.

Surface-enhanced Raman spectroscopy: fundamental considerations

The SERS spectrum of a molecule is strongly influenced by: (1) the SERS-active substrate, (2) the emission wavelength of the excitation laser, and (3) the molecule–metal interaction (Scheme 1). The present section does not aim to give a thorough description of the fundamental theory of SERS, but it will focus on specific theoretical aspects that affect the appearance of the SERS spectrum.

Surface-enhanced spectroscopies, such as surface-enhanced fluorescence (SEF), surface-enhanced infrared spectroscopy (SEIRA), or SERS, are governed by the plasmon, defined by Le Ru and Etchegoin as: "a quantum quasi-particle representing the elementary excitations, or modes, of the charge density oscillations in a plasma".[134] If the frequency of an incident electromagnetic wave matches the oscillation frequency of the plasmon modes of a metallic particle, the particle will act as a dipole antenna and will emit light. As a consequence, a local field enhancement, referred to as the dipolar localized surface plasmon polariton (LSPP), is induced. Additionally, under appropriate experimental conditions, Kretschmann or Otto configuration, at the interface between a dielectric and a

J. Popp

Jürgen Popp studied chemistry at the universities of Erlangen and Würzburg. After his PhD in Chemistry, he joined Yale University for his postdoctoral work. He subsequently returned to Würzburg University, where he finished his habilitation in 2002. Since 2002, he has held a chair for Physical Chemistry at the Friedrich-Schiller University Jena, Germany. Since 2006, he has also been the Scientific Director of the Leibniz Institute of Photonic Technology, Jena, Germany. His research interests are mainly concerned with biophotonics. In particular, his expertise in the development and application of innovative Raman techniques for biomedical diagnosis should be emphasized.

View Article Online
Critical Review Analyst

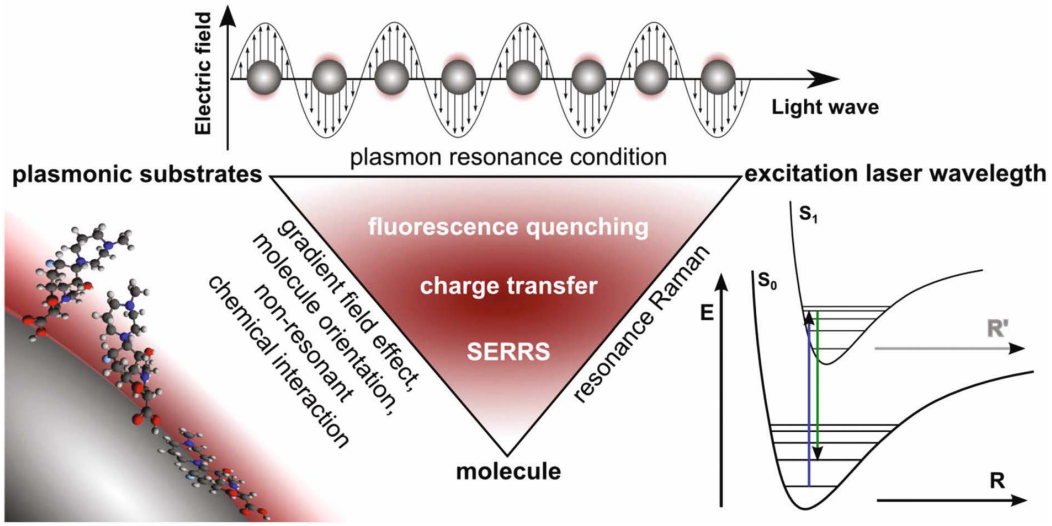

Scheme 1 Surface-enhanced Raman spectroscopy: the parameters that play a major role in the appearance of the SERS spectra.

metallic layer, propagating surface plasmon polaritons (PSPPs) can be created.[134] The increased local electric field caused by the dipolar LSPP or PSPP is the source of the Raman signal enhancement and the basis of the electromagnetic mechanism of SERS. In the case of a spherical particle, in the electrostatic approximation, the plasmon resonance condition is fulfilled when the dielectric function of the material out of which the particle is made of meets the relationship: $\varepsilon(\lambda) = -2\varepsilon_m$ (where ε_m is the dielectric constant of the surrounding medium).[135] This condition is met, partially, only in the case of metallic materials, where $\mathrm{Re}(\varepsilon(\lambda)) < 0$, because of the nonzero imaginary part, $\mathrm{Im}(\varepsilon(\lambda))$. In the visible spectral range, silver and gold SERS-active substrates are widely used. Even though gold has a considerably higher chemical stability under atmospheric conditions, silver is preferred when the aim is a high signal enhancement. The difference between the strength of the LSPP of the two metals is due to their slightly different optical properties. In the case of silver, the contribution of inter-band electronic transitions to the dielectric function in the visible spectral range is constant and real. In the case of gold, the natural oscillations of the free electron plasma are strongly affected by the presence of the inter-band transitions at wavelengths bellow 600 nm, and thus, $\mathrm{Im}(\varepsilon(\lambda))$ is significant in this spectral range.[135]

As foreseen from the plasmon resonance condition, optimal signal enhancements can be achieved only for specific wavelengths of the excitation laser. Generally, the position of the LSPP resonance can be easily tailored *via* the fabrication protocols. As a result, numerous synthesis approaches yielding a high diversity of metallic structures have been reported. Nonetheless, the Lee and Meisel[136] (cited 2935 times) and Leopold and Lendl[137] (cited 552 times) protocols are the most commonly employed ones for carrying out SERS studies. The reported extinction spectra of these colloids exhibit one main band, centered at around 410 nm. Based on this, one would expect that by applying a laser with an emission wavelength at 410 nm, one would obtain a very strong SERS spectrum. Nevertheless, the connection between the extinction spectrum and the magnitude of the electromagnetic SERS enhancements is, generally, indirect. In Fig. 2, the extinction coefficient, defined as the ratio of the extinction over the geometrical cross-section, and the enhancement factor of a single sphere and dimers with a 10 and 2 nm gap separation are depicted.[138] According to calculations performed with generalized Mie theory, the overall extinction coefficient is comparable for the three considered cases, while the maximum

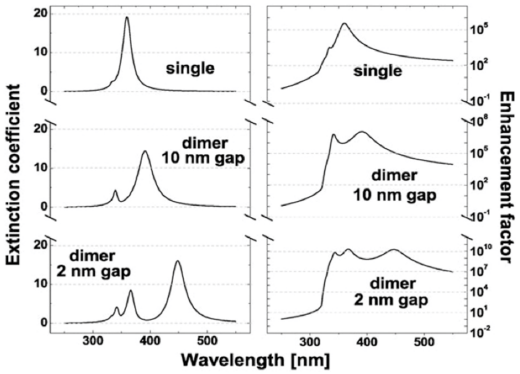

Fig. 2 Extinction (on a linear scale) coefficient and enhancement factor (on a log-scale) for a single sphere (d = 50 nm) and for dimers with 10 and 2 nm gap separation, respectively (reproduced from Le Ru *et al.*[138] with permission from the PCCP Owner Societies).

View Article Online
Analyst Critical Review

enhancement, on the contrary, changes by several orders of magnitude. Thus, single particle LSP resonances present the same extinction magnitude as dimers, despite their no or very low SERS signal enhancement.[138] The extinction band located at 410 nm in the UV-Vis spectrum of the colloids prepared *via* the two mentioned particles is due to the dipolar LSPP resonances of the single spherical particles. In practice, the red-shifted, respective to the position of the plasmon resonance, emission wavelength of the excitation laser is used for colloidal particles. In the case of solid substrates, if the analyte molecule or the medium used as a solvent does not affect the morphology or optical properties of the nanostructures, one can expect that the position of the plasmon resonance derived from the optical measurements or theoretical calculations would give more accurate information about the magnitude of the electromagnetic enhancement.[139] This is because of the fixed geometry and position of the hotspots. However, when performing theoretical calculations, the measurement conditions, especially the dielectric properties of the surrounding medium, have to be considered for accurate results.

The electromagnetic enhancement is present also in the absence of an adsorbed molecule[140] and although it brings interesting fundamental knowledge, the applicability of SERS can be assessed only in the presence of an analyte. The interaction of molecules with the plasmonic nanostructures can lead to SERS spectra showing spectral features significantly different from the ones observed in the reference Raman spectra. These changes may be caused by the gradient field effect, the specific orientation of the molecule on the surface, and the quenching of fluorescence.

Generally, Raman bands are observed for those vibrational modes of the molecule that present a change in their dipole electric polarizability during vibration. However, if the size of the molecule is comparable with the spatial distribution of the LSPP local electric field gradient, excitation of the multi-pole transitions becomes significant.[141] As a result, forbidden vibrational modes are present in the recoded SERS spectrum and they have to be considered for a correct interpretation of the results.

A second parameter influencing the SERS spectrum is the orientation of the molecules on the metallic surface, referred to as 'surface selection rules'.[142] If the polarizability of the local electric field is perpendicular to the metallic surface, Raman modes of the adsorbed molecule with a strong polarizability tensor component normal to the surface are selectively enhanced as compared with the Raman modes with strong parallel polarizability tensor components. By following these rules, many publications report the orientation of the molecules on the metallic surface. However, these statements are valid only if the local field polarization is predominantly perpendicular to the surface at positions with the highest enhancements and if the molecule have several Raman modes with very different symmetries.[143] A consequence of the selective enhancement of specific Raman modes is that, at different concentrations, new bands can appear or some can vanish in the SERS spectrum. This happens especially in the case of molecules with multiple functional groups with high affinity toward the metallic surface. This, combined with the steric hindrance, can lead to reorientation of the molecule on the metallic surface, and hence to new spectral features.

Lastly, when the energy of the excitation laser matches a dipolar electronic transition within the interrogated free molecule, the fluorescence emission most often covers the weak Raman spectrum. Nevertheless, if the molecule is in the proximity of metallic surfaces, new channels for the absorption of the fluorescence emission are provided and fluorescence quenching occurs. This phenomenon is especially prominent for molecule–metal distances of a few nanometers.[135] In this case, one might refer to surface-enhanced resonance Raman spectroscopy (SERRS), where, besides the electromagnetic enhancement provided by the SERS-active substrates, also the resonant excitation of the molecule contributes to the overall signal. One should also take into consideration, that when measuring under resonant Raman conditions, the vibrational modes with the greatest Franck–Condon overlap integrals will be the ones most visible.

The electromagnetic enhancement mechanism was proved to account for signal enhancements of up to 10^{11}.[144] However, factors of 10^{14}–10^{15} have been reported in the literature. The additional signal gain was attributed to the chemical enhancement mechanism. Three different processes have been suggested to contribute to this: (1) chemical interaction of the nanoparticle and the molecule in the electronic ground state; (2) resonant excitation of the charge-transfer process between the molecule and the nanoparticle; and (3) the resonance Raman enhancement of the chemically bound molecule. In the first case, the molecule is not covalently bound to the surface of the nanoparticle. However, the presence of the metal perturbs the electronic structure of the analyte, inducing a slight change in its electronic distribution. In the second case, it was shown, depending on the relative energies of the Fermi level of the nanoparticle, the highest occupied molecular orbital, and the lowest unoccupied molecular orbital of the molecule, charge transfer from the molecule to metal or from the metal to molecule can occur. Lastly, an effect similar to SERRS can occur, but here the energy of the incident radiation does not induce an electronic transition in the free molecule, but instead it resonantly excites the molecule with a modified electronic structure due to the interaction with the metallic surface. Overall, due to the chemical interaction of the molecule with the metallic surface, the position of the SERS bands can be shifted respective to their original position in the reference Raman spectrum. This is particularly strong for the vibrations of functional groups in the proximity of the metallic surface.

Microfluidic platforms for SERS

Continuous flow platforms

Colloidal nanoparticles. The approach of utilizing continuously flowing streams of completely miscible liquid phases

was the first route toward scaling down reaction volumes and increasing the throughput of measurements. SERS-active substrates in the form of colloidal nanoparticles synthesized *via* chemical reduction are the most accessible metallic nanostructures. In the last four years, the focus of the reported studies combining colloidal nanoparticles with continuous flow microfluidics[72–81] has been directed toward the trapping of nanoparticles and enrichment of the analyte at the detection area,[75,76,78,80] the on-demand formation of nanoparticle aggregates,[72,74,77,109] and on the enhancement of the collection efficiency of the SERS signal.[73,95]

The interaction of analyte molecules with the colloidal nanoparticles inside a conventional microfluidic channel is governed by the slow diffusion forces. This leads to high signal variations and thus to low reproducibility. The concentration of analyte–nanoparticle conjugates in the detection volume can be achieved *via* passive or active processes. White and coworkers used a passive concentration strategy by employing a 3D nanofluidic network with packed nanoporous silica microspheres.[75,76,78] The platform evolved from a single microchannel chip, where the analyte and colloidal nanoparticles were mixed off-chip and were injected *via* the same port to a multiport injector with meander channels and an integrated competitive displacement unit for DNA sequence detection (Fig. 3(a)). The microfluidic chip requires no nanofabrication processes, while delivery of the excitation laser and the collection of the SERS signal are achieved *via* optical fibers. Although this approach overcomes the limitations of open channel microfluidics, where the nanoparticles are typically poorly concentrated in the detection volume, the trapping of the analyte–nanoparticle conjugates is irreversible and the device is thus for single use only. An alternative approach for trapping analyte–nanoparticle conjugates was demonstrated by Gao and coworkers by using an active concentration strategy.[80] They implemented an automatic competitive immunoassay into a solenoid-embedded dual channel microfluidic device containing a sensing and a control channel (see Fig. 3b). The authors took advantage of antibody–antigen binding reactions and magnetic separation. After the competitive reaction between the free antigen and antigen-conjugated gold nanoparticles for binding sites on the surface of antibody-conjugated magnetic beads, the magnetic immunocomplexes were trapped by yoke-type solenoids, and the resulting SERS spectra were recorded. The integration of a control channel considerably increased the reliability of the device by minimizing the influence of most of the experimental variables.

The formation of hotspots *via* the aggregation of colloids is essential for sensitive SERS detection. The passive or active trapping of nanoparticles is one way to achieve this. In the search for improved measurement conditions, scientists orientated their attention toward the reversible and on-demand concentration and formation of nanoparticle aggregates. In this way, new hotspots can be created for each measurement and the chip can be used for multiple analysis. Following this goal, Zhou *et al.*[77] fabricated a poly(dimethylsiloxane) (PDMS) microfluidic chip with a pneumatic valve and nanopost arrays at the bottom of the microchannel. The trapping and releasing of gold nanoparticles is shown in Fig. 4(a). The opening and closing of the valve is controlled *via* the applied pressure. By optimizing the amount of pressure, the thin elastomeric membrane deforms and contacts the nanoposts at the bottom of the channel. The diameter of the used gold nanoparticles was 250 nm and they were larger than the height of the deformed PDMS relief structures. In this way, the particles can be trapped while the solvent can still flow through. In order to get a reliable SERS spectrum, 10–15 minutes were needed for complete formation of the aggregates. After the measurement was performed, the pressure could be released and the aggregates were flushed away. Nevertheless, nanoparticles with small diameters cannot be efficiently trapped and high-throughput measurements are hindered by the slow formation of aggregates. An alternative strategy for aggregates formation was reported by Hwang *et al.*[72] They used an optoelectrofluidic

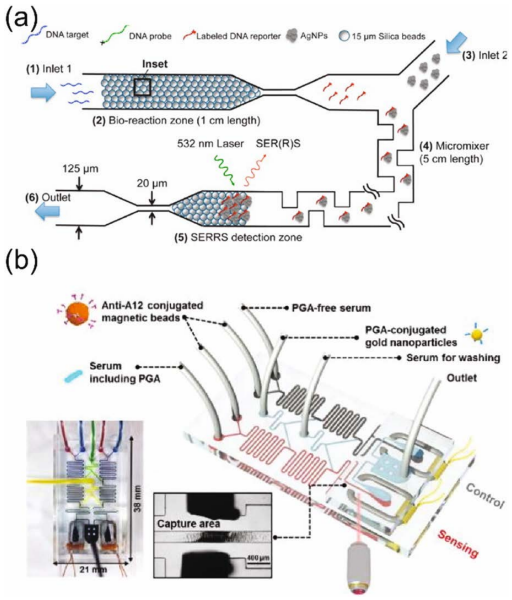

Fig. 3 (a) Microfluidic SERS microsystem with integrated competitive displacement for DNA sequence detection. Silica microspheres functionalized with DNA probe-reporter pairs are packed against a frit. When the target sequence is introduced at the inlet, Raman-labeled reporter oligos are displaced. As they flow along the channel, they are mixed with metal nanoclusters and trapped in the microfluidic SERRS detection region. (Reprinted with permission from Yazdi *et al.*[78] Copyright 2012 American Chemical Society.) (b) Schematic illustration of the solenoid-embedded dual channel microfluidic sensor for SERS-based competitive immunoassay, optical images of the solenoid chip filled with four different colors of inks, photograph of the capture area for the magnetic immunocomplexes (reprinted from R. Gao, J. Ko, K. Cha, J. H. Jeon, G. Rhie, J. Choi, A. J. deMello, J. Choo, Fast and sensitive detection of an anthrax biomarker using SERS-based solenoid microfluidic sensor, *Biosens. Bioelectron.*, **72**, 230–236,[80] Copyright 2015, with permission from Elsevier).

View Article Online
Analyst Critical Review

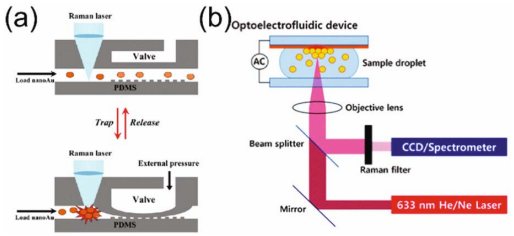

Fig. 4 (a) Schematics of the trapping and releasing of gold nanoparticles using a modified pneumatic microvalve for SERS detection (Springer, J. Zhou, K. Ren, Y. Zhao, W. Dai, H. Wu, Convenient formation of nanoparticle aggregates on microfluidic chips for highly sensitive SERS detection of biomolecules, *Anal. Bioanal. Chem.*, 2011, **402**, 1601–1609,[77] Copyright Springer-Verlag 2011). (b) Reversible, on-demand formation of nanoparticle aggregates by using an opto-electronic platform (reproduced from Hwang *et al.*[72] with permission from The Royal Society of Chemistry).

platform consisting of three layers: a photoconductive layer on a transparent electrode, a liquid chamber, and a ground electrode (Fig. 4(b)). When electromagnetic radiation is shone on the photoconductive layer, current flows through the illuminated area and creates a nonuniform electric field in the liquid chamber. As a result, metal nanoparticles can be efficiently concentrated and SERS-active sites can form in a reliable and stable manner. The recorded SERS signals become saturated into a steady state after about 2 min. The authors also demonstrated dynamic control of the SERS-active sites by adjusting the position of the laser spot during the voltage application. The presented platform required no fluidic components or complicated fabrication processes, and the on-demand formation of colloidal aggregates at a specific place could be easily achieved. In contrast with this method, the electrokinetic concentration of gold nanoparticles reported by Kim *et al.*[84] required a more complicated fabrication protocol of the microfluidic chip, and the aggregates could be formed only at the predesigned positions.

Stationary SERS-active substrates. The sophisticated engineering of materials and their integration in microfluidic platforms is a hot topic in nanoscience. As a result, many metallic nanostructures with elaborate morphologies have been reported. Gold layers roughened *via* UV laser pulse irradiation,[85] silver nanodot arrays obtained *via* the use of a through-hole ultrathin anodic aluminum oxide template,[88] nanopillar forests realized by an oxygen-plasma-stripping-of-the-photoresist technique,[89] nanoporous gold disks,[91] plasmonic nanodomes,[93] metal–elastomer nanostructures,[97] Ag-coated TiO_2 nanotubes,[98] plasmonic nanopillar arrays,[100] and silver-covered electron beam lithography patterned quartz substrates[101] are just some of the SERS-active substrates implemented within continuous flow cells. Soft lithography on PDMS is the most often applied fabrication procedure for obtaining these microfluidic platforms.

Among the designed SERS-active substrates, 3D plasmonic structures offer a considerably large surface area for the adsorption of analyte molecules. Mao and coworkers[89] fabricated a SERS sensor consisting of a PDMS microchannel cap and a nanopillar forest based upon a SERS-active substrate (see Fig. 5(a)). The nanopillar forest was obtained *via* a new oxygen–plasma-stripping procedure and consisted of Si pillars covered by a thin layer (50 nm) of sputtered Ag. The performance of the embedded substrates was compared with the results obtained by the traditional drop-casting of an analyte solution onto the open metallic surface. The reproducibility of the measurements was improved considerably by the flow cell method, and had a relative error of only 13%. However, the overall signal intensity was four times decreased compared with the open surface, because the SERS spectra were recorded through the PDMS cover. Unfortunately, the authors did not indicate the required time to achieve a steady and stable SERS signal of the target molecule. Furthermore, this platform, as many others reported, seals the SERS-active substrate in an irreversible way in the PDMS channel. Therefore, either an effective cleaning procedure has to be applied before reusing the microfluidic chip or they have to be considered as disposable devices. An alternative to these platforms was reported by Patze *et al.*[101] They embedded silver substrates prepared by

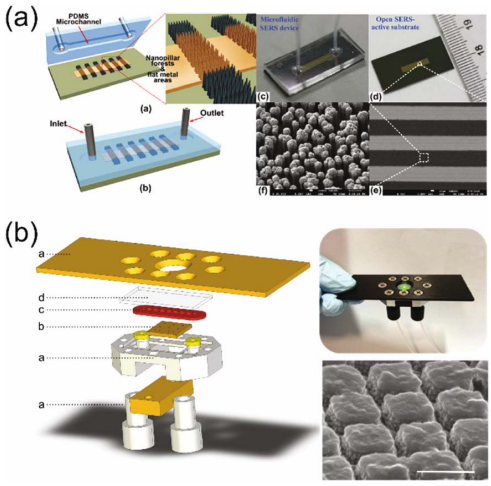

Fig. 5 (a) Microfluidic SERS sensor based on nanopillar forests realized by a technique involving oxygen–plasma stripping of the photoresist: schematic structure, the entire chip with the inlet and outlet depicted, photo of the chip, and SEM images of the nanopillar forest. (Reprinted from Mao *et al.*[89] Copyright 2013. With permission from Wiley-VCH Verlag GmbH & Co. KGaA, Weinheim.) (b) Microfluidic cartridge setup applied for SERS experiments: the microfluidic cartridge (a), the implemented SERS substrate (b), the silicon channel (c), and the glass cover (d) are shown with an offset for better visibility; photographical image of the entire cartridge and SEM image of the silver-covered electron beam lithography patterned quartz substrates (reprinted from S. Patze, U. Huebner, F. Liebold, K. Weber, D. Cialla-May, J. Popp, SERS as an analytical tool in environmental science: The detection of sulfamethoxazole in the nanomolar range by applying a microfluidic cartridge setup, *Anal. Chim. Acta*, **949**, 1–7 (ref. 101) Copyright 2016 with permission from Elsevier).

electron beam lithography into a microfluidic cartridge. On top of the plasmonic structures, a silicone cover with a microfluidic channel was positioned and covered by an optical glass window (see Fig. 5(b)). The system was closed with screws, allowing the easy replacement of the SERS-active substrate. The system offered many possibilities as it could be used for a large variety of stationary SERS-active substrates.

Although the two above-described platforms have different designs, they share the same limitation as most continuous flow devices. Namely, the transport of analyte molecules toward the surface of the metallic surface relies on diffusion, which is especially slow in parabolic velocity flow profiles with zero velocity at the channel walls. Hydrodynamic focusing,[87,94] electrokinetic concentration,[86] or chemical functionalization of the metallic surface[91,92,145] are some of the solutions to overcome this challenge. The incorporation of hydrodynamic focusing into a microfluidic device with embedded fluidic tubing and a SERS-active electrode was reported by Bailey *et al.*[94] On this platform, both SERS and electrochemical measurements could be carried out. The sample was injected *via* a capillary embedded into the chip and *via* an additional inlet. Due to the perpendicular flow of the two streams, a sheath-flow profile was created, where the analyte molecules were confined near the SERS-active substrate. An alternative way to increase the amount of the target analyte on the metallic surface is by applying an electrokinetic concentration. In this way, pathogens could be concentrated by combining the discriminating capability of short-range dielectrophoresis with the long-range transporting capability of DC-biased AC electroosmosis.[86]

As in the case of the platforms employing colloidal nanoparticles, immunoassay-like platforms have also been fabricated with stationary SERS-active substrates.[83,92,145] Due to the very strong binding reaction between antibodies and antigens, the capturing of the target molecules can be significantly enhanced. Lee and coworkers[83] combined the immunoassay concept with a fully automated gold array-embedded gradient microfluidic chip. A schematic illustration of the device is shown in Fig. 6. The top layer consists of a PDMS panel for uniform distribution of the antibody-conjugated hollow gold nanospheres, followed by a middle PDMS gradient panel for the generation of various concentrations of the biomarker, and a bottom panel featuring a gold-embedded glass substrate for immobilization of the sandwich immunocomplexes. The tedious manual dilution process involving repetitive pipetting and inaccurate dilutions is eliminated in this way. Another interesting approach was reported by Wu and coworkers.[145] They realized a concept of a SERS-assisted 3D barcode, where different SERS probes labeled with different Raman reporters allow quantitative multiplex detection. The platform, therefore, has multiple channels and allows the simultaneous detection of $m \times k$ kinds of antigens in n kinds of samples when k kinds of Raman reporters are used.

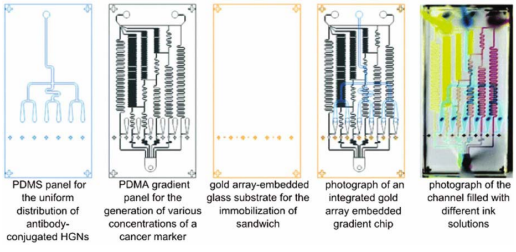

Fig. 6 Schematic of a gold-array-embedded gradient chip consisting of three layers and its photographs (reproduced from Lee *et al.*[83] with permission from The Royal Society of Chemistry).

***In situ* synthesized SERS-active substrates.** The platforms described up to now in the present review implement SERS-active substrates that were prepared *via* off-chip methods. This requires additional lab equipment and skilled personnel and increases the overall time of the analysis. However, the *in situ* synthesis of plasmonic nanostructures opens a new avenue for system integration, miniaturization, and on-site applications.

Leem *et al.*[131] applied the polyol method to synthesize silver-patterned surfaces in a microfluidic chip (Fig. 7(a)). In the chemical reaction, ethylene glycol acts as a solvent as well as the reducing agent for silver. As silver ions are reduced to silver atoms, the concentration of silver atoms in the precursor solution increases and silver nuclei start to form and grow into nanoparticles. In order to enhance the crystalline structure of the nanoparticles, polyvinylpyrrolidone (PVP) and copper(II) chloride are added to a precursor containing silver nitrate. A thin layer of nanoparticles forms on the walls of the microfluidic platform, consisting of a PDMS channel on the Si wafer substrate. After fabrication, the substrate is washed with ethanol in order to remove the PVP from the surface. For the measurements, the silver-patterned-PDMS channel was afterwards attached to a glass substrate.

Parisi and coworkers[106,110] published two subsequent studies where they made use of the galvanic replacement reaction for the *in situ* synthesis of rough metallic structures. In their approach, after the *in situ* electrodeposition of Cu-core/C-sheath nanowalls, a facile in-channel silver galvanic replacement reaction method took place at room temperature. For this, the electrodes had to be integrated into the microfluidic channel. These electrodes were prepatterned on a Si substrate using photolithography and lift-off techniques. The PDMS microfluidic channel was plasma-bonded to the Si substrate. The as-prepared platform offered high sensitivity due to the large available surface of the silver-nanoparticle-decorated nanowalls for analyte absorption and a large number of nanocavities, which could confine the surface plasmons in very small volumes.

Zhao *et al.*[114] used the PDMS–PDMS–glass "sandwich" microfluidic device illustrated in Fig. 7(b) for the *in situ* synthesis of composite Ag film@nano Au structures. For this, first, silver ammonia solution and glucose were filled into the channel in order to create a silver mirror. This was followed by the addition of poly(dimethyldiallylammonium chloride) and self-assembly of the Au nanoparticles. Finally, a chemical-

View Article Online
Analyst Critical Review

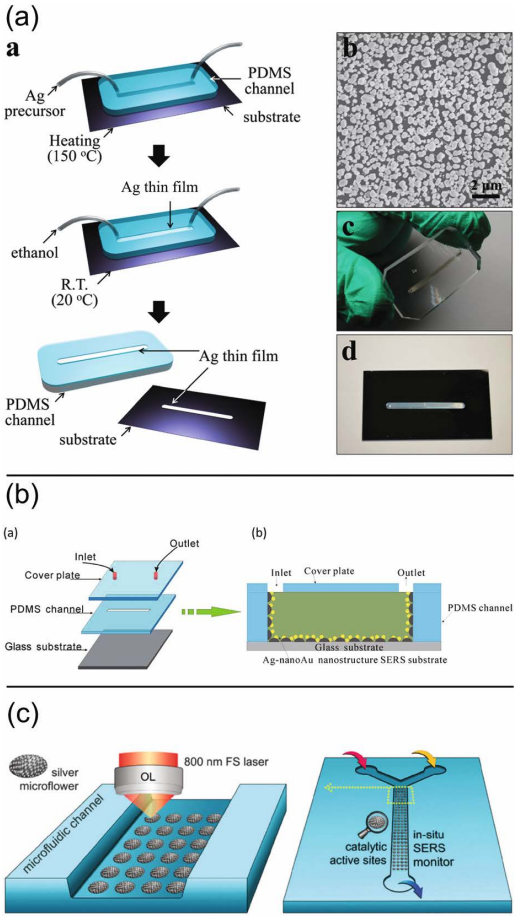

Fig. 7 (a) Schematic of the microfluidic patterning system, the SEM image of the Ag thin film, and photographs of the Ag-patterned PDMS and Si wafer. (Reproduced from Leem *et al.*[131] with permission from The Royal Society of Chemistry.) (b) Components of the "sandwich" microfluidic chip and a cross-section of the microfluidic channel. (Reproduced from Zhao *et al.*[114] with permission from The Royal Society of Chemistry.) (c) Scheme for the laser fabrication of silver microflowers inside a microfluidic channel (reproduced from Xu *et al.*[104] with permission from The Royal Society of Chemistry).

plating solution flowed over the nanostructure. Although the authors claim the *in situ* synthesis of the SERS-active substrate, gold colloids synthesized *a priori* were used in order to obtain the final nanostructures.

These three approaches and some others[107,112] published during the last four years have yet to deal with the challenge of cross-contamination and single-measurement design. A solution for this was published by Bjerneld *et al.*[146] and it involved the photochemical reduction of silver nitrate. More exactly, upon illumination with laser radiation, a chemical reaction between silver nitrate and citric acid is induced and colloidal silver, acetone-1,3-dicarboxylate, and carbon dioxide is formed. El-Zahry and coworkers[105,113] applied this synthesis principle for the *in situ* preparation of silver substrates. This was combined with a measurement protocol, where the memory effects did not play any role anymore in the SERS detection. Namely, in the procedure, a sequential injection analysis was used and the flow cell was moved by a few micrometers after each SERS detection. The formation of 3D Ag@ZnO nanostructures at any predefined position inside the microfluidic channels was also achieved by using a weak-focused, continuous-wave laser beam on the surface of a gold film serving as the bottom of the chip.[108] Due to light absorption of the Au film, the solution was locally heated up and then, by applying a precursor, 3D Ag@ZnO structures were formed. Light–matter interaction was also used by Xu *et al.*[104] to create silver microflower arrays *in situ* (see Fig. 7(c)). The authors used femtosecond-laser-induced photoreduction on the bed of a glass microchannel, and they attributed the formation of the structures to multi-photon-absorption-induced photoreduction. Nevertheless, the whole microflower array was created at once and then sealed in a PDMS template. Therefore, the advantage offered by the creation of a new hotspot after each SERS measurement is cancelled out.

Segmented flow platforms

In continuous flow platforms, cross-contamination and a weak analyte–plasmonic-substrate interaction are the main challenges. As described above, multiple strategies have been applied during the last few years to try to overcome these limitations. In parallel with this work, microfluidic platforms with segmented flow were also developed.[60,115–124] Here, segments can be formed by separating the liquid of interest by an immiscible fluid phase or by gas bubbles.[129] Although the liquid containing the sample wets the channel walls, cross-contamination is less relevant, as liquid exchange between the segments might happen only due to the thin wetting layer on the channel walls. Furthermore, by functionalizing the surface of the channels with a hydrophobic layer,[147] the aqueous segments do not wet the channel walls and precipitation of the substances is thus avoided. The challenge of cross-contamination is completely overcome only if the molecules or ions in the liquid sample cannot diffuse between segments.

Droplet-based microfluidic chips are the most popular segmented flow microfluidic platforms. Here, mixing is considerably enhanced by the convective flow inside the droplets.[129] Operational units, such as the droplet generator, splitting, fusion and mixing, solution dosing, phase separation, and distance control can be easily integrated.[65] Many of these units do not require an external trigger and they act thanks to the interplay of the interface generated forces with the hydrodynamic forces. As the SERS-active substrates, colloidal nanoparticles are applied.

Batch-synthesized SERS-active substrates. Citrate-[116–118,121] and hydroxylamine hydrochloride[60,123,124]-reduced silver colloidal nanoparticles are commonly encountered in the field of droplet-based microfluidic platforms. In the first case, the authors followed the protocol published by Lee and Meisel[136]

View Article Online

Critical Review Analyst

in 1982, which consisted of the chemical reaction between silver nitrate and sodium citrate at the boiling temperature of water. The reaction took up to one hour, and thus, other protocols have been considered in order to reduce this time. An almost instantaneous reduction of silver nitrate by hydroxylamine hydrochloride in the presence of sodium hydroxide can be carried out at room temperature. The preparation protocol[137] was published in 2003 and in the literature, the resultant products are referred to as 'Leopold–Lendl nanoparticles'. The same microfluidic platform was combined by Popp *et al.*[60,117,118,121,123,124] with both types of colloidal nanoparticles for various applications. The glass-based platform is depicted in Fig. 8(a). Glass has a low Raman scattering cross-section, and, as compared with PDMS, no signals interfere with the fingerprint of the molecules of interest. The successful generation of droplets in the continuous phase of oil was assured by a T-junction and in the hydrophobic channel walls due to the silanization procedure. Through a dosing unit, additional aqueous solutions could be injected into the already-existing droplets. The efficient mixing of substances was assured *via* the two meandering channels, while a long measurement loop allowed fine tuning of the measurement position. Generally, the analyte solutions and the solvents are pumped through ports 1–3, while the silver nanoparticles and their activation agent are injected *via* ports 4 and 5. In this way, the in-droplet concentration of the analytes could be easily and automatically adjusted and the addition of the SERS-active substrate can then be done in a reproducible manner. Lu and coworkers[116] employed a PDMS microfluidic chip very similar to the one depicted in Fig. 8(a), demonstrating the versatility of the microfluidic platform. Gold-core silver-shell nanocomposite particles were also employed in droplet-based microfluidics due to their proven SERS-signal-enhancement properties. For the synthesis of the gold core, Chung and co-workers[115] used the citrate reduction protocol followed by the addition of a DNA probe and encapsulation in a 4 nm thin silver layer. A pentagon-shaped microfluidic channel was designed to control the droplet size, as depicted in Fig. 8(b). After droplet formation, the samples in each compartment were mixed during the transport through the winding channels, and a long measuring loop is implemented. Wu *et al.*[120] prepared gold nanorods, as cores, using a previously developed seed-mediated growth method.[148] After a purification step, the cores were coated with silver. For this, L-ascorbic acid, hexadecyltrimethylammonium bromide, and silver nitrate were used. The as-prepared nanoparticles, the carrier oil, and the sample were injected at three different inlets of the microfluidic platform (Fig. 8(c)), which had a single, long, meandering channel.

Recently, Gao and coworkers[122] reported an approach for a wash-free magnetic immunoassay combined with droplet microfluidics. The starting point for this platform was based on the microfluidic device depicted in Fig. 3(b). There, the same authors used yoke-type solenoids for separation of the magnetic immunocomplexes from the solution. Nevertheless, the removal of unbound reagents was challenging and complicated-to-fabricate solenoids were required. In their recent study, the same authors designed and implemented a droplet-based microfluidic system embedded with a rectangular magnetic bar. The platform, depicted in Fig. 9, has four distinct operational units: microdroplet generator, immunocomplex and supernatant separator, isolation of magnetic immunocomplex droplets, and collection of unbound SERS nanotag droplets for SERS detection. The microdroplet generator had the same pentagon design as the platform in Fig. 8(b). The key parameters of this platform were the last two operational units. Namely, after the separation of the magnetic beads by the magnetic bar, the initial droplet was split into two smaller

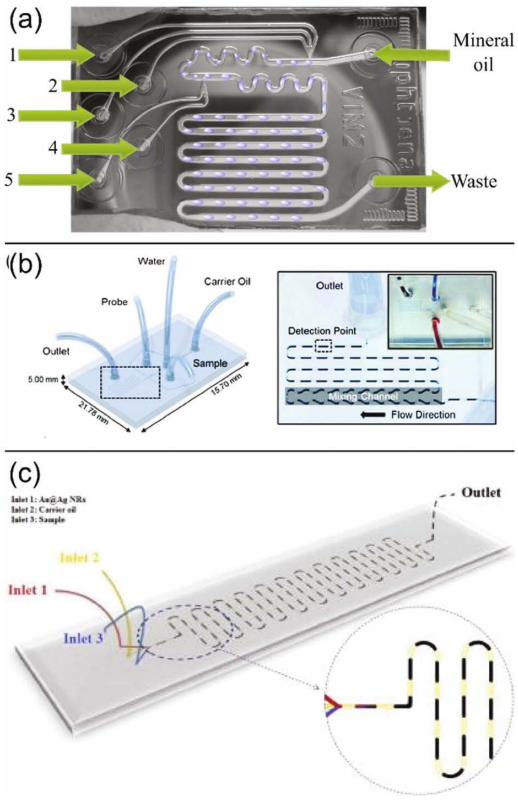

Fig. 8 (a) LoC-SERS system made out of glass: ports 1–5 are used for the injection of an aqueous solution containing the sample, the SERS-active substrates, and their aggregation agent. (Reprinted with permission from Hidi *et al.*[123] Copyright 2016 American Chemical Society.) (b) Microdroplet channel layout for the SERS detection of mercury(II) ions. Photograph of the channel filled with different colors of ink (blue and red), injected through the two inlets for the formation of aqueous droplets. (Reproduced from Chung *et al.*[115] with permission from The Royal Society of Chemistry.) (c) Schematic of a droplet-based microfluidic device (reprinted from L. Wu, Z. Wang, S. Zong, Y. Cui, Rapid and reproducible analysis of thiocyanate in real human serum and saliva using a droplet SERS-microfluidic chip, *Biosens. Bioelectron.*, **62**, 13–18.[120] Copyright 2014 with permission from Elsevier with the permission of Elsevier).

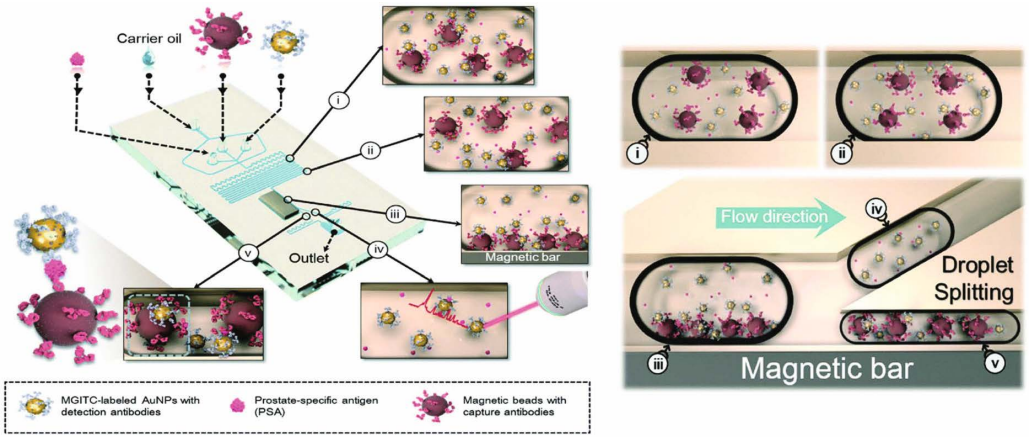

Fig. 9 Wash-free magnetic immunoassay combined with droplet-based microfluidics having five compartments (i–v) (reproduced from Gao *et al.*[122] with permission from The Royal Society of Chemistry).

droplets due to the presence of the y-shaped channels. The large droplets contained unbound SERS nanotags, while the smaller ones contained the magnetic immunocomplexes. Therefore, washing steps for removal of any unbound targets were not required.

***In situ* synthesized SERS-active substrates.** As already mentioned, the *in situ* synthesis of SERS-active substrates provides numerous advantages. Nonetheless, during the last four years, only two publications, to the best of our knowledge, have reported the synthesis of SERS-active colloids in droplet-based microfluidic platforms. This low number may be for many reasons. First, due to the formation of gaseous reaction products in most of the existing synthesis protocols, the stability of the droplets can be affected. Second, the slow reduction reaction of metal salts requires long microfluidic channels in order to assure the completeness of the reaction. The Leopold–Lendl nanoparticles are formed instantaneously and at room temperature. Gao *et al.*[125] took advantage of this fast reaction and synthesized these nanoparticles in a droplet-based microfluidic platform, as illustrated in Fig. 10. For this, they used a PDMS chip with two compartments. The first one had multiple winding channels in order to assure a good mixing of the reactants used for the colloidal synthesis and a long diffusion channel for the fast growth of silver nucleation. The second compartment had a T-junction, where the analyte-containing solutions were pumped into the droplets containing silver colloids. Although this is a promising approach, this synthesis protocol cannot be used in the case of the microfluidic chip shown in Fig. 8(a) because the sodium hydroxide used for assuring an alkaline pH during the synthesis will react with the silane layer deposited on the surface of the microchannel. To overcome this, Dugandžić *et al.*[126] used instead a chemical reaction between silver nitrate and hydrazine hydrate in ammonium hydroxide solution and trisodium citrate as a protective agent.

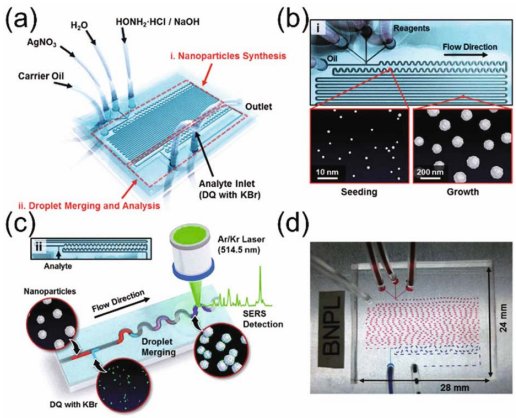

Fig. 10 Schematic of a droplet-based microfluidic platform used for the *in situ* synthesis of silver nanoparticles and the detection of a diaquat dibromide (reproduced from Gao *et al.*[125] with permission from The Royal Society of Chemistry).

Both described strategies show the superiority of the *in situ* synthesized colloidal solution over the batch protocols. Namely, each droplet contains a freshly prepared batch of colloids synthesized in an automatic and reproducible way. Also, colloid formation and SERS measurements can be performed on the same platform. And finally, the aging of the colloids no longer plays a role anymore.

Powerful application schemes in biophotonics

As discussed above, the combination of SERS as an optical detection method with nano/microfluidics offers the possi-

bility to tackle the challenges of conventional SERS measurements without compromising the sensitivity and specificity of the technique. This synergy opened the door for new applications, such as the immunoassay-based reliable SERS detection of biomarkers. The present section aims to offer an overview of the current hot topics of applications addressed by SERS and microfluidics.

Environmental and food monitoring

Even micromolar concentrations of pollutants in food or water can bring potential public health risks, so it is highly important to control any presence of naturally occurring or intentionally added chemical hazards in the environment. During the last few years, many studies have demonstrated that SERS combined with microfluidics is a powerful analytical tool for this purpose.[96,149–152]

Chung *et al.*[115] realized the SERS-based trace analysis of Hg(II) ions in water down to 10 pM concentration using Cy3-labeled aptamer-modified Au/Ag core–shell nanoparticles in the microdroplet channel (Fig. 8(b)). Namely, in the presence of Hg(II) ions, aptamer DNAs formed stable T–Hg(II)–T mediated hairpin structures, displacing the Raman reporter Cy3 from the surface of the nanoparticles and causing a decrease in the SERS signal (Fig. 11(a)). Similarly, an indirect strategy was used for the detection of As(III) ions by mixing them in a zigzag microfluidic chip with glutathione (GSH)/4-mercaptopyridine (4-MPY)-functionalized silver colloids (Fig. 11(b)). The binding of As(III) ions with GSH led to the aggregation of Ag colloids, and a SERS signal of 4-MPY could be recorded. Such sensors exhibited selectivity to the As(III) ions with an estimated limit of detection (LOD) of 0.67 ppb.[153]

Some toxic chemicals are widely used in agricultural areas and can contaminate waterways. Zhou *et al.*[154] reported the SERS-based trace analysis of the fungicide methyl parathion in lake water samples using a capillary with incorporated electrical heating constantan wire covered with vertically aligned ZnO nanotapers decorated with Ag nanoparticles (Fig. 11(c)). For SERS measurements, the capillary was filled with a mixture of a thermoresponsive microgel, Au-nanorod colloids, and an analyte solution, and then heated up. The heating process induced the shrinkage of the microgels, which caused the immobilization of the analyte and the reduction of the gaps between the plasmonic nanostructures. As a result, highly dense hotspots were formed and strong SERS signals were recorded.

An alternative strategy for creating hotspots was presented by Yazdi and White and was described in the previous section (Fig. 3(a)).[75] The passive trapping of Ag nanoparticles with adsorbed analyte molecules into the SERS detection volume in the measurement system allowed the detection of the organophosphate insecticide malathion down to a concentration of 12 ppb. Thereafter, the system was improved by implementing a passive micromixer for mixing the analyte and colloids on-chip. With the new design, detection of the fungicide thiram, with an estimated LOD of 50 ppt, and of the food contaminant melamine, with an LOD of 63 ppb, were reported.[76] For on-field analysis, the authors simplified the system by using a portable Raman spectrometer and a simple pipette instead of a bulky pump for sample loading. The authors successfully performed the multi-detection of 5 ppm methyl parathion, 0.1 ppb malachite green, and 5 ppb thiram.[155] Thiram down to 1×10^{-8} M concentration was also detected by Wang *et al.*[156] in a microfluidic channel, using a SERS optrode fabricated *in situ* by light-controlled polymerization and silver deposition. Gao *et al.*[125] used SERS to identify the herbicide diaquat dibromide monohydrate in microdroplets (see Fig. 10) with *in situ*

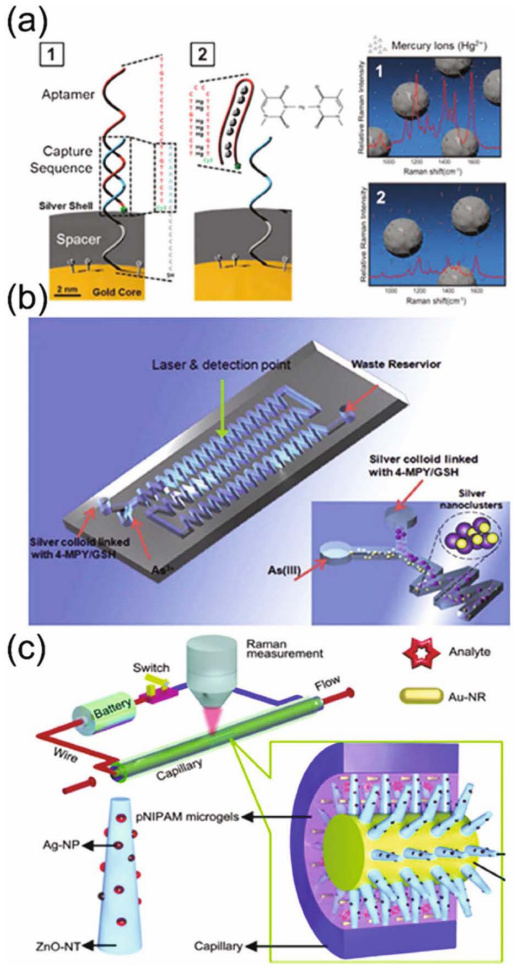

Fig. 11 (a) In the presence of Hg(II) ions, aptamer DNAs form stable T–Hg(II)–T mediated hairpin structures and move the Raman reporter Cy3 far away from the nanoparticles, resulting in a decrease in the SERS signal (two right). (Reproduced from Chung *et al.*[115] with permission from The Royal Society of Chemistry.) (b) Schematic diagram of the microfluidic chip used for analyzing As(III) and the mixing of As(III) ions with GSH/4-MPY-functionalized AgNPs. (Reproduced from Qi *et al.*[79] with permission from The Royal Society of Chemistry.) (c) Schematic of a battery-controlled SERS-based fluidic system (reproduced from Zhou *et al.*[112] with permission from Nature Publishing Group).

synthesized Ag colloids, reaching concentration levels below 5 nM.

Parisi *et al.*[110] presented the direct fabrication of Ag-nanoparticles-based SERS substrates in a microchannel followed by the detection of the pesticide Carbofuran and the herbicide Alachor, with determined LODs as low as 5 ppb for both targets. Patze *et al.*[101] developed a microfluidic cartridge setup using structured quartz wafers covered with a 40 nm layer of silver as the SERS substrate (see Fig. 5(b)). A real-world application of such a system was proven by its successful detection of the antibiotic sulfamethoxazole, as a drinking water pollutant, in spiked tap, river and lake waters in the nanomolar range.[101]

Many toxins threaten health and the life of humans and animals throughout the various food supply chains. One of them, ochratoxin A (OTA), was detected utilizing a microfluidic chip with a Au nanostructure *in situ* functionalized with an OTA-binding aptametric sequence. The injection of OTA to the microfluidic channel resulted in a change in the structural conformation of the aptamer sequence, which was possible to monitor with SERS. Unfortunately, only a single solution with a concentration of 2.5 μM was tested during the study.[157] The animal food additive clenbuterol was also detected by a SERS-based paper microfluidic platform with an LOD of 0.1 pg mL^{-1}.[158]

Detection of biomolecules

The ability to isolate, detect, and quantify certain biomolecules, such as DNA or proteins, from biological matrices opens up plenty of opportunities in clinical and diagnostic medical science. Optofluidic SERS sensors, benefiting from ultrasensitive, repeatable, and label-free detection, have been successfully applied in this area.[85,108]

Zhou *et al.*[77] developed a SERS-based microfluidic platform with a pneumatic valve and nanorod arrays at the bottom of the microchannel for Au nanoparticle aggregation and the creation of SERS hotspots (see Fig. 4(a)). The potential of this device was shown not only by detecting a typical protein, namely bovine serum albumin (BSA), down to the picomolar level, but also by distinguishing cytochrome C from BSA in a mixture of these two proteins. Wang and coworkers[159] obtained SERS spectra from the nerve agent simulant MP at a concentration as low as 10^{-8} M, using capillaries coated with 3D-clustered nanostructures decorated with Ag nanoparticles (Fig. 12(a)), which also exhibited good recycling performance. Leem *et al.*[131] developed a simple and low-cost microfluidic pattering system for the fabrication of Ag thin films in a microfluidic channel and then utilized them as an adenosine-sensing SERS probe (Fig. 7(a)) that worked down to the 500 nM concentration level.

The aggregation of amyloid beta peptide (Aβ), a biomarker for Alzheimer's disease, was studied using micro/nanofluidic junctions and a gold-nanoparticles-based SERS-active substrate. The Aβ aggregates were injected into the chip and, due to their large size, they were trapped at the micro/nanojunction and then examined with SERS (Fig. 12(b)). The authors proved their initial hypothesis that Aβ aggregation and its resulting structural characteristics are dependent on the initial Aβ concentration and on the time.[133] Neugebauer *et al.*[160] used a combination of droplet microfluidics (see Fig. 8(a)) and SERRS to successfully detect hemin at a 55 μM concentration in a binary mixture with cytochrome C, DNA, and glutathione.

The detection of specific DNA/RNA sequences is a major challenge in the fields of molecular biology and diagnosis, in which probing of a particular disease is based on nucleic acid identification. Prado *et al.*[161] reported the selective SERS detection of label-free purine and pyrimidine bases at low concentrations in continuous and in segmented flow microfluidic devices with silver colloids. Both platforms exhibited homogeneous mixing with silver colloids, but the microdroplet system inhibited the formation of large clusters that might clog the channel.

Zhao *et al.*[100] presented a fast method for the detection of natural sources double-strand DNA. This was done by

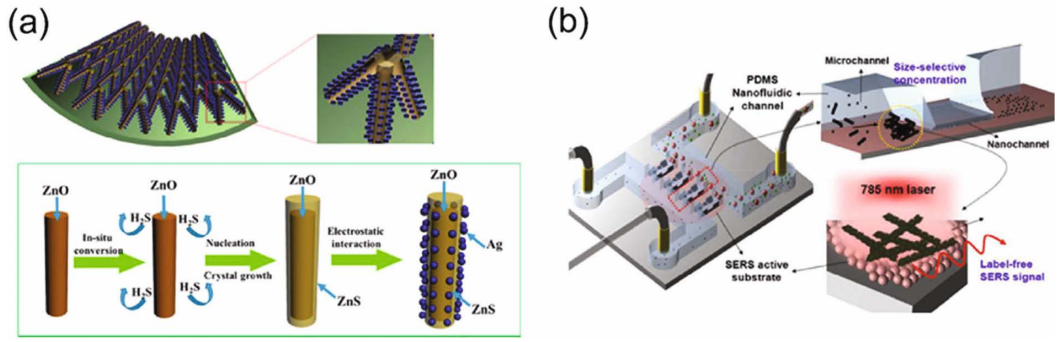

Fig. 12 (a) Schematic of the preparation of 3D-clustered nanostructures for bovine serum albumin detection (reprinted with permission from Wang *et al.*[159] Copyright 2016 American Chemical Society). (b) Schematic description of a SERS-active nanofluid device (Springer, I. Choi, Y. S. Huh, D. Erickson, Ultrasensitive, label-free probing of the conformational characteristics of amyloid beta aggregates with a SERS-active nanofluidic device, *Microfluid. Nanofluid.*, 2011, **12**.[133] Copyright 2011 with permission of Springer).

embedding a Ag/Si nanopillar array in a microfluidic chip for SERS monitoring. Because of the wide-range enhancing field and sufficient interpillar space, DNA molecules can easily enter the enhancing sites and yield reproducible signals upon excitation.

Saha *et al.*[162] adapted SERS in a simple paper-based microfluidic system. Using silver-coated gold nanoparticles, functionalized with a Raman reporter molecule, namely 4-mercaptopyridine, and glucose or biotin, they could detect the proteins concanavalin (Con) A and streptavidin. The presence of these proteins, due to the high affinity to glucose or biotin, induces the aggregation of nanoparticles, and the SERS signal of 4-mercaptopyridine could be detected. The authors reported the detection sensitivity for Con A as 1×10^{-15} M and for streptavidin as 1×10^{-14} M. It was found that the SERS signal intensity reached a maximum value within 3–4 min, independent of the protein concentration.

Drug and narcotics detection

The capability of LoC-SERS platforms to detect low molecular weight substances at low concentrations has also found use in drug monitoring and narcotics detection.[163]

Underlining the importance of therapeutic drug monitoring, Hidi *et al.*[60,117,123] assessed the potential and limitation of LoC-SERS platforms to detect drugs using silver colloids as SERS agents and a segmented flow microfluidic chip (Fig. 8(a)). The authors successfully detected methotrexate in the target therapeutic concentration range in distilled water. Thereafter, moving closer to real-world applications, the detection of the antibiotic levofloxacin was realized in complex matrices, such as artificial and human urine. Prior to the measurements, the urine samples were filtrated and diluted in order to reduce the matrix effects and to optimize the SERS signal. The system showed it held great promise in point-of-care applications, even with a portable Raman setup.[60] The authors also proved that such a technique is suitable for quantitative measurements and, combined with the standard addition method, it is able to predict unknown concentrations of an antibiotic in clinical samples. For example, for the detection of nitroxoline in spiked human urine, the achieved LOD was 3 μM and the limit of quantification (LOQ) was 6.5 μM. Furthermore, by applying chemometric approaches, the molecule was successfully quantified in simulated clinical samples with an unknown nitroxoline concentration.[123]

El-Zahry *et al.*[113] simultaneously detected aspirin and vitamin C in their pharmaceutical dosage forms and in spiked urine samples using a microfluidic chip with an *in situ*-produced SERS silver substrate. SERS detection was combined with sequential injection analysis, offering possibilities for automation of the analytical procedures. The authors found that a slower flow leads to an increased SERS signal. The detection limits were 32 and 3 ng ml^{-1} for aspirin and vitamin C, respectively. Bailey *et al.*[94] combined SERS and electrochemical detection in a sheath-flow microfluidic channel, and detected riboflavin with a detection limit near 1 nM. The fast-moving sheath flow limits the analyte diffusion within the region close to the SERS-active surface and stimulates the interactions between the analyte and substrate for a more sensitive SERS detection.

Yüksel *et al.*[103] demonstrated that SERS combined with microfluidics could be applied for narcotics monitoring. The authors realized the detection of the main component of cannabis, *i.e.*, tetrahydrocannabinol (THC), by the use of a SERS-based capillary platform created by *in situ* microwave-synthesized Ag nanoparticles. Such a system benefited from a simple and fast production of capillaries, which took only around 3 min. After loading the analyte, SERS measurements along the capillary exhibited good reproducibility and THC was detected down to a concentration of 1 nM. Another drug of abuse, methamphetamine, was determined down to 10 nM concentration in saliva using a microfluidic flow-focusing device, which allowed the analyte to be first adsorbed on the surface of the silver colloids before introducing the aggregation agent (Fig. 13(a)). In this way, the analyte was present in the created hotspots and not just surrounding them as it would be if the analyte were to be added to already-aggregated nanoparticles.[164]

Wu *et al.*[120] successfully detected a small molecule, namely thiocyanate (SCN^-), in complex matrices, such as human serum and saliva, by implementing a droplet SERS-microfluidic device using Au@Ag nanorods (Fig. 8(c)). The rapid detec-

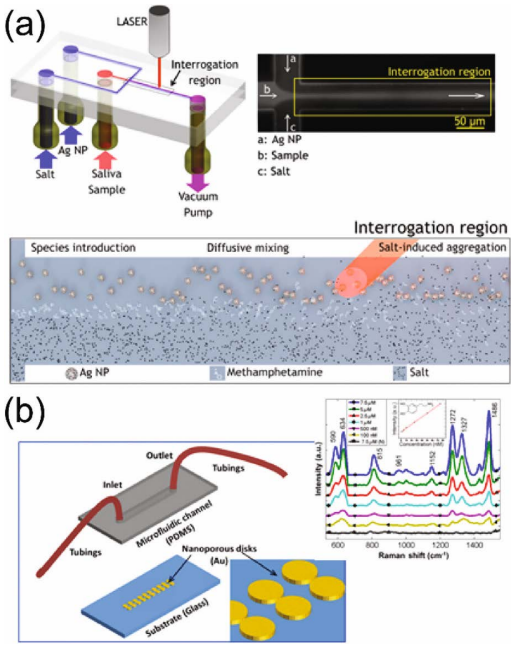

Fig. 13 (a) Flow-focusing device used for controlled Ag colloids aggregation. (Reprinted with permission from Andreou *et al.*[164] Copyright 2013 American Chemical Society.) (b) Schematic of the sensor architecture and concentration-dependent SERS spectra of dopamine (reproduced from Li *et al.*[165] with permission from SPIE).

tion of SCN^- in human saliva was also achieved and the result could be used to distinguish between smokers and nonsmokers.

Li *et al.*[165] employed nanoporous gold disks in a microchannel to increase the total usable area of a nanostructured surface, thus providing more adsorption sites for biomolecules (Fig. 13(b)). The efficiency of such a microfluidic SERS sensor was demonstrated by detecting dopamine in the nanomolar range and urea in artificial urine with an LOD 0.67 mM. Another urine component, namely creatinine, was measured in artificial urine down to 0.9 mg dL^{-1} using nanostructured capillary tubes with an inverse opal photonic crystal decorated with gold nanoparticles.[111]

Cell and bacteria detection

The combination of SERS and a microfluidic system provides an efficient platform for the sensitive, rapid, low-cost, and automatic separation, online detection, and identification of cells and bacteria without the risk of contamination of the sample as well as the operator.[130]

Chrimes *et al.*[166] developed a microfluidic system integrating dielectrophoresis (DEP) and SERS for the trapping and real-time investigation of the cell functions of isolated and grouped yeast cell clusters, as shown in Fig. 14(a). Yeast cells were coated with silver nanoparticles first to enable highly sensitive SERS analysis. Then, DEP was applied to immobilize a desired number of cells into the condition of being in intimate contact (grouped) or at a spacing greater than 10 μm from each other (isolated) in the microfluidic environment to observe the effect of such conditions on the live cells' chemical secretions. Principal component analysis (PCA) was used to visualize and examine hidden patterns in the SERS signals obtained from the two types of cells, and the significant systematic difference was found in the PCA score plot. The presence of chemicals and proteins around isolated cells before the budding process was found by analyzing the results

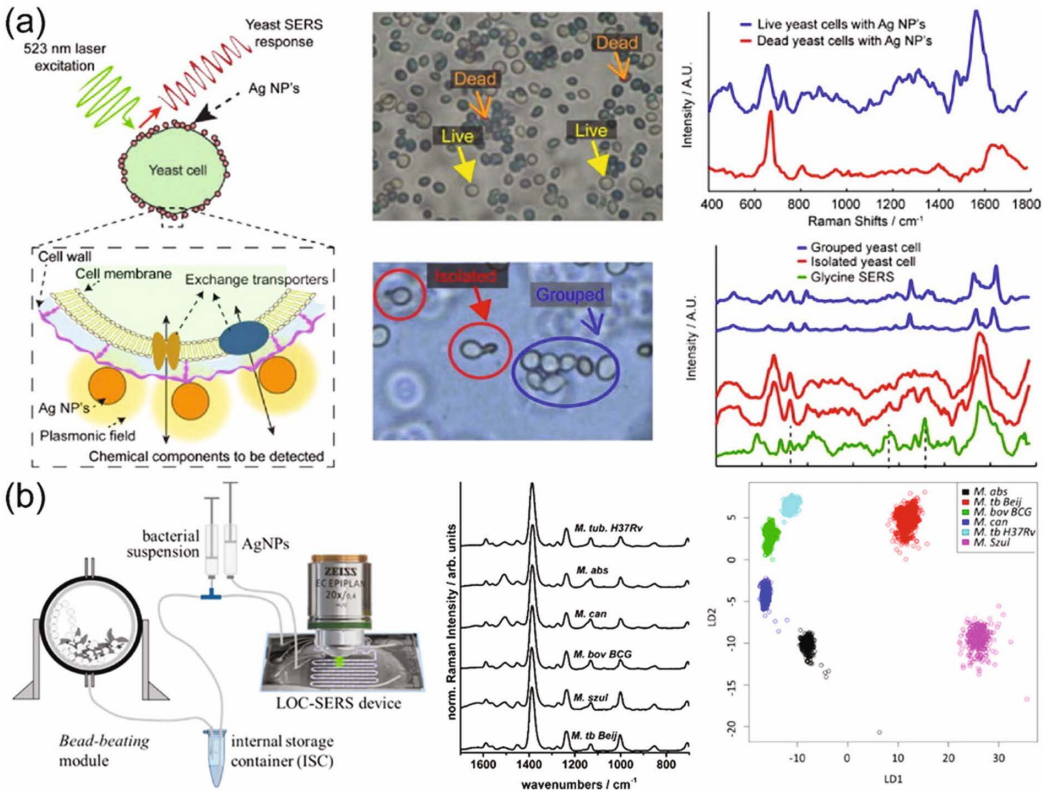

Fig. 14 (a) Schematic of silver bonding to the yeast cell-wall, followed by exposure to the light source, and the consequent generation of SERS signals (left). Results from the SERS of live *versus* dead yeast cells and grouped *versus* isolated yeast cells (middle and right) (reprinted from A. F. Chrimes, K. Khoshmanesh, S.-Y. Tang, B. R. Wood, P. R. Stoddart, S. S. E. Collins, A. Mitchell, K. Kalantar-zadeh, *In situ* SERS probing of nano-silver-coated individual yeast cells, *Biosens. Bioelectron.*, **49**, 536–541.[166] Copyright 2013, with permission from Elsevier.) (b) Schematic of the microfluidic device with a sample preparation module mounted to the microscope stage (left). Mean spectra of the three batches for every mycobacterial species (middle). PCA–LDA model trained to separate the six species for data visualization (right). (Reprinted with permission from Mühlig *et al.*[124] Copyright 2016 American Chemical Society.)

compared with grouped cells. This microfluidic SERS–DEP system enabled the *in situ* monitoring of cell secretion. A SERS substrate composed of 3D Ag@ZnO nanostructures was also integrated into a single-cell trapping microfluidic device by Xie *et al.*[108] for the SERS fingerprint detection of a single living HeLa cell surface, and multiple peaks from proteins, carbohydrates, and lipids were detectable.

The long-range concentration and rapid (<5 min) identification of rare pathogens from human blood were realized by Cheng *et al.*[86] by using SERS and a microfluidic platform with a hybrid electrokinetic mechanism for the isolation and concentration of bacteria. By capturing low concentrations of bacteria from a sample containing very dense blood cells, the approach showed high promise for the determination of blood infections. Besides this study, the fast online SERS detection of a single bacterium with high specificity and sensitivity was also realized by Lin *et al.*[167] They combined specific antibody-conjugated SERS tags with a microfluidic DEP device. Recently, a closed system for sample preparation and analysis based on LoC-SERS was developed by Mühlig *et al.*[124] and successfully applied to the identification of six species of *Mycobacterium tuberculosis* complex (MTC) and nontuberculous mycobacteria (NTM), as shown in Fig. 14(b). First, the bacteria were disrupted by using a bead-beating module and then they were directly injected into the LoC device after a washing step in the closed system, which ensured the operator safety as well as higher stability and reproducibility of the measurement conditions. Then, the AgNPs were also injected into the system to generate the SERS signals. The vibrational signals of the cell-wall component mycolic acid specific for each species dominated the SERS spectra and were thus used for the identification of the mycobacteria. The identification of the six species was realized with high accuracy and reliability by introducing chemometric methods.

The synergy between SERS and microfluidics appears to be useful also for the detection of most common foodborne pathogenic bacteria. Applying chemometric analysis to SERS data, Mungroo *et al.*[81] could effectively discriminate between eight different pathogen species: *E. coli*, *S. typhimirium*, *S. enteritis*, *Pseudomonas aeruginosa*, *L. monocytogenes*, *L. innocua, MRSA 35*, and *MRSA 86.* To simulate a more realistic industry scenario, the authors also studied polymicrobial cultures, but could reach only 64.5% accuracy in differentiation between individual bacterial species and 72.6% for detecting Gram-negative *versus* Gram-positive bacteria.

Immunoassays and biomarker detection for diagnosis

Microfluidic SERS immunoassays and biomarker detection dramatically improve the sensitivity and selectivity, and reduce the reaction volume as well as the time-cost of the assay and detection, which could simplify the diagnostic process and promote their further practical applications in the field of early diagnosis.[132,168,169]

A robust and sensitive SERS-microfluidic bioassay platform was developed by Wang *et al.*[92] for the simultaneous detection of two pathogen antigens, as shown in Fig. 15(a).

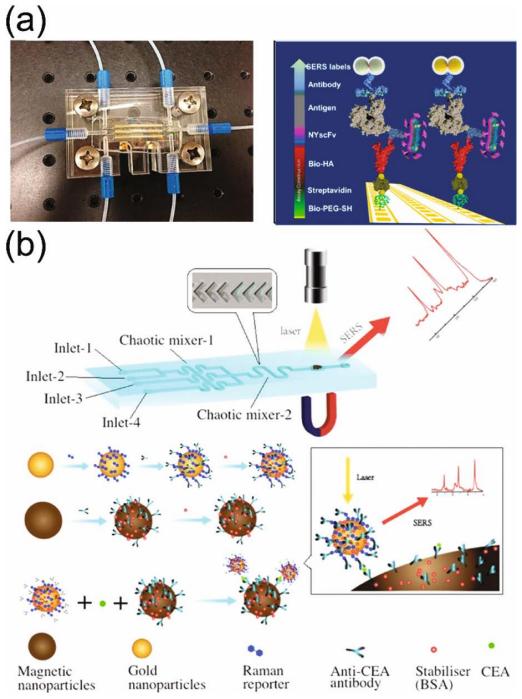

Fig. 15 (a) Image of the 3-channel microfluidic device containing gold patterns (left) and schematic illustration of the SERS biosensor platform with NYscFv for duplex antigen detection (right) (reproduced from Wang *et al.*[92] with permission from American Chemical Society). (b) Design of the microfluidic sensor and the principle of the sandwich immunoassay (reproduced from Zou *et al.*[170] Copyright 2015. With permission from WILEY-VCH Verlag GmbH & Co. KGaA, Weinheim).

The nanoyeast single-chain variable fragments (NYscFv), with the advantages of cost-effective production, stability in solution, and target-specificity, were developed as alternative affinity reagents. Highly purified, silica-coated Au nanoparticles with a self-assembled monolayer of Raman reporters were introduced to generate maximum Raman signals and to minimize the coadsorption of other molecules. The use of a microfluidic device with multiple channels enables the rapid detection of multiple targets simultaneously. Finally, the highly sensitive detection of the individual *Entamoeba histolytica* antigen EHI_115350 (LOD = 1 pg mL^{-1}) and EHI_182030 (LOD = 10 pg mL^{-1}) with high specificity has been achieved by using this platform. Gao and coworkers[80] developed a fully automated SERS-based solenoid-embedded microfluidic device with magnetic immunocoplexes for the quantitative and sensitive detection of the anthrax biomarker in solution, as shown in Fig. 3(a). In their further work,[122] the rapid and sensitive detection of prostate-specific antigen (PSA) cancer markers in serum was also realized by using a SERS-based microdroplet sensor for a wash-free magnetic immunoassay, as shown in Fig. 9. The LOD was estimated to be below 0.1 ng mL^{-1} for the PSA cancer

marker, which is much lower than the clinical cut-off value for the diagnosis of prostate cancer.

Zou and coworkers[170] developed a microfluidic sensing platform based on the sandwich immunoassay to detect the carcinoembryonic antigen (CEA), which serves as a reference for the diagnosis and prognosis of various malignant carcinoma in whole raw blood samples, as shown in Fig. 15(b). The sensing platform comprised a microfluidic chip, magnetic immunosensors, and SERS probes, which enabled analysis of the whole blood sample without sample pretreatment. All the immunoassay steps could be completed in the microchannel network for high-throughput analysis. The LOD for CEA in blood samples was as low as 10^{-12} M by using this method. Perozziello and coworkers[171,172] established a SERS-microfluidic platform composed of a microfluidic filtering device and a super hydrophobic surface integrating SERS sensors for the filtering, concentration, and analysis of specific peptides derived from the breast-cancer-related (BRCA1) protein, a vital tumor-suppressor molecule in the development of breast cancers. A concentration of the peptide down to 1 ng μL^{-1} could be detected, demonstrating the efficacy of the microfluidic device to purify the complex biological sample. Distinguishing cancerous prostate cells from normal cells was also realized by Pallaoro *et al.*[173] by combining microfluidics with SERS for the identification of individual cells incubated with SERS biotags continuously flowing in a microfluidics channel. This work provided a way for one-step cell labeling and continuous cell analysis for tumor cell identification at the single-cell level with a disposable device. Aimed at practical application, a paper-membrane-based SERS-microfluidic platform was also developed to separate glucose from a blood matrix and to detect the glucose level by using a nitrocellulose membrane as the substrate paper, a wax-printing method to construct the microfluidic channel, and gold nanorods with Raman labels as the SERS probes.[174] This paper-based microfluidic SERS device offered a cost-effective method to simplify the diagnostic process for diabetes mellitus.

Multiplex detection

SERS-based multiplex detection has a number of superior advantages, such as (1) facile labeling, (2) stable signal, (3) narrow peak width and high spectral resolution, (4) allowing simultaneous labeling of multiple reporters, and (5) multiple signals with a single wavelength excitation. When combined with the merits of microfluidics, it permits the capabilities to perform rapid, low-volume, and high-throughput multiplex detection with high sensitivity and reproducibility.[88,175,176]

Choi *et al.*[82] developed a programmable SERS-based micro-network gradient platform to simultaneously and quantitatively detect two breast cancer-related DNA oligomer mixtures, as shown in Fig. 16(a). The microfluidic network was designed by using an electric–hydraulic analogy to generate on-demand concentration gradients and to automatically produce different concentration gradients by continuously mixing Cy3-labeled

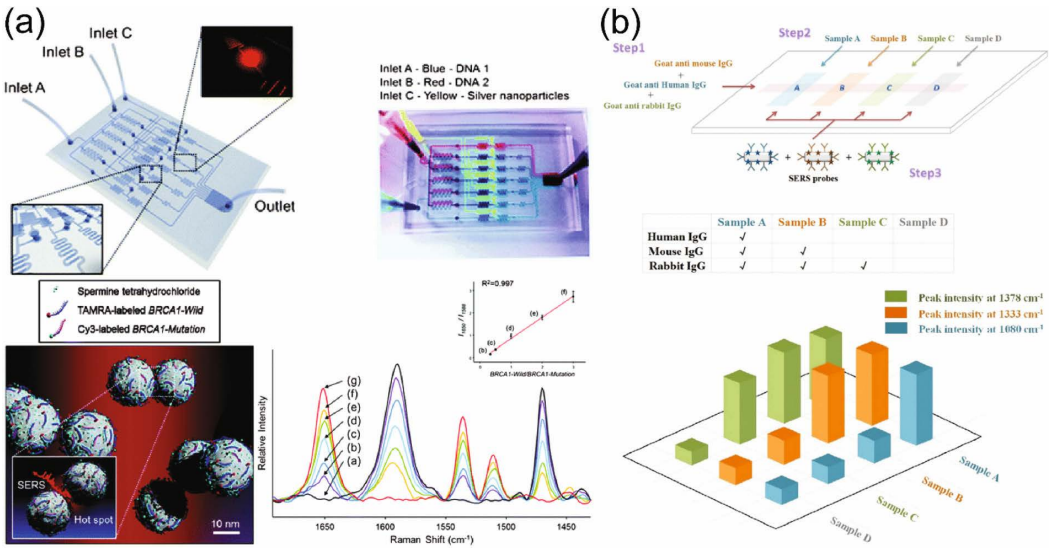

Fig. 16 (a) Three-layer integrated micro-network gradient channel and photograph of the channel filled with different colors of ink injected through the three inlets (top). SERS signal coming from the DNA oligomers adsorbed on the silver nanoparticle aggregates in the microfluidic channel and confocal SERS spectra of different molar ratios of the duplex DNA oligomer mixtures (below). (Reproduced from Choi *et al.*[82] with permission from The Royal Society of Chemistry.) (b) Simultaneous detection of human IgG, mouse IgG, and rabbit IgG. Schematic illustration of the multiplex immunoassay using one channel containing three antibodies (top). Components in each sample (middle). The results of the multiplex immunoassays are represented in 3D barcode (below) (reproduced from Wu *et al.*[145] Copyright 2015. With permission from Wiley-VCH Verlag GmbH & Co. KGaA, Weinheim).

DNA oligomers (BRAC1-Mutation) with TAMRA-labeled DNA oligomers (BRAC1-Wild). AgNPs were used to measure the SERS signals for different ratios of the duplex DNA oligomer mixtures under flowing conditions, and a good linear response was achieved. The detection time (less than 10 min) was reduced dramatically compared with the traditional PCR technique. The multiplex detection of DNA sequences was also demonstrated by Yazdi and coworkers[78] through a SERS-based competitive displacement assay in an integrated microsystem, as shown in Fig. 3(a). The LOD was as low as 100 pM for the target DNA sequence. Nguyen *et al.*[177] designed a SERS-microfluidic system for a multiplex immunoassay to detect four biomarkers of breast cancer from mimicked-patient serum. Gold nanostars conjugated with intact antibodies (IgG) and fragments of antigen binding (Fab) were used to determine the SERS signals.

The Fab-immunosenor demonstrated a 2.4-times higher signal than that of the IgG-immunosensor. The microfluidic device with four reaction chambers was designed for the detection of the four approved biomarkers. This improved SERS-microfluidic platform has been successfully used for the multiplex detection of a panel of breast cancer biomarkers, including cancer antigen (CA125), HER2, epididymis protein (HE4), and Eotaxin-1 from patient-mimicked serum samples. Wu *et al.*[145] developed a SERS-assisted 3D barcode microfluidic chip for a simultaneous, high-throughput, and multiplex immunoassay, as shown in Fig. 16(b). A microfluidic patterned antibody barcode substrate was designed for the spatial separation of multiple proteins in different samples. Au@Ag nanorods with different Raman labels served as SERS tags to generate spectroscopic information. The 3D barcode joins 2D spatial encoding with Raman spectroscopic encoding to store all the information for multiplex detection, including the sample sequence number, the presence of different proteins, and the concentration of the corresponding proteins in each sample. The one-step multiplex detection of human IgG, mouse IgG, and rabbit IgG within 30 min could be achieved with an ultrasensitivity down to 10 fg mL^{-1}.

In situ monitoring of biological processes and chemical reactions

SERS-microfluidic systems have also found important applications in the *in situ* monitoring of chemical reactions and processes. This is possibly due to the unique advantage they offer whereby complex reactions can be easily carried out in different microchannels, which act as microreactors allowing reactant injection as well as procedure monitoring and the sensitive detection of reaction products with SERS.[104]

Qi *et al.*[91] developed a SERS-based label-free approach for the *in situ* monitoring of the individual DNA hybridization by immobilizing molecular sentinel (MS) on nanoporous gold (NPG) disks inside microfluidics, as shown in Fig. 17(a). The microfluidic environment allowed agile fluid manipulation with a small volume. MS involves the complementary sequencing of a target ssDNA into a hairpin probe, which has a thiol group at the 5′ end for robust binding and cyanine 3 (Cy3) at the 3′ end for SERS detection. The strong SERS signal of Cy3 decreases during the hybridization process when the hairpin structure is open. By using this approach, the onset of hybridization events within 10 min after introducing 20 pM target ssDNA molecules could be detected with the sensitivity down to the single-molecule limit. The *in situ* monitoring of the enzymatic breakdown of organophosphate (OP) was carried out by Liberman *et al.*[109] by forming SERS-active AgNP clusters to enhance the Raman signals of the thiolated breakdown products inside a microfluidic device. Recently, Xie and coworkers[178] investigated the platinum-catalyzed reduction of 4-nitrothiophenol (4-NTP) to 4-aminothiophenol (4-ATP) by using label-free SERS monitoring in a microfluidic reactor, as shown in Fig. 17(b). Bifunctional Au–Pt–Au hybrid NPs were used as metal catalysts and SERS-active substrates. A microfluidic reactor chip with 30 alternatingly combined channels was used for completely mixing, eliminating unwanted photocatalytic side reactions, and providing the necessary time resolution for kinetic monitoring. A strong pH-dependent catalytic reduction of 4-NTP in aqueous solution of sodium borohydride was revealed based on kinetic analysis. This work demonstrated the potential of the microfluidics-based kinetic SERS monitoring of heterogeneous catalysis in colloidal suspension.

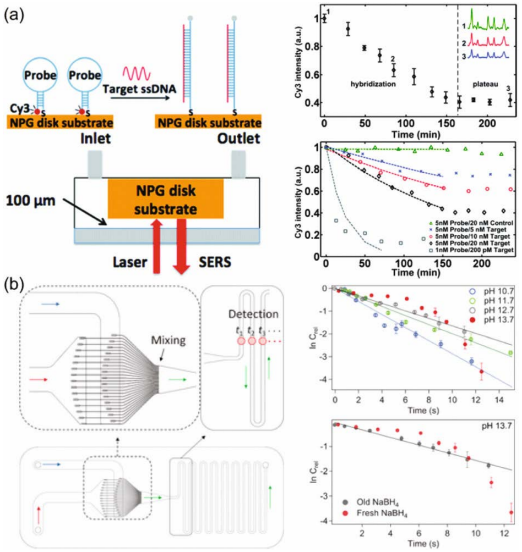

Fig. 17 (a) Schematic of MS sensing mechanism in microfluidics (left). *In situ* hybridization monitoring using SERS line-spectra (right). (Reproduced from Qi *et al.*[91] with permission from The Royal Society of Chemistry.) (b) The microfluidic reactor chip used for label-free SERS monitoring of the reduction of 4-NTP on Au–Pt–Au bifunctional NPs in aqueous borohydride solution (left). Kinetic SERS monitoring of the catalytic reactions at different pH values and comparison of the reaction kinetics by using freshly prepared and aged sodium borohydride solutions at pH 13.7 (reproduced from Xie *et al.*[178] Copyright 2016. With permission from Wiley-VCH Verlag GmbH & Co. KGaA, Weinheim).

View Article Online
Analyst Critical Review

Chemometric methods

This section gives an overview and a short explanation of the chemometric methods applied in the LoC-SERS papers reviewed in the previous sections. Chemometrics is generally utilized to translate the SERS spectra into meaningful information, normally either concentration estimates or diagnostic values. In order to take advantage of the unique potential of SERS for chemical analytics or diagnostic purposes, methods that allow 'control' of the SERS enhancement have to be developed. The reason for this is that an uncontrolled enhancement leads to unreliable varying information. Control can be achieved by either controlling all the experimental parameters, as demonstrated in the experimental sections above, or exercising control within the data analysis pipeline. In the second route, the robustness of the prediction is enhanced within the chemometric data pipeline used to analyse the SERS spectra. Both experimental and computational control methods try to reduce variations of the signal that do not arise from the analyte of interest. The results of both approaches are reliable and robust SERS spectra and/or extracted information (either concentration estimates or diagnostic values).

The computational approach will be described in the following pages. To the best of the author's knowledge, general investigations on the chemometric workflow for SERS spectra are not reported, therefore the usual data pipeline used for Raman spectra with minor modifications is employed.[179] This Raman spectroscopic data pipeline is composed of a spectral pre-processing and construction of the analysis models. These models are, ultimately, evaluated with validation schemes, *e.g.*, cross-validation or bootstrapping, to calculate the model characteristics. These characteristics may be the root-mean square error of prediction (RMSEP) for regression models or accuracies in the case of classification models. These characteristics are calculated to estimate the generalization performance of the models, *e.g.*, which error may result when predicting unknown SERS spectra with the evaluated models. The chemometrical models applied are standard chemometrical models, such as factor, classification, and regression techniques, which are widely described in textbooks.[180] The evaluation procedures and the calculated characteristics do not differ from the ones used in classical Raman spectroscopic analysis. Beside these similarities in the data pipeline of classical Raman spectroscopic analysis and SERS analysis, the pre-processing features a few differences. In the following, we give an overview of the analytical models used, the evaluation procedures,[181] and the pre-processing routines.[182]

Preprocessing of LoC-SERS spectra

The preprocessing routines used for the pretreatment of LoC-SERS spectra are slightly changed in comparison to the preprocessing routines used for Raman spectra. This change results from the fact that most of the microfluidic platforms allow the use of internal/external standards or certain spectra that can be used as such. The usual preprocessing for Raman spectra consists of a spike correction, a wavenumber calibration,[183] intensity calibration, a baseline correction,[101,124,164] a smoothing, and a normalization.[179,182] For Raman spectra, this data pipeline is intensively investigated and optimized. For example, Guo *et al.*[184] developed a marker that can be used to estimate the baseline correction quality and therefore can combine different background correction algorithms for the same dataset.[184] In this study,[184] a sensitive nonlinear iterative peak (SNIP) clipping, an asymmetric least squares baseline fit (ALS), and a modified polynomial fitting (Modpoly) were combined. These algorithms are widely used for the analysis of Raman and SERS spectra (see references of the study[184]). All these methods try to separate a slowly varying background from fast changing Raman bands. While ALS and Modpoly fit a low order polynomial, the SNIP algorithm uses the Low Statistic Digital Filter, then the Peak Clipping Loop and the inverse filter to determine a background estimation. For the normalization, often the vector norm or the area norm of a certain band or of the whole spectrum are utilized. While the area norm is the sum of all intensities, the vector norm is the squared root of the sum of all the squared intensities. Often LoC-SERS devices allow measuring either an internal standard[147] or spectra of a different channel within the device or the spectra of some separation medium,[183] which can then be used as the standard spectra. With the help of these additional spectra wavenumber or intensity, changes[183] can be corrected. This is visualized in Fig. 18, where a marker band of the separation medium (oil) is used to perform additionally a wavenumber calibration. Other researchers often try to correct for colloid properties[118,147] by means of new calibration concepts. These calibration procedures aim to standardize the SERS spectra in such a way that a robust and reliable analysis of these spectra is possible. The utilized analytical models will be described in the next section.

Statistical models and their quality measures

The statistical models used to analyze every kind of data, including LoC-SERS spectra, depend on the spectroscopic task to be solved. In principle, regression models and classification algorithms are used depending on if a continuous or a discrete variable should be extracted from the data.[180] Such a continuous variable is most often the concentration of an analyte of interest. In this case, regression algorithms, like partial least squares regression (PLS)[185] or principal component regression (PCR), can be applied. The basis is always to optimize the correlation of the spectra and the analyte concentration. All of these methods construct a predictive linear model for the given analyte based on a training dataset and their performance is then evaluated using evaluation procedures, like the cross-validation procedure.[181] Based on these evaluation procedures, the generalization performance of the model is estimated and quantified. As a quantitative marker for the performance, the average relative prediction error (ARPE)[151] or the root-mean squared error (RMSE)[180] can be utilized. The ARPE can be interpreted as the mean relative error, while the RMSE results in an absolute quantification of the average error.

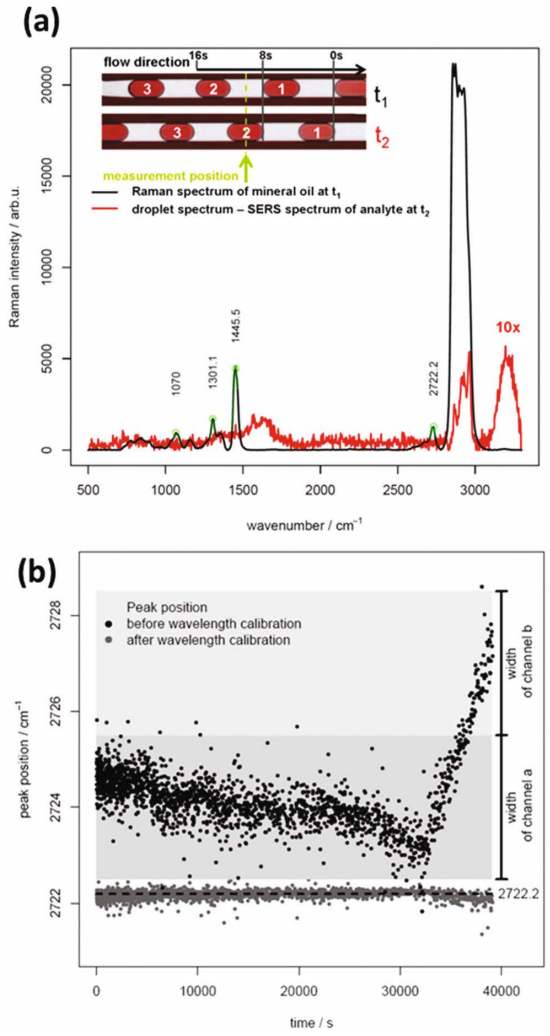

Fig. 18 (a) Segmented flow applied within a microfluidic device with a fixed measurement position and continuous movement of the droplets during detection; baseline-corrected Raman spectrum of mineral oil measured at t_1 (measured outside a droplet) and a baseline-corrected SERS spectrum of an analyte detected at t_2 (measured inside a droplet). (b) Plot of the peak position of a fitted oil band at 1445 cm^{-1} before and after wavenumber calibration. (Reprinted with permission from März *et al.*[183] Copyright 2011 American Chemical Society.)

Sometimes a 'P' for prediction or 'CV' for cross-validation is appended to the abbreviation to emphasize how this value was derived.

Beside the presented regression techniques, other techniques exist that can be used as regression tools. Two of these techniques are the classical least squares,[173,175] where known SERS spectra are fitted as the sum of the constituents spectra and the fitting coefficients are used as concertation estimates, and the multivariate curve resolution alternating least squares (MCR-ALS), which is used due to its flexibility to incorporate constraints[123,186–188] into the data pipeline.

If, in contrast, a discrete variable should be extracted, classification algorithms are utilized. Most common for the analysis of LoC-SERS data is a combination of principal component analysis (PCA) and linear discriminant analysis (LDA).[81,124,160] These two methods are over 100 years old, but their advantage is their robustness. This robustness results from the fact that the LDA constructs a linear classification model after a PCA has been utilized to reduce the dimensionality. Again, these models are evaluated based on evaluation procedures, like cross-validation.[181] From this evaluation or from the application to an independent dataset, quantitative markers for the model performance are extracted. This can be the accuracy, which is the overall working of the classification model, or the sensitivity of an important group.[189] As we have already mentioned, the applied statistical models are standard models, which are also applied in classical Raman spectroscopy. Nevertheless, there are a few studies that have tried to standardize LoC-SERS specific characteristics, which will be described at the end of this section.

Computational ways to deal with LoC-SERS-specific characteristics

There are two ways to deal with variations within LoC-SERS measurements: one is based on (extended) multiplicative signal correction (EMSC/MSC)[190,191] and the other one is based on the standard addition method (SAM).[192] The first way was investigated by Xia and coworkers.[151] They combined the 'optical path-length estimation and correction' (OPLEC) and a MSC to a method called 'multiplicative effects model for SERS (MEM_{SERS})'. They showed that their model was superior to PLS in terms of RMSEP and ARPE. Another approach is the combination of LoC-SERS and SAM, where a known concentration of the analyte of interest is added to the test sample and *via* recalculation the unknown concentration of the test sample can be determined.[192] In principle, this method corrects for matrix effects, which is thus a great advantage.[121,123] The SAM procedure for the determination of the unknown concentration of Congo red in the presence of methyl red in an aqueous solution by applying microfluidic SERS is illustrated in Fig. 19. Namely, by keeping a constant flowrate for the sample and adjusting the flowrates of water and the standard solution while keeping a constant total droplet volume (Fig. 19(a)), the unknown concentration of the target molecule could be determined. After a dimension reduction, where the SERS spectra were converted (Fig. 19(b)) to a 1D score (Fig. 19(c)), the unknown concentration of Congo red in the binary solution was accurately estimated.

Future perspectives and conclusions

The body of literature focusing on the development of LoC-SERS platforms is exhaustive, as demonstrated in the previous sections of this review. Much effort has been done to

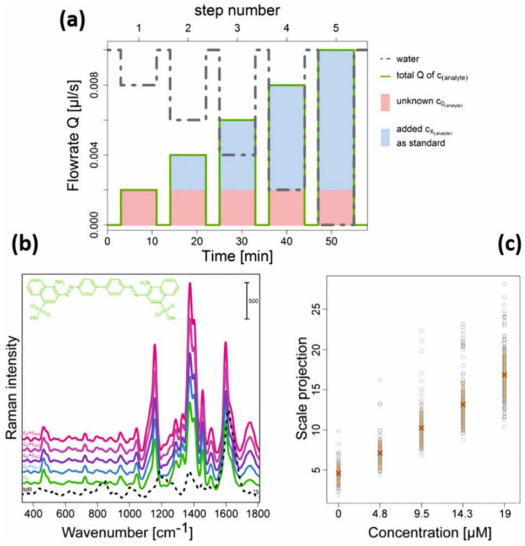

Fig. 19 (a) LoC-SERS-SAM gradient flow: the flow rate of water (gray dashed line) and the sum of the flow rates of an unknown sample and of an added standard are illustrated (green solid line). The colored areas illustrate the corresponding fraction of the analyte concentrations of the unknown sample (pink) and the standard (blue). (b) SERS spectrum of methyl red (black dotted line) used as an interfering molecule for the determination of the unknown concentration of Congo red (green line) in a binary matrix. The following spectra belong to the stepwise additions of the standard. (c) The gray points represent the prediction from the PCR. Also, the mean and standard deviation of the scale projection are shown. (Springer, E. Kämmer, K. Olschewski, S. Stöckel, P. Rösch, K. Weber, D. Cialla-May, T. Bocklitz, J. Popp, Quantitative SERS studies by combining LoC-SERS with the standard addition method, *Anal. Bioanal. Chem.*, 2015, **407**, 8925–8929.[121] Copyright Springer-Verlag Berlin Heidelberg 2015. With permission of Springer.)

improve the reliability and feasibility of these systems. Namely, LoC-SERS systems with on-demand and reversible formation of nanoparticle aggregates, with efficient analyte trapping in the detection area, with integrated competitive assay designs, and with *in situ* synthesis of SERS-active substrates have been reported over the last four years. Nevertheless, in a marketplace where numerous devices are well established, the implementation of new technologies is challenging. In order to overcome this, the research activities should be directed toward developing field-ready hardware and test kits with multiplexing capabilities, but without compromising their specificity and sensitivity.

LoC-SERS-integrated systems have a high potential for on-field, low-cost applications. The footprint and the costs of these platforms can be considerably reduced thanks to the continuous development of miniaturized, fiber-based Raman setups. Furthermore, moving away from low-scale, clean-room fabrication toward large-scale or *in situ*, right before measurement, synthesis of reliable SERS-active substrates will also promote a wide range of applications of these systems. Although in the research laboratory setting the reusability of microfluidic chips is of high interest for reducing costs, single-use, disposable and finger-nail sized chips with integrated operational units are desirable for large-scale applications. Furthermore, bulky syringe pumps have to be replaced with small units or ideally, by self-acting capillary forces.

In the last two sections of the present review, we showed that LoC-SERS systems combined with chemometric approaches have a high potential for a multitude of applications. Among these, multiplex detection is of high interest, as *i.e.*, for medical diagnosis, a whole panel of biomarkers has to be detected in order to confirm the presence of a disease. Microfluidic SERS in combination with competitive immunoassay designs can offer 3D barcode information with high sensitivity. Furthermore, considerable advances have been done in pathogen, drug, and pollutant detection in clinically and environmentally relevant matrices. Therefore, the latest studies have transited from ideal, easy-to-handle solvents to real-world situations. Nevertheless, the reliable quantification of substances by means of SERS is still challenging to realize. The quality of SERS-active substrates, the high chemical variability of clinical and environmental samples, and the fact that SERS is by definition a surface-sensitive technique are some of the factors contributing to these challenges.

In conclusion, although there is still much work to be done on the field of LoC-SERS platforms before the technique can be commercialized and implemented in practice, we are optimistic that the individual contribution of each research group focused on this topic will lead to a powerful bioanalytical tool of the future.

Acknowledgements

The funding of the grants InfectoGnostics (13GW0096F) and EXASENS (13N13856) by the Federal Ministry of Education and Research, Germany (BMBF) supporting this study is gratefully acknowledged.

References

1 M. Cauchi, D. P. Fowler, C. Walton, C. Turner, W. J. Jia, R. N. Whitehead, L. Griffiths, C. Dawson, H. Bai, R. H. Waring, D. B. Ramsden, J. O. Hunter, J. A. Cole and C. Bessant, *Metabolomics*, 2014, **10**, 1113–1120.
2 M. Niimi, T. Masuda, K. Kaihatsu, N. Kato, S. Nakamura, T. Nakaya and F. Arai, *Sens. Actuators, B*, 2014, **201**, 185–190.
3 E. Zerbini, M. M. Cardoso, M. D. Sequeira, M. N. Santi, H. Taher, D. Larpin, O. Latini and G. Tonarelli, *Medicina*, 1999, **59**, 453–458.
4 J. Y. Zhou, J. Hanfelt and J. M. Peng, *Proteomics: Clin. Appl.*, 2007, **1**, 1342–1350.
5 P. Baumann, K. Baumgartner and J. Hubbuch, *J. Chromatogr., A*, 2015, **1396**, 77–85.

6 G. Bazylak and L. J. Nagels, *Curr. Med. Chem.*, 2002, **9**, 1547–1566.
7 P. G. Varley, A. J. Brown, H. C. Dawkes and N. R. Burns, *Eur. Biophys. J. Biophys. Lett.*, 1997, **25**, 437–443.
8 D. Dasgupta and T. K. Sengupta, in *The Battle Against Microbial Pathogens: Basic Science, Technological Advances and Educational Programs*, ed. A. Méndez-Vilas, Formatex Research Center, 2015, pp. 1084–1090.
9 S. Grimalt, J. V. Sancho, O. J. Pozoa and F. E. Hernándeza, *J. Mass Spectrom.*, 2010, **45**, 421–436.
10 A. Masiá, J. Campo, C. Blasco and Y. Picó, *J. Chromatogr., A*, 2014, **1345**, 86–97.
11 G. Amendola, P. Pelosi and D. A. Barbini, *J. Environ. Sci. Health, Part B*, 2015, **50**, 109–120.
12 H. H. Lim and H. S. Shin, *J. Chromatogr., A*, 2014, **1361**, 117–124.
13 G. E. Morlock and W. Schwack, *J. Planar Chromatogr.–Mod. TLC*, 2007, **20**, 399–406.
14 J. A. G. Roach, D. Andrzejewski, M. L. Gay, D. Nortrup and S. M. Musser, *J. Agric. Food Chem.*, 2003, **51**, 7547–7554.
15 Y. H. Zhu, G. R. Li, Y. P. Duan, S. Q. Chen, C. Zhang and Y. F. Li, *Food Chem.*, 2008, **109**, 899–908.
16 F. Chen, G. G. Ying, J. F. Yang, J. L. Zhao and L. Wang, *J. Environ. Sci. Health, Part B*, 2010, **45**, 682–693.
17 B. Kapalavavi, Y. Yang, R. Marple and C. Gamsky, *Sep. Purif. Technol.*, 2016, **158**, 308–312.
18 J. L. Perez and M. A. Bello, *Talanta*, 1999, **48**, 1199–1202.
19 S. L. Yuan, X. F. Li, X. M. Jiang, H. X. Zhang and S. K. Zheng, *Chin. J. Anal. Chem.*, 2013, **41**, 49–56.
20 C. R. Bommarito, A. B. Sturdevant and D. W. Szymanski, *J. Forensic Sci.*, 2007, **52**, 24–30.
21 Y. Ehara and Y. Marumo, *Forensic Sci. Int.*, 1998, **96**, 1–10.
22 H. H. Maurer, *Ther. Drug Monit.*, 2002, **24**, 247–254.
23 J. F. Van Bocxlaer, K. M. Clauwaert, W. E. Lambert, D. L. Deforce, E. G. Van den Eeckhout and A. P. De Leenheer, *Mass Spectrom. Rev.*, 2000, **19**, 165–214.
24 G. Brandhorst, M. Oellerich, G. Maine, P. Taylor, G. Veen and P. Wallemacq, *Clin. Chem. Lab. Med.*, 2012, **58**, 821–825.
25 S.-S. Kim and B. Mizaikoff, in *Handbook of Spectroscopy*, Wiley-VCH Verlag GmbH & Co. KGaA, 2014, ch. 46, pp. 1557–1584, DOI: 10.1002/9783527654703.
26 L. Malic and A. G. Kirk, *Sens. Actuators, A*, 2007, **135**, 515–524.
27 M. Pokrzywnicka, D. J. Cocovi-Solberg, M. Miró, V. Cerdà, R. Koncki and Ł. Tymecki, *Anal. Bioanal. Chem.*, 2011, **399**, 1381–1387.
28 C. Moldovan, R. Iosub, C. Codreanu, B. Firtat, D. Necula, C. Brasoveanu and I. Stan, *Sensors*, 2012, **12**, 11372–11390.
29 H. M. Fang, S. J. Huang, C. L. Yang, K. C. Young and C. K. Yu, *J. Med. Biol. Eng.*, 2013, **33**, 117–123.
30 T. Schuster, R. Herschel, N. Neumann and C. G. Schaffer, *J. Lightwave Technol.*, 2012, **30**, 1003–1008.
31 Y. C. Dong and Z. Q. Yang, *Chin. Sci. Bull.*, 2013, **58**, 2557–2562.
32 D. King, M. O'Sullivan and J. Ducree, *J. Mod. Opt.*, 2014, **61**, 85–101.
33 O. Avci, N. L. Unlu, A. Y. Ozkumur and M. S. Unlu, *Sensors*, 2015, **15**, 17649–17665.
34 P. Couceiro, S. Gomez-de Pedro and J. Alonso-Chamarro, *Microfluid. Nanofluid.*, 2015, **18**, 649–656.
35 A. Thiha and F. Ibrahim, *Sensors*, 2015, **15**, 11431–11441.
36 Q. Zhang, D. M. Zhang, Y. L. Lu, Y. Yao, S. Li and Q. J. Liu, *Biosens. Bioelectron.*, 2015, **68**, 494–499.
37 L. G. Carrascosa, C. S. Huertas and L. M. Lechuga, *TrAC, Trends Anal. Chem.*, 2016, **80**, 177–189.
38 M. Fleischmann, P. J. Hendra and A. J. McQuillan, *Chem. Phys. Lett.*, 1974, **26**, 163–166.
39 H. Ilkhani, T. Hughes, J. Li, C. J. Zhong and M. Hepel, *Biosens. Bioelectron.*, 2016, **80**, 257–264.
40 T. Iliescu, M. Baia and I. Pavel, *J. Raman Spectrosc.*, 2006, **37**, 318–325.
41 M. Potara, M. Baia, C. Farcau and S. Astilean, *Nanotechnol.*, 2012, **23**, 1–10.
42 E. J. Liang, C. Engert and W. Kiefer, *Vib. Spectrosc.*, 1995, **8**, 435–444.
43 S. Schneider, G. Brehm and P. Freunscht, *Phys. Status Solidi B*, 1995, **189**, 37–42.
44 E. J. Liang, X. L. Ye and W. Kiefer, *J. Phys. Chem. A*, 1997, **101**, 7330–7335.
45 C. Yuen, W. Zheng and Z. W. Huang, *Biosens. Bioelectron.*, 2010, **26**, 580–584.
46 R. F. Huang, S. Y. Han and X. Li, *Anal. Bioanal. Chem.*, 2013, **405**, 6815–6822.
47 A. Bonifacio, S. Dalla Marta, R. Spizzo, S. Cervo, A. Steffan, A. Colombatti and V. Sergo, *Anal. Bioanal. Chem.*, 2014, **406**, 2355–2365.
48 O. Alharbi, Y. Xu and R. Goodacre, *Analyst*, 2015, **140**, 5965–5970.
49 R. L. Dong, S. Z. Weng, L. B. Yang and J. H. Liu, *Anal. Chem.*, 2015, **87**, 2937–2944.
50 Z. Z. Han, H. L. Liu, J. Meng, L. B. Yang, J. Liu and J. H. Liu, *Anal. Chem.*, 2015, **87**, 9500–9506.
51 C. Wang and C. X. Yu, *Nanotechnol.*, 2015, **26**, 1–26.
52 L. Litti, V. Amendola, G. Toffoli and M. Meneghetti, *Anal. Bioanal. Chem.*, 2016, **408**, 2123–2131.
53 D. Cialla, S. Pollok, C. Steinbrücker, K. Weber and J. Popp, *Nanophotonics*, 2014, **3**, 383–411.
54 X. M. Lin, Y. Cui, Y. H. Xu, B. Ren and Z. Q. Tian, *Anal. Bioanal. Chem.*, 2009, **394**, 1729–1745.
55 B. Sharma, R. R. Frontiera, A. I. Henry, E. Ringe and R. P. Van Duyne, *Mater. Today*, 2012, **15**, 16–25.
56 J. F. Betz, W. W. Yu, Y. Cheng, I. M. White and G. W. Rubloff, *Phys. Chem. Chem. Phys.*, 2014, **16**, 2224–2239.
57 M. Jahn, S. Patze, I. J. Hidi, R. Knipper, A. I. Radu, A. Muhlig, S. Yuksel, V. Peksa, K. Weber, T. Mayerhofer, D. Cialla-May and J. Popp, *Analyst*, 2016, **141**, 756–793.
58 Y. Zhang, B. Walkenfort, J. H. Yoon, S. Schlücker and W. Xie, *Phys. Chem. Chem. Phys.*, 2015, **17**, 21120–21126.

59 E. C. Le Ru and P. G. Etchegoin, in *Principles of Surface-Enhanced Raman Spectroscopy*, Elsevier, Amsterdam, 2009, pp. 367–413, DOI: 10.1016/B978-0-444-52779-0.00013-1.
60 I. J. Hidi, M. Jahn, M. W. Pletz, K. Weber, D. Cialla-May and J. Popp, *J. Phys. Chem. C*, 2016, **120**, 20613–20623.
61 W. Shen, X. Lin, C. Jiang, C. Li, H. Lin, J. Huang, S. Wang, G. Liu, X. Yan, Q. Zhong and B. Ren, *Angew. Chem., Int. Ed.*, 2015, **54**, 7308–7312.
62 B. L. Darby and E. C. Le Ru, *J. Am. Chem. Soc.*, 2014, **136**, 10965–10973.
63 L. Chen and J. Choo, *Electrophoresis*, 2008, **29**, 1815–1828.
64 C. Lim, J. Hong, B. G. Chung, A. J. deMello and J. Choo, *Analyst*, 2010, **135**, 837–844.
65 A. Marz, T. Henkel, D. Cialla, M. Schmitt and J. Popp, *Lab Chip*, 2011, **11**, 3584–3592.
66 J. Kim, *Lab Chip*, 2012, **12**, 3611–3623.
67 I. M. White, S. H. Yazdi and W. W. Yu, *Microfluid. Nanofluid.*, 2012, **13**, 205–216.
68 Q. L. Li, B. W. Li and Y. Q. Wang, *RSC Adv.*, 2013, **3**, 13015–13026.
69 H. Lee, L. F. Xu, D. Koh, N. Nyayapathi and K. W. Oh, *Sensors*, 2014, **14**, 17008–17036.
70 J. A. Huang, Y. L. Zhang, H. Ding and H. B. Sun, *Adv. Opt. Mater.*, 2015, **3**, 618–633.
71 Q. Zhou and T. Kim, *Sens. Actuators, B*, 2016, **227**, 504–514.
72 H. Hwang, D. Han, Y.-J. Oh, Y.-K. Cho, K.-H. Jeong and J.-K. Park, *Lab Chip*, 2011, **11**, 2518–2525.
73 Y. B. Guo, M. K. K. Oo, K. Reddy and X. D. Fan, *ACS Nano*, 2012, **6**, 381–388.
74 K. B. Kim, J.-H. Han, H. Choi, H. C. Kim and T. D. Chung, *Small*, 2012, **8**, 378–383.
75 S. H. Yazdi and I. M. White, *Biomicrofluidics*, 2012, **6**, 014105.
76 S. H. Yazdi and I. M. White, *Anal. Chem.*, 2012, **84**, 7992–7998.
77 J. H. Zhou, K. N. Ren, Y. H. Zhao, W. Dai and H. K. Wu, *Anal. Bioanal. Chem.*, 2012, **402**, 1601–1609.
78 S. H. Yazdi, K. L. Giles and I. M. White, *Anal. Chem.*, 2013, **85**, 10605–10611.
79 N. Qi, B. Li, H. You, W. Zhang, L. Fu, Y. Wang and L. Chen, *Anal. Methods*, 2014, **6**, 4077–4082.
80 R. Gao, J. Ko, K. Cha, J. H. Jeon, G. E. Rhie, J. Choi, A. J. deMello and J. Choo, *Biosens. Bioelectron.*, 2015, **72**, 230–236.
81 N. A. Mungroo, G. Oliveira and S. Neethirajan, *Microchim. Acta*, 2016, **183**, 697–707.
82 N. Choi, K. Lee, D. W. Lim, E. K. Lee, S. I. Chang, K. W. Oh and J. Choo, *Lab Chip*, 2012, **12**, 5160–5167.
83 M. Lee, K. Lee, K. H. Kim, K. W. Oh and J. Choo, *Lab Chip*, 2012, **12**, 3720–3727.
84 D. Kim, A. R. Campos, A. Datt, Z. Gao, M. Rycenga, N. D. Burrows, N. G. Greeneltch, C. A. Mirkin, C. J. Murphy, R. P. Van Duyne and C. L. Haynes, *Analyst*, 2014, **139**, 3227–3234.
85 W. Huttner, K. Christou, A. Gohmann, V. Beushausen and H. Wackerbarth, *Microfluid. Nanofluid.*, 2012, **12**, 521–527.
86 I. F. Cheng, H.-C. Chang, T.-Y. Chen, C. Hu and F.-L. Yang, *Sci. Rep.*, 2013, **3**, 1–8.
87 P. Negri, K. T. Jacobs, O. O. Dada and Z. D. Schultz, *Anal. Chem.*, 2013, **85**, 10159–10166.
88 G. Chen, Y. Y. Wang, H. L. Wang, M. Cong, L. Chen, Y. G. Yang, Y. J. Geng, H. B. Li, S. P. Xu and W. Q. Xu, *RSC Adv.*, 2014, **4**, 54434–54440.
89 H. Mao, W. Wu, D. She, G. Sun, P. Lv and J. Xu, *Small*, 2014, **10**, 127–134.
90 Y. J. Oh and K. H. Jeong, *Lab Chip*, 2014, **14**, 865–868.
91 J. Qi, J. Zeng, F. Zhao, S. H. Lin, B. Raja, U. Strych, R. C. Willson and W.-C. Shih, *Nanoscale*, 2014, **6**, 8521–8526.
92 Y. Wang, S. Rauf, Y. S. Grewal, L. J. Spadafora, M. J. A. Shiddiky, G. A. Cangelosi, S. Schlücker and M. Trau, *Anal. Chem.*, 2014, **86**, 9930–9938.
93 H. Y. Wu and B. T. Cunningham, *Nanoscale*, 2014, **6**, 5162–5171.
94 M. R. Bailey, A. M. Pentecost, A. Selimovic, R. S. Martin and Z. D. Schultz, *Anal. Chem.*, 2015, **87**, 4347–4355.
95 J. Choi, K. S. Lee, J. H. Jung, H. J. Sung and S. S. Kim, *RSC Adv.*, 2015, **5**, 922–927.
96 Y. Deng, M. N. Idso, D. D. Galvan and Q. M. Yu, *Anal. Chim. Acta*, 2015, **863**, 41–48.
97 A. Lamberti, A. Virga, A. Angelini, A. Ricci, E. Descrovi, M. Cocuzza and F. Giorgis, *RSC Adv.*, 2015, **5**, 4404–4410.
98 A. Lamberti, A. Virga, A. Chiado, A. Chiodoni, K. Bejtka, P. Rivolo and F. Giorgis, *J. Mater. Chem. C*, 2015, **3**, 6868–6875.
99 S. Uusitalo, J. Hiltunen, P. Karioja, S. Siitonen, V. Kontturi, R. Myllyla, M. Kinnunen and I. Meglinski, *J. Eur. Opt. Soc.-Rapid*, 2015, **10**, 150431–150438.
100 Y. Q. Zhao, Y. L. Zhang, J. A. Huang, Z. Y. Zhang, X. F. Chen and W. J. Zhang, *J. Mater. Chem. A*, 2015, **3**, 6408–6413.
101 S. Patze, U. Huebner, F. Liebold, K. Weber, D. Cialla-May and J. Popp, *Anal. Chim. Acta*, 2017, **949**, 1–7.
102 A. Yamaguchi, T. Fukuoka, R. Takahashi, R. Hara and Y. Utsumi, *Sens. Actuators, B*, 2016, **230**, 94–100.
103 S. Yüksel, A. M. Schwenke, G. Soliveri, S. Ardizzone, K. Weber, D. Cialla-May, S. Hoeppener, U. S. Schubert and J. Popp, *Anal. Chim. Acta*, 2016, **939**, 93–100.
104 B. B. Xu, R. Zhang, X. Q. Liu, H. Wang, Y. L. Zhang, H. B. Jiang, L. Wang, Z. C. Ma, J. F. Ku, F. S. Xiao and H. B. Sun, *Chem. Commun.*, 2012, **48**, 1680–1682.
105 M. R. El-Zahry, A. Genner, I. H. Refaat, H. A. Mohamed and B. Lendl, *Talanta*, 2013, **116**, 972–977.
106 J. Parisi, L. Su and Y. Lei, *Lab Chip*, 2013, **13**, 1501–1508.
107 G. Wang, G. Shi, H. Wang, Q. Zhang and Y. Li, *Adv. Funct. Mater.*, 2014, **24**, 1017–1026.
108 Y. Xie, S. Yang, Z. Mao, P. Li, C. Zhao, Z. Cohick, P.-H. Huang and T. J. Huang, *ACS Nano*, 2014, **8**, 12175–12184.

109 V. Liberman, K. Hamad-Schifferli, T. A. Thorsen, S. T. Wick and P. A. Carr, *Nanoscale*, 2015, **7**, 11013–11023.
110 J. Parisi, Q. C. Dong and Y. Lei, *RSC Adv.*, 2015, **5**, 14081–14089.
111 X. W. Zhao, J. Y. Xue, Z. D. Mu, Y. Huang, M. Lu and Z. Z. Gu, *Biosens. Bioelectron.*, 2015, **72**, 268–274.
112 Q. Zhou, G. Meng, P. Zheng, S. Cushing, N. Wu, Q. Huang, C. Zhu, Z. Zhang and Z. Wang, *Sci. Rep.*, 2015, **5**, 12865–12866.
113 M. R. El-Zahry, I. H. Refaat, H. A. Mohamed and B. Lendl, *Anal. Bioanal. Chem.*, 2016, **408**, 4733–4741.
114 H. Z. Zhao, Y. Xu, C. Y. Wang, R. Wang, S. T. Xiang and L. Chen, *RSC Adv.*, 2016, **6**, 14105–14111.
115 E. Chung, R. Gao, J. Ko, N. Choi, D. W. Lim, E. K. Lee, S. I. Chang and J. Choo, *Lab Chip*, 2013, **13**, 260–266.
116 X. N. Lu, D. R. Samuelson, Y. H. Xu, H. W. Zhang, S. Wang, B. A. Rasco, J. Xu and M. E. Konkel, *Anal. Chem.*, 2013, **85**, 2320–2327.
117 I. J. Hidi, A. Muhlig, M. Jahn, F. Liebold, D. Cialla, K. Weber and J. Popp, *Anal. Methods*, 2014, **6**, 3943–3947.
118 E. Kammer, K. Olschewski, T. Bocklitz, P. Rosch, K. Weber, D. Cialla and J. Popp, *Phys. Chem. Chem. Phys.*, 2014, **16**, 9056–9063.
119 B. D. Piorek, C. Andreou, M. Moskoyits and C. D. Meinhart, *Anal. Chem.*, 2014, **86**, 1061–1066.
120 L. Wu, Z. Y. Wang, S. F. Zong and Y. P. Cui, *Biosens. Bioelectron.*, 2014, **62**, 13–18.
121 E. Kammer, K. Olschewski, S. Stockel, P. Rosch, K. Weber, D. Cialla-May, T. Bocklitz and J. Popp, *Anal. Bioanal. Chem.*, 2015, **407**, 8925–8929.
122 R. K. Gao, Z. Y. Cheng, A. J. Demello and J. Choo, *Lab Chip*, 2016, **16**, 1022–1029.
123 I. J. Hidi, M. Jahn, K. Weber, T. Bocklitz, M. W. Pletz, D. Cialla-May and J. Popp, *Anal. Chem.*, 2016, **88**, 9173–9180.
124 A. Mühlig, T. Bocklitz, I. Labugger, S. Dees, S. Henk, E. Richter, S. Andres, M. Merker, S. Stockel, K. Weber, D. Cialla-May and J. Popp, *Anal. Chem.*, 2016, **88**, 7998–8004.
125 R. Gao, N. Choi, S. I. Chang, E. K. Lee and J. Choo, *Nanoscale*, 2014, **6**, 8781–8786.
126 V. Dugandžić, I. J. Hidi, K. Weber, D. Cialla-May and J. Popp, *Anal. Chim. Acta*, 2016, **946**, 73–79.
127 T. A. Meier, E. Poehler, F. Kemper, O. Pabst, H. G. Jahnke, E. Beckert, A. Robitzki and D. Belder, *Lab Chip*, 2015, **15**, 2923–2927.
128 J. Zhang, R. J. Coulston, S. T. Jones, J. Geng, O. A. Scherman and C. Abell, *Science*, 2012, **335**, 690–694.
129 R. Seemann, M. Brinkmann, T. Pfohl and S. Herminghaus, *Rep. Prog. Phys.*, 2012, **75**, 1–41.
130 M. Knauer, N. P. Ivleva, R. Niessner and C. Haisch, *Anal. Bioanal. Chem.*, 2012, **402**, 2663–2667.
131 J. Leem, H. W. Kang, S. H. Ko and H. J. Sung, *Nanoscale*, 2014, **6**, 2895–2901.
132 A. Kaminska, E. Witkowska, K. Winkler, I. Dziecielewski, J. L. Weyher and J. Waluk, *Biosens. Bioelectron.*, 2015, **66**, 461–467.
133 I. Choi, Y. S. Huh and D. Erickson, *Microfluid. Nanofluid.*, 2012, **12**, 663–669.
134 E. C. Le Ru and P. G. Etchegoin, in *Principles of Surface-Enhanced Raman Spectroscopy*, Elsevier, Amsterdam, 2009, pp. 121–183, DOI: 10.1016/B978-0-444-52779-0.00009-X.
135 P. G. Etchegoin and E. C. Le Ru, in *Surface Enhanced Raman Spectroscopy*, Wiley-VCH Verlag GmbH & Co. KGaA, 2010, ch. 1, pp. 1–37, DOI: 10.1002/9783527632756.
136 P. C. Lee and D. Meisel, *J. Phys. Chem.*, 1982, **86**, 3391–3395.
137 N. Leopold and B. Lendl, *J. Phys. Chem. B*, 2003, **107**, 5723–5727.
138 E. C. Le Ru, C. Galloway and P. G. Etchegoin, *Phys. Chem. Chem. Phys.*, 2006, **8**, 3083–3087.
139 E. C. Ru, P. G. Etchegoin, J. Grand, N. Felidj, J. Aubard, G. Levi, A. Hohenau and J. R. Krenn, *Curr. Appl. Phys.*, 2008, **8**, 467–470.
140 M. Moskovits, *J. Raman Spectrosc.*, 2005, **36**, 485–496.
141 C. M. Aikens, L. R. Madison and G. C. Schatz, *Nat. Photonics*, 2013, **7**, 508–510.
142 M. Moskovits and J. S. Suh, *J. Phys. Chem.*, 1984, **88**, 5526–5530.
143 E. C. Le Ru, S. A. Meyer, C. Artur, P. G. Etchegoin, J. Grand, P. Lang and F. Maurel, *Chem. Commun.*, 2011, **47**, 3903–3905.
144 H. Xu, J. Aizpurua, M. Käll and P. Apell, *Phys. Rev. E: Stat. Phys., Plasmas, Fluids, Relat. Interdiscip. Top.*, 2000, **62**, 4318–4324.
145 L. Wu, Z. Wang, K. Fan, S. Zong and Y. Cui, *Small*, 2015, **11**, 2798–2806.
146 E. J. Bjerneld, K. V. G. K. Murty, J. Prikulis and M. Käll, *ChemPhysChem*, 2002, **3**, 116–119.
147 A. März, K. R. Ackermann, D. Malsch, T. Bocklitz, T. Henkel and J. Popp, *J. Biophotonics*, 2009, **2**, 232–242.
148 I. Gorelikov and N. Matsuura, *Nano Lett.*, 2008, **8**, 369–373.
149 B. X. Liu, W. Jiang, H. T. Wang, X. H. Yang, S. J. Zhang, Y. F. Yuan, T. Wu and Y. P. Du, *Microchim. Acta*, 2013, **180**, 997–1004.
150 H. Yang, M. Deng, S. Ga, S. H. Chen, L. Kang, J. H. Wang, W. W. Xin, T. Zhang, Z. R. You, Y. An, J. L. Wang and D. X. Cui, *Nanoscale Res. Lett.*, 2014, **9**, 1–6.
151 T. H. Xia, Z. P. Chen, Y. Chen, J. W. Jin and R. Q. Yu, *Anal. Methods*, 2014, **6**, 2363–2370.
152 Y. A. Yang, S. P. Xu, Y. Y. Wang, G. H. Qi and W. Q. Xu, *Chem. J. Chin. Univ.*, 2015, **36**, 254–259.
153 N. Qi, B. W. Li, H. Y. You, W. Zhang, L. W. Fu, Y. Q. Wang and L. X. Chen, *Anal. Methods*, 2014, **6**, 4077–4082.
154 Q. T. Zhou, G. W. Meng, P. Zheng, S. Cushing, N. Q. Wu, Q. Huang, C. H. Zhu, Z. Zhang and Z. W. Wang, *Sci. Rep.*, 2015, **5**, 1–11.
155 S. H. Yazdi and I. M. White, *Analyst*, 2013, **138**, 100–103.

156 S. Y. Wang, C. Y. Liu, H. L. Wang, G. Chen, M. Cong, W. Song, Q. Jia, S. P. Xu and W. Q. Xu, *ACS Appl. Mater. Interfaces*, 2014, **6**, 11706–11713.
157 B. C. Galarreta, M. Tabatabaei, V. Guieu, E. Peyrin and F. Lagugne-Labarthet, *Anal. Bioanal. Chem.*, 2013, **405**, 1613–1621.
158 T. T. Zheng, Z. G. Gao, Y. Luo, X. M. Liu, W. J. Zhao and B. C. Lin, *Electrophoresis*, 2016, **37**, 418–424.
159 G. Wang, K. R. Li, F. J. Purcell, D. Zhao, W. Zhang, Z. Y. He, S. Tan, Z. G. Tang, H. Z. Wang and E. Reichnianis, *ACS Appl. Mater. Interfaces*, 2016, **8**, 24974–24981.
160 U. Neugebauer, A. Marz, T. Henkel, M. Schmitt and J. Popp, *Anal. Bioanal. Chem.*, 2012, **404**, 2819–2829.
161 E. Prado, A. Colin, L. Servant and S. Lecomte, *J. Phys. Chem. C*, 2014, **118**, 13965–13971.
162 A. Saha and N. R. Jana, *ACS Appl. Mater. Interfaces*, 2015, **7**, 996–1003.
163 C. Delhaye, J. L. Bruneel, D. Talaga, M. Guirardel, S. Lecomte and L. Servant, *J. Phys. Chem. C*, 2012, **116**, 5327–5332.
164 C. Andreou, M. R. Hoonejani, M. R. Barmi, M. Moskovits and C. D. Meinhart, *ACS Nano*, 2013, **7**, 7157–7164.
165 M. Li, F. S. Zhao, J. B. Zeng, J. Qi, J. Lu and W. C. Shih, *J. Biomed. Opt.*, 2014, **19**, 1116111–1116118.
166 A. F. Chrimes, K. Khoshmanesh, S.-Y. Tang, B. R. Wood, P. R. Stoddart, S. S. E. Collins, A. Mitchell and K. Kalantar-zadeh, *Biosens. Bioelectron.*, 2013, **49**, 536–541.
167 H. Y. Lin, C. H. Huang, W. H. Hsieh, L. H. Liu, Y. C. Lin, C. C. Chu, S. T. Wang, I. T. Kuo, L. K. Chau and C. Y. Yang, *Small*, 2014, **10**, 4700–4710.
168 Y. L. Xing, A. Wyss, N. Esser and P. S. Dittrich, *Analyst*, 2015, **140**, 7896–7901.
169 H. Liu, X. Qian, Z. J. Wu, R. Yang, S. Q. Sun and H. Ma, *J. Mater. Chem. B*, 2016, **4**, 482–488.
170 K. Zou, Z. G. Gao, Q. F. Deng, Y. Luo, L. J. Zou, Y. Lu, W. J. Zhao and B. C. Lin, *Electrophoresis*, 2016, **37**, 786–789.
171 G. Perozziello, P. Candeloro, F. Gentile, A. Nicastri, A. Perri, M. L. Coluccio, A. Adamo, F. Pardeo, R. Catalano, E. Parrotta, H. D. Espinosa, G. Cuda and E. Di Fabrizio, *RSC Adv.*, 2014, **4**, 55590–55598.
172 G. Perozziello, P. Candeloro, F. Gentile, M. L. Coluccio, M. Tallerico, A. De Grazia, A. Nicastri, A. M. Perri, E. Parrotta, F. Pardeo, R. Catalano, G. Cuda and E. Di Fabrizio, *Microelectron. Eng.*, 2015, **144**, 37–41.
173 A. Pallaoro, M. R. Hoonejani, G. B. Braun, C. D. Meinhart and M. Moskovits, *ACS Nano*, 2015, **9**, 4328–4336.
174 H. Torul, H. Ciftci, D. Cetin, Z. Suludere, I. H. Boyaci and U. Tamer, *Anal. Bioanal. Chem.*, 2015, **407**, 8243–8251.
175 M. R. Hoonejani, A. Pallaoro, G. B. Braun, M. Moskovits and C. D. Meinhart, *Nanoscale*, 2015, **7**, 16834–16840.
176 C. Novara, A. Lamberti, A. Chiado, A. Virga, P. Rivolo, F. Geobaldo and F. Giorgis, *RSC Adv.*, 2016, **6**, 21865–21870.
177 A. H. Nguyen, J. Lee, H. I. Choi, H. S. Kwak and S. J. Sim, *Biosens. Bioelectron.*, 2015, **70**, 358–365.
178 W. Xie, R. Grzeschik and S. Schlücker, *Angew. Chem., Int. Ed.*, 2016, **55**, 13729–13733.
179 T. W. Bocklitz, S. Guo, O. Ryabchykov, N. Vogler and J. Popp, *Anal. Chem.*, 2016, **88**, 133–151.
180 T. Hastie, R. Tibshirani and J. Friedman, *The Elements of Statistical Learning – Data Mining, Inference, and Prediction*, Springer, 2008.
181 R. Kohavi, presented in part at the Proceedings of the 14th international joint conference on Artificial intelligence - Volume 2, Montreal, Quebec, Canada, 1995.
182 T. Bocklitz, A. Walter, K. Hartmann, P. Rösch and J. Popp, *Anal. Chim. Acta*, 2011, **704**, 47–56.
183 A. März, T. Bocklitz and J. Popp, *Anal. Chem.*, 2011, **83**, 8337–8340.
184 S. Guo, T. Bocklitz and J. Popp, *Analyst*, 2016, **141**, 2396–2404.
185 S. Wold, M. Sjöström and L. Eriksson, *Chemom. Intell. Lab. Syst.*, 2001, **58**, 109–130.
186 C. Ruckebusch and L. Blanchet, *Anal. Chim. Acta*, 2013, **765**, 28–36.
187 J. E. L. Villa and R. J. Poppi, *Analyst*, 2016, **141**, 1966–1972.
188 M. B. Mamián-López and R. J. Poppi, *Anal. Bioanal. Chem.*, 2013, **405**, 7671–7677.
189 C. Beleites, U. Neugebauer, T. Bocklitz, C. Krafft and J. Popp, *Anal. Chim. Acta*, 2013, **760**, 25–33.
190 Z.-P. Chen, J. Morris and E. Martin, *Anal. Chem.*, 2006, **78**, 7674–7681.
191 K. H. Liland, A. Kohler and N. K. Afseth, *J. Raman Spectrosc.*, 2016, **47**, 643–650.
192 K. Booksh, J. M. Henshaw, L. W. Burgess and B. R. Kowalski, *J. Chemom.*, 1995, **9**, 263–282.

REFERENCES

[1] Petersen, I.; Hayward, A.C. "Antibacterial prescribing in primary care". *The Journal of antimicrobial chemotherapy*, 2007, **60 Suppl 1**, i43-47, DOI 10.1093/jac/dkm156.

[2] Shapiro, D.J.; Hicks, L.A.; Pavia, A.T.; Hersh, A.L. "Antibiotic prescribing for adults in ambulatory care in the USA, 2007-09". *The Journal of antimicrobial chemotherapy*, 2014, **69**(1), 234-240, DOI 10.1093/jac/dkt301.

[3] Zweigner, J.; Meyer, E.; Gastmeier, P.; Schwab, F. "Rate of antibiotic prescriptions in German outpatient care - are the guidelines followed or are they still exceeded?". *GMS hygiene and infection control*, 2018, **13**, DOI 10.3205/dgkh000310.

[4] WHO, WHO: *The top 10 causes of death* [online], [Zugriff am: 02.12].

[5] Gerritsen, J. "Series: Basic Sciences: Host defence mechanisms of the respiratory system". *Paediatric Respiratory Reviews*, 2000, **1**(2), 128-134, DOI 10.1053/prrv.2000.0041.

[6] Dropulic, L.K.; Lederman, H.M. "Overview of Infections in the Immunocompromised Host". *Microbiology spectrum*, 2016, **4**(4), DOI 10.1128/microbiolspec.DMIH2-0026-2016.

[7] Fishman, J.A. "Infections in immunocompromised hosts and organ transplant recipients: essentials". *Liver transplantation : official publication of the American Association for the Study of Liver Diseases and the International Liver Transplantation Society*, 2011, **17 Suppl 3**, S34-37, DOI 10.1002/lt.22378.

[8] Cortegiani, A.; Madotto, F.; Gregoretti, C.; Bellani, G.; Laffey, J.G.; Pham, T.; Van Haren, F.; Giarratano, A.; Antonelli, M.; Pesenti, A.; Grasselli, G.; Investigators, L.S.; Group, E.T. "Immunocompromised patients with acute respiratory distress syndrome: secondary analysis of the LUNG SAFE database". *Critical Care*, 2018, **22**(1), 157, DOI 10.1186/s13054-018-2079-9.

[9] Konduri, S.R.; Soubani, A.O. "Chapter 9 - Respiratory infections in immunosuppressed patients". In: Kon, K., Rai, M. eds. *The Microbiology of Respiratory System Infections.* Academic Press, 2016, vol. 1, S. 125-142, ISBN 24519006, DOI 10.1016/B978-0-12-804543-5.00009-9.

[10] Parameswaran, G.I.; Murphy, T.F. "Infections in Chronic Lung Diseases". *Infectious Disease Clinics of North America*, 2007, **21**(3), 673-695, DOI 10.1016/j.idc.2007.06.006.

[11] Busse, W.W.; Lemanske, R.F., Jr.; Gern, J.E. "Role of viral respiratory infections in asthma and asthma exacerbations". *Lancet (London, England)*, 2010, **376**(9743), 826-834, DOI 10.1016/S0140-6736(10)61380-3.

[12] Perng, D.W.; Chen, P.K. "The Relationship between Airway Inflammation and Exacerbation in Chronic Obstructive Pulmonary Disease". *Tuberculosis and respiratory diseases*, 2017, **80**(4), 325-335, DOI 10.4046/trd.2017.0085.

[13] Lyczak, J.B.; Cannon, C.L.; Pier, G.B. "Lung infections associated with cystic fibrosis". *Clinical microbiology reviews*, 2002, **15**(2), 194-222, DOI 10.1128/CMR.15.2.194-222.2002.

[14] Wardlaw, T.M.J., Emily White; Hodge, Matthew; World Health Organization; UNICEF. *Pneumonia: the forgotten killer of children*. Geneva: World Health Organization, 2006. ISBN 9789280640489 9280640488.

[15] Forum of International Respiratory Societies. The Global Impact of Respiratory Disease – Second Edition. Sheffield: 2017.

[16] Geffen, L. "Common upper respiratory tract problems in the elderly—A guide to clinical diagnosis and prudent prescription". *South African Family Practice*, 2006, **48**(5), 20-23, DOI 10.1080/20786204.2006.10873390.

[17] Belongia, E.A.; Kieke, B.A.; Donahue, J.G.; Greenlee, R.T.; Balish, A.; Foust, A.; Lindstrom, S.; Shay, D.K. "Effectiveness of inactivated influenza vaccines varied substantially with antigenic match from the 2004-2005 season to the 2006-2007 season". *The Journal of infectious diseases*, 2009, **199**(2), 159-167, DOI 10.1086/595861.

[18] Kissling, E.; Valenciano, M.; Buchholz, U.; Larrauri, A.; Cohen, J.M.; Nunes, B.; Rogalska, J.; Pitigoi, D.; Paradowska-Stankiewicz, I.; Reuss, A.; Jimenez-Jorge, S.; Daviaud, I.; Guiomar, R.; O'Donnell, J.; Necula, G.; Gluchowska, M.; Moren, A. "Influenza vaccine effectiveness estimates in Europe in a season with three influenza type/subtypes circulating: the I-MOVE multicentre case-control study, influenza season 2012/13". *Euro surveillance : bulletin Europeen sur les maladies transmissibles = European communicable disease bulletin*, 2014, **19**(6).

[19] Vu, T.; Farish, S.; Jenkins, M.; Kelly, H. "A meta-analysis of effectiveness of influenza vaccine in persons aged 65 years and over living in the community". *Vaccine*, 2002, **20**(13), 1831-1836, DOI 10.1016/S0264-410X(02)00041-5.
[20] Moberley, S.A.; Holden, J.; Tatham, D.P.; Andrews, R.M. "Vaccines for preventing pneumococcal infection in adults". *The Cochrane database of systematic reviews*, 2008, (1), Cd000422, DOI 10.1002/14651858.CD000422.pub2.
[21] Shah, A.; Panjabi, C. "Allergic Bronchopulmonary Aspergillosis: A Perplexing Clinical Entity". *Allergy, asthma & immunology research*, 2016, **8**(4), 282-297, DOI 10.4168/aair.2016.8.4.282.
[22] Haas, K.M.; Poe, J.C.; Steeber, D.A.; Tedder, T.F. "B-1a and B-1b cells exhibit distinct developmental requirements and have unique functional roles in innate and adaptive immunity to S. pneumoniae". *Immunity*, 2005, **23**(1), 7-18, DOI 10.1016/j.immuni.2005.04.011.
[23] Milczewska, J.; Wolkowicz, T.; Zacharczuk, K.; Kwiatkowska, M. "Cross-infections with Pseudomonas aeruginosa in patients with cystic fibrosis attending the Warsaw Centre". *Developmental period medicine*, 2015, **19**(1), 60-65.
[24] Hagaman, J.T.; Rouan, G.W.; Shipley, R.T.; Panos, R.J. "Admission chest radiograph lacks sensitivity in the diagnosis of community-acquired pneumonia". *The American journal of the medical sciences*, 2009, **337**(4), 236-240, DOI 10.1097/MAJ.0b013e31818ad805.
[25] Laursen, C.B.; Sloth, E.; Lambrechtsen, J.; Lassen, A.T.; Madsen, P.H.; Henriksen, D.P.; Davidsen, J.R.; Rasmussen, F. "Diagnostic performance of chest X-ray for the diagnosis of community acquired pneumonia in acute admitted patients with respiratory symptoms". *Scandinavian Journal of Trauma, Resuscitation and Emergency Medicine*, 2013, **21**(Suppl 2), A21-A21, DOI 10.1186/1757-7241-21-S2-A21.
[26] Hayden, G.E.; Wrenn, K.W. "Chest radiograph vs. computed tomography scan in the evaluation for pneumonia". *The Journal of emergency medicine*, 2009, **36**(3), 266-270, DOI 10.1016/j.jemermed.2007.11.042.
[27] Charles, P.G. "Early diagnosis of lower respiratory tract infections (point-of-care tests)". *Current Opinion in Pulmonary Medicine*, 2008, **14**(3), 176-182, DOI 10.1097/MCP.0b013e3282f7642f.
[28] Laupland, K.B.; Valiquette, L. "The changing culture of the microbiology laboratory". *The Canadian journal of infectious diseases & medical microbiology*, 2013, **24**(3), 125-128.
[29] Morshed, M.G.; Lee, M.-K.; Jorgensen, D.; Isaac-Renton, J.L. "Molecular methods used in clinical laboratory: prospects and pitfalls". *FEMS Immunology & Medical Microbiology*, 2007, **49**(2), 184-191, DOI 10.1111/j.1574-695X.2006.00191.x.
[30] Chisanga, M.; Muhamadali, H.; Ellis, D.I.; Goodacre, R. "Surface-Enhanced Raman Scattering (SERS) in Microbiology: Illumination and Enhancement of the Microbial World". *Applied Spectroscopy*, 2018, **72**(7), 987-1000, DOI 10.1177/0003702818764672.
[31] Cialla-May, D.; Zheng, X.S.; Weber, K.; Popp, J. "Recent progress in surface-enhanced Raman spectroscopy for biological and biomedical applications: from cells to clinics". *Chemical Society Reviews*, 2017, **46**(13), 3945-3961, DOI 10.1039/c7cs00172j.
[32] Pence, I.; Mahadevan-Jansen, A. "Clinical instrumentation and applications of Raman spectroscopy". *Chemical Society Reviews*, 2016, **45**(7), 1958-1979, DOI 10.1039/C5CS00581G.
[33] Santos, I.P.; Barroso, E.M.; Bakker Schut, T.C.; Caspers, P.J.; van Lanschot, C.G.F.; Choi, D.-H.; van der Kamp, M.F.; Smits, R.W.H.; van Doorn, R.; Verdijk, R.M.; Noordhoek Hegt, V.; von der Thüsen, J.H.; van Deurzen, C.H.M.; Koppert, L.B.; van Leenders, G.J.L.H.; Ewing-Graham, P.C.; van Doorn, H.C.; Dirven, C.M.F.; Busstra, M.B.; Hardillo, J.; Sewnaik, A.; ten Hove, I.; Mast, H.; Monserez, D.A.; Meeuwis, C.; Nijsten, T.; Wolvius, E.B.; Baatenburg de Jong, R.J.; Puppels, G.J.; Koljenović, S. "Raman spectroscopy for cancer detection and cancer surgery guidance: translation to the clinics". *Analyst*, 2017, **142**(17), 3025-3047, DOI 10.1039/C7AN00957G.
[34] Raman, C.V.; Krishnan, K.S. "A New Type of Secondary Radiation". *Nature*, 1928, **121**, 501, DOI 10.1038/121501c0.
[35] Long, D.A. "Vibrational Raman Scattering". In: *The Raman Effect.* 2002, DOI 10.1002/0470845767.ch5.
[36] Popp, J.; Kiefer, W. *Raman Scattering, Fundamentals*. 2006. DOI 10.1002/9780470027318.a6405.
[37] Puppels, G.J.; de Mul, F.F.; Otto, C.; Greve, J.; Robert-Nicoud, M.; Arndt-Jovin, D.J.; Jovin, T.M. "Studying single living cells and chromosomes by confocal Raman microspectroscopy". *Nature*, 1990, **347**(6290), 301-303, DOI 10.1038/347301a0.
[38] Brauchle, E.; Schenke-Layland, K. "Raman spectroscopy in biomedicine - non-invasive in vitro analysis of cells and extracellular matrix components in tissues". *Biotechnol. J.*, 2013, **8**(3), 288-297, DOI 10.1002/biot.201200163.

[39] Chan, J.; Fore, S.; Wachsman-Hogiu, S.; Huser, T. "Raman spectroscopy and microscopy of individual cells and cellular components". *Laser Photon. Rev.*, 2008, **2**(5), 325-349, DOI 10.1002/lpor.200810012.
[40] Das, R.S.; Agrawal, Y.K. "Raman spectroscopy: Recent advancements, techniques and applications". *Vib. Spectrosc.*, 2011, **57**(2), 163-176, DOI 10.1016/j.vibspec.2011.08.003.
[41] Ellis, D.I.; Cowcher, D.P.; Ashton, L.; O'Hagan, S.; Goodacre, R. "Illuminating disease and enlightening biomedicine: Raman spectroscopy as a diagnostic tool". *Analyst*, 2013, **138**(14), 3871-3884, DOI 10.1039/c3an00698k.
[42] Kim, H.; Kosuda, K.M.; Van Duyne, R.P.; Stair, P.C. "Resonance Raman and surface- and tip-enhanced Raman spectroscopy methods to study solid catalysts and heterogeneous catalytic reactions". *Chemical Society Reviews*, 2010, **39**(12), 4820-4844, DOI 10.1039/C0CS00044B.
[43] Cialla, D.; Marz, A.; Bohme, R.; Theil, F.; Weber, K.; Schmitt, M.; Popp, J. "Surface-enhanced Raman spectroscopy (SERS): progress and trends". *Anal Bioanal Chem*, 2012, **403**(1), 27-54, DOI 10.1007/s00216-011-5631-x.
[44] Schatz, G.C.; Van Duyne, R.P. "Electromagnetic Mechanism of Surface-Enhanced Spectroscopy". In: *Handbook of Vibrational Spectroscopy.* 2006, DOI 10.1002/0470027320.s0601.
[45] Schmitt, M., Mayerhöfer, T. , Popp, J. , Kleppe, I. and Weisshart, K. "Light–Matter Interaction". In: *Handbook of Biophotonics.* 2013, DOI 10.1002/9783527643981.bphot003.
[46] Asher, S.A. "UV Resonance Raman Spectroscopy for Analytical, Physical, and Biophysical Chemistry". *Analytical Chemistry*, 1993, **65**(4), 201A-210A, DOI 10.1021/ac00052a715.
[47] Fleischmann, M.; Hendra, P.J.; McQuillan, A.J. "Raman spectra of pyridine adsorbed at a silver electrode". *Chemical Physics Letters*, 1974, **26**(2), 163-166, DOI 10.1016/0009-2614(74)85388-1.
[48] Ahmed, A.; Gordon, R. "Single molecule directivity enhanced Raman scattering using nanoantennas". *Nano letters*, 2012, **12**(5), 2625-2630, DOI 10.1021/nl301029e.
[49] Le Ru, E.C.; Blackie, E.; Meyer, M.; Etchegoin, P.G. "Surface enhanced Raman scattering enhancement factors: a comprehensive study". *J. Phys. Chem. C*, 2007, **111**(37), 13794-13803, DOI 10.1021/jp0687908.
[50] Xu, H.; Aizpurua, J.; Kall, M.; Apell, P. "Electromagnetic contributions to single-molecule sensitivity in surface-enhanced raman scattering". *Physical review. E, Statistical physics, plasmas, fluids, and related interdisciplinary topics*, 2000, **62**(3 Pt B), 4318-4324.
[51] Doering, W.E.; Nie, S. "Single-Molecule and Single-Nanoparticle SERS: Examining the Roles of Surface Active Sites and Chemical Enhancement". *The Journal of Physical Chemistry B*, 2002, **106**(2), 311-317, DOI 10.1021/jp011730b.
[52] Kneipp, K. "Chemical Contribution to SERS Enhancement: An Experimental Study on a Series of Polymethine Dyes on Silver Nanoaggregates". *The Journal of Physical Chemistry C*, 2016, **120**(37), 21076-21081, DOI 10.1021/acs.jpcc.6b03785.
[53] Yu, X.; Cai, H.; Zhang, W.; Li, X.; Pan, N.; Luo, Y.; Wang, X.; Hou, J.G. "Tuning Chemical Enhancement of SERS by Controlling the Chemical Reduction of Graphene Oxide Nanosheets". *ACS Nano*, 2011, **5**(2), 952-958, DOI 10.1021/nn102291j.
[54] Mishra, S.; Singh, R.K.; Ojha, A.K. "Investigation on bonding interaction of benzonitrile with silver nano particles probed by surface enhanced Raman scattering and quantum chemical calculations". *Chemical Physics*, 2009, **355**(1), 14-20, DOI 10.1016/j.chemphys.2008.10.006.
[55] Moskovits, M.; Suh, J.S. "Surface selection rules for surface-enhanced Raman spectroscopy: calculations and application to the surface-enhanced Raman spectrum of phthalazine on silver". *The Journal of Physical Chemistry*, 1984, **88**(23), 5526-5530, DOI 10.1021/j150667a013.
[56] Fan, M.; Andrade, G.F.S.; Brolo, A.G. "A review on the fabrication of substrates for surface enhanced Raman spectroscopy and their applications in analytical chemistry". *Analytica Chimica Acta*, 2011, **693**(1), 7-25, DOI 10.1016/j.aca.2011.03.002.
[57] Jahn, M.; Patze, S.; Hidi, I.J.; Knipper, R.; Radu, A.I.; Muhlig, A.; Yuksel, S.; Peksa, V.; Weber, K.; Mayerhofer, T.; Cialla-May, D.; Popp, J. "Plasmonic nanostructures for surface enhanced spectroscopic methods". *Analyst*, 2016, **141**(3), 756-793, DOI 10.1039/c5an02057c.
[58] Jeon, T.Y.; Kim, D.J.; Park, S.G.; Kim, S.H.; Kim, D.H. "Nanostructured plasmonic substrates for use as SERS sensors". *Nano Converg.*, 2016, **3**, 20, DOI 10.1186/s40580-016-0078-6.
[59] Doern, G.V.; Vautour, R.; Gaudet, M.; Levy, B. "Clinical impact of rapid in vitro susceptibility testing and bacterial identification". *Journal of clinical microbiology*, 1994, **32**(7), 1757-1762.
[60] Hameed, S.; Xie, L.; Ying, Y. "Conventional and emerging detection techniques for pathogenic bacteria in food science: A review". *Trends in Food Science & Technology*, 2018, **81**, 61-73, DOI 10.1016/j.tifs.2018.05.020.

[61] Rajapaksha, P.; Elbourne, A.; Gangadoo, S.; Brown, R.; Cozzolino, D.; Chapman, J. "A review of methods for the detection of pathogenic microorganisms". *Analyst*, 2019, **144**(2), 396-411, DOI 10.1039/C8AN01488D.

[62] Váradi, L.; Luo, J.L.; Hibbs, D.E.; Perry, J.D.; Anderson, R.J.; Orenga, S.; Groundwater, P.W. "Methods for the detection and identification of pathogenic bacteria: past, present, and future". *Chemical Society Reviews*, 2017, **46**(16), 4818-4832, DOI 10.1039/C6CS00693K.

[63] Maurer, J.J. "Rapid Detection and Limitations of Molecular Techniques". *Annual Review of Food Science and Technology*, 2011, **2**(1), 259-279, DOI 10.1146/annurev.food.080708.100730.

[64] Verma, J.; Saxena, S.; Babu, S.G. "ELISA-Based Identification and Detection of Microbes". In: Arora, D.K., Das, S., Sukumar, M. eds. *Analyzing Microbes: Manual of Molecular Biology Techniques.* Berlin, Heidelberg: Springer Berlin Heidelberg, 2013, S. 169-186, ISBN 978-3-642-34410-7, DOI 10.1007/978-3-642-34410-7_13.

[65] Yang, S.; Rothman, R.E. "PCR-based diagnostics for infectious diseases: uses, limitations, and future applications in acute-care settings". *The Lancet Infectious Diseases*, 2004, **4**(6), 337-348, DOI 10.1016/S1473-3099(04)01044-8.

[66] Dalterio, R.A.; Nelson, W.H.; Britt, D.; Sperry, J.F. "An Ultraviolet (242 nm Excitation) Resonance Raman Study of Live Bacteria and Bacterial Components". *Applied Spectroscopy*, 1987, **41**(3), 417-422, DOI 10.1366/0003702874448931.

[67] Ashton, L.; Lau, K.; Winder, C.L.; Goodacre, R. "Raman spectroscopy: lighting up the future of microbial identification". *Future microbiology*, 2011, **6**(9), 991-997, DOI 10.2217/fmb.11.89.

[68] Harz, M.; Rösch, P.; Popp, J. "Vibrational spectroscopy—A powerful tool for the rapid identification of microbial cells at the single-cell level". *Cytometry Part A*, 2009, **75A**(2), 104-113, DOI 10.1002/cyto.a.20682.

[69] Jarvis, R.M.; Goodacre, R. "Characterisation and identification of bacteria using SERS". *Chem Soc Rev*, 2008, **37**(5), 931-936, DOI 10.1039/b705973f.

[70] Stöckel, S.; Kirchhoff, J.; Neugebauer, U.; Rösch, P.; Popp, J. "The application of Raman spectroscopy for the detection and identification of microorganisms". *Journal of Raman Spectroscopy*, 2016, **47**(1), 89-109, DOI 10.1002/jrs.4844.

[71] Reddy, R.K.; Bhargava, R. "Chemometric Methods for Biomedical Raman Spectroscopy and Imaging". In: Matousek, P., Morris, M.D. eds. *Emerging Raman Applications and Techniques in Biomedical and Pharmaceutical Fields.* Berlin, Heidelberg: Springer Berlin Heidelberg, 2010, S. 179-213, ISBN 978-3-642-02649-2, DOI 10.1007/978-3-642-02649-2_8.

[72] Hamasha, K.; Mohaidat, Q.I.; Putnam, R.A.; Woodman, R.C.; Palchaudhuri, S.; Rehse, S.J. "Sensitive and specific discrimination of pathogenic and nonpathogenic Escherichia coli using Raman spectroscopy-a comparison of two multivariate analysis techniques". *Biomedical optics express*, 2013, **4**(4), 481-489, DOI 10.1364/boe.4.000481.

[73] Rebrošová, K.; Šiler, M.; Samek, O.; Růžička, F.; Bernatová, S.; Holá, V.; Ježek, J.; Zemánek, P.; Sokolová, J.; Petráš, P. "Rapid identification of staphylococci by Raman spectroscopy". *Scientific Reports*, 2017, **7**(1), 14846, DOI 10.1038/s41598-017-13940-w.

[74] Espagnon, I.; Ostrovskii, D.; Mathey, R.; Dupoy, M.; Joly, P.L.; Novelli-Rousseau, A.; Pinston, F.; Gal, O.; Mallard, F.; Leroux, D.F. "Direct identification of clinically relevant bacterial and yeast microcolonies and macrocolonies on solid culture media by Raman spectroscopy". *Journal of biomedical optics*, 2014, **19**(2), 027004, DOI 10.1117/1.Jbo.19.2.027004.

[75] Mathey, R.; Dupoy, M.; Espagnon, I.; Leroux, D.; Mallard, F.; Novelli-Rousseau, A. "Viability of 3h grown bacterial micro-colonies after direct Raman identification". *J Microbiol Methods*, 2015, **109**, 67-73, DOI 10.1016/j.mimet.2014.12.002.

[76] Kloß, S.; Kampe, B.; Sachse, S.; Rösch, P.; Straube, E.; Pfister, W.; Kiehntopf, M.; Popp, J. "Culture Independent Raman Spectroscopic Identification of Urinary Tract Infection Pathogens: A Proof of Principle Study". *Analytical Chemistry*, 2013, **85**(20), 9610-9616, DOI 10.1021/ac401806f.

[77] Kloß, S.; Lorenz, B.; Dees, S.; Labugger, I.; Rösch, P.; Popp, J. "Destruction-free procedure for the isolation of bacteria from sputum samples for Raman spectroscopic analysis". *Analytical and Bioanalytical Chemistry*, 2015, **407**(27), 8333-8341, DOI 10.1007/s00216-015-8743-x.

[78] Schroder, U.C.; Ramoji, A.; Glaser, U.; Sachse, S.; Leiterer, C.; Csaki, A.; Hubner, U.; Fritzsche, W.; Pfister, W.; Bauer, M.; Popp, J.; Neugebauer, U. "Combined dielectrophoresis-Raman setup for the classification of pathogens recovered from the urinary tract". *Anal Chem*, 2013, **85**(22), 10717-10724, DOI 10.1021/ac4021616.

[79] Pahlow, S.; Meisel, S.; Cialla-May, D.; Weber, K.; Rösch, P.; Popp, J. "Isolation and identification of bacteria by means of Raman spectroscopy". *Advanced drug delivery reviews*, 2015, **89**, 105-120, DOI 10.1016/j.addr.2015.04.006.

[80] Ghosal, S.; Macher, J.M.; Ahmed, K. "Raman Microspectroscopy-Based Identification of Individual Fungal Spores as Potential Indicators of Indoor Contamination and Moisture-Related Building Damage". *Environmental Science & Technology*, 2012, **46**(11), 6088-6095, DOI 10.1021/es203782j.

[81] Verwer, P.E.B.; van Leeuwen, W.B.; Girard, V.; Monnin, V.; van Belkum, A.; Staab, J.F.; Verbrugh, H.A.; Bakker-Woudenberg, I.A.J.M.; van de Sande, W.W.J. "Discrimination of Aspergillus lentulus from Aspergillus fumigatus by Raman spectroscopy and MALDI-TOF MS". *European Journal of Clinical Microbiology & Infectious Diseases*, 2014, **33**(2), 245-251, DOI 10.1007/s10096-013-1951-4.

[82] Silge, A.; Heinke, R.; Bocklitz, T.; Wiegand, C.; Hipler, U.C.; Rösch, P.; Popp, J. "The application of UV resonance Raman spectroscopy for the differentiation of clinically relevant Candida species". *Anal Bioanal Chem*, 2018, **410**(23), 5839-5847, DOI 10.1007/s00216-018-1196-2.

[83] Jarvis, R.M.; Goodacre, R. "Ultra-violet resonance Raman spectroscopy for the rapid discrimination of urinary tract infection bacteria". *FEMS Microbiology Letters*, 2004, **232**(2), 127-132, DOI 10.1016/S0378-1097(04)00040-0.

[84] Lopez-Diez, E.C.; Goodacre, R. "Characterization of microorganisms using UV resonance Raman spectroscopy and chemometrics". *Anal Chem*, 2004, **76**(3), 585-591, DOI 10.1021/ac035110d.

[85] Liu, Y.; Zhou, H.B.; Hu, Z.W.; Yu, G.X.; Yang, D.T.; Zhao, J.S. "Label and label-free based surface-enhanced Raman scattering for pathogen bacteria detection: A review". *Biosens. Bioelectron.*, 2017, **94**, 131-140, DOI 10.1016/j.bios.2017.02.032.

[86] Wang, Y.; Yan, B.; Chen, L. "SERS Tags: Novel Optical Nanoprobes for Bioanalysis". *Chemical Reviews*, 2013, **113**(3), 1391-1428, DOI 10.1021/cr300120g.

[87] Lin, Y.; Hamme Ii, A.T. "Targeted highly sensitive detection/eradication of multi-drug resistant Salmonella DT104 through gold nanoparticle-SWCNT bioconjugated nanohybrids". *Analyst*, 2014, **139**(15), 3702-3705, DOI 10.1039/c4an00744a.

[88] Zhang, H.; Ma, X.; Liu, Y.; Duan, N.; Wu, S.; Wang, Z.; Xu, B. "Gold nanoparticles enhanced SERS aptasensor for the simultaneous detection of Salmonella typhimurium and Staphylococcus aureus". *Biosens Bioelectron*, 2015, **74**, 872-877, DOI 10.1016/j.bios.2015.07.033.

[89] Avci, E.; Kaya, N.S.; Ucankus, G.; Culha, M. "Discrimination of urinary tract infection pathogens by means of their growth profiles using surface enhanced Raman scattering". *Analytical and Bioanalytical Chemistry*, 2015, **407**(27), 8233-8241, DOI 10.1007/s00216-015-8950-5.

[90] Culha, M.; Kahraman, M.; Çam, D.; Sayın, I.; Keseroğlu, K. "Rapid identification of bacteria and yeast using surface-enhanced Raman scattering". *Surface and Interface Analysis*, 2010, **42**(6-7), 462-465, DOI 10.1002/sia.3256.

[91] Kahraman, M.; Keseroğlu, K.; Çulha, M. "On Sample Preparation for Surface-Enhanced Raman Scattering (SERS) of Bacteria and the Source of Spectral Features of the Spectra". *Applied Spectroscopy*, 2011, **65**(5), 500-506, DOI 10.1366/10-06184.

[92] Yang, D.; Zhou, H.; Haisch, C.; Niessner, R.; Ying, Y. "Reproducible E. coli detection based on label-free SERS and mapping". *Talanta*, 2016, **146**, 457-463, DOI 10.1016/j.talanta.2015.09.006.

[93] Sengupta, A.; Mujacic, M.; Davis, E.J. "Detection of bacteria by surface-enhanced Raman spectroscopy". *Analytical and Bioanalytical Chemistry*, 2006, **386**(5), 1379-1386, DOI 10.1007/s00216-006-0711-z.

[94] Cam, D.; Keseroglu, K.; Kahraman, M.; Sahin, F.; Culha, M. "Multiplex identification of bacteria in bacterial mixtures with surface-enhanced Raman scattering". *Journal of Raman Spectroscopy*, 2010, **41**(5), 484-489, DOI 10.1002/jrs.2475.

[95] Efrima, S.; Bronk, B.V. "Silver Colloids Impregnating or Coating Bacteria". *The Journal of Physical Chemistry B*, 1998, **102**(31), 5947-5950, DOI 10.1021/jp9813903.

[96] Alula, M.T.; Krishnan, S.; Hendricks, N.R.; Karamchand, L.; Blackburn, J.M. "Identification and quantitation of pathogenic bacteria via in-situ formation of silver nanoparticles on cell walls, and their detection via SERS". *Microchimica Acta*, 2017, **184**(1), 219-227, DOI 10.1007/s00604-016-2013-2.

[97] Chen, L.; Mungroo, N.; Daikuara, L.; Neethirajan, S. "Label-free NIR-SERS discrimination and detection of foodborne bacteria by in situ synthesis of Ag colloids". *Journal of Nanobiotechnology*, 2015, **13**(1), 45, DOI 10.1186/s12951-015-0106-4.

[98] Zhou, H.; Yang, D.; Ivleva, N.P.; Mircescu, N.E.; Niessner, R.; Haisch, C. "SERS detection of bacteria in water by in situ coating with Ag nanoparticles". *Anal Chem*, 2014, **86**(3), 1525-1533, DOI 10.1021/ac402935p.

[99] Zhou, H.; Yang, D.; Mircescu, N.E.; Ivleva, N.P.; Schwarzmeier, K.; Wieser, A.; Schubert, S.; Niessner, R.; Haisch, C. "Surface-enhanced Raman scattering detection of bacteria on microarrays at single cell levels using silver nanoparticles". *Microchimica Acta*, 2015, **182**(13), 2259-2266, DOI 10.1007/s00604-015-1570-0.
[100] Dina, N.E.; Zhou, H.; Colniţă, A.; Leopold, N.; Szoke-Nagy, T.; Coman, C.; Haisch, C. "Rapid single-cell detection and identification of pathogens by using surface-enhanced Raman spectroscopy". *Analyst*, 2017, **142**(10), 1782-1789, DOI 10.1039/C7AN00106A.
[101] Dina, N.E.; Gherman, A.M.R.; Chiş, V.; Sârbu, C.; Wieser, A.; Bauer, D.; Haisch, C. "Characterization of Clinically Relevant Fungi via SERS Fingerprinting Assisted by Novel Chemometric Models". *Analytical Chemistry*, 2018, **90**(4), 2484-2492, DOI 10.1021/acs.analchem.7b03124.
[102] Witkowska, E.; Jagielski, T.; Kamińska, A. "Genus- and species-level identification of dermatophyte fungi by surface-enhanced Raman spectroscopy". *Spectrochimica Acta Part A: Molecular and Biomolecular Spectroscopy*, 2018, **192**, 285-290, DOI 10.1016/j.saa.2017.11.008.
[103] Xu, J.; Turner, J.W.; Idso, M.; Biryukov, S.V.; Rognstad, L.; Gong, H.; Trainer, V.L.; Wells, M.L.; Strom, M.S.; Yu, Q. "In situ strain-level detection and identification of Vibrio parahaemolyticus using surface-enhanced Raman spectroscopy". *Anal Chem*, 2013, **85**(5), 2630-2637, DOI 10.1021/ac3021888.
[104] Henderson, K.C.; Benitez, A.J.; Ratliff, A.E.; Crabb, D.M.; Sheppard, E.S.; Winchell, J.M.; Dluhy, R.A.; Waites, K.B.; Atkinson, T.P.; Krause, D.C. "Specificity and Strain-Typing Capabilities of Nanorod Array-Surface Enhanced Raman Spectroscopy for Mycoplasma pneumoniae Detection". *PloS one*, 2015, **10**(6), e0131831-e0131831, DOI 10.1371/journal.pone.0131831.
[105] Premasiri, W.R.; Lee, J.C.; Sauer-Budge, A.; Théberge, R.; Costello, C.E.; Ziegler, L.D. "The biochemical origins of the surface-enhanced Raman spectra of bacteria: a metabolomics profiling by SERS". *Analytical and bioanalytical chemistry*, 2016, **408**(17), 4631-4647, DOI 10.1007/s00216-016-9540-x.
[106] Muhlig, A.; Bocklitz, T.; Labugger, I.; Dees, S.; Henk, S.; Richter, E.; Andres, S.; Merker, M.; Stockel, S.; Weber, K.; Cialla-May, D.; Popp, J. "LOC-SERS: A Promising Closed System for the Identification of Mycobacteria". *Anal Chem*, 2016, **88**(16), 7998-8004, DOI 10.1021/acs.analchem.6b01152.
[107] Muhamadali, H.; Subaihi, A.; Mohammadtaheri, M.; Xu, Y.; Ellis, D.I.; Ramanathan, R.; Bansal, V.; Goodacre, R. "Rapid, accurate, and comparative differentiation of clinically and industrially relevant microorganisms via multiple vibrational spectroscopic fingerprinting". *Analyst*, 2016, **141**(17), 5127-5136, DOI 10.1039/C6AN00883F.
[108] Wilson J, J.G. Principles and practice of screening for disease. Organization, W.H. *Public Health paper No 34. edn.* Geneva: World Health Organization, 1986.
[109] Maxim, L.D.; Niebo, R.; Utell, M.J. "Screening tests: a review with examples". *Inhalation toxicology*, 2014, **26**(13), 811-828, DOI 10.3109/08958378.2014.955932.
[110] Burton, C.; Ma, Y. "Current Trends in Cancer Biomarker Discovery Using Urinary Metabolomics: Achievements and New Challenges". *Current medicinal chemistry*, 2017, DOI 10.2174/0929867324666170914102236.
[111] Pacchiarotta, T.; Deelder, A.M.; Mayboroda, O.A. "Metabolomic investigations of human infections". *Bioanalysis*, 2012, **4**(8), 919-925, DOI 10.4155/bio.12.61.
[112] Baker, M.J.; Hussain, S.R.; Lovergne, L.; Untereiner, V.; Hughes, C.; Lukaszewski, R.A.; Thiéfin, G.; Sockalingum, G.D. "Developing and understanding biofluid vibrational spectroscopy: a critical review". *Chemical Society Reviews*, 2016, **45**(7), 1803-1818, DOI 10.1039/C5CS00585J.
[113] Mitchell, A.L.; Gajjar, K.B.; Theophilou, G.; Martin, F.L.; Martin-Hirsch, P.L. "Vibrational spectroscopy of biofluids for disease screening or diagnosis: translation from the laboratory to a clinical setting". *Journal of biophotonics*, 2014, **7**(3-4), 153-165, DOI 10.1002/jbio.201400018.
[114] Guo, S.; Bocklitz, T.; Neugebauer, U.; Popp, J. "Common mistakes in cross-validating classification models". *Analytical Methods*, 2017, **9**(30), 4410-4417, DOI 10.1039/C7AY01363A.
[115] Gonzalez-Solis, J.L.; Martinez-Espinosa, J.C.; Salgado-Roman, J.M.; Palomares-Anda, P. "Monitoring of chemotherapy leukemia treatment using Raman spectroscopy and principal component analysis". *Lasers in medical science*, 2014, **29**(3), 1241-1249, DOI 10.1007/s10103-013-1515-y.
[116] Pichardo-Molina, J.L.; Frausto-Reyes, C.; Barbosa-Garcia, O.; Huerta-Franco, R.; Gonzalez-Trujillo, J.L.; Ramirez-Alvarado, C.A.; Gutierrez-Juarez, G.; Medina-Gutierrez, C. "Raman spectroscopy and multivariate analysis of serum samples from breast cancer patients". *Lasers in medical science*, 2007, **22**(4), 229-236, DOI 10.1007/s10103-006-0432-8.

[117] Ullah, I.; Ahmad, I.; Nisar, H.; Khan, S.; Ullah, R.; Rashid, R.; Mahmood, H. "Computer assisted optical screening of human ovarian cancer using Raman spectroscopy". *Photodiagnosis and photodynamic therapy*, 2016, **15**, 94-99, DOI 10.1016/j.pdpdt.2016.05.011.
[118] Khan, S.; Ullah, R.; Javaid, S.; Shahzad, S.; Ali, H.; Bilal, M.; Saleem, M.; Ahmed, M. "Raman Spectroscopy Combined with Principal Component Analysis for Screening Nasopharyngeal Cancer in Human Blood Sera". *Appl Spectrosc*, 2017, **71**(11), 2497-2503, DOI 10.1177/0003702817723928.
[119] Khan, S.; Ullah, R.; Khan, A.; Ashraf, R.; Ali, H.; Bilal, M.; Saleem, M. "Analysis of hepatitis B virus infection in blood sera using Raman spectroscopy and machine learning". *Photodiagnosis and photodynamic therapy*, 2018, **23**, 89-93, DOI 10.1016/j.pdpdt.2018.05.010.
[120] Sohail, A.; Khan, S.; Ullah, R.; Qureshi, S.A.; Bilal, M.; Khan, A. "Analysis of hepatitis C infection using Raman spectroscopy and proximity based classification in the transformed domain". *Biomedical optics express*, 2018, **9**(5), 2041-2055, DOI 10.1364/BOE.9.002041.
[121] Khan, S.; Ullah, R.; Khan, A.; Sohail, A.; Wahab, N.; Bilal, M.; Ahmed, M. "Random Forest-Based Evaluation of Raman Spectroscopy for Dengue Fever Analysis". *Appl Spectrosc*, 2017, **71**(9), 2111-2117, DOI 10.1177/0003702817695571.
[122] Neugebauer, U.; Trenkmann, S.; Bocklitz, T.; Schmerler, D.; Kiehntopf, M.; Popp, J. "Fast differentiation of SIRS and sepsis from blood plasma of ICU patients using Raman spectroscopy". *Journal of biophotonics*, 2014, **7**(3-4), 232-240, DOI 10.1002/jbio.201400010.
[123] Harris, A.T.; Lungari, A.; Needham, C.J.; Smith, S.L.; Lones, M.A.; Fisher, S.E.; Yang, X.B.; Cooper, N.; Kirkham, J.; Smith, D.A.; Martin-Hirsch, D.P.; High, A.S. "Potential for Raman spectroscopy to provide cancer screening using a peripheral blood sample". *Head & neck oncology*, 2009, **1**, 34, DOI 10.1186/1758-3284-1-34.
[124] Ryzhikova, E.; Kazakov, O.; Halamkova, L.; Celmins, D.; Malone, P.; Molho, E.; Zimmerman, E.A.; Lednev, I.K. "Raman spectroscopy of blood serum for Alzheimer's disease diagnostics: specificity relative to other types of dementia". *Journal of biophotonics*, 2015, **8**(7), 584-596, DOI 10.1002/jbio.201400060.
[125] Wang, H.; Zhang, S.; Wan, L.; Sun, H.; Tan, J.; Su, Q. "Screening and staging for non-small cell lung cancer by serum laser Raman spectroscopy". *Spectrochimica acta. Part A, Molecular and biomolecular spectroscopy*, 2018, **201**, 34-38, DOI 10.1016/j.saa.2018.04.002.
[126] Sahu, A.; Dalal, K.; Naglot, S.; Aggarwal, P.; Murali Krishna, C. "Serum based diagnosis of asthma using Raman spectroscopy: an early phase pilot study". *PloS one*, 2013, **8**(11), e78921-e78921, DOI 10.1371/journal.pone.0078921.
[127] Bonifacio, A.; Cervo, S.; Sergo, V. "Label-free surface-enhanced Raman spectroscopy of biofluids: fundamental aspects and diagnostic applications". *Anal Bioanal Chem*, 2015, **407**(27), 8265-8277, DOI 10.1007/s00216-015-8697-z.
[128] Zhang, Y.Y.; Mi, X.; Tan, X.Y.; Xiang, R. "Recent Progress on Liquid Biopsy Analysis using Surface-Enhanced Raman Spectroscopy". *Theranostics*, 2019, **9**(2), 491-525, DOI 10.7150/thno.29875.
[129] Shao, L.; Zhang, A.; Rong, Z.; Wang, C.; Jia, X.; Zhang, K.; Xiao, R.; Wang, S. "Fast and non-invasive serum detection technology based on surface-enhanced Raman spectroscopy and multivariate statistical analysis for liver disease". *Nanomedicine: Nanotechnology, Biology and Medicine*, 2018, **14**(2), 451-459, DOI 10.1016/j.nano.2017.11.022.
[130] Feng, S.; Lin, D.; Lin, J.; Li, B.; Huang, Z.; Chen, G.; Zhang, W.; Wang, L.; Pan, J.; Chen, R.; Zeng, H. "Blood plasma surface-enhanced Raman spectroscopy for non-invasive optical detection of cervical cancer". *Analyst*, 2013, **138**(14), 3967-3974, DOI 10.1039/C3AN36890D.
[131] Lin, D.; Pan, J.; Huang, H.; Chen, G.; Qiu, S.; Shi, H.; Chen, W.; Yu, Y.; Feng, S.; Chen, R. "Label-free blood plasma test based on surface-enhanced Raman scattering for tumor stages detection in nasopharyngeal cancer". *Scientific Reports*, 2014, **4**, 4751, DOI 10.1038/srep04751.
[132] Yu, Y.; Lin, Y.; Xu, C.; Lin, K.; Ye, Q.; Wang, X.; Xie, S.; Chen, R.; Lin, J. "Label-free detection of nasopharyngeal and liver cancer using surface-enhanced Raman spectroscopy and partial lease squares combined with support vector machine". *Biomedical optics express*, 2018, **9**(12), 6053-6066, DOI 10.1364/BOE.9.006053.
[133] Guo, J.; Rong, Z.; Li, Y.; Wang, S.Q.; Zhang, W.X.; Xiao, R. "Diagnosis of chronic kidney diseases based on surface-enhanced Raman spectroscopy and multivariate analysis". *Laser Physics*, 2018, **28**(7), 7, DOI 10.1088/1555-6611/aabec5.
[134] Lu, Y.; Lin, Y.; Zheng, Z.; Tang, X.; Lin, J.; Liu, X.; Liu, M.; Chen, G.; Qiu, S.; Zhou, T.; Lin, Y.; Feng, S. "Label free hepatitis B detection based on serum derivative surface enhanced Raman

spectroscopy combined with multivariate analysis". *Biomedical optics express*, 2018, **9**(10), 4755-4766, DOI 10.1364/BOE.9.004755.
[135] Han, H.W.; Yan, X.L.; Dong, R.X.; Ban, G.; Li, K. "Analysis of serum from type II diabetes mellitus and diabetic complication using surface-enhanced Raman spectra (SERS)". *Applied Physics B*, 2009, **94**(4), 667-672, DOI 10.1007/s00340-008-3299-5.
[136] Bonifacio, A.; Dalla Marta, S.; Spizzo, R.; Cervo, S.; Steffan, A.; Colombatti, A.; Sergo, V. "Surface-enhanced Raman spectroscopy of blood plasma and serum using Ag and Au nanoparticles: a systematic study". *Anal Bioanal Chem*, 2014, **406**(9-10), 2355-2365, DOI 10.1007/s00216-014-7622-1.
[137] Paraskevaidi, M.; Ashton, K.M.; Stringfellow, H.F.; Wood, N.J.; Keating, P.J.; Rowbottom, A.W.; Martin-Hirsch, P.L.; Martin, F.L. "Raman spectroscopic techniques to detect ovarian cancer biomarkers in blood plasma". *Talanta*, 2018, **189**, 281-288, DOI 10.1016/j.talanta.2018.06.084.
[138] Bispo, J.A.; de Sousa Vieira, E.E.; Silveira, L., Jr.; Fernandes, A.B. "Correlating the amount of urea, creatinine, and glucose in urine from patients with diabetes mellitus and hypertension with the risk of developing renal lesions by means of Raman spectroscopy and principal component analysis". *Journal of biomedical optics*, 2013, **18**(8), 87004, DOI 10.1117/1.Jbo.18.8.087004.
[139] Elumalai, B.; Prakasarao, A.; Ganesan, B.; Dornadula, K.; Ganesan, S. "Raman spectroscopic characterization of urine of normal and oral cancer subjects". *Journal of Raman Spectroscopy*, 2014, **46**(1), 84-93, DOI 10.1002/jrs.4601.
[140] Phan, H.T.; Haes, A.J. "Impacts of pH and Intermolecular Interactions on Surface-Enhanced Raman Scattering Chemical Enhancements". *The Journal of Physical Chemistry C*, 2018, **122**(26), 14846-14856, DOI 10.1021/acs.jpcc.8b04019.
[141] Del Mistro, G.; Cervo, S.; Mansutti, E.; Spizzo, R.; Colombatti, A.; Belmonte, P.; Zucconelli, R.; Steffan, A.; Sergo, V.; Bonifacio, A. "Surface-enhanced Raman spectroscopy of urine for prostate cancer detection: a preliminary study". *Analytical and Bioanalytical Chemistry*, 2015, **407**(12), 3271-3275, DOI 10.1007/s00216-015-8610-9.
[142] Huang, S.; Wang, L.; Chen, W.; Feng, S.; Lin, J.; Huang, Z.; Chen, G.; Li, B.; Chen, R. "Potential of non-invasive esophagus cancer detection based on urine surface-enhanced Raman spectroscopy". *Laser Physics Letters*, 2014, **11**(11), 115604, DOI 10.1088/1612-2011/11/11/115604.
[143] Zou, Y.; Huang, M.Z.; Wang, K.H.; Song, B.; Wang, Y.; Chen, J.; Liu, X.; Li, X.; Lin, L.L.; Huang, G.Z. "Urine surface-enhanced Raman spectroscopy for non-invasive diabetic detection based on a portable Raman spectrometer". *Laser Physics Letters*, 2016, **13**(6), 5, DOI 10.1088/1612-2011/13/6/065604.
[144] Yang, H.; Zhao, C.; Li, R.; Shen, C.; Cai, X.; Sun, L.; Luo, C.; Yin, Y. "Noninvasive and prospective diagnosis of coronary heart disease with urine using surface-enhanced Raman spectroscopy". *Analyst*, 2018, **143**(10), 2235-2242, DOI 10.1039/C7AN02022H.
[145] Gonchukov, S.; Sukhinina, A.; Bakhmutov, D.; Biryukova, T.; Tsvetkov, M.; Bagratashvily, V. "Periodontitis diagnostics using resonance Raman spectroscopy on saliva". *Laser Physics Letters*, 2013, **10**(7), 075610, DOI 10.1088/1612-2011/10/7/075610.
[146] Li, X.; Yang, T.; Lin, J. "Spectral analysis of human saliva for detection of lung cancer using surface-enhanced Raman spectroscopy". *Journal of biomedical optics*, 2012, **17**(3), 037003, DOI 10.1117/1.Jbo.17.3.037003.
[147] Qian, K.; Wang, Y.; Hua, L.; Chen, A.Y.; Zhang, Y. "New method of lung cancer detection by saliva test using surface-enhanced Raman spectroscopy". *Thorac. Cancer*, 2018, **9**(11), 1556-1561, DOI 10.1111/1759-7714.12837.
[148] Connolly, J.M.; Davies, K.; Kazakeviciute, A.; Wheatley, A.M.; Dockery, P.; Keogh, I.; Olivo, M. "Non-invasive and label-free detection of oral squamous cell carcinoma using saliva surface-enhanced Raman spectroscopy and multivariate analysis". *Nanomedicine : nanotechnology, biology, and medicine*, 2016, **12**(6), 1593-1601, DOI 10.1016/j.nano.2016.02.021.
[149] Rekha, P.; Aruna, P.; Brindha, E.; Koteeswaran, D.; Baludavid, M.; Ganesan, S. "Near-infrared Raman spectroscopic characterization of salivary metabolites in the discrimination of normal from oral premalignant and malignant conditions". *Journal of Raman Spectroscopy*, 2016, **47**(7), 763-772, DOI 10.1002/jrs.4897.
[150] Nicholas D. Magee, R.J.B., Robert Gray, Margaret Imrie, Madeleine Ennis, John McGarvey, and Joseph S. Elborn. "Raman Spectroscopy Analysis Of Induced Sputum In Lung Cancer". In: *B62. LUNG CANCER BIOMARKERS AND THERAPEUTIC RESPONSE.* 2010, S. A3492-A3492, DOI 10.1164/ajrccm-conference.2010.181.1_MeetingAbstracts.A3492.

[151] Rusciano, G.; Capriglione, P.; Pesce, G.; Abete, P.; Carnovale, V.; Sasso, A. "Raman spectroscopy as a new tool for early detection of bacteria in patients with cystic fibrosis". *Laser Physics Letters*, 2013, **10**(7), 075603, DOI 10.1088/1612-2011/10/7/075603.
[152] Strimbu, K.; Tavel, J.A. "What are biomarkers?". *Current opinion in HIV and AIDS*, 2010, **5**(6), 463-466, DOI 10.1097/COH.0b013e32833ed177.
[153] Arya, S.K.; Estrela, P. "Recent Advances in Enhancement Strategies for Electrochemical ELISA-Based Immunoassays for Cancer Biomarker Detection". *Sensors (Basel, Switzerland)*, 2018, **18**(7), DOI 10.3390/s18072010.
[154] de la Rica, R.; Stevens, M.M. "Plasmonic ELISA for the ultrasensitive detection of disease biomarkers with the naked eye". *Nature nanotechnology*, 2012, **7**(12), 821-824, DOI 10.1038/nnano.2012.186.
[155] Nimse, S.B.; Sonawane, M.D.; Song, K.S.; Kim, T. "Biomarker detection technologies and future directions". *Analyst*, 2016, **141**(3), 740-755, DOI 10.1039/c5an01790d.
[156] Tagit, O.; Hildebrandt, N. "Fluorescence Sensing of Circulating Diagnostic Biomarkers Using Molecular Probes and Nanoparticles". *ACS Sensors*, 2017, **2**(1), 31-45, DOI 10.1021/acssensors.6b00625.
[157] Shan, B.; Pu, Y.; Chen, Y.; Liao, M.; Li, M. "Novel SERS labels: Rational design, functional integration and biomedical applications". *Coordination Chemistry Reviews*, 2018, **371**, 11-37, DOI 10.1016/j.ccr.2018.05.007.
[158] Smolsky, J.; Kaur, S.; Hayashi, C.; Batra, S.K.; Krasnoslobodtsev, A.V. "Surface-Enhanced Raman Scattering-Based Immunoassay Technologies for Detection of Disease Biomarkers". *Biosensors*, 2017, **7**(1), DOI 10.3390/bios7010007.
[159] Blasi, F.; Stolz, D.; Piffer, F. "Biomarkers in lower respiratory tract infections". *Pulmonary pharmacology & therapeutics*, 2010, **23**(6), 501-507, DOI 10.1016/j.pupt.2010.04.007.
[160] Oved, K.; Cohen, A.; Boico, O.; Navon, R.; Friedman, T.; Etshtein, L.; Kriger, O.; Bamberger, E.; Fonar, Y.; Yacobov, R.; Wolchinsky, R.; Denkberg, G.; Dotan, Y.; Hochberg, A.; Reiter, Y.; Grupper, M.; Srugo, I.; Feigin, P.; Gorfine, M.; Chistyakov, I.; Dagan, R.; Klein, A.; Potasman, I.; Eden, E. "A novel host-proteome signature for distinguishing between acute bacterial and viral infections". *PloS one*, 2015, **10**(3), e0120012, DOI 10.1371/journal.pone.0120012.
[161] Pupelis, G.; Drozdova, N.; Mukans, M.; Malbrain, M.L. "Serum procalcitonin is a sensitive marker for septic shock and mortality in secondary peritonitis". *Anaesthesiology intensive therapy*, 2014, **46**(4), 262-273, DOI 10.5603/ait.2014.0043.
[162] Haran, J.P.; Beaudoin, F.L.; Suner, S.; Lu, S. "C-reactive protein as predictor of bacterial infection among patients with an influenza-like illness". *The American journal of emergency medicine*, 2013, **31**(1), 137-144, DOI 10.1016/j.ajem.2012.06.026.
[163] Mehanic, S.; Baljic, R. "The importance of serum procalcitonin in diagnosis and treatment of serious bacterial infections and sepsis". *Materia socio-medica*, 2013, **25**(4), 277-281, DOI 10.5455/msm.2013.25.277-281.
[164] Liu, B.; Ni, H.; Zhang, D.; Wang, D.; Fu, D.; Chen, H.; Gu, Z.; Zhao, X. "Ultrasensitive Detection of Protein with Wide Linear Dynamic Range Based on Core–Shell SERS Nanotags and Photonic Crystal Beads". *ACS Sensors*, 2017, **2**(7), 1035-1043, DOI 10.1021/acssensors.7b00310.
[165] Nguyen, A.H.; Shin, Y.; Sim, S.J. "Development of SERS substrate using phage-based magnetic template for triplex assay in sepsis diagnosis". *Biosensors and Bioelectronics*, 2016, **85**, 522-528, DOI 10.1016/j.bios.2016.05.043.
[166] Kim, H.; Kim, E.; Choi, E.; Baek, C.S.; Song, B.; Cho, C.H.; Jeong, S.W. "Label-free C-reactive protein SERS detection with silver nanoparticle aggregates". *RSC Adv.*, 2015, **5**(44), 34720-34729, DOI 10.1039/c5ra00040h.
[167] van de Veerdonk, F.L.; Wever, P.C.; Hermans, M.H.; Fijnheer, R.; Joosten, L.A.; van der Meer, J.W.; Netea, M.G.; Schneeberger, P.M. "IL-18 serum concentration is markedly elevated in acute EBV infection and can serve as a marker for disease severity". *The Journal of infectious diseases*, 2012, **206**(2), 197-201, DOI 10.1093/infdis/jis335.
[168] Kamińska, A.; Winkler, K.; Kowalska, A.; Witkowska, E.; Szymborski, T.; Janeczek, A.; Waluk, J. "SERS-based Immunoassay in a Microfluidic System for the Multiplexed Recognition of Interleukins from Blood Plasma: Towards Picogram Detection". *Scientific Reports*, 2017, **7**(1), 10656, DOI 10.1038/s41598-017-11152-w.
[169] *List of Qualified Biomarkers* [online], [Zugriff am: 11.12].
[170] Yao, Y.; Ji, J.; Zhang, H.; Zhang, K.; Liu, B.; Yang, P. "Three-Dimensional Plasmonic Trap Array for Ultrasensitive Surface-Enhanced Raman Scattering Analysis of Single Cells". *Analytical Chemistry*, 2018, **90**(17), 10394-10399, DOI 10.1021/acs.analchem.8b02252.

[171] Cowcher, D.P.; Xu, Y.; Goodacre, R. "Portable, Quantitative Detection of Bacillus Bacterial Spores Using Surface-Enhanced Raman Scattering". *Analytical Chemistry*, 2013, **85**(6), 3297-3302, DOI 10.1021/ac303657k.
[172] Davies, J.C. "Pseudomonas aeruginosa in cystic fibrosis: pathogenesis and persistence". *Paediatric Respiratory Reviews*, 2002, **3**(2), 128-134, DOI 10.1016/S1526-0550(02)00003-3.
[173] Gellatly, S.L.; Hancock, R.E.W. "Pseudomonas aeruginosa : new insights into pathogenesis and host defenses". *Pathogens and Disease*, 2013, **67**(3), 159-173, DOI 10.1111/2049-632X.12033.
[174] Hunter, R.C.; Klepac-Ceraj, V.; Lorenzi, M.M.; Grotzinger, H.; Martin, T.R.; Newman, D.K. "Phenazine content in the cystic fibrosis respiratory tract negatively correlates with lung function and microbial complexity". *American journal of respiratory cell and molecular biology*, 2012, **47**(6), 738-745, DOI 10.1165/rcmb.2012-0088OC.
[175] Wilson, R.; Sykes, D.A.; Watson, D.; Rutman, A.; Taylor, G.W.; Cole, P.J. "Measurement of Pseudomonas aeruginosa phenazine pigments in sputum and assessment of their contribution to sputum sol toxicity for respiratory epithelium". *Infection and immunity*, 1988, **56**(9), 2515-2517.
[176] Wu, X.; Chen, J.; Li, X.; Zhao, Y.; Zughaier, S.M. "Culture-free diagnostics of Pseudomonas aeruginosa infection by silver nanorod array based SERS from clinical sputum samples". *Nanomedicine : nanotechnology, biology, and medicine*, 2014, **10**(8), 1863-1870, DOI 10.1016/j.nano.2014.04.010.
[177] Nguyen, C.Q.; Thrift, W.J.; Bhattacharjee, A.; Ranjbar, S.; Gallagher, T.; Darvishzadeh-Varcheie, M.; Sanderson, R.N.; Capolino, F.; Whiteson, K.; Baldi, P.; Hochbaum, A.I.; Ragan, R. "Longitudinal Monitoring of Biofilm Formation via Robust Surface-Enhanced Raman Scattering Quantification of Pseudomonas aeruginosa-Produced Metabolites". *ACS Applied Materials & Interfaces*, 2018, **10**(15), 12364-12373, DOI 10.1021/acsami.7b18592.
[178] Bodelón, G.; Montes-García, V.; López-Puente, V.; Hill, E.H.; Hamon, C.; Sanz-Ortiz, M.N.; Rodal-Cedeira, S.; Costas, C.; Celiksoy, S.; Pérez-Juste, I.; Scarabelli, L.; La Porta, A.; Pérez-Juste, J.; Pastoriza-Santos, I.; Liz-Marzán, L.M. "Detection and imaging of quorum sensing in Pseudomonas aeruginosa biofilm communities by surface-enhanced resonance Raman scattering". *Nature materials*, 2016, **15**(11), 1203-1211, DOI 10.1038/nmat4720.
[179] Bauer, H.; Schueller, E.; Weinke, G.; Berger, A.; Hitzenberger, R.; Marr, I.L.; Puxbaum, H. "Significant contributions of fungal spores to the organic carbon and to the aerosol mass balance of the urban atmospheric aerosol". *Atmospheric Environment*, 2008, **42**(22), 5542-5549, DOI 10.1016/j.atmosenv.2008.03.019.
[180] Jaenicke, R.; Matthias-Maser, S.; Gruber, S. "Omnipresence of biological material in the atmosphere". *Environmental Chemistry*, 2007, **4**(4), 217-220, DOI 10.1071/EN07021.
[181] Baxi, S.N.; Portnoy, J.M.; Larenas-Linnemann, D.; Phipatanakul, W.; Environmental Allergens, W. "Exposure and Health Effects of Fungi on Humans". *The journal of allergy and clinical immunology. In practice*, 2016, **4**(3), 396-404, DOI 10.1016/j.jaip.2016.01.008.
[182] Sorenson, W.G. "Fungal spores: hazardous to health?". *Environmental health perspectives*, 1999, **107 Suppl 3**, 469-472, DOI 10.1289/ehp.99107s3469.
[183] Agarwal, R.; Gupta, D. "Severe asthma and fungi: current evidence". *Medical Mycology*, 2011, **49**(Supplement_1), S150-S157, DOI 10.3109/13693786.2010.504752.
[184] King, J.; Brunel, S.F.; Warris, A. "Aspergillus infections in cystic fibrosis". *The Journal of infection*, 2016, **72 Suppl**, S50-55, DOI 10.1016/j.jinf.2016.04.022.
[185] De Gussem, K.; Vandenabeele, P.; Verbeken, A.; Moens, L. "Chemotaxonomical identification of spores of macrofungi: possibilities of Raman spectroscopy". *Analytical and Bioanalytical Chemistry*, 2007, **387**(8), 2823-2832, DOI 10.1007/s00216-007-1150-1.
[186] Asher, S.A.; Johnson, C.R. "Raman spectroscopy of a coal liquid shows that fluorescence interference is minimized with ultraviolet excitation". *Science (New York, N.Y.)*, 1984, **225**(4659), 311-313.
[187] Gaus, K.; Rösch, P.; Petry, R.; Peschke, K.D.; Ronneberger, O.; Burkhardt, H.; Baumann, K.; Popp, J. "Classification of lactic acid bacteria with UV-resonance Raman spectroscopy". *Biopolymers*, 2006, **82**(4), 286-290, DOI 10.1002/bip.20448.
[188] Manoharan, R.; Ghiamati, E.; Dalterio, R.A.; Britton, K.A.; Nelson, W.H.; Sperry, J.F. "UV resonance Raman spectra of bacteria, bacterial spores, protoplasts and calcium dipicolinate". *Journal of Microbiological Methods*, 1990, **11**(1), 1-15, DOI 10.1016/0167-7012(90)90042-5.
[189] Neugebauer, U.; Schmid, U.; Baumann, K.; Holzgrabe, U.; Ziebuhr, W.; Kozitskaya, S.; Kiefer, W.; Schmitt, M.; Popp, J. "Characterization of bacterial growth and the influence of antibiotics by means of UV resonance Raman spectroscopy". *Biopolymers*, 2006, **82**(4), 306-311, DOI 10.1002/bip.20447.

[190] Jahn, B.; Koch, A.; Schmidt, A.; Wanner, G.; Gehringer, H.; Bhakdi, S.; Brakhage, A.A. "Isolation and characterization of a pigmentless-conidium mutant of Aspergillus fumigatus with altered conidial surface and reduced virulence". *Infection and immunity*, 1997, **65**(12), 5110-5117.
[191] Kumamoto, Y.; Taguchi, A.; Smith, N.I.; Kawata, S. "Deep UV resonant Raman spectroscopy for photodamage characterization in cells". *Biomedical optics express*, 2011, **2**(4), 927-936, DOI 10.1364/BOE.2.000927.
[192] Wen, Z.Q.; Thomas, G.J. "UV resonance Raman spectroscopy of DNA and protein constituents of viruses: Assignments and cross sections for excitations at 257, 244, 238, and 229 nm". *Biopolymers*, 1998, **45**(3), 247-256, DOI 10.1002/(SICI)1097-0282(199803)45:3<247::AID-BIP7>3.0.CO;2-R.
[193] Josse, J.; Husson, F. "Selecting the number of components in principal component analysis using cross-validation approximations". *Computational Statistics & Data Analysis*, 2012, **56**(6), 1869-1879, DOI 10.1016/j.csda.2011.11.012.
[194] Jung, S.; Lee, M.H.; Ahn, J. "On the number of principal components in high dimensions". *Biometrika*, 2018, **105**(2), 389-402, DOI 10.1093/biomet/asy010.
[195] Mousavi, B.; Hedayati, M.T.; Hedayati, N.; Ilkit, M.; Syedmousavi, S. "Aspergillus species in indoor environments and their possible occupational and public health hazards". *Current medical mycology*, 2016, **2**(1), 36-42, DOI 10.18869/acadpub.cmm.2.1.36.
[196] Rocchi, S.; Reboux, G.; Larosa, F.; Scherer, E.; Daguindeau, E.; Berceanu, A.; Deconinck, E.; Millon, L.; Bellanger, A.P. "Evaluation of invasive aspergillosis risk of immunocompromised patients alternatively hospitalized in hematology intensive care unit and at home". *Indoor air*, 2014, **24**(6), 652-661, DOI 10.1111/ina.12108.
[197] Tashiro, T.; Izumikawa, K.; Tashiro, M.; Takazono, T.; Morinaga, Y.; Yamamoto, K.; Imamura, Y.; Miyazaki, T.; Seki, M.; Kakeya, H.; Yamamoto, Y.; Yanagihara, K.; Yasuoka, A.; Kohno, S. "Diagnostic significance of Aspergillus species isolated from respiratory samples in an adult pneumology ward". *Medical Mycology*, 2011, **49**(6), 581-587, DOI 10.3109/13693786.2010.548084.
[198] Sugui, J.A.; Kwon-Chung, K.J.; Juvvadi, P.R.; Latgé, J.-P.; Steinbach, W.J. "Aspergillus fumigatus and related species". *Cold Spring Harbor perspectives in medicine*, 2015, **5**(2), a019786-a019786, DOI 10.1101/cshperspect.a019786.
[199] Mondon, P.; De Champs, C.; Donadille, A.; Ambroise-Thomas, P.; Grillot, R. "Variation in virulence of Aspergillus fumigatus strains in a murine model of invasive pulmonary aspergillosis". *Journal of medical microbiology*, 1996, **45**(3), 186-191, DOI 10.1099/00222615-45-3-186.
[200] Bouatra, S.; Aziat, F.; Mandal, R.; Guo, A.C.; Wilson, M.R.; Knox, C.; Bjorndahl, T.C.; Krishnamurthy, R.; Saleem, F.; Liu, P.; Dame, Z.T.; Poelzer, J.; Huynh, J.; Yallou, F.S.; Psychogios, N.; Dong, E.; Bogumil, R.; Roehring, C.; Wishart, D.S. "The human urine metabolome". *PloS one*, 2013, **8**(9), e73076, DOI 10.1371/journal.pone.0073076.
[201] Ali, R.; Ozkalemkas, F.; Ozcelik, T.; Ozkocaman, V.; Ozkan, A.; Bayram, S.; Ener, B.; Ursavas, A.; Ozal, G.; Tunali, A. "Invasive pulmonary aspergillosis: role of early diagnosis and surgical treatment in patients with acute leukemia". *Annals of Clinical Microbiology and Antimicrobials*, 2006, **5**, 17-17, DOI 10.1186/1476-0711-5-17.
[202] Kliasova, G.A.; Petrova, N.A.; Galstian, G.M.; Gotman, L.N.; Vishnevskaia, E.S.; Sysoeva, E.P.; Khoroshko, N.D.; Mikhailova, E.A.; Parovichnikova, E.N.; Isaev, V.G. "Invasive aspergillosis in immunocompromised patients". *Terapevticheskii arkhiv*, 2003, **75**(7), 63-68.
[203] Adamko, D.J.; Saude, E.; Bear, M.; Regush, S.; Robinson, J.L. "Urine metabolomic profiling of children with respiratory tract infections in the emergency department: a pilot study". *BMC infectious diseases*, 2016, **16**(1), 439-439, DOI 10.1186/s12879-016-1709-6.
[204] Saude, E.J.; Skappak, C.D.; Regush, S.; Cook, K.; Ben-Zvi, A.; Becker, A.; Moqbel, R.; Sykes, B.D.; Rowe, B.H.; Adamko, D.J. "Metabolomic profiling of asthma: diagnostic utility of urine nuclear magnetic resonance spectroscopy". *The Journal of allergy and clinical immunology*, 2011, **127**(3), 757-764.e751-756, DOI 10.1016/j.jaci.2010.12.1077.
[205] Tuuminen, T. "Urine as a specimen to diagnose infections in twenty-first century: focus on analytical accuracy". *Frontiers in immunology*, 2012, **3**, 45, DOI 10.3389/fimmu.2012.00045.
[206] Kavanagh, C.; Uy, N.S. "Nephrogenic Diabetes Insipidus". *Pediatric clinics of North America*, 2019, **66**(1), 227-234, DOI 10.1016/j.pcl.2018.09.006.
[207] Yaxley, J.; Pirrone, C. "Review of the Diagnostic Evaluation of Renal Tubular Acidosis". *The Ochsner journal*, 2016, **16**(4), 525-530.
[208] Moreira, L.P.; Silveira, L.; da Silva, A.G.; Fernandes, A.B.; Pacheco, M.T.T.; Rocco, D.D.F.M. "Raman spectroscopy applied to identify metabolites in urine of physically active subjects". *Journal of*

Photochemistry and Photobiology B: Biology, 2017, **176**, 92-99, DOI 10.1016/j.jphotobiol.2017.09.019.
[209] Premasiri, W.R.; Clarke, R.H.; Womble, M.E. "Urine analysis by laser Raman spectroscopy". *Lasers in surgery and medicine*, 2001, **28**(4), 330-334, DOI 10.1002/lsm.1058.
[210] Sands, J.M.; Bichet, D.G. "Nephrogenic diabetes insipidus". *Annals of internal medicine*, 2006, **144**(3), 186-194.
[211] Hennings, J.C.; Picard, N.; Huebner, A.K.; Stauber, T.; Maier, H.; Brown, D.; Jentsch, T.J.; Vargas-Poussou, R.; Eladari, D.; Hübner, C.A. "A mouse model for distal renal tubular acidosis reveals a previously unrecognized role of the V-ATPase a4 subunit in the proximal tubule". *EMBO molecular medicine*, 2012, **4**(10), 1057-1071, DOI 10.1002/emmm.201201527.
[212] Zumla, A. "Current trends and newer concepts on diagnosis, management and prevention of respiratory tract infections". *Current opinion in pulmonary medicine*, 2013, **19**(3), 189-191, DOI 10.1097/MCP.0b013e32835f8265.
[213] Mosier-Boss, P.A. "Review of SERS Substrates for Chemical Sensing". *Nanomaterials (Basel, Switzerland)*, 2017, **7**(6), 142, DOI 10.3390/nano7060142.
[214] Leopold, N.; Lendl, B. "A New Method for Fast Preparation of Highly Surface-Enhanced Raman Scattering (SERS) Active Silver Colloids at Room Temperature by Reduction of Silver Nitrate with Hydroxylamine Hydrochloride". *The Journal of Physical Chemistry B*, 2003, **107**(24), 5723-5727, DOI 10.1021/jp027460u.
[215] Chowdhury, J.; Mukherjee, K.M.; Misra, T.N. "A pH dependent surface-enhanced Raman scattering study of hypoxanthine". *Journal of Raman Spectroscopy*, 2000, **31**(5), 427-431, DOI 10.1002/1097-4555(200005)31:5<427::AID-JRS553>3.0.CO;2-L.
[216] de Almeida Pdel, V.; Gregio, A.M.; Machado, M.A.; de Lima, A.A.; Azevedo, L.R. "Saliva composition and functions: a comprehensive review". *The journal of contemporary dental practice*, 2008, **9**(3), 72-80.
[217] Han, H.; Huang, Z.; Lee, W. "Metal-assisted chemical etching of silicon and nanotechnology applications". *Nano Today*, 2014, **9**(3), 271-304, DOI 10.1016/j.nantod.2014.04.013.
[218] Huang, Z.; Geyer, N.; Werner, P.; de Boor, J.; Gösele, U. "Metal-Assisted Chemical Etching of Silicon: A Review". *Advanced Materials*, 2011, **23**(2), 285-308, DOI 10.1002/adma.201001784.
[219] Becker, M.; Stelzner, T.; Steinbrück, A.; Berger, A.; Liu, J.; Lerose, D.; Gösele, U.; Christiansen, S. "Selectively Deposited Silver Coatings on Gold-Capped Silicon Nanowires for Surface-Enhanced Raman Spectroscopy". *ChemPhysChem*, 2009, **10**(8), 1219-1224, DOI 10.1002/cphc.200800809.
[220] Hidi, I.J.; Jahn, M.; Pletz, M.W.; Weber, K.; Cialla-May, D.; Popp, J. "Toward Levofloxacin Monitoring in Human Urine Samples by Employing the LoC-SERS Technique". *The Journal of Physical Chemistry C*, 2016, **120**(37), 20613-20623, DOI 10.1021/acs.jpcc.6b01005.
[221] Peksa, V.; Jahn, M.; Štolcová, L.; Schulz, V.; Proška, J.; Procházka, M.; Weber, K.; Cialla-May, D.; Popp, J. "Quantitative SERS Analysis of Azorubine (E 122) in Sweet Drinks". *Analytical Chemistry*, 2015, **87**(5), 2840-2844, DOI 10.1021/ac504254k.
[222] Madzharova, F.; Heiner, Z.; Gühlke, M.; Kneipp, J. "Surface-Enhanced Hyper-Raman Spectra of Adenine, Guanine, Cytosine, Thymine, and Uracil". *The Journal of Physical Chemistry C*, 2016, **120**(28), 15415-15423, DOI 10.1021/acs.jpcc.6b02753.

CONFERENCE CONTRIBUTIONS

1. **Detection of pneumonia pathogens from sputum samples with the use of Raman spectroscopy**, O. Žukovskaja, S. Kloß, M. Dahms, U. Neugebauer, D. Cialla-May, K. Weber, J. Popp, *Raman4Clinics – Summer School in Clinical Biophotonics*, Jena (Germany), 29.05-01.06.2016. *(Poster)*

2. **Detection of the *Pseudomonas aeruginosa* metabolite pyocyanin by SERS combined with a microfluidic platform**, O. Žukovskaja, I. J. Jahn, K. Weber, D. Cialla-May, J. Popp, *Molecular Plasmonics 2017,* Jena (Germany), 18.05-20.05.2017. *(Poster)*

3. **Detection of *Pseudomonas aeruginosa* metabolite pyocyanin in water and saliva by employing the SERS technique**, O. Žukovskaja, I. J. Jahn, K. Weber, D. Cialla-May, J. Popp, *Raman4Clinics Annual Scientific Meeting*, Belgrade (Serbia), 06.07-07.07.2017. *(Poster)*

4. **Detection of *Pseudomonas aeruginosa* metabolite Pyocyanin in water and respiratory tract samples by employing the SERS technique**, O. Žukovskaja, I. J. Jahn, K. Weber, D. Cialla-May, J. Popp, *DoKDoK 2017,* Suhl (Germany), 18.09-22.09.2017 *(Poster)*

5. **Detection of *Pseudomonas aeruginosa* metabolite Pyocyanin in water and respiratory tract samples by employing SERS-based detection schemes**, O. Žukovskaja, I. J. Jahn, K. Weber, D. Cialla-May, J. Popp, *Bunsentagung 2018*, Hannover (Germany), 10.05-12.05.2018. *(Poster)*

6. **UV-Raman spectroscopic identification of fungal spores important for respiratory diseases**, O. Žukovskaja, S. Kloß, M. G. Blango, O. Ryabchykov, O. Kniemeyer, A. A. Brakhage, T. Bocklitz, D. Cialla-May, K. Weber, J. Popp, *SPEC 2018*, Glasgow (Great Britain), 10.06-15.06.2018 *(Poster)*

7. **SERS based detection of *Pseudomonas aeruginosa* metabolite pyocyanin in water and respiratory tract body-fluids**, O. Žukovskaja, I. J. Jahn, S. Shevchenko, L. Osminkina, K. Weber, D. Cialla-May, J. Popp, *ICORS 2018*, Jeju (South Korea), 26.08-31.08.2018. *(Poster)*

8. **UV-Raman spectroscopic identification of fungal spores important for respiratory disease**, O. Žukovskaja, S. Kloß, M. G. Blango, O. Ryabchykov, O. Kniemeyer, A. A. Brakhage, T. Bocklitz, D. Cialla-May, K. Weber, J. Popp, *DoKDoK 2018,* Friedrichroda (Germany),17.09-21.09.2018. *(Talk)*

ACKNOWLEDGEMENT

I would like to express my profound gratitude to Prof. Dr. Jürgen Popp for giving me the opportunity to be part of his research group. His trust, expertise and guidance helped me a lot throughout my PhD time.

My deepest appreciation goes to my two supervisors, Dr. Karina Weber and Dr. Dana Cialla-May, for their continuous help and support, for the magnitude of their advices and plenty of given opportunities for the improvement of my scientific and personal skills.

I would like also to thank Prof. Dr. Michael Schmitt for his constant encouragement and often provided constructive feedback on my manuscripts, as well as on this thesis.

The scientific cooperations with Dr. Izabella Jahn, PD Dr. Thomas Bocklitz, Dr. Sandra Kloß, Dr. Vladimir Sivakov, Dr. Liubov Osminkina and Svetlana Agafilushkina have largely contributed to my improvement and are highly acknowledged.

The special thankfulness I would like to pay to Oleg Ryabchykov for his help and support with the statistical data analysis and the endless patience with which he answered all of my questions.

I would like to thank to Dr. Maria Straßburger, Dr. Christopher Hennings and Dr. Michael Wegmann for providing me mice urine samples and for Dr. Matthew G. Blango for fungal spores samples.

I am very grateful for the nice working atmosphere and the continuous support of all the people who at some point were the part of JBCI group. I would particularly like to single out Dr. Izabella Jahn, who kindly shared her expertise with me and Dr. Andreea Radu, who gave me plenty of advices and invested her time for the proofreading of this thesis.

I especially thank for all my friends in ‘Jena’s cool Kids’ and my dearest friend Melina for all our discussions, travels, picnics and parties. Every one of you has touched my life and made my stay in Jena a wonderful adventure.

My genuine thanks go to my beloved family for believing in me and supporting me throughout my whole life.

Last, but not least, I would like to pay special thankfulness, warmth and appreciation to my Florian, who has been together with me since the first days of this ‘expedition to PhD world’. I thank you for always being caring, supporting and understanding, for being ready to help me with any problem I faced, for dedicating your time to make this thesis more beautiful and my life easier. Words are not enough to express my gratitude.

Thank you for your part in my journey.

ERKLÄRUNGEN

Selbstständigkeitserkärung

Ich erkläre, dass ich die vorliegende Arbeit selbständig und unter Verwendung der angegebenen Hilfsmittel, persönlichen Mitteilungen und Quellen angefertigt habe.

_____	_____
Ort, Datum	Olga Žukovskaja

Für alle in dieser kumulativen Dissertation verwendeten Manuskripte liegen die notwendigen Genehmigungen der Verlage (reprint permissions) für die Zweitpublikation vor.

_____	_____
Ort, Datum	Olga Žukovskaja

Bestätigung des Einverständnisses der Koautoren

Die Co-Autoren der in dieser kumulativen Dissertation verwendeten Manuskripte sind sowohl über die Nutzung, als auch über die oben angegebenen Eigenanteile der weiteren Doktoranden/ Doktorandinnen als Koautoren an den Publikationen und Zweitpublikationsrechten bei einer kumulativen Dissertation informiert und stimmen dem zu. Die Anteile der Co-Autoren an den Publikationen sind vor der jeweiligen Publikation aufgeführt.

_____	_____
Ort, Datum	Olga Žukovskaja

Einverständniserklärung des Betreuers

Ich bin mit der Abfassung der Dissertation als publikationsbasiert, d.h. kumulativ, einverstanden und bestätige die vorstehenden Angaben. Eine entsprechend begründete Befürwortung mit Angabe des wissenschaftlichen Anteils des Doktoranden an den verwendeten Publikationen werde ich parallel an den Rat der Fakultät der Chemisch-Geowissenschaftlichen Fakultät richten.

_____	_____
Ort, Datum	Prof. Dr. Jürgen Popp